U. S. Department of Energy
1000 Independence Avenue, S.W.
Washington, D.C. 20585

Fiscal Year 2018: Third Quarter

Progress Reports:

Advanced Battery Materials Research (BMR) Program
&
Battery500
Consortium Program

Released September 2018
for the period of April – June 2018

Approved by

Tien Q. Duong, Program Manager
Advanced Battery Materials Research Program & Battery500 Consortium Program
Vehicle Technologies and Electrification Program
Energy Efficiency and Renewable Energy

TABLE OF CONTENTS

A Message from the Advanced Battery Materials Research Program Manager xvi

Advanced Battery Materials Research Program

Task 1 – Liquid/Polymer Solid-State Electrolytes 1

Task 1.1 – Advanced Lithium-Ion Battery Technology: High-Voltage Electrolyte (Joe Sunstrom, Ron Hendershot, and Alec Falzone, Daikin) 3

Task 1.2 – Multi-Functional, Self-Healing Polyelectrolyte Gels for Long-Cycle-Life, High-Capacity Sulfur Cathodes in Lithium-Sulfur Batteries (Alex Jen and Jihui Yang, University of Washington) 6

Task 1.3 – Development of Ion-Conducting Inorganic Nanofibers and Polymers (Nianqiang (Nick) Wu, West Virginia University; Xiangwu Zhang, North Carolina State University) 10

Task 1.4 – High Conductivity and Flexible Hybrid Solid-State Electrolyte (Eric Wachsman, Liangbing Hu, and Yifei Mo, University of Maryland) 13

Task 1.5 – Self-Forming Thin Interphases and Electrodes Enabling 3D Structured High-Energy-Density Batteries (Glenn Amatucci, Rutgers University) 16

Task 1.6 – Dual Function Solid-State Battery with Self-Forming, Self-Healing Electrolyte and Separator (Esther Takeuchi, Stony Brook University).. 19

Task 1.7 – High-Conductivity, Low-Temperature Polymer Electrolytes for Lithium-Ion Batteries (Bryan D. McCloskey, University of California at Berkeley).................................. 22

Task 1.8 – Advanced Polymer Materials for Batteries (Zhenan Bao and Yi Cui, Stanford University) 25

Task 1.9 – Improving the Stability of Lithium-Metal Anodes and Inorganic-Organic Solid Electrolytes (Nitash Balsara, Lawrence Berkeley National Laboratory)....................... 28

Task 1.10 – Electrolyte/Binder for High Efficiency Lithium-Sulfur Battery: New Materials Design and Computation (Larry A. Curtiss, Zhengcheng Zhang, and Ahn Ngo, Argonne National Laboratory).. 30

Task 2 – Diagnostics 32

Task 2.1 – Model System Diagnostics for High-Energy Cathode Development (Guoying Chen, Lawrence Berkeley National Laboratory).. 34

Task 2.2 – Interfacial Processes – Diagnostics (Robert Kostecki, Lawrence Berkeley National Laboratory) 37

Task 2.3 – Advanced *In Situ* Diagnostic Techniques for Battery Materials (Xiao-Qing Yang and Seongmin Bak, Brookhaven National Laboratory) 40

Task 2.4 – Advanced Microscopy and Spectroscopy for Probing and Optimizing Electrode-Electrolyte Interphases in High-Energy Lithium Batteries (Shirley Meng, University of California at San Diego) 43

Task 2.5 – *In Situ* Diagnostics of Coupled Electrochemical-Mechanical Properties of Solid Electrolyte Interphases on Lithium-Metal Rechargeable Batteries (Xingcheng Xiao, General Motors; Brian W. Sheldon, Brown University; Yue Qi, Michigan State University; and Y. T. Cheng, University of Kentucky) 46

Task 2.6 – Microscopy Investigation on the Fading Mechanism of Electrode Materials (Chongmin Wang, Pacific Northwest National Laboratory) 50

Task 2.7 – Understanding and Mitigating Interfacial Reactivity between Electrode and Electrolyte (Khalil Amine and Zhonghai Chen, Argonne National Laboratory) 53

Task 2.8 – Correlative Microscopy Characterization of Electrochemical Hotspots in Oxide Electrodes (Yi Cui, William Chueh, and Michael Toney; Stanford/SLAC) 55

Task 3 – Modeling 58

Task 3.1 – Design of High-Energy, High-Voltage Lithium Batteries through First-Principles Modeling (Kristin Persson, Lawrence Berkeley National Laboratory) 59

Task 3.2 – Addressing Heterogeneity in Electrode Fabrication Processes (Dean Wheeler and Brian Mazzeo, Brigham Young University) 61

Task 3.3 – Understanding and Strategies for Controlled Interfacial Phenomena in Lithium-Ion Batteries and Beyond (Perla Balbuena and Jorge Seminario, Texas A&M University; Partha Mukherjee, Purdue University) 64

Task 3.4 – Electrode Materials Design and Failure Prediction (Venkat Srinivasan, Argonne National Laboratory) 67

Task 3.5 – First-Principles Calculations of Existing and Novel Electrode Materials (Gerbrand Ceder, Lawrence Berkeley National Laboratory) 70

Task 3.6 – Dendrite Growth Morphology Modeling in Liquid and Solid Electrolytes (Yue Qi, Michigan State University) 72

Task 3.7 – First-Principles Modeling and Design of Solid-State Interfaces for the Protection and Use of Lithium-Metal Anodes (Gerbrand Ceder, University of California at Berkeley) 75

Task 3.8 – Large-Scale *Ab Initio* Molecular Dynamics Simulations of Liquid and Solid Electrolytes (Lin-Wang Wang, Lawrence Berkeley National Laboratory) 77

Task 3.9 – *In Operando* Thermal Diagnostics of Electrochemical Cells (Ravi Prasher, Lawrence Berkeley National Laboratory) 80

Task 3.10 – Multi-Scale Modeling of Solid-State Electrolytes for Next-Generation Lithium Batteries (Anh Ngo, Larry A. Curtiss, and Venkat Srinivasan, Argonne National Laboratory) 82

Task 4 – Metallic Lithium 84

Task 4.1 – Lithium Dendrite Prevention for Lithium Batteries (Wu Xu and Ji-Guang Zhang, Pacific Northwest National Laboratory) 86

Task 4.2 – Self-Assembling and Self-Healing Rechargeable Lithium Batteries (Yet-Ming Chiang, Massachusetts Institute of Technology; Venkat Viswanathan, Carnegie Mellon University)... 89

Task 4.3 – Engineering Approaches to Dendrite-Free Lithium Anodes (Prashant Kumta, University of Pittsburgh) 92

Task 4.4 – Nanoscale Interfacial Engineering for Stable Lithium-Metal Anodes (Yi Cui, Stanford University) 95

Task 4.5 – Composite Electrolytes to Stabilize Metallic Lithium Anodes (Nancy Dudney and X. Chelsea Chen, Oak Ridge National Laboratory) 98

Task 4.6 – Lithium Batteries with Higher Capacity and Voltage (John B. Goodenough, University of Texas at Austin)... 101

Task 4.7 – Advancing Solid-State Interfaces in Lithium-Ion Batteries (Nenad M. Markovic and Larry A. Curtiss, Argonne National Laboratory) 103

Task 4.8 – Mechanical and Defect Properties at the Protected Lithium Interface (Nancy Dudney, Oak Ridge National Laboratory; Erik Herbert, Michigan Technological University; Jeff Sakamoto, University of Michigan).................................... 106

Task 5 – Sulfur Electrodes...109

Task 5.1 – Novel Chemistry: Lithium Selenium and Selenium Sulfur Couple (Khalil Amine, Argonne National Laboratory)... 111

Task 5.2 – Development of High-Energy Lithium-Sulfur Batteries (Jun Liu and Dongping Lu, Pacific Northwest National Laboratory) 113

Task 5.3 – Nanostructured Design of Sulfur Cathodes for High-Energy Lithium-Sulfur Batteries (Yi Cui, Stanford University).. 116

Task 5.4 – Addressing Internal “Shuttle” Effect: Electrolyte Design and Cathode Morphology Evolution in Lithium-Sulfur Batteries (Perla Balbuena, Texas A&M University; Partha Mukherjee, Purdue University) 119

Task 5.5 – Investigation of Sulfur Reaction Mechanisms (Deyang Qu, University of Wisconsin at Milwaukee; Xiao-Qing Yang, Brookhaven National Laboratory).. 122

Task 5.6 – Statically and Dynamically Stable Lithium-Sulfur Batteries (Arumugam Manthiram, University of Texas at Austin) 125

Task 5.7 – Electrochemically Responsive, Self-Formed Lithium-Ion Conductors for High-Performance Lithium-Metal Anodes (Donghai Wang, Pennsylvania State University)... 128

Task 5.8 – Materials and Cell Design Optimization for Lithium-Sulfur Battery Technology (Hong Gan, Brookhaven National Laboratory) 132

Task 6 – Air Electrodes / Electrolytes 135

Task 6.1 – Rechargeable Lithium-Air Batteries
(Ji-Guang Zhang and Wu Xu, Pacific Northwest National Laboratory) 136

Task 6.2 – Lithium-Air Batteries
(Khalil Amine and Larry A. Curtiss, Argonne National Laboratory).......... 138

Task 7 – Sodium-Ion Batteries 141

Task 7.1 – Exploratory Studies of Novel Sodium-Ion Battery Systems
(Xiao-Qing Yang and Seongmin Bak, Brookhaven National Laboratory) 142

Battery500 Consortium Program

Innovation Center for Battery500
(Jun Liu, Pacific Northwest National Laboratory; Yi Cui, Stanford University) **.......... 145**

TABLE OF FIGURES

Figure 1. Carbon (left) and aluminum (middle) depth profiling using atomic emission spectroscopy with Ar(g) ionization. Elemental survey scan (right) of NMC-111 cathode (cycled at 4.6 V, 15% FEC v/v). 4

Figure 2. 3D images of a cycled (left) and uncycled (right) NMC-111 cathode at low (top) and high (bottom) magnifications. Calculated surface characteristics are tabulated for each cathode (right). 4

Figure 3. Photo of solvate ionogel 1 (SIG 1) formula cured into film of Celgard 2500.......... 7

Figure 4. Tensile stress-strain tests of PP-1/LiTFSI and PP-1/Li(G4)TFSI. 7

Figure 5. Cycling performance of sulfur cathodes with PP and PVDF as binder. 8

Figure 6. Schematic description of the formation of an ionic surface group, and its interaction with a solvate ionic liquid electrolyte. 8

Figure 7. (a) Raman spectra and (b) Fourier transform infrared spectra of pure polyvinylidene fluoride (PVDF), PVDF-hexafluoropropylene (HFP)/LiTFSI, and PVDF-HFP/LiTFSI /$Li_{0.33}La_{0.557}TiO_3$ (LLATO) nanofiber-based membrane. 11

Figure 8. (a) Rate capability (0.2-10 C) and (b) charge-discharge profiles (at different C rates) of all-solid-state Li|s@LLAZO-PCLP-DA(50)|LFP cell operated at 25°C.......... 12

Figure 9. Hybrid composite electrolyte with the thickness < 20 µm. 14

Figure 10. Electrochemical impedance spectrum of the Li/electrolyte/Li symmetric cell at room temperature. 14

Figure 11. Initial symmetrical cell cycled at 0.1mA/cm^2, 0.5 mA/cm^2, and 3 mA/cm^2. 14

Figure 12. Comparison of discharge capacities for the 1st, 2nd, 3rd, and 6th cycles for a standard self-formed single cell versus an environmentally encapsulated self-formed single cell. Cells were submitted to a formation period over the first three cycles with a lower charge capacity cutoff that was increased upon subsequent cycling. Encapsulated cells responded with higher discharge capacity regardless of the charge capacity utilization.......... 17

Figure 13. Addition of silver iodide in the composite solid electrolyte demonstrated reduced pre-charge AC impedance in coin cell construction A. 20

Figure 14. Schematic of energy dispersive X-ray diffraction experiment. 20

Figure 15. Intensity maps of as-assembled cell (top right) and three locations of charged cell. 20

Figure 16. Quantitative profiles of as-assembled cell (top right) and three locations of charged cell. 20

Figure 17. Conductivity and viscosity of Li+-neutralized sulfonated polysulfones of various molecular weights dissolved in dimethyl sulfoxide. The Li^+ concentration in each case was 0.1 M. 23

Figure 18. Diffusion coefficient of each species in 0.1-M Li^+ solutions of various molecular weight Li^+-neutralized sulfonated polysulfones in dimethyl sulfoxide as measured using pulse field gradient nuclear magnetic resonance 23

Figure 19. Li^+ transference number (t_+) of Li^+-neutralized sulfonated polysulfones of various molecular weights dissolved in dimethyl sulfoxide. The Li^+ concentration in each case was 0.1 M. 24

Figure 20. (a) Chemical structures of the polymer coatings used in this study. Coloring of the label corresponds to the chemical functionality of the polymer. (b) Diagram of the conditions used to study the initial stages of lithium metal growth under polymer. 26

Figure 21. (a) Chemical structures of the dynamic crosslinking of the self-healing polymer and covalent crosslinking of the self-healing elastomer. (b-e) Scanning electron microscopy images of 0.1 mAh/cm^2 of lithium electrodeposited on polymer-coated copper. The electrodes are coated with (b-c) a supramolecular adaptive coating and (d-e) a covalently crosslinked self-healing elastomer with similar chemistry to the supramolecular coating. Scale bars are 50 µm for b/d, and 1 µm for c/e. 27

Figure 22. Scanning electron microscopy images of 0.1 mAh/cm^2 of lithium electrodeposited on copper with (a) no polymer coating, (b) PEO coating, (c) PVDF coating, (d) self-healing polymer coating, (e) PU coating, and (f) PVDF-HFP coating. Scale bars for all images are 5 um. 27

Figure 23. (a) Transference number measurements of poly(ethylene oxide) - b- poly(acryloisobutyl polyhedral oligomeric silsesquioxane) (PEO-POSS(5-6)). (b) phase diagram of PEO-POSS(5-1.9) 29

Figure 24. Structures of synthesized fluorinated ethers. 31

Figure 25. Voltage profiles of the Li-S cell with tetrafluorethylene – pentafluorinated perfluoro-polyether (TFE-PFPE) and TFE perfluorobutyl ethylene (TFE-PFBE) electrolytes. The sulfur electrode is made of commercial sulfur power, carbon black conducting agent, and polyvinylidene fluoride binder. 31

Figure 26. Oxygen K-edge X-ray absorption spectroscopy profiles of chemically delithiated $Li_0Nb_{0.3}Mn_{0.4}O_2$ (a-b) and $Li_{1.3}Nb_{0.3}Mn_{0.4}O_2$ cathodes charged to 4.8 V after various cycle numbers (c-d). (e-f) Intensity of the TM_{3d}-$O2_p$ absorption band as a function of the cycle number. (a), (c), and (e) were collected in the total electron yield mode; (b), (d), and (f) were collected in fluorescent yield mode. 35

Figure 27. Manganese L-edge X-ray absorption spectroscopy profiles of chemically delithiated $Li_0Nb_{0.3}Mn_{0.4}O_2$ (a-b) and $Li_{1.3}Nb_{0.3}Mn_{0.4}O_2$ cathodes charged to 4.8 V after various cycle numbers (c-d). (e/f) Manganese oxidation state derived from average L3 and L2 band energies, respectively. (a) and (c) were collected in the totally electron yield mode; (b) and (d) were collected in in fluorescence yield mode. 35

Figure 28. (a/d) Atomic force microscopy (AFM) morphology image of the pristine NMC thin-film electrode. (b) AFM morphology image and (c) near-field infrared (IR) adsorbance image of cycled NMC thin film after 5 s washing in diethyl carbonate (DEC). (e) AFM morphology image and (c) near-field IR absorbance image of cycled NMC thin film with 5 min washing in DEC. 38

Figure 29. (a) X-ray pair distribution function data of pristine sample (symbol) and the O-O pair contribution (solid line). (b) Neutron pair distribution function data of both pristine and charged sample (symbol) and the O-O pair contribution (solid line). (c) The relative scattering power/length of lithium, cobalt, and oxygen for X-ray and for neutron scattering. (d) The change of the shortest O-O pair distance from pristine sample to charged sample. 41

Figure 30. High-resolution transmission electron microscopy image, electron diffraction (ED), and intensity of reciprocal lattice from line-scanning on single particle for the Li-rich layered oxide (LRLO) sample after 50 cycles (a) and after heat treatment at 300°C (b). Models of cycled and heat treated LRLO for ED simulation (c). Simulated ED patterns for LRLO with different degree of stacking faults (d). 44

Figure 31. Cryo - transmission electron microscopy images (a, b, d, e) with their corresponding area fast Fourier transform analysis (c, f) of the deposited lithium metal using electrolytes containing Cs^+ (a-c) and Zn^{2+} (d-f) additives at 400 kx magnification. The current density of the deposition is 0.5 mA/cm^2, and deposition time is 5 minutes. 45

Figure 32. A phase diagram of wrinkling and delamination of a thin-film protective coating on a Li-metal electrode. 47

Figure 33. X-ray photoelectron spectroscopy depth profiling spectra (Li 1s, C 1s, O 1s, F 1s, N 1s, S 2p) of plated lithium surfaces after a half cycle (0.5 mA cm^{-2}, 4 mAh cm^{-2}) in four different electrolytes (4 M LiFSI DME, 0.4 LiTFSI + 0.6 M $LiNO_3$ DOL-DME, 1 M LiTFSI DOL-DME, and 1 M $LiPF_6$ EC-DEC). 48

Figure 34. Infusion of Li_3PO_4 into secondary particles eliminates structural degradation. The structural degradations are evaluated by a combination of selected area electron diffraction (a-c), bright-field transmission electron microscopy imaging (d-f), scanning transmission electron microscopy – high-angle annular dark field (STEM HAADF) imaging (g-i), and atomic-level STEM-HAADF imaging (j-l, corresponding to the high magnification image of the redline marked regions). The left column corresponds to the pristine electrode without cycling, the middle column is the pristine electrode after 200 cycles, and the right column shows the Li_3PO_4-infused electrode after 200 cycles. These observations demonstrate that after 200 cycles, the pristine electrode shows significant structural degradation, featuring intergranular cracking and formation of amorphous phase within the grain boundaries (e), formation of surface reaction layer on each grain surface (indicated in h by the yellow arrows), and layered-to-spinel transformation (k), while these degradation features do not occur in the Li_3PO_4-infused electrode. The scale bars are 5 nm^{-1} in a-c, 500 nm in d-f, 100 nm in g-i, and 2 nm in j-l. 51

Figure 35. Dependence of (a) reversible capacity, (b) irreversible capacity loss, and (c) relative irreversible capacity loss of Li/C composite cathode on the loading density of sulfur in S/C composite. 54

Figure 36. Dependence of the static leakage current on both the working potential and the loading density of sulfur in S/C composite. 54

Figure 37. Rate-dependent *operando* X-ray diffraction of NMC-111 during first-cycle charging. 56

Figure 38. Predicted potential profiles for (a) silicon and (b) SiO_2, as referenced to the phase diagram. 60

Figure 39. Lithium self-diffusivity diffusion coefficients in lithium silicides and lithium silicates as a function of voltage versus lithium. 60

Figure 40. The experimental setup of micro-probe with a sample of delaminated cathode. 62

Figure 41. Electrochemical impedance spectroscopy Nyquist spectra of different electrolyte samples with conductivities varying from 82 to 443 µS/cm. 62

Figure 42. Charge density difference profile when a lithium ion is deposited on top of a defective lithium surface. Yellow: charge accumulation. Light blue: charge depletion. 65

Figure 43. (a) One-dimensional model geometry for the electrode-electrolyte interfacial region. (b) Phase field model converts the sharp interface into a continuous interfacial region by a phase parameter. (c) Electrochemical reactions assumed for the Li_2S precipitation process in the battery discharge process. (d) Electrochemical/chemical reactions assumed for Li_2S removal during battery charge process. 68

Figure 44. (a) Modeled Li_2S film growth on the active carbon surface in the discharge, and Li_2S film removal in the charge. (b) Li_2S film thickness growth under different discharge current conditions: 100 mA/cm^2, 200 mA/cm^2, and 480 mA/cm^2. (c) Simulated Li_2S film thickness variation under different charge current conditions. 68

Figure 45. Computed phase diagram of the MnO/Li_2VO_3/LiF alloy space. 71

Figure 46. Computed voltage profile and evolution of manganese and vanadium oxidation states (from density functional theory). 71

Figure 47. The equilibrium electron, Li-ion concentration, and the electric field distribution profile under different applied voltages. 73

Figure 48. Single lithium vacancy migration path in a nitride lattice. 76

Figure 49. Mechanical model to study stress concentration at rough surface. 76

Figure 50. The sandwich structure of hexaaminobenzene and Li-S. (Left, side view; Right, top view) 78

Figure 51. The decomposition energy as phase separation (into ternaries) and moisture reaction. Negative value means unstable. 78

Figure 52. Process flow showing integration of 3-omega sensors onto electrodes within electrochemical cells. 81

Figure 53. Raw data from *in situ* measurement of full electrochemical cell using internally integrated 3ω sensors. 81

Figure 54. The x, y components of the Young's Modulus obtained from the project's model. (a) and (b) are for the bulk region, while (c) and (d) are for grain boundary regions of the Σ_3(112) grain boundary. 83

Figure 55. (a) Temperature dependence of ionic conductivity of a polymer-in-salt electrolyte. (b) Electrochemical stability of the polymer-in-salt electrolyte in Li||SS cells at a scan rate of 0.1 mV/s and room temperature. (c) Charge/discharge voltage profiles for the first three cycles of a Li||LFP cell with the polymer-in-salt electrolyte at 60°C. 87

Figure 56. Comparison of cycling stability of Li||Li symmetric cells using electrolytes with different amounts of lithium difluorophosphate additive and scanning electron microscopy images of lithium morphologies from cycled cells. 87

Figure 57. X-ray photoelectron spectroscopy studies of the SEI formed in $LiPF_6$/carbonate-based electrolyte with fluoroethylene carbonate additive. 90

Figure 58. Sand's time experiment showing potential versus time for symmetric Li/Li cells for pristine lithium and surface-engineered lithium. 93

Figure 59. Scanning electron microscopy images of (a) surface-engineered lithium (SE-Li), (b) lithium plating on SE-Li, and (c) cycled SE-Li. 93

Figure 60. Cycling behavior of $LiMn_2O_4$ cathode tested against pristine lithium and surface-engineered lithium. 93

Figure 61. Schematic of lithium plating/stripping in lithium hosts (a) without and (b) with the sealing layer. 96

Figure 62. Scanning electron microscopy of hollow carbon spheres (HCS) and atomic layer deposition Al_2O_3/HCS electrodes soaked and dried in saturated NaCl solution. $LiPF_6$/EC/DEC electrolyte or saturated NACL/H_2O solution. 96

Figure 63. Cycling performance. 96

Figure 64. (left) Discharge and charge capacity as a function of cycle number for two all-solid-state cells at 50°C. (middle) Discharge and charge voltage profile at cycle 80. (right) Impedance spectra of Li|PE|CPE|LFP cells at different stages. 99

Figure 65. Discharge and charge capacity as a function of cycle number for Li|LiPON|CPE|LFP cell (left) and Li|CPE|LFP cell (middle), at 50°C. Right, discharge and charge voltage profile at cycle 15 for Li|Lipon|CPE|LFP cell and cycle 40 for Li|CPE|LFP cell. 99

Figure 66. Ionic conductivity of previous composite electrolytes and composite gel electrolyte at 30°C. 99

Figure 67. Charge/discharge voltage curves of bare and graphene-coated copper current collectors at 0.5 mA cm^{-2} (discharge for 2 h, charge up to 2 V; 5th cycle). 102

Figure 68. Scanning electron microscopy images of lithium deposit on the bare and graphene-coated copper current collectors. Lithium deposition was performed at 1 mA cm^{-2} for 6 h at room temperature. 102

Figure 69. Survey (top) and S 2p and P 2p (bottom) core level X-ray photoelectron spectra before (red) and after (black) lithium sputtering show clear reaction of LPS with lithium metal. 104

Figure 70. The impedance spectrum of unpolished (left) and polished (right) Li-LPS-Li symmetric cells at room temperature. 104

Figure 71. Li-LLZO-Li room-temperature cycling data. A critical current density of 2.7 mA/cm^2 (avg; stdev ~ 0.5 mA/cm^2; n=12) was achieved. 107

Figure 72. Critical current density (CCD) as a function of temperature in Li-LLZO-Li cells (top left) and the logarithm of CCD as a function of the inverse of temperature (top right). Both plots include reported CCDs from the literature for comparison. 107

Figure 73. Initial (left) and optimized (right) structure of high-concentration siloxane-based electrolytes using *ab initio* molecular dynamic simulation. 112

Figure 74. Computed structure of Li_2S_6 in high-concentration siloxane-based electrolytes...................... 112

Figure 75. Electrochemical impedance spectra (EIS) evolution in the first 20 hours of In-SE-LE-SS cell with electrolytes (a) 1 M LiTFSI/ DME and (b) 1 M LiTFSI/DOL. (c) EIS evolution of InLi/SE/LE/SS and (d) InLi/SE/LE/S with 1 M LiTFSI/DOL. EIS test (5 mv, 105-10-1 Hz). 114

Figure 76. The specific burning time test of sulfur electrodes with (a) sulfur – polyvinylidene fluoride (S-PVDF) electrode and (b) sulfur – ammonium polyphosphate (S-APP) electrode. The time indicated in the pictures is counted as soon as the electrodes are exposed to the direct flame from a lighter, indicated by the white arrow in (a). (c) The specific burning time of the sulfur cathodes with APP and PVDF binders. (d) Schematic showing the flame-retardant mechanism of the APP binder based sulfur electrode. 117

Figure 77. (a) Chemical reaction for flame-retardant mechanism. (b) X-ray photoelectron spectroscopy (XPS) spectra of the surface chemical composition of the sulfur – ammonium polyphosphate (S-APP), before and after burning. (c) S 2p XPS spectra of the S-PVDF electrode before and after burning. (d) Scanning electron microscopy (SEM) image and the corresponding (e) sulfur and (f) phosphorus elemental maps of the S-APP electrode after burning. (g) Energy dispersive spectroscopy (EDS) of the S-APP electrode after burning. (h) SEM image and the corresponding (i) sulfur and (j) fluorine elemental maps of the S-PVDF electrode after burning. (k) EDS of the S-PVDF electrode after burning. 118

Figure 78. Multilayer graphene structure showing the incorporation of nitrogen into the C rings in pyridinic (not shown), graphitic (blue circle), and pyrrolic (green circle) positions and their interactions with lithium. Note that: (1) graphitic nitrogen does not interact with lithium, (2) pyrrolic nitrogen bonds to lithium, and (3) as discussed last quarter, carbon backbone also participates in the electrochemical reduction of sulfur. 120

Figure 79. Photographs of S/Xant- copolymer with 90% (a), 70% (b), and 50% sulfur (c). 123

Figure 80. Rate performance of S/Xant- (70% sulfur). The testing was done in a coin cell. 123

Figure 81. Long-term cyclability of the cells fabricated with the three-dimensional carbon-paper cathodes with a sulfur loading, sulfur content, and electrolyte/sulfur ratio of, respectively, (a) 13 mg cm^{-2}, 75 wt%, and 4.0 $\mu L\ mg^{-1}$, and (b) 17 mg cm^{-2}, 80 wt%, and 3.9 $\mu L\ mg^{-1}$. 126

Figure 82. Cycling performance of a lithium-sulfur pouch cell with a sulfur loading of 7 mg cm^{-2}, sulfur content of 70 wt% based on the total mass of the cathode, and an electrolyte/sulfur ratio of 5 µL mg^{-1}: (a) charge/discharge curves and (b) cyclability at a C/5 rate. 126

Figure 83. The X-ray photoelectron spectroscopy (XPS) spectra of SEI layers formed from the electrolytes containing different additives. S 2p XPS spectra (a), C 1s XPS spectra (b), and F 1s XPS spectra (c) of the SEI layers formed from different electrolytes. 129

Figure 84. Fourier transform infrared of SEI layers obtained from theC-Ely (C-SEI) and the PSD-90-Ely (PSD-90-SEI). 129

Figure 85. Atomic force microscopy (AFM) images and indentation study of SEI layers obtained from C-Ely (a/c) and PSD-90-Ely (b/d). Scanning electron microscopy images of SEI layers obtained from C-Ely (e) and PSD-90-Ely (f). The scan size for AFM images is 10×10 μm^2. 130

Figure 86. Cycling performance of cells using PSD-90-Ely electrolyte. 130

Figure 87. Two-dimensional TiS_2 sheet synthesis 133

Figure 88. XPD of two-dimensional sheet TiS_2. 133

Figure 89. Polysulfide adsorbing color test. 133

Figure 90. Electrochemical testing. 133

Figure 91. (a) Optical image of as-prepared high-loading (4 mg cm^{-2}) air-electrode based on RuO_2/CNT composite catalysts. (b) Deep discharge/charge curves of Li-O_2 cells cycled between 2.2 V and 4.2 V at a current density of 0.1 mA cm^{-2} in 1 M LiTf-TEGDME electrolyte at room temperature 137

Figure 92. High-resolution transmission electron microscopy image of annealed Ir_8 clusters on an rGO cathode showing crystalline facets of the iridium nanoparticles. 139

Figure 93. Green rectangle shows a typical ~ 5 x 10 nm particle formed on the Ir-rGO cathode with white lines corresponding to Ir_3Li spacing; the upper left inset shows a fast Fourier transform (FFT) on the nanoparticle surface with the diffraction peaks consistent with Ir_3Li; lower right inset shows a close up of the nanoparticle with a thin layer of ~ 1-2 nm marked by dashed cyan line on the surface of the nanoparticle, due to the discharge product 139

Figure 94. *In situ* X-ray diffraction patterns collected during the first charge/discharge and the second charge of Na/$Na_{0.66}Mn_{0.6}Ni_{0.2}Mg_{0.2}O_2$ cells at a current rate of 0.2 C in the potential range between 1.5 and 4.3 V. 143

Figure 95. Differential scanning calorimetry profiles of (a) NMC-811 and (b) NCA charged to different cut-off voltages. (c) Capacity retention of a graphite/NMC-811 cell, compared with a Li/NMC-811 cell. 146

Figure 96. Characterization of fire-retardant localized high-concentration electrolyte (LHCE). (a) Schematic illustration for dilution by BTFE of an HCE consisting of 3.2 M LiFSI/TEP to form LHCEs. (b-c) Photographs of ignition tests of glass fibers saturated with the conventional electrolyte (b) and the 1.2 M LHCE (c). (d) Raman spectra of pure TEP, pure BTFE, LiFSI, the HCE, and LHCEs with different LiFSI salt concentrations and TEP/BTFE molar ratios. (e) Viscosity of different electrolytes. 147

Figure 97. (a) Chemical structures of PEO and PTHF precursors that are used in the crosslinking reaction to create robust, free-standing solid polymer electrolyte (SPE) films. (b) Graph showing the ionic conductivity versus the degree of polymerization of the polymers in the crosslinked network for xPEO and xPTHF SPEs. The inset shows molecular dynamics simulations of LiTFSI dissolved in the polymer backbones. (c) Density-weighted lithium-oxygen radial distribution functions (atoms per nm^3) in PTHF and PEO. (d) Experimental ^{7}Li NMR spectra for LiTFSI in PEO and PTHF. 148

Figure 98. Discharge curves at ~ 6 mA/cm^2 to understand cathode utilization (right). Current density variation computations (left) of cathode chemistries. 149

TABLE OF TABLES

Table 1. Composition and resulting time-to-short-circuit data for solvate ionogel formulations 1-5 in comparison to neat Li(G4)TFSI. 7

Table 2. Atomic compositions collected by XPS of pristine, thiol, and sodium sulfate modified samples. 8

Table 3. Comparison of several solid electrolytes. 73

Table 4. Averages and standard deviations for critical current density as a function of temperature. 107

Table 5. The reduced modulus of SEI layers formed from the C-Ely and PSD-90-Ely. 130

Table 6. The relationship between the physical properties and electrochemical performance of the Ni-rich NMC thick electrodes provided by Maxwell Technology. 149

A MESSAGE FROM THE PROGRAM MANAGER

We have added a new topic area, Sodium Ion Batteries, to the BMR portfolio. Na-ion batteries offer an appealing, potentially more-affordable, and sustainable alternative to Li-ion batteries. Although a considerable number of investigators has pursued this electrochemical couple over the last 10 years, the technology remains far from practical commercialization. Most scholars agree that considerable R&D must be conducted to identify optimal electrode materials, electrolytes, separators, and binders before the Na-ion battery can reach its full potential. Over the next three years, the BMR Program will pursue a limited effort focusing on improving the rechargeability of the negative electrode. In this issue, we report on the study by Drs. Xiao-Qing Yang and Seongmin Bak (Brookhaven National Laboratory): Exploratory Studies of Novel Sodium-Ion Battery Systems.

BMR Team

A few notable achievements from the BMR Team for this quarter are summarized below:

- **Pacific Northwest National Laboratory (Xu and Zhang Team).** Lithium difluorophosphate (LiDFP) was shown to be effective as a dendrite-suppressing additive for standard $LiPF_6$/carbonate electrolyte by forming a compact and stable solid electrolyte interface on the lithium anode. With an optimal LiDFP content, Li||Li symmetric cells cycled stably for more than 500 and 200 h at 0.5 and 1.0 mA cm^{-2}, respectively, which is much longer than the control electrolyte without LiDFP additive.

- **Stanford University (Cui Team).** Novel 3D electrodes were prepared using atomic layer deposition (ALD)-coated hollow carbon spheres (HCS). The thin ALD coating seals the micropores of HCS to keep the electrolyte from contacting lithium occupying the center; the liquid electrolyte only contacts the outer surface of ALD Al_2O_3/HCS. 500 cycles, over 3 months, was achieved without the initiation of fluctuations in the measured Coulombic efficiency.

- **Lawrence Berkeley National Laboratory (Chen Team).** X-ray absorption spectroscopy was used to reveal the chemical origin of cycling instability in a cation-disordered $Li_{1.3}Nb_{0.3}Mn_{0.4}O_2$ cathode.

- **Brookhaven National Laboratory (Yang and Bak Team).** Combined X-ray and neutron diffraction experiments were conducted to study the structure change associated with oxygen-related redox reactions. The investigation provided evidence for possible formation of O-O dimers in highly delithiated $LiCoO_2$.

- **Argonne National Laboratory (Srinivasan Group).** A mathematical model was developed to evaluate the precipitation process of lithium-sulfide during battery discharge. The model revealed that high C-rates can potentially lead to Li_2S accumulation on the active electrode surface in discharge-charge cycles. This occurs because the time needed for Li_2S film growth can be longer than that needed for Li_2S film removal.

Battery500 Consortium Team

Highlights from the Battery500 Consortium team are provided below:

- **Keystone Project 1 (Electrode Architectures).** University of California, San Diego, continued evaluation of thick electrodes fabricated by Maxwell Technology using a dry-electrode process. A study utilizing NMC-622 electrodes indicated that reducing electrode porosity improves electrochemical performance. Although the result goes against conventional wisdom, the team speculates that this may be due to a more compact electronic conductive network with reduced tortuosity in an electrode with lower porosity.

- **Keystone Project 3 (Cell Fabrication, Testing, and Diagnosis).** A calendar life study on Li-metal pouch cells containing NMC-811, showed little loss in performance over the course of more than six months.

We encourage you to follow our progress as we proceed. Our next report is expected to be available in December 2018.

Sincerely,

Tien Q. Duong

Tien Q. Duong
Manager, Advanced Battery Materials Research Program & Battery500 Consortium Program
Vehicle Technologies and Electrification Program
Energy Efficiency and Renewable Energy
U.S. Department of Energy

TASK 1 – Liquid/Polymer Solid-State Electrolytes

Summary and Highlights

The BMR Program goal is to develop long-life batteries superior to commercial Li-ion systems in terms of cost, vehicle range, and safety. The BMR Program addresses the fundamental problems of electrode chemical and mechanical instabilities that have slowed development of affordable, high performance, automotive batteries. The aim is to identify electrode/electrolyte materials that yield enhanced battery performance and lead to greater acceptance of electric vehicles (EVs). Currently, the U. S. Department of Energy (DOE) Vehicle Technologies Office (VTO) supports ten projects in the BMR Program under this Electrolytes Task. These projects can be categorized into three general topics:

- **Liquid.** The projects for liquid electrolyte aim to develop electrolyte formulations, based on fluoro-chemistries, to achieve significantly improved operating voltage, increased durability, and increased energy density of Li-ion batteries at a reasonable cost. Nonaqueous polyelectrolyte solutions with high Li^+ transference numbers will be developed to achieve high rate capabilities at room temperature. In addition, electrolytes with new polymer binders bearing a pentafluorophenyl group on the backbone will be designed, synthesized, and tested.
- **Polymer.** The targets of polymer electrolyte projects include inorganic/polymer and polymer/gel hybrid electrolytes that have flexibility, mechanical strength, thermal stability, high ionic conductivity, stable interfaces against lithium metal, and polysulfide-trapping capability enabling energy density Li-S batteries, with comparable cycle life.
- **Self-Forming & Self-Healing.** The self-forming, self-healing electrolyte projects are focused on developing and implementing Li-metal-based metal fluorite and metal iodide batteries, capable of energy densities > 400-500 Wh/kg and 1000 Wh/L.

Highlights

At the Daikin group, as the first step toward determining the elemental composition and thickness of cathode solid electrolyte interphase (SEI) layers, the team successfully used Auger electron spectroscopy (AES) depth profiling to calibrate known carbon film thicknesses. In addition, surface roughness and morphology were studied for pristine and cycled cathodes. They found that the cycled cathode has approximately 20% more surface along with more noticeable surface roughness.

The University of California (UC) at Berkeley group has completed transport measurements for polyelectrolyte solutions comprised of various molecular weight polymers. The higher molecular weight produces a higher viscosity solution, as the larger chains provide a greater number of entanglements that impede bulk fluid motion. Interestingly, it was found that the conductivity of each solution is approximately equivalent despite the differences in viscosity. They also found that the transference number is above 0.9 at all molecular weights, and that it increases as a function of molecular weight, demonstrating that adjusting the polymer molecular weight is a straightforward method to increase transference number without sacrificing conductivity.

At Argonne National Laboratory (ANL), the pentafluorinated perfluoropolyether–tetrafluorethylene (PFPE–TFE) and TFE perfluorobutyl ethylene (TFE-PFBE) compounds possessing strong electron-withdrawing fluorines on the benzene ring were synthesized. In addition, voltage profiles of the Li-S cell with TFE-PFPE and TFE-PFBE electrolytes were collected and analyzed.

The University of Maryland (UMD) group has continued to reduce thickness of the hybrid composite electrolyte to an average thickness of 11 microns. The electrochemical performance of symmetrical cell was evaluated by charge-discharge cycling. In addition, lithium plating/stripping performance at 3 mA/cm^2 was tested, which shows an overpotential around 1 V without shorting.

At the University of Washington (UW), the group has performed time-to-short-circuit experiments for their solvate ionogels. These results agree with their previous cyclic stripping/plating results. They also doped the self-healing polymer system PP-1 with the solvate ionic liquid (SIL), achieving a high doping concentration of 33 wt% Li(G_4)TFSI without phase separation, which shows complete self-healing ability at the facile temperature of 40°C when heated for 12 h. To improve the wetting of thick electrodes by the electrolyte, ionic functional groups are being investigated as a means to strongly attract the liquid ionic species. For proof-of-concept, they studied the differences between a neutral thiol surface and a charged sodium sulfonate surface.

The West Virginia University (WVU) group progressed on studying the interaction between the aluminum doped-$Li_{0.33}La_{0.56}TiO_3$ (LLTO) nanofibers and the polymer matrix. Plasticized cross-linked polymer was integrated with a silane-coated $Li_{6.4}La_3Al_{0.24}Zr_2O_{12}$ (LLAZO) nanofiber to achieve an ionic conductivity of 5.7×10^{-4} S cm^{-1} at room temperature. Electrochemical performance of Li|$LiFePO_4$ cells with the silane-coated LLAZO-incorporated cross-linked polymer composite electrolytes was also investigated, showing high rate capability.

The Stanford University group has prepared a number of polymer coatings with various chemical and mechanical properties to investigate the importance of these parameters to the quality of the electrodeposited lithium metal. They found that the polymer coatings increased the density of lithium nucleation, leading to more uniform electrode coverage, and that the shape or size of the lithium particles changed depending on the polymer coating.

The Lawrence Berkeley National Laboratory (LBNL) group has successfully characterized the transference number of hybrid organic-inorganic diblock copolymer electrolytes, and characterized the effect of salt on the diblock copolymer morphology in PEO-POSS(5-1.9) using small angle x-ray scattering.

At Stony Brook University (SBU), cell construction A for Li/I_2 batteries with or without silver iron is completed. The team found that the impedance of the silver-ion-containing cell was substantially lower than the cell without silver. The cells were examined *in situ* using energy dispersive X-ray diffraction (EDXRD).

At Rutgers University, the tam has commenced the systematic development and implementation stages of the self-formed battery of 12 V architecture, and successfully obtained a 12 V formation. They are beginning complete electrochemical performance analysis.

Task 1.1 – Advanced Lithium-Ion Battery Technology: High-Voltage Electrolyte (Joe Sunstrom, Ron Hendershot, and Alec Falzone, Daikin)

Project Objective. The project objective is to identify electrolyte formulations, based on fluoro-chemistries, that will allow significantly improved operating voltage, increased durability, and increased energy density of Li-ion batteries at a reasonable cost. The project seeks to understand the conditions under which the electrolyte degrades, the effect on battery performance, and solutions that can overcome current limitations of the electrolyte. Gassing in Li-ion batteries is one of the most common failure mechanisms and poses the greatest safety risk in consumer devices. This project aims to investigate gas composition as a function of cathode material, electrolyte formulation, and operating voltage, and proposes optimal cell compositions at decomposition voltages.

Project Impact. Developing an understanding of the operating conditions in which gasses form in Li-ion batteries enables the project to propose optimized cell compositions, which operate at higher voltages for a longer period. Different fluorinated electrolyte components and additives may suppress and/or eliminate gas generation at or above hypothesized decomposition voltages. To investigate these topics, it is imperative that the project utilize multiple approaches, including, but not limited to: cathode material, electrolyte composition, operating voltage, and cycle number.

Approach. The evolving composition of the electrolyte in the battery will be examined by various analytical instruments to study volatiles [gas chromatography – mass spectrometry (GC-MS)/thermal conductivity detector (TCD)], liquid [liquid chromatography MS (LC-MS)], and solid [time-of-flight secondary ion mass spectrometry (TOF-SIMS), thermogravimetric analysis MS (TGA-MS), X-ray photoelectron spectroscopy (XPS), and AES] electrolyte decomposition products during battery operation. In the first year, the team addressed the gas composition and kinetics for both hydrocarbon and fluorocarbon as a function of several charge/discharge conditions. In the second year, the project will transition into analysis of the solid-state electrolyte (SSE) decomposition components of its tested batteries to obtain valuable information about SEI layer formation and how it manifests change in both the anode (graphite) and cathode (LCO and NMC).

Out-Year Goals. Work will progress toward understanding how electrolyte formulation and cell operation affect SEI layer formation/properties. Specifically, measurements of thickness and elemental composition as a function of fluorinated electrolyte composition and voltage will be performed. Understanding the SEI layer and other solid-state components of Li-ion batteries will provide valuable information on the required surface properties for increased performance at high voltage.

Collaborations. The project has collaborated with Dr. Majid Beidaghi (Auburn University) for atomic force microscopy (AFM) measurements on the carbon and aluminum film standards.

Milestones

1. Film thickness versus time/voltage complete. (Milestone 2.1; In progress)
2. Film composition (elemental) versus time/voltage complete. (Milestone 2.2; In progress)

Progress Report

To determine the elemental composition and thickness of cathode SEI layers, a reproducible method had to be developed. The project's initial approach utilized AES depth profiling, which will be calibrated to known carbon film thicknesses. Figure 1 depicts the depth profiling of 500 Å and 1000 Å carbon film samples, in addition to the underlying aluminum layer that will serve as a spectroscopic reflector for additional experiments.

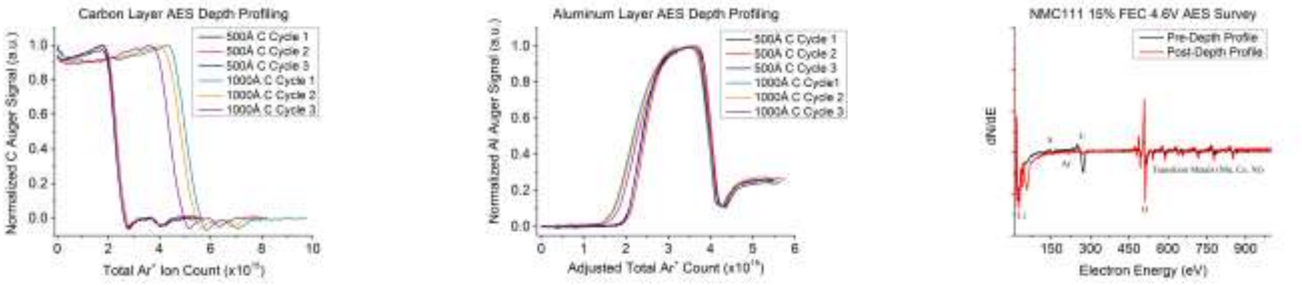

Figure 1. Carbon (left) and aluminum (middle) depth profiling using Auger electron spectroscopy with Ar(g) ionization. Elemental survey scan (right) of NMC-111 cathode (cycled at 4.6 V, 15% FEC v/v).

The project obtained three depth profile measurements on a wafer that had a 500 Å carbon film deposited on a 1000 Å aluminum layer. In addition, it measured a separate wafer with 1000 Å of carbon and 1000 Å of aluminum with an identical method. On average, the 1000 Å carbon film took twice as many sputter cycles to reach the underlying aluminum layer, confirming that the film thickness is approximately twice as thick. High-resolution scanning electron microscopy (SEM) imaging and film reflectometer measurements are being performed to quantitatively determine the thicknesses.

In addition to investigating the chemical properties of the SEI layer, physical changes of the bulk cathode material are also evident. Immediately following AES analysis of both cycled (4.6 V, 15% FEC, NMC-111) and uncycled (NMC-111) cathodes, the samples were mounted on a laser confocal microscope in order to observe physical changes to the surface following a cycle life test producing 3D contrast images of surface roughness. Figure 2 depicts both the optical images obtained in addition to 3D contrast images of surface roughness. The cycled cell has approximately 20% more surface as compared to the pristine cathode, along with more noticeable surface roughness.

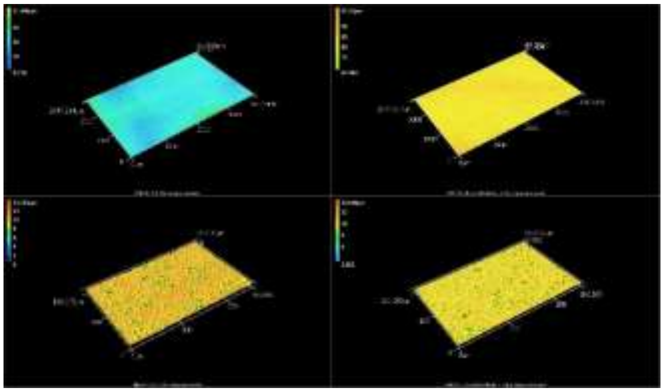

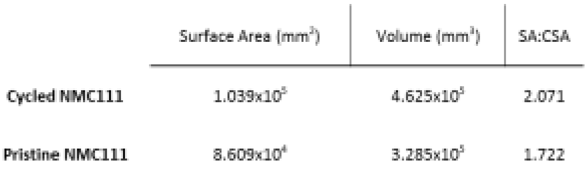

	Surface Area (mm^2)	Volume (mm^3)	SA:CSA
Cycled NMC111	1.039x10^5	4.625x10^5	2.071
Pristine NMC111	8.609x10^4	3.285x10^5	1.722

Figure 2. 3D images of a cycled (left) and uncycled (right) NMC-111 cathode at low (top) and high (bottom) magnifications. Calculated surface characteristics are tabulated for each cathode (right).

Several collaborative efforts have been and are being pursued, primarily revolving around surface analysis: Auburn University (sample prep) and University of Texas, Dallas (TOF-SIMS).

Patents/Publications/Presentations

Presentation

- DOE Annual Merit Review (AMR) Meeting, Washington, D. C. (June 18–21, 2018): “Daikin Advanced Lithium Ion Battery Technology – High Voltage Electrolyte”; Joe Sunstrom, Alec Falzone, and Ron Hendershot. Poster.

Task 1.2 – Multi-Functional, Self-Healing Polyelectrolyte Gels for Long-Cycle-Life, High-Capacity Sulfur Cathodes in Lithium-Sulfur Batteries
(Alex Jen and Jihui Yang, University of Washington)

Project Objective. The project objective is to develop self-healing and polysulfide-trapping polyelectrolyte gels containing room-temperature ionic liquid (RTIL) for the Li-S battery system. The battery design will be able to achieve gravimetric and volumetric energy densities of ≥ 800 Wh/kg and ≥ 1000 Wh/L, respectively.

Project Impact. The Li-S battery system is currently hampered by poor capacity retention, primarily caused by dissolution of polysulfide reaction intermediates in typical organic electrolytes, as well as poor electrical contact between insulating sulfur and the conductive carbon matrix. This project aims to produce a high-capacity, long-cycle-life Li-S battery system by using rational molecular design strategies to address each capacity loss mechanism directly. A long-cycle-life Li-S battery system with the capability of doubling Li-ion energy density would enable production of lighter, longer range EVs at a cost that is affordable to the average U. S. household.

Approach. The team will develop Li-S coin cells that utilize self-healing, interpenetrated ionomer gel electrolytes in both the cathode and separator. The team will synthesize necessary starting materials and fabricate components of these gels while testing their relevant electrochemical and mechanical properties. All components will be combined into interpenetrating structures, which will be tested both alone and in cell configurations. Device performance data will be collected and used to further optimize designs of both material and cell, culminating in an optimized Li-S battery design capable of doubling the energy density of traditional Li-ion batteries. During the first year, the team is focusing on (1) synthesis of a variety of precursors for gel electrolytes, (2) fabrication and testing of both baseline materials and novel materials made from these precursors, and (3) iterative validation and improvement of design principles through both materials and device testing.

Out-Year Goals. Work will progress toward developing structure-property relationships for the self-healing, interpenetrated gel ionomer electrolyte and its individual components, as well as successful incorporation of such an electrolyte into a working Li-S cell. The team plans to demonstrate significant improvements in both capacity and retention when using the project's novel materials, as compared to state-of-the-art baseline systems.

Collaborations. This project funds work at the UW. Dr. Alex Jen, principal investigator (PI), focuses on design, synthesis, and testing of novel materials, as well as device-based verification of design principles. Dr. Jihui Yang (co-PI) focuses on optimization of device fabrication and testing, as well as investigation of failure mechanisms in devices using novel materials. Pacific Northwest National Laboratory (PNNL) facilities will be used for detailed study of device operation.

Milestones

1. Select a particular self-healing gel formulation (set of organic starting materials) for continued study based on electrochemical and mechanical properties. (Q2, FY 2018)
2. Provide detailed cell performance data for concept cells containing currently-best materials designs. (Q4, FY 2018)

Progress Report

Multifunctional Ionomer Gels. Several additional tests were performed on the five established solvate ionogel formulas (SIGs 1-5) to enhance the team's understanding of the system. Time-to-short-circuit (T_{sc}) experiments were performed at 0.1 mA/cm^2 on Li|Li symmetric cells containing 0.25-mm-thick gel films as separators and compared to neat Li(G4)TFSI in a glass fiber separator (0.125-mm thick). The results are summarized in Table 1. The project notes that formulas containing longer-chain P_{3500} uniformly resist short-circuiting for longer than SIG 1 or Li(G4)TFSI alone, and that SIG 3, being less-crosslinked due to lower P_{3500} content, displays a shorter T_{sc} value than SIGs 2, 4, and 5, which last outstandingly long. SIG 4, despite also being less-crosslinked, contains a higher concentration of TFSI$^-$, which may have contributed to its longer lifetime than SIG 3. These results agree with the previous cyclic stripping/plating results for SIGs 2 and 5 (no short circuiting after 100 cycles/600 hours), and also suggest a complex relationship between conductivity, lithium transference number, electrolyte chemistry (that is, mobile anion concentration), mechanical properties of the gel network, and lithium dendrite resistance. Also, the team has found that Li(G4)TFSI, along with ionogel precursor solution, is able to wet the pores of a Celgard 2500 polypropylene (PP) separator. This stands in stark contrast to other ionic liquid electrolytes based on TFSI$^-$/FSI$^-$, which require much thicker glass fiber separators. The team has successfully cured a solution of SIG 1 that had been wetted into Celgard to form a thin (~ 30 µm) composite separator (Figure 3), which the team hopes will retain the favorable aspects of the ionogel, but in a much thinner, lighter, and more mechanically stable form. This composite separator is being tested.

Table 1. Composition and resulting time-to-short-circuit data for solvate ionogel formulations 1-5 in comparison to neat Li(G4)TFSI.

Formula	Composition [% volume added]						T_{sc} [hr]
	P_{750}	P_{3500}	TEGMA	PyrTFSIMA	Li(G4)TFSI	1,4-dioxane	
Li(G4)TFSI	0%	0%	0%	0%	100%	0%	10.6
SIG 1	20%	0%	0%	0%	80%	0%	10.8
SIG 2	0%	20%	0%	0%	80%	0%	113.9
SIG 3	0%	10%	10%	0%	80%	0%	25.0
SIG 4	0%	10%	0%	10%	80%	0%	99.3
SIG 5	0%	20%	0%	0%	66.6%	13.3%	118.3

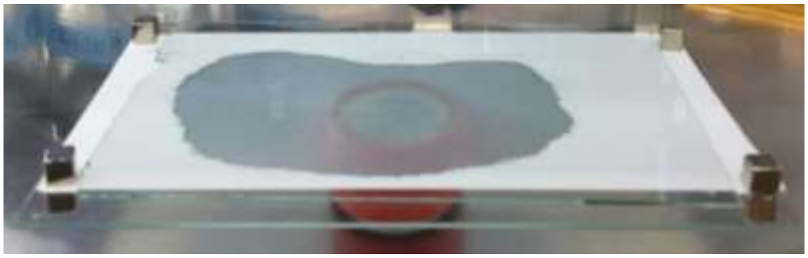

Figure 3. Photo of solvate ionogel 1 (SIG 1) formula cured into film of Celgard 2500.

Self-Healing Materials. As reported, the project's self-healing polymer system (PP-1) can achieve high ionic conductivity (~ 1x10^{-6} S/cm) when doped with LiTFSI. This conductivity was achieved at an ethylene oxide (EO) to Li$^+$ molar ratio of 20:1 [EO]:[Li$^+$] at 50°C. Recently, to further improve the ionic conductivity and test its compatibility with Li(G4)TFSI, the team doped PP-1 with the SIL, achieving a high doping concentration of 33 wt% Li(G4)TFSI without phase separation, which it is postulated is due to the polarity of the PP-1 EO units. This high doping concentration improved the ionic conductivity by an order of magnitude, to 1.01x10^{-5} S/cm at room temperature. In addition to measuring the ionic conductivity of the project's doped films, the team studied the mechanical properties with both additives, as reported in Figure 4. Here, the team found plasticization upon swelling with Li(G4)TFSI,

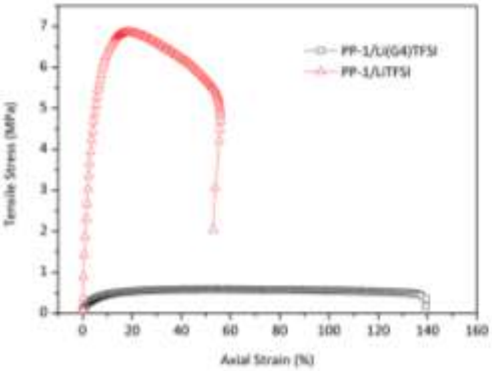

Figure 4. Tensile stress-strain tests of PP-1/LiTFSI and PP-1/Li(G4)TFSI.

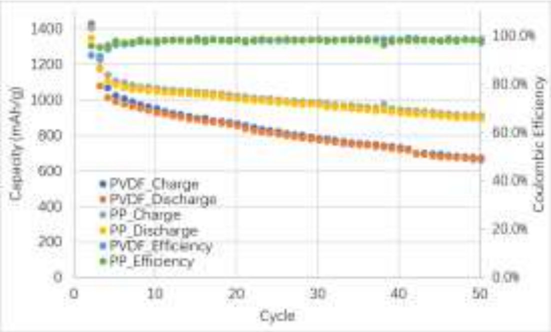

Figure 5. Cycling performance of sulfur cathodes with polypropylene and polyvinylidene fluoride as binder.

in contrast to doping LiTFSI alone into the network, which stiffens it due to the EO-Li^+ interactions. The lack of such interactions when Li^+ is contained as a SIL would also support the increased conductivity, as the ionic species should be more mobile. Furthermore, the PP-1/Li(G4)TFSI system shows complete self-healing ability at the facile temperature of 40°C when heated for 12 hours. Finally, the team measured the effect of the PP [with a naphthalene diimide:pyrene (NDI:Py) molar ratio of 3:1] system in Li-S coin cells. Cells were configured with Li-metal anodes, Celgard separators, dioxolane:dimethoxyethane (DOL:DME) based organic electrolyte, and C/S composite cathodes. The polymer binders used (that is, PP and polyvinylidene fluoride, or PVDF, as a control), made up 20 wt% of the cathode materials. The cells fabricated with the PP binder show stable cycling behavior, high Coulombic efficiency (CE > 98%), and an improved capacity retention over the PVDF-based counterparts, as presented in Figure 5. Presumably, at this low sulfur loading (around 1.1 mg/cm^2), the increase in capacity retention is due to the ability of polar naphthalene diisocyanate (NDI) and EO units in the PP binder system to trap solvated polysulfide species. However, the role of the polysulfide trapping and self-healing properties of the PP system in cell performance is being investigated.

Table 2. Atomic compositions collected by X-ray photoelectron spectroscopy of pristine, thiol, and sodium sulfate modified samples.

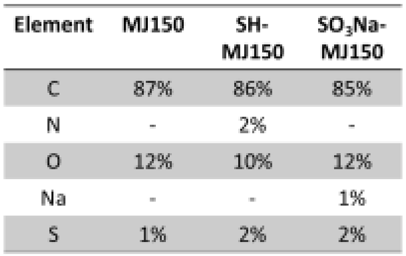

Element	MJ150	SH-MJ150	SO_3Na-MJ150
C	87%	86%	85%
N	-	2%	-
O	12%	10%	12%
Na	-	-	1%
S	1%	2%	2%

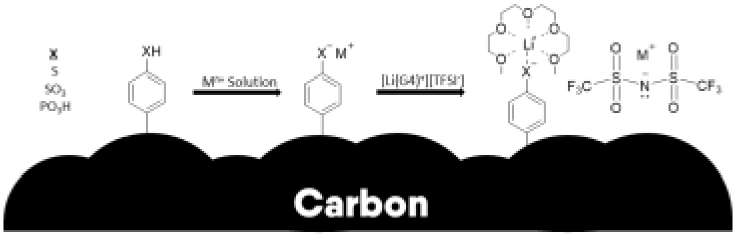

Figure 6. Schematic description of the formation of an ionic surface group, and its interaction with a solvate ionic liquid electrolyte.

Mesoporous Carbon Functionalization. Further efforts were devoted to improving the wetting of thick electrodes by the electrolyte. As the project's system focuses on using SIL electrolytes, ionic functional groups are being investigated as a means to strongly attract the liquid ionic species, as depicted in Figure 6. For proof-of-concept, the team compared the differences between a neutral thiol surface and a charged sodium sulfonate surface. The chemical composition of these surfaces was confirmed by XPS, and is reported in Table 2. The ratio of sulfur to sodium in the SO_3Na-MJ150 samples shows a 1:1 ratio of S:Na, implying that all sulfate groups are coordinated to a sodium counter-ion (after correcting for the 1% sulfur found even in pristine samples). With an ionic surface confirmed, the difference in wetting will be determined by contact angle measurements with the Li(G4)TFSI electrolyte on various surfaces, including both functionalized graphite foils and mesoporous C/S composites. These measurements are being conducted.

Patents/Publications/Presentations

Publications

- Qin, J., F. Lin, D. Hubble, Y. Wang, Y. Li, I. A. Murphy, S.-H. Jang, J. Yang, and A. K.-Y. Jen. "Tuning Self-Healing Properties of Stiff, Ion-Conductive Polymers." Submitted to *Advanced Functional Materials*.
- Li, Y.,* I. A. Murphy,* Y. Chen, F. Lin, X. Wang, S. Wang, D. Hubble, S.-H. Jang, K. T. Mueller, C. Wang, A. K.-Y. Jen, and J. Yang (*co-first author). "Surface Functionalization of Mesoporous Carbon for Polysulfide Trapping in Lithium Sulfur Batteries." Submitted to *Advanced Energy Materials*.
- Hubble, D., J. Qin, F. Lin, I. A. Murphy, S.-H. Jang, J. Yang, and A. K.-Y. Jen. "Rational Design of High-Conductivity Lithium Solvate Ionogels Using a Poly(Ethylene Glycol) Dimethacrylate Matrix." In preparation.

Presentations

- 233rd Electrochemical Society (ECS) Meeting, Seattle, Washington (May 2018): "Tuning Self-Healing Property of Stiff Supramolecular Polymer for Flexible Electronics"; J. Qin, F. Lin, Y. Wang, D. Hubble, Y. Li, S.-H. Jang, J. Yang, and A. K.-Y. Jen.
- 233rd ECS Meeting, Seattle, Washington (May 2018): "Rationally-Designed Solvate Ionogel Electrolytes for Improved Lithium-Sulfur Battery Performance"; D. Hubble, J. Qin, F. Lin, I. A. Murphy, Y. Li, J. Yang, and A. K.-Y. Jen. Poster.
- 233rd ECS Meeting, Seattle, Washington (May 2018): "Tunable Surface Modification of Mesoporous Carbon Nanoparticles for Polysulfide Trapping in Lithium-Sulfur Batteries"; I. A. Murphy, Y. Li, S.-H. Jang, J. Yang, and A. K.-Y. Jen. Poster.

Task 1.3 – Development of Ion-Conducting Inorganic Nanofibers and Polymers (Nianqiang (Nick) Wu, West Virginia University; Xiangwu Zhang, North Carolina State University)

Project Objective. The project objective is to develop SSEs based on the highly-conductive inorganic nanofibrous network in the polymer matrix for lithium batteries.

Project Impact. The research team will conduct research and development (R&D) on solid-state inorganic nanofiber-polymer composite electrolytes that will not only provide higher ionic conductivity, improved mechanical strength, and better stability than the polyethylene oxide (PEO) polymer electrolyte, but also exhibit better mechanical integrity, easier incorporation, and better compatibility with the Li-metal anode than the planar ceramic membrane counterparts. The proposed inorganic nanofiber-polymer composite electrolytes will enable practical use of high-energy-density, high-power-density Li-metal batteries, and Li-S batteries.

Approach. Integration of the highly Li^+-conductive inorganic nanofiber network into the polymer matrix not only provides the continuous Li^+ transport channels, but also kinetically inhibits crystallization from the amorphous state of polymer electrolyte. The inorganic nanofibers will be fabricated with an electrospinning technique; the ionic conductivity of inorganic nanofibers will be improved by chemical substitution or doping. Highly ionic-conductive polymers will be developed by cross-linking and/or creation of a block-copolymer structure. The composition and microstructure of the composite electrolyte will be designed to suppress the Li-dendrite formation.

Out-Year Goals. Work will progress toward synthesis of the inorganic nanofibers and the polymer matrix. The goal is to find the optimal synthetic route to achieve the desirable conductivity.

Collaborations. This project funds work at WVU and North Carolina State University (NCSU). Dr. Nianqiang (Nick) Wu at WVU serves as PI, and Dr. Xiangwu Zhang at NCSU acts as co-PI. Peng Zheng and Xuefei Gao (Ph.D. student at WVU), Hui Yang (Postdoctoral Fellow at WVU), Botong Liu (Ph.D. student at WVU), Chaoyi Yan (Ph.D. student at NCSU), and Mahmut Dirican (Postdoctoral Fellow at NCSU) contributed to the project.

Milestones

1. Synthesize the inorganic nanofiber-polymer composite electrolytes by *in situ* polymerization of polymer on the surface of inorganic nanofibers – Subtask 2.1. (Q4, FY 2018; Completed)
2. Characterize the microstructure of composite electrolytes, and study the nanofiber-polymer interface – Subtask 2.2. (Q4, FY 2018; 70% Complete)
3. Measure the temperature-dependent ionic conductivity of composite electrolytes, the transference number, and the electrochemical stability window – Subtask 2.3. (Q3, FY 2018; Completed)
4. Measure the mechanical properties such as the Young's modulus, the shear modulus, and the tensile and shear strengths – Subtask 2.4. (Q3, FY 2018; Completed)
5. Study the geometry (length, diameter) and surface functional groups of nanofibers on the overall performance of composite electrolytes – Subtask 2.5. (Q4, FY 2018; 70% Complete)
6. Study the effects of different types of polymer on the overall performance of composite electrolytes – Subtask 2.6. (Q4, FY 2018; 60% Complete)
7. Optimize the fiber-to-polymer ratio in composite electrolytes – Subtask 2.7. (Q4, FY 2018; 50% Complete)

Progress Report

This quarter, the team investigated the interaction between the aluminum-doped LLTO nanofibers and the polymer matrix. Plasticized cross-linked polymer was integrated with a silane-coated LLAZO nanofiber (s@LLAZO) to achieve an ionic conductivity of 5.7×10^{-4} S cm^{-1} at room temperature. Electrochemical performance of Li|$LiFePO_4$ cells with the silane-coated LLAZO-incorporated cross-linked polymer composite electrolytes was also investigated.

Task 2.1 - Development of Inorganic Nanofibers-Polymer Composites

2.1.1 Synergistic Coupling between Al-Doped $Li_{0.33}La_{0.557}TiO_3$ (LLATO) and PVDF–Hexafluoropropylene (HFP). Raman and Fourier transform infrared (FTIR) spectra were acquired to investigate the interaction between the LLATO nanofibers and the PVDF/LiTFSI polymer matrix, and the resulting change in the structure of the polymer electrolyte (Figure 7). The intensity of FTIR peaks corresponding to the α-phase PVDF-HFP at 795 cm^{-1}, 873 cm^{-1}, and 1426 cm^{-1} decreased after addition of LiTFSI; the intensity of these peaks diminished with an increase in the LLATO content in the composite electrolyte. This indicated the deprotonation of CH_2. CF_2 stretching vibration mode at 1200 cm^{-1} decreased dramatically, suggesting the dehydrofluorination of PVDF-HFP chains. This implied the interactions between the lithium salt and the CF_2 groups in the polymer molecular chains. The FTIR results suggested the similar reaction mechanism. A new peak appeared at 1510 cm^{-1}, corresponding to the C=C stretching vibration modes of polyenes, suggesting the dehydrofluorination of PVDF-HFP chains. Also, the peak at 2980 cm^{-1} attributed to the CH_2 bending vibration mode almost disappeared after adding the LLATO nanofibers, indicating the deprotonation of CH_2. These changes in the chemical structure were in agreement with those of PVDF after alkaline treatment, which means that the LLATO addition is likely to create an alkaline-like condition for PVDF, leading to partial dehydrofluorination of PVDF.

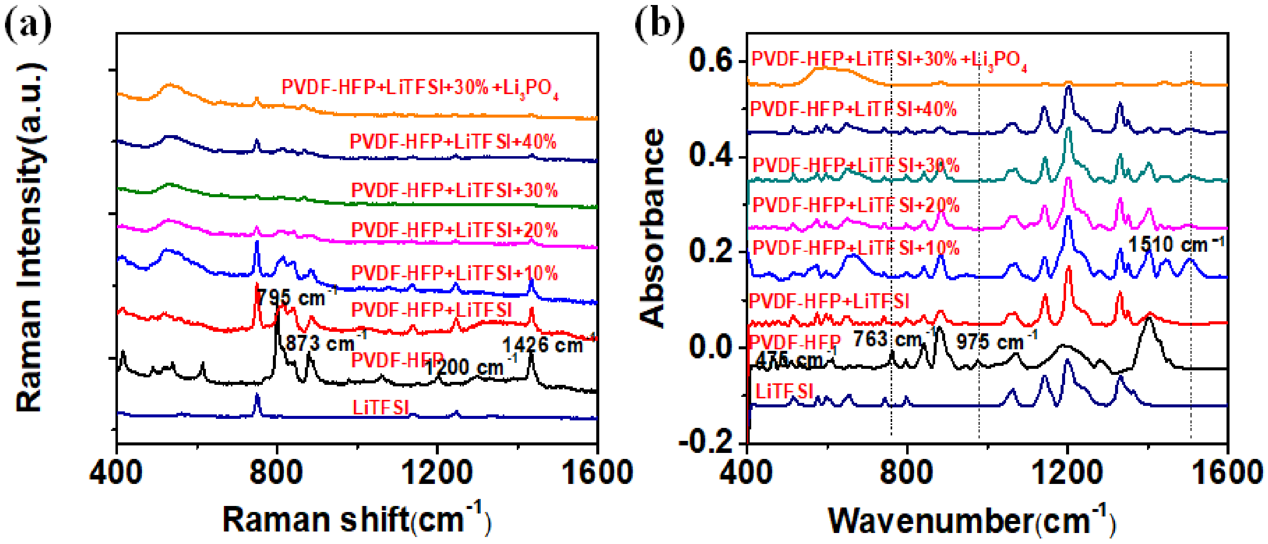

Figure 7. (a) Raman spectra and (b) Fourier transform infrared spectra of pure polyvinylidene fluoride (PVDF), PVDF-hexafluoropropylene (HFP)/LiTFSI, and PVDF-HFP/LiTFSI /$Li_{0.33}La_{0.557}TiO_3$ (LLATO) nanofiber-based membrane.

2.1.2 Silane-Coated LLAZO-Incorporated Cross-Linked Polymer Composite Electrolytes. The plasticized cross-linked polymer was integrated with the LLAZO nanofibers to improve the ionic conductivity. The prepolymer solution was composed of 60 wt% poly(ethylene glycol) diacylate (PEGDA) as monomer and 40 wt% poly(ethylene glycol) dimethyl ether (PEG-DME) as the plastizer. PEGDA contained dual acrylate (DA) groups, the resultant plasticized cross-linked polymer (PCLP) is denoted as PCLP-DA. LiTFSI was added with a controlled [EO]/[Li^+] ratio of 12:1. The composite electrolytes were then fabricated with 70 wt% s@LLAZO nanofibers and 30 wt% PCLP-DA polymer. The DA groups in PEGDA increased the degree of cross linking, which supported connections between nanofibers. The as-prepared composite solid electrolytes are denoted as s@LLAZO-PCLP-DA-1, 2, 3, and 4, respectively, based on different silane coating thicknesses achieved by 3, 6, 12, and 24 h treatment. The s@LLAZO-PCLP-DA, s@LLAZO-PCLP-DA-1, s@LLAZO-PCLP-DA-2, s@LLAZO-PCLP-DA-3, and s@LLAZO-PCLP-DA-4 demonstrated ionic conductivities of 2.2×10^{-4}, 2.8×10^{-4}, 5.7×10^{-4}, 5.4×10^{-4}, and 5.1×10^{-4} S cm^{-1}, respectively, indicating the reduced interfacial resistance between the PCLP-DA polymer and the nanofibers.

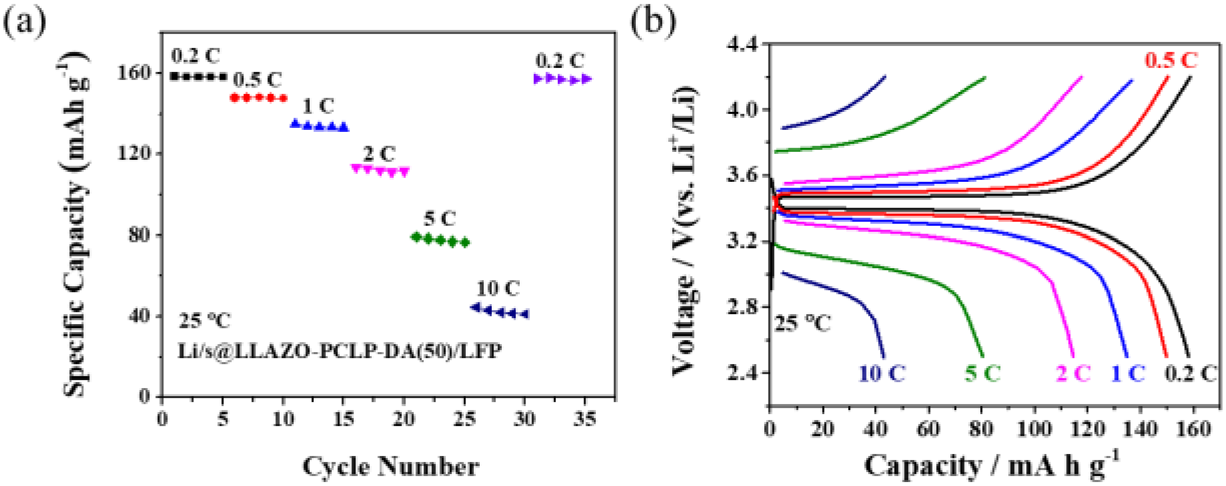

Figure 8. (a) Rate capability (0.2-10 C) and (b) charge-discharge profiles (at different C rates) of all-solid-state Li|s@LLAZO-PCLP-DA(50)|LFP cell operated at 25°C.

The electrochemical performance of Li|$LiFePO_4$ cells with silane-coated LLAZO-incorporated cross-linked polymer composite electrolytes was investigated. The Li|$LiFePO_4$ cells assembled with different composite solid electrolytes were galvanostatically charged and discharged at 25°C between 2.5 and 4.2 V at a current density of 85 mA g^{-1} (that is, 0.5 C-rate). Among all three cells tested, the cell assembled with s@LLAZO-PCLP-DA(50) showed the optimum cycling performance, with relatively high capacity of 147 mAh g^{-1} and relatively high capacity retention of 95% after 100 cycles.

The all-solid-state Li|s@LLAZO-PCLP-DA(50)|$LiFePO_4$ cells also showed high rate capability, which is shown in Figure 8a. The discharge capacities of 158, 147, 135, 113,78, and 44 mAh g^{-1} were obtained at the varied C rates of 0.2, 0.5, 1, 2, 5, and 10, respectively. After applying cycles at higher current densities, the discharge capacity increased up to 158 mAh g^{-1} when the current density reduced back to 0.05 C. Figure 8b shows the typical charge-discharge curves of the all-solid-state Li|s@LLAZO-PCLP-DA(50)|$LiFePO_4$ cells at different C rates. Stable charge and discharge plateaus of all-solid-state cells were consistent with those of conventional liquid cells, indicating no mechanical failure and excellent stability at high C rates.

Patents/Publications/Presentations

The project did not have any patents, publications, or presentations to report this quarter.

Task 1.4 – High Conductivity and Flexible Hybrid Solid-State Electrolyte (Eric Wachsman, Liangbing Hu, and Yifei Mo, University of Maryland)

Project Objective. The project objective is to develop flexible hybrid electrolyte with garnet nanofibers to achieve the following: (1) flexible, with greater mechanical strength (~ 10 MPa) and thermal stability than polymer electrolytes; (2) high room-temperature ionic conductivity, ~ 0.5 mS/cm; (3) stable interface with lithium metal and effective blocking of lithium dendrites at current densities up to 3 mA/cm^2; and (4) battery performance with Li-S chemistry with an energy density of ≥ 450 Wh/kg (and ≥ 1000 Wh/L) and maintaining ≥ 80% of capacity up to 500 cycles.

Project Impact. Instability and/or high resistance at the interface of lithium metal with various solid electrolytes limit the use of the metallic anode for batteries with high energy density, such as Li-air and Li-S batteries. The critical impact of this endeavor will be focused on developing a new type of SSE that is highly conductive, highly flexible, and electrochemically stable. The new SSE will enable Li-metal anodes with excellent interfacial impedance and blocking of lithium dendrite formation.

Approach. The project will synthesize garnet nanofibers, fill the porous region with polymer electrolyte, and characterize the flexible hybrid membrane properties. The flexible hybrid SSE microstructure will be determined using focused ion beam (FIB)/SEM and integrated with electrochemical methods to investigate the properties and stability with Li-metal anode.

Out-Year Goals. The project will develop a fundamental understanding of the mechanism of Li-ionic diffusion in garnet nanofibers and their mechanical properties, as well as these properties for hybrid garnet-fiber/polymer hybrids. Work will progress toward study of the electrode assembly during electrochemical cycling of the anode.

Collaborations. This project funds work at UMD, College Park. Dr. Eric D. Wachsman (PI) will focus on optimizing the garnet network to achieve high ionic conductivity and flexibility using FIB/SEM and electrochemical impedance spectroscopy (EIS) characterization. Dr. Liangbing Hu (co-PI) focuses on synthesis of the hybrid electrolyte and test for Li-metal anode with the hybrid electrolyte. Dr. Yifei Mo (co-PI) will lead efforts on computational modeling of the garnet nanofiber hybrid electrolytes for fundamental mechanistic understanding.

Milestones

1. Fully characterize electrochemical, mechanical, and thermal properties of hybrid SSE. (Q1, FY 2018; Completed December 2017)

2. Fabricate hybrid SSE with 20-µm thickness and understand the Li-hybrid SSE interface through Li-SSE-Li symmetric cells. (Q2, FY 2018; Completed March 2018)

3. Understand lithium stripping and plating in thin SSE at a current density of 3 mA/cm^2 without shorting. (Q3, FY 2018; Completed June 2018)

4. *Go/No-Go Decision*: No lithium dendrites at 3 mA/cm^2 for 500 cycles. (Q4, FY 2018; Initiated June 2018)

Progress Report

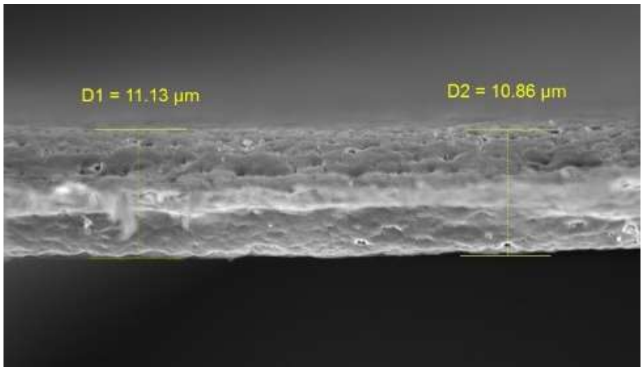

Figure 9. Hybrid composite electrolyte with the thickness < 20 µm.

This quarter, the team continued to reduce thickness of the hybrid composite electrolyte. They were able to fabricate very thin hybrid composite electrolyte. Figure 9 shows the SEM image of the electrolyte with an average thickness of 11 microns. The electrolyte appears to be homogenous, dense, and flexible.

Using a thin hybrid composite electrolyte, the team assembled a symmetrical cell for electrochemical characterization. The symmetrical cell was fabricated by pressing two pieces of lithium metal on both sides of the electrolyte by hydraulic crimping. The cell was analyzed by solatron 1260 and 1287. The initial impedance of the cell was measured from 10^7 to 10 Hz with an AC amplitude of 100 mV at room temperature. Two arcs are observed for the cell as shown in Figure 10. The first suppressed arc at high-frequency range is from the resistance of electrolyte. The second arc at low-frequency range originated from the interface between lithium metal and electrolyte. As the team has seen, the interface resistance is higher than that from the electrolyte. The high interfacial resistance can be addressed by cleaning the surface impurity of the lithium metal in the next quarter.

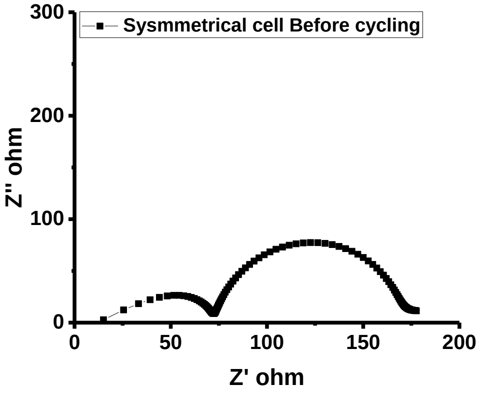

Figure 10. Electrochemical impedance spectrum of the Li/electrolyte/Li symmetric cell at room temperature.

The electrochemical performance of the cell was evaluated by charge-discharge cycling. Figure 11 shows the preliminary cycling results. The voltage profiles of the cell show stable performance at different current densities of 0.1 mA/cm^2 and 0.5 mA/cm^2. The resistance calculated from the cycling matched well the AC impedance. The team further tested the lithium plating/stripping performance at 3 mA/cm^2 in Figure 11. The symmetric Li/electrolyte/Li cell shows an overpotential around 1 V without shorting. The cycling performance at 3 mA/cm^2 will be further demonstrated next quarter.

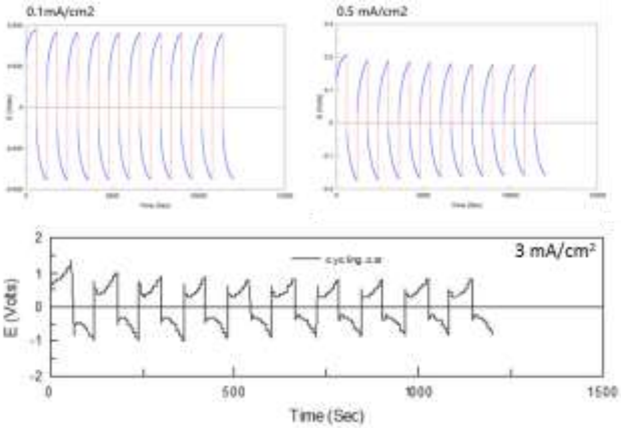

Figure 11. Initial symmetrical cell cycled at 0.1mA/cm^2, 0.5 mA/cm^2, and 3 mA/cm^2.

Patents/Publications/Presentations

The project did not have any patents, publications, or presentations to report this quarter.

Task 1.5 – Self-Forming Thin Interphases and Electrodes Enabling 3D Structured High-Energy-Density Batteries
(Glenn Amatucci, Rutgers University)

Project Objective. The project objective is to develop and implement a novel *in situ* formed Li-metal-based metal fluoride battery that will enable packaged 10-mAh batteries of energy densities > 1000 Wh/L and > 400 Wh/kg at 12 V.

Impact. Successful realization of 3D batteries formed *in situ* with a practical approach to large-scale fabrication would address some of the DOE EV performance goals, including: (1) areal capacity increase, (2) improved rates, and (3) designs to enable high-voltage unit cells.

Approach. The project is divided into two main tasks that focus on the advance of the self-forming chemistry concurrent to the cell design and fabrication. The self-forming chemistry task is comprised of three subtasks encompassing the negative and positive reactive current collectors, and the bi-ion glass conductor. The cell design and fabrication target the development and integration of the bipolar configuration to achieve the 12-V single cell goal.

Out-Year Goals. Work will continue toward improving reactive current collectors and cell design to optimize electrochemical performance of the cell stack in terms of energy density both gravimetric and volumetric as well as capacity retention upon cycling. A secondary focus will be implementation of bipolar design within the cell structure.

Collaborations. All project tasks will be performed at Rutgers University.

Milestones

1. Establish negative reactive current collector compositions that enable high efficiency of lithium plating and stripping in excess of 90% during the *in situ* formation step and > 95% during subsequent cycles. (Q2, FY 2018; Completed)
2. Establish optimal type and composition of bi-ion conductors that achieve ionic conductivities in excess of $1\text{x}10^{-4}$ S/cm after *in situ* formation. (Q3, FY 2018; Completed)
3. Establish cell-stack design with 75% utilization of the positive reactive current collector and 12 V. (Q1, FY 2018; In progress)
4. *Go/No-Go Decision*: Achieve self-formed cell-stack of at least 750 Wh/L and 200 Wh/kg, and > 80% capacity retention after 20 cycles at a rate of C/10. Achieve an output voltage of 12 V.

Progress Report

Transport is a critical factor impacting all aspects of the *in situ* formed battery electrochemical performance, including the positive reactive current collector utilization, cell stack energy density, cycle life, and rate capability used as metrics in the project milestones. Transport limitations were addressed through a multi-prong approach that encompasses modifications of the cell architecture and hybridization of transport pathways, as well as fabrication of multicomponent nanolayered structure architectures of tunable conductivity type (ionic, electronic, mixed) and relative concentration within the bulk of the solid-state structure of the reactive positive current collector. Transport hybridization and nanolayered positive current collector compositions of mixed conductivity were found to improve performance.

Last quarter, the team also identified mechanical-stress-induced fracture and subsequent impact on transport as the limiting factor creating a barrier to reaching beyond current cycling capabilities. As such, this quarter focused on developing pathways to mitigate impact of stress/strain energy without negatively influencing cell electrochemical properties. Several avenues are being pursued to produce more uniform transformations during reactions, including modifications to cycling protocols, electrode design reorientation, and application of previously identified beneficial chemistry compositions. Herein, the project reports on modification to cycling protocols with investigation of both pulsing and intermediate slow formation and charging protocols. The most beneficial results came from a brief period of slow discharge after charge with incorporation of this into the charging process. It had been determined that this brief "priming" step after charge prior to discharge allows for a more uniform distribution in nucleation so that transformations during reactions are less likely to create areas highly concentrated in active component and leading to mechanical failure. These formation steps will be included in all testing protocols moving forward. In addition, efforts to optimize electrode design and chemistry compositions are in progress and are continually adjusted and implemented as the project advances.

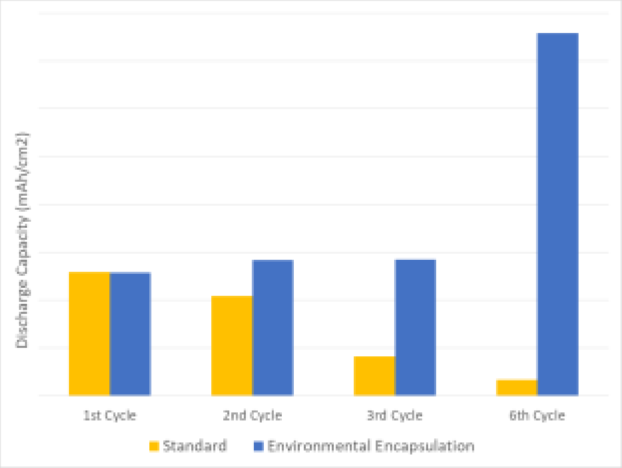

Figure 12. Comparison of discharge capacities for the 1st, 2nd, 3rd, and 6th cycles for a standard self-formed single cell versus an environmentally encapsulated self-formed single cell. Cells were submitted to a formation period over the first three cycles with a lower charge capacity cutoff that was increased upon subsequent cycling. Encapsulated cells responded with higher discharge capacity regardless of the charge capacity utilization.

Another key aspect investigated this quarter included the effect of the environment on electrochemical performance through cell encapsulation. To determine if cell exposure affected performance, several compositions were tested by encapsulating their chemistry and applying light pressure. A standard composition and its encapsulated homologue are compared in Figure 12. While both samples were submitted to a formation protocol in the first three cycles, with a lower controlled charge capacity cutoff than in subsequent cycles, the standard sample showed discharge capacity loss during the formation period and, ultimately, failure occurred rapidly. In contrast, encapsulation of chemistry seemed to improve reaction uniformity in the formation step, as demonstrated by good capacity retention followed by increased capacity output at a higher rate. Encapsulation is clearly beneficial and will be applied for future analysis and application in the self-formed 12-V architecture.

Finally, the project also began systematic development and implementation of the self-formed battery of 12-V architecture. Late this quarter, the team successfully obtained a 12-V formation and is now beginning complete electrochemical performance analysis. Initial results with the 12-V architecture were only able to reach an 8-V formation with application of the original self-forming battery design. However, with reengineering of the architecture, improvements were seen, and the former issues resulting in barriers to the goal were resolved, as demonstrated by the team's ability to achieve a 12-V cell.

Next quarter, the team will focus on achieving performance within the 12-V architecture, which exceeds that of the project's lower voltage benchmark cells. The cycling protocols and chemistry combinations will be optimized to achieve the remaining milestones.

Patents/Publications/Presentations

The project has no patents, publications, or presentations to report this quarter.

Task 1.6 – Dual Function Solid-State Battery with Self-Forming, Self-Healing Electrolyte and Separator

(Esther Takeuchi, Stony Brook University)

Project Objective. The project objective is to demonstrate a solid-state rechargeable battery based on a Li-metal anode and iodine cathode with a self-forming, self-healing electrolyte and separator with high gravimetric and volumetric energy density.

Project Impact. This program will enable demonstration of the proposed rechargeable battery with improved power capability, high energy density, and a self-forming, self-healing SSE/separator. Technical insight will be gained regarding improved conductivity of the solid lithium iodide (LiI) based electrolyte, power capability of the proposed system, the self-healing nature of the LiI layer, the nature of the electrode-electrolyte interfaces, and feasibility of the system to reach the DOE targets.

Approach. The proposed concept is a dual function rechargeable solid-state battery utilizing LiI combined with silver iodide (AgI) as the electrolyte, with lithium metal (and small quantities of silver metal) as the anode and iodine as the cathode with a self-forming, self-healing separator/electrolyte. The battery will be assembled in the discharged state where the anode and cathode will be created during the first formation (charge) step. Initially, silver ion (Ag^+) will diffuse toward the negative electrode and be reduced to silver metal (Ag^0), and iodine ion (I^-) will be oxidized to elemental iodine (I_2) at the cathode side. As the formation of the battery continues, lithium ion (Li^+) will form a Li-metal layer at the anode, with generation of iodine at the cathode. LiI will remain and serve as both the separator and electrolyte.

Out-Year Goals. This is a multiyear program where the effort is divided into three major tasks.

- Year 1 involves electrolyte preparation and characterization including preparation of SSEs and conductivity measurements.
- Year 2 will focus on cell construction and testing including both *in situ* and *ex situ* analysis.
- Year 3 will focus on cell characterization. Under the program, cycle life, efficiency, energy density, and the functional capacity of cells will be determined.

Collaborations. This project collaborates with Amy Marschilok and Kenneth Takeuchi of SBU.

Milestones

1. Prepare construction A cells with the three most conductive electrolytes from Subtask 2.1.0. (June 30, 2018; Completed)
2. *Go/No-Go Decision*: Formation of Li^0, Ag^0 at anode and iodine at cathode with charging. (September 30, 2018; Initiated)
3. Determine functional capacity and energy density of construction A cells. (December 31, 2018; Initiated)

Progress Report

Cell Construction A for Li/I_2 Batteries with or without Silver Ion. This quarter's milestone was assembly of cells with cell construction A using the conductive electrolytes identified earlier. Figure 13 shows the impedance of as-assembled cells using electrolyte including LiI:LiI(HPN)$_2$ with and without the inclusion of a silver-containing component. The impedance of the silver-ion-containing cell was substantially lower than the cell without silver. Several ratios were examined, and the trend was observed over multiple samples. Next quarter, silver-containing cells will be tested, and their functional electrochemistry will be determined and compared to cells with no silver-ion content.

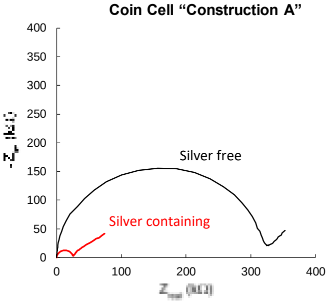

Figure 13. Addition of silver iodide in the composite solid electrolyte demonstrated reduced pre-charge AC impedance in coin cell construction A.

Figure 14. Schematic of energy dispersive X-ray diffraction experiment.

***In Situ* Investigation of Cell Construction A.** A series of cells with cell construction A using LiI:LiI(HPN)$_2$ was assembled. The cells were examined *in situ* using EDXRD, which can be used to investigate the structure of electrode materials as a function of spatial location inside the cells. Performed at high-energy synchrotron facilities, the technique uses a multi-wavelength "white beam" of X-rays. Use of EDXRD provides several advantages over angle resolved X-ray. First, the high-energy white beam is able to penetrate engineering materials, including steel, allowing for *in situ* diffraction measurements to be collected without the need for specially designed cells with X-ray windows. Second, as EDXRD operates at a fixed scattering angle, a goniometer is not needed, and full diffraction patterns can be collected quickly. Finally, the measurement collected with an automated sample stage having micron-scale positioning control enables spatial resolution of the diffraction phase(s) within the electrode. Figure 14 shows the experiment schematic.

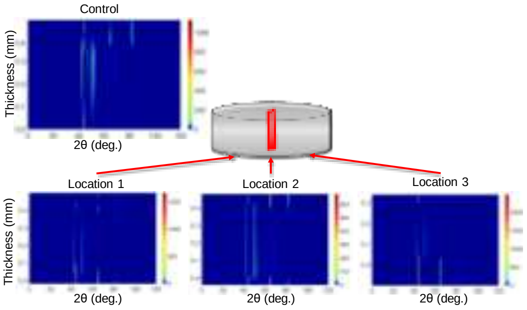

Figure 15. Intensity maps of as-assembled cell (top right) and three locations of charged cell.

Three types of cells were examined: as-assembled, charged, and cycled. Figure 15 shows the intensity maps of the major peaks of the LiI diffraction pattern. Figure 16 shows quantitative comparison of the peak intensities. The locational information obtained from these data indicates that the intensity profiles of the charged cell and the as-assembled cell differ. As the LiI is consumed during the charge process to form lithium and iodine, the results are consistent with the mechanism of cell formation. Further, results from the charged cell show that the distributions at the three locations probed for the charged cell are not identical, indicating that the charge process did not result in uniform consumption of the LiI present in the parent electrolyte. This provides insight for the next-generation cell design.

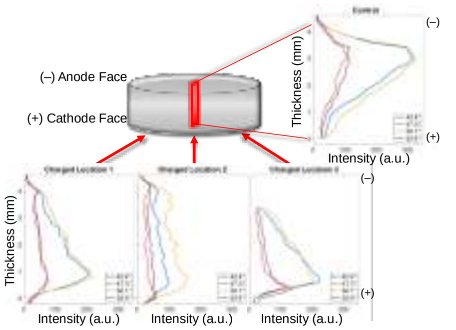

Figure 16. Quantitative profiles of as-assembled cell (top right) and three locations of charged cell.

Patents/Publications/Presentations

Publication

- Abraham, A., J. Huang, P. F. Smith, A. C. Marschilok, K. J. Takeuchi, and E. S. Takeuchi. "Demonstration of a Self-Forming Solid State Rechargeable Li/I_2 Battery." Accepted.

Presentations

- Program Officer Site Visit, Stony Brook University, Stony Brook, New York (June 14, 2018): "Dual Function Solid State Battery with Self-Forming Self-Healing Electrolyte and Separator"; E. Takeuchi, A. Marschilok, and K. Takeuchi.
- DOE AMR Meeting, Washington, D. C. (June 18–21, 2018): "Dual Function Solid State Battery with Self-Forming Self-Healing Electrolyte and Separator"; E. Takeuchi, A. Marschilok, and K. Takeuchi. Poster.

Task 1.7 – High-Conductivity, Low-Temperature Polymer Electrolytes for Lithium-Ion Batteries (Bryan D. McCloskey, University of California at Berkeley)

Project Objective. Design of electrolytes with enhanced transport properties compared to conventional liquid organic electrolytes is key to improving the rate at which a Li-ion battery can be discharged or charged. Ideally, electrolytes would allow high mobility for lithium ions and disallow mobility of inactive ions (for example, the counteranion of the Li^+). However, current liquid electrolyte compositions usually provide higher mobility for the counteranion than Li^+, which results in high concentration polarization that disallows fast charging, particularly in batteries that employ thick porous electrodes, as is necessary for EVs to provide high energy densities. The project objective is to develop a high Li^+ transference number (t_{Li}, the fraction of ionic current carried by Li^+ in an electrolyte of uniform composition) polymer-based electrolyte that, when used in a Li-ion battery, can support current rate capabilities sufficient for EV propulsion at room temperature.

Impact. Development of practical high t_{Li} polymer-based electrolytes for Li-ion batteries would enable safer Li-metal and graphitic anode cycling and thicker porous electrode designs, leading to improved specific and volumetric battery energy densities consistent with the EV Everywhere Grand Challenge. High-energy anode and cathode materials, such as lithium metal, silicon, and high-voltage layered or spinel structures, could be enabled by electrolytes with high t_{Li} and large operating voltage windows, such as those based on sulfones, as proposed here.

Approach. Lowering the operating temperature of polymer electrolytes has been cited as an important challenge to their viability as Li-ion battery electrolytes. The project will address this challenge by using Li^+ neutralized anionically charged polymers as salts in conventional liquid solvents. Using these so-called polyelectrolyte solutions, initial results indicate that the project can access t_{Li} values typical of single-ion conducting polymer electrolytes ($t_{Li} > 0.9$) and conductivity values (> 1 mS/cm at room temperature) that approach those of traditional battery electrolytes.

Out-Year Goals. The optimization of transport and stability properties of these polyelectrolyte systems, through understanding of appropriate polymer and solvent design, is the objective. The goal is to develop new polyelectrolyte compositions that provide superior transport properties (specifically, higher t_{Li} and conductivity) than conventional liquid electrolytes and enable use of high-energy electrode materials, such as lithium metal.

Collaborations. Collaborations on this project include Vince Battaglia (porous electrode preparation) and Kristin Persson (atomistic modeling) at LBNL.

Milestones

1. Complete COMSOL modeling to identify target transference number and conductivities for electrolytes that enable efficient fast charging (~ 3 C). (Q1, FY 2018; Completed October 2017)
2. Complete synthesis and physical characterization of polysulfone and PEO-based ionomers of various molecular weights. Progress measure: Publish a comprehensive article on understanding of design criteria of high transference number/high conductivity electrolytes. (Q2, FY 2018; Completed February 2018)
3. Complete transport measurements for polyelectrolyte solutions comprised of various molecular weight polymers. *Go/No-Go Decision*: Switch polymer chemistries if optimized polyelectrolyte solution transference number is less than 0.9 and conductivity at room temperature is less than 0.1 mS/cm. (Q3, FY 2018; Completed June 2018)
4. Complete polyelectrolyte solution cycling measurements using Li-metal electrodes to confirm that high transference number electrolytes suppress dendrite formation. (Q4, FY 2018; On schedule)

Progress Report

Nonaqueous polyelectrolyte solutions have been shown as promising candidates for high transference number, high-conductivity electrolytes.[1] Previously, the project investigated poly(allyl glycidyl ether)-based polyelectrolyte solutions, finding conductivity on the order of 0.1-1 mS/cm and transference number above 0.8.[2] While polyelectrolytes have been studied for many years, the effect of polymer molecular weight on the transport properties of the solution is not well known.

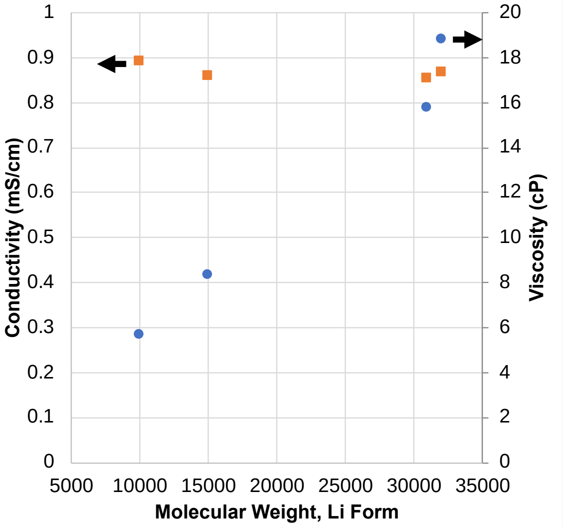

Figure 17. Conductivity and viscosity of Li$^+$-neutralized sulfonated polysulfones of various molecular weights dissolved in dimethyl sulfoxide. The Li$^+$ concentration in each case was 0.1 M.

Last quarter, several different molecular weight sulfonated polysulfone polymers were synthesized to investigate the effect of molecular weight on conductivity and transference number. Utilizing these polymers, the team characterized the complete transport properties of polyelectrolyte solutions as a function of the molecular weight of the polymer. Figure 17 displays the conductivity and viscosity for 0.1-M lithium solutions, as a function of molecular weight of the polymer. The higher molecular weight produces a higher viscosity solution, as the larger chains provide a greater number of entanglements that impede bulk fluid motion. Interestingly, the conductivity of each solution is approximately equivalent despite the differences in viscosity.

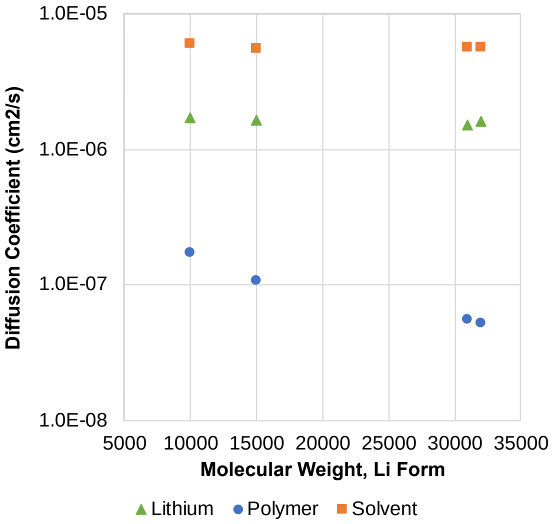

Figure 18. Diffusion coefficient of each species in 0.1-M Li$^+$ solutions of various molecular weight Li$^+$-neutralized sulfonated polysulfones in dimethyl sulfoxide as measured using pulse field gradient nuclear magnetic resonance.

To deconvolute the relative contribution of each species in solution on conductivity and viscosity, the team employed pulse field gradient nuclear magnetic resonance (PFG-NMR) to measure the diffusion coefficient of each species (that is, the solvent, Li$^+$, and polymer backbone). Figure 18 shows the diffusion coefficient of the solvent, dimethyl sulfoxide (DMSO-d6), lithium, and the polymer backbone. It is important to note that this technique does not distinguish between lithium species that are well-solvated and those that may exist as Li$^+$-sulfonate ion pairs, instead averaging the motion of both Li$^+$ species. Here it is apparent that the average Li$^+$ species and the solvent do not diffuse differently as a function of polymer molecular weight. Again, this result is somewhat surprising given the increased viscosity of the higher molecular weight solutions. This suggests that the local environment felt by each small molecule is relatively unperturbed by the long-range motion that is impeded by the polymer flow in a viscosity measurement. The polymer backbone diffusion coefficient does, however, decrease as a function of molecular weight, as would be expected given a larger radius of gyration with more repeat units.

Utilizing these diffusion coefficients, the team calculates the apparent transference number of the electrolyte as $t_+ = D_{Li}/(D_{Li} + D_{polymer})$. This approximation is not explicitly equivalent to the true electrochemical transference number unless each diffusion coefficient ideally corresponds to the electrophoretic mobility of each species. However, this transference number does approximate the relative motion of lithium to the anion in solution. As plotted in Figure 19, it is apparent that the transference number is above 0.9 at all molecular weights, and that it increases as a function of molecular weight. This is a result of the reduced diffusion of the bulkier polymer backbone at higher molecular weights. This clearly demonstrates that adjusting the polymer molecular weight is a straightforward method to increase transference number, without sacrificing conductivity. The data presented in Figures 17 and 19 satisfy the go/no-go decision point (a polyelectrolyte solution that has transference number > 0.9 and conductivity > 0.1 mS/cm).

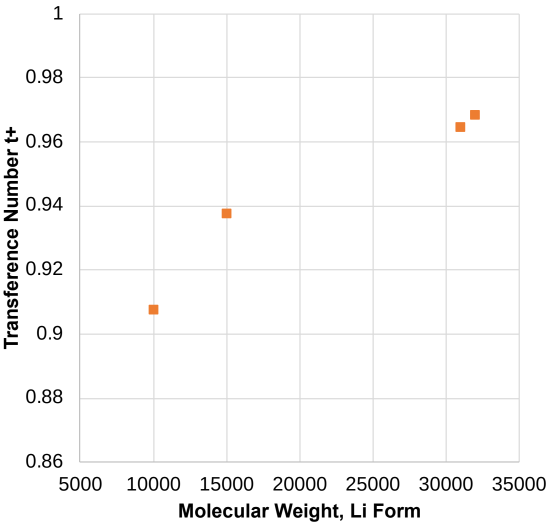

Figure 19. Li$^+$ transference number (t_+) of Li$^+$-neutralized sulfonated polysulfones of various molecular weights dissolved in dimethyl sulfoxide. The Li$^+$ concentration in each case was 0.1 M.

1. Diederichsen, K. M., E. J. McShane, and B. D. McCloskey. "Promising Routes to a High Li$^+$ Transference Number Electrolyte for Lithium-Ion Batteries." American Chemical Society (ACS) *Energy Letters* 2 (2017): 2563–2575. doi: 10.1021/acsenergylett.7b00792.
2. Buss, H. G., S. Y. Chan, N. A. Lynd, and B. D. McCloskey. "Nonaqueous Polyelectrolyte Solutions as Liquid Electrolytes with High Lithium-Ion Transference Number and Conductivity." ACS *Energy Letters* 2 (2017): 481–487. doi: 10.1021/acsenergylett.6b00724.

Patents/Publications/Presentations

The project has no patents, publications, or presentations to report this quarter.

Task 1.8 – Advanced Polymer Materials for Batteries (Zhenan Bao and Yi Cui, Stanford University)

Project Objective. This project will develop new polymer materials for batteries. The team will develop polymer coatings with specific mechanical properties that can accommodate the volume expansion and contraction of the Li-metal anode associated with deposition and stripping (charging and discharging).

Project Impact. The cycling stability and CE of Li-metal electrodes will be increased by implementation of a polymer-based protective layer that functions as an artificial SEI with desired properties. The improved performance will enable further development toward practical utilization of Li-metal anodes with higher cycling efficiency and less susceptibility to dendrite-based failure.

Approach. The project uses soft polymer coatings with dynamic crosslinking to give the resulting polymers liquid-like rheological properties and stretchable and self-healing properties. In previous work, the project has shown that such coatings resulted in uniform deposition/stripping of lithium metal and improved cycling stability of Li-metal electrodes. To understand the design rules for effective polymer coatings, the team chose a few representative polymers to systematically understand structure property relationships. Here, the team investigates the correction between surface energy of the polymer and exchange current for lithium deposition.

Out-Year Goals. Work will progress toward the correlation between dielectric constant and exchange current. These findings will enable further understanding and development of various polymer coatings for protecting Li-metal anodes.

Collaborations. There are no active collaborations this quarter.

Milestones

1. Explore the effects of various commercial polymers on lithium nucleation and interfacial kinetics. (Q1, FY 2018; Completed)
2. Develop polymer coating to mechanically suppress lithium dendrites and improve cycle life. (Q2–Q3, FY 2018; Completed)
3. Understand effects of polymer coating properties such as dielectric constant and surface energy, among others, on lithium electrochemistry and electrode performance. (Q3–Q4, FY 2018; In progress)

Progress Report

Selection of Polymers for Systematic Understanding. To develop a clear fundamental picture of the processes affecting Li-metal deposition, the team prepared a number of polymer coatings with various chemical and mechanical properties to investigate the importance of these parameters to the quality of the electrodeposited lithium metal. For this study, the team systematically chose several polymers previously used in battery applications. PEO is a common solid polymer electrolyte, and polyurethane (PU) and PVDF are common gel electrolytes. Additionally, PVDF and PVDF-HFP are also common binder materials for composite electrodes. Poly (dimethylsiloxane) (PDMS) was tested because it has been used as a coating to stabilize lithium metal. The team also modified the mechanical properties of its previously reported adaptive (self-healing) polymer (SHP) coating with chemical crosslinking to obtain a self-healing elastomer (SHE) with different mechanical properties but almost identical chemistry. The thermal and mechanical properties of the polymers were characterized in detail, and the following distinct groupings can be observed (Figure 20). PEO, PVDF, and PVDF-HFP are rigid, semi-crystalline solids exhibiting high initial modulus and plastic deformation after strain is applied. They are characterized by frequency-independent storage modulus and clear first-order phase transitions corresponding to the melting of the crystalline domains. The stress-strain curves show that these properties will give rise to tough, but deformable polymer coatings at room temperature. The SHP and PDMS coatings are highly adaptable to mechanical strain due to the viscoelastic nature of these two polymers. Both polymers have liquid-like mechanical properties at low frequencies with the loss modulus dominating over the storage modulus. While the SHP is a flowable viscoelastic material, the SHE is a covalently crosslinked elastic solid. Similarly, the PU used here is a soft elastomer with high stretchability and low glass transition temperature (T_g). These elastic coatings should be able to deform and potentially recover from applied strain, but these films will not have the adaptive qualities of the SHP and PDMS due to solid-like properties of both elastomers. Even at long time scales, the SHE and PU both behave as solids and will not significantly flow or adapt without external stimuli. Overall, PEO, PVDF, and PVDF-HFP have the mechanical properties of traditional thermoplastics, PU and SHE are soft elastomers, and PDMS and SHP are viscoelastic materials.

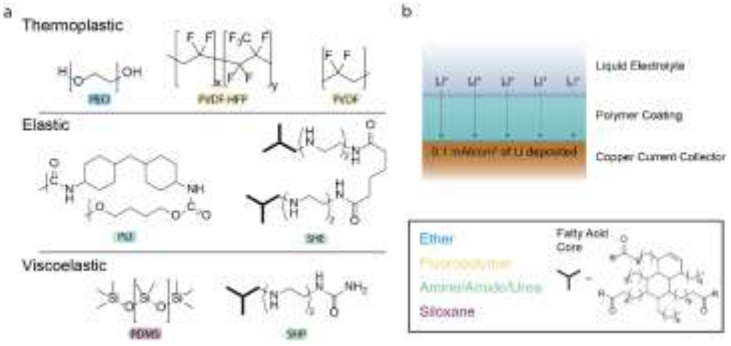

Figure 20. (a) Chemical structures of the polymer coatings used in this study. Coloring of the label corresponds to the chemical functionality of the polymer. (b) Diagram of the conditions used to study the initial stages of lithium metal growth under polymer.

Coating Chemistry and Lithium Morphology. The team compared the SHP and SHE coatings to understand the effects of polymer coating mechanics on lithium deposition. Both polymers have similar chemistry, but the SHP is a flowable viscoelastic material, while the SHE is a covalently crosslinked elastic solid. The high density of hydrogen bonding groups in the SHE still allows for self-healing to occur. The team observed that the overall uniformity of the lithium deposition was very poor for the SHE compared to the flowable SHP (Figure 21b/d), indicating that the mechanical properties and coating quality of a polymer film are important for uniform deposition. However, when closely examining the individual lithium deposits, the team noticed that both the SHP and SHE coatings grew lithium with nearly identical shapes (Figure 21c/e). This suggests that the chemical functionality of the polymer is a main factor dictating the local lithium morphology.

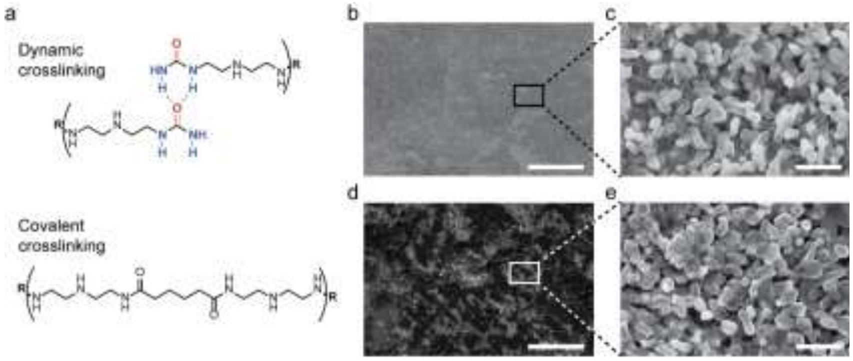

Figure 21. (a) Chemical structures of the dynamic crosslinking of the self-healing polymer and covalent crosslinking of the self-healing elastomer. (b-e) Scanning electron microscopy images of 0.1 mAh/cm^2 of lithium electrodeposited on polymer-coated copper. The electrodes are coated with (b-c) a supramolecular adaptive coating and (d-e) a covalently crosslinked self-healing elastomer with similar chemistry to the supramolecular coating. Scale bars are 50 μm for b/d, and 1 μm for c/e.

To further investigate the effects of the chemistry of the polymer coating, the team tested the other polymers described above. Every polymer coating tested was found to improve the coverage of initial lithium deposits on the electrode over that of uncoated copper, which showed many exposed regions of bare surface (Figure 22a). This suggests that the polymer coatings increased the density of lithium nucleation, leading to more uniform electrode coverage. However, this increased density of lithium particles is not correlated to increases in the overpotential measured for the deposition, as one would expect from classical nucleation theory.

Interestingly, the team also noticed that the shape or size of the lithium particles changed depending on the polymer coating. For example, SHP and PEO altered the lithium deposits to be very small in diameter (10^2 nm) and nearly filamentary or rod-like in shape (Figure 22b/d), while PVDF and PVDF-HFP changed the lithium particles to be much larger (10^3 nm) and globular (Figure 22c/f). Since there is no clear correlation of lithium deposit behavior with the modulus or visco-elasticity, it suggests that the polymer mechanical properties do not solely dictate lithium morphology and cannot fully predict the intricate chemistry of lithium growth dynamics. This is especially clear when comparing the PEO and PVDF polymer coatings. Even though these materials have similar modulus and stress-strain behavior, the size and shape of the lithium deposits differed drastically. These differences in particle size depend on both the nucleation and growth processes of the lithium metal, which are influenced by the specific coating chemistry and will be discussed in later sections. Ideally, lithium metal would be deposited as a dense, uniform film on the electrode to minimize the contact area with the electrolyte and the potential for forming dead lithium particles electronically separated from the electrode. Coatings that promote this type of growth and are electrochemically stable over long-term battery cycling should provide the best performance.

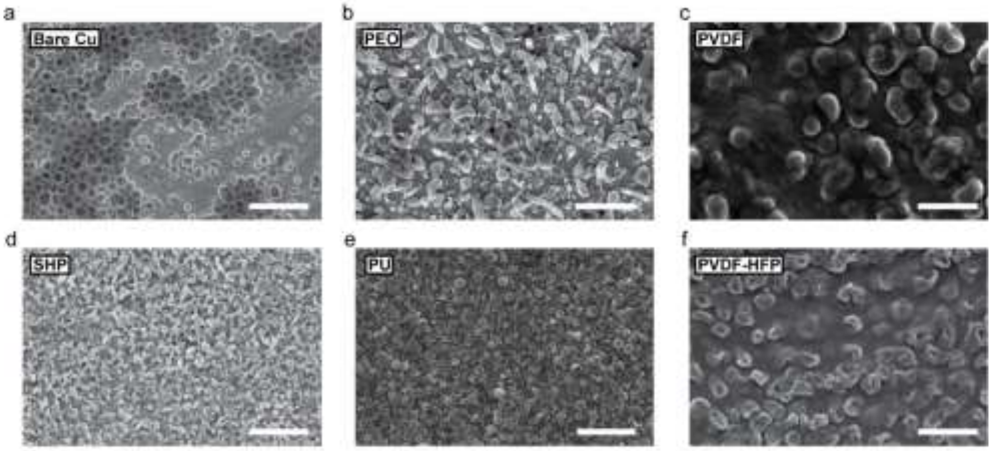

Figure 22. Scanning electron microscopy images of 0.1 mAh/cm^2 of lithium electrodeposited on copper with (a) no polymer coating, (b) PEO coating, (c) PVDF coating, (d) self-healing polymer coating, (e) PU coating, and (f) PVDF-HFP coating. Scale bars for all images are 5 um.

Patents/Publications/Presentations

The project has no patents, publications, or presentations to report this quarter.

Task 1.9 – Improving the Stability of Lithium-Metal Anodes and Inorganic-Organic Solid Electrolytes (Nitash Balsara, Lawrence Berkeley National Laboratory)

Project Objective. The project objective is to establish a new hybrid electrolyte that will be stable against cells with a Li-metal anode.

Project Impact. Polymer electrolytes offer increased stability in lithium batteries in comparison to more widely used liquid electrolytes. Nanostructured electrolytes containing both soft, ion-conducting domains and rigid non-conducting domains offer the opportunity to tune both mechanical and electrical properties separately. Such electrolytes are conveniently made by block copolymer self-assembly. Most of the block copolymer electrolytes studied thus far comprise organic polymer chains for both the conducting and rigid domains. The team hopes to synthesize new electrolytes that simulataneously have high transport properties and have greater stability against lithium in comparison to organic diblock copolymers.

Approach. First, the team synthesizes hybrid diblock copolymers by incorporating monomers that contain an inorganic component. Then electrolytes are prepared by mixing these diblock copolymers with salt. Electrochemical and mechanical characterization of these materials are performed before carrying out cycling X-ray tomography experiments. The combination of these approaches enables rational design of materials that exhibit improved stability against lithium metal.

Out-Year Goals. The project will synthesize a new hybrid electrolyte that is designed to be stable against lithium metal. The material is a block copolymer wherein acryloisobutyl polyhedral oligomeric silsesquioxane (POSS) is covalently bonded to the chain. The second block is a conventional polymer electrolyte, PEO. Electrochemical characterization of this polymer will include measurement of all transport properties including conductivity, diffusion coefficient, and the transference number. The stability against lithium metal will be evaluated by cyclic voltammetry (CV), while its applications as an electrolyte will be evaluated and visualized using cycling X-ray tomography experiments on symmetric Li-hybrid-Li cells.

Collaborations. There are no active collaborations this quarter.

Milestones

1. Synthesis of POSS-PEO block copolymer hybrid electrolyte. (Q1, FY 2018; Completed)
2. Measurement of conductivity of the hybrid copolymer. (Q2, FY 2018; Completed)
3. Measurement of diffusion coefficient and transference number of electrolytes. (Q3, FY 2018; Completed)
4. Completion of the first Li-electrolyte-Li tomography experiments. (Q4, FY 2018; In progress)

Progress Report

The third milestone has been completed. The team successfully characterized the transference number of hybrid organic-inorganic diblock copolymer electrolytes: poly(ethylene oxide) -*b*- poly(acryloisobutyl polyhedral oligomeric silsesquioxane) (PEO-POSS(5-6)) mixed with lithium bis(trifluoromethane)sulfonimide (LiTFSI) salt. The molecular weight of the PEO block is 5 kg mol^{-1} and POSS block 6 kg mol^{-1} The steady-state current experiment is used to determine the transference number, $t_{+,SS}$, defined in Figure 23. ΔV is the applied potential (10 mV), i_{Ω} is the initial current, i_{SS} is the current measured at steady-state, and $R_{i,0}$ and $R_{i,SS}$ are the initial and steady-state resistances of the interface. The results are shown for salt concentration of [Li]/[EO] = $r \leq 0.20$.

Further, this quarter the team characterized the effect of salt on the diblock copolymer morphology in PEO-POSS(5-1.9) using small angle x-ray scattering (SAXS). The phase diagram in Figure 23b shows morphology as a function of temperature (y-axis), *r* (x-axis), and volume fraction of the EO/salt rich phase, $\phi_{EO/LiTFSI}$ (top x-axis). Disordered (D), lamellar (L) and coexisting hexagonally packed cylinders with lamellar (C/L) morphologies are shown.

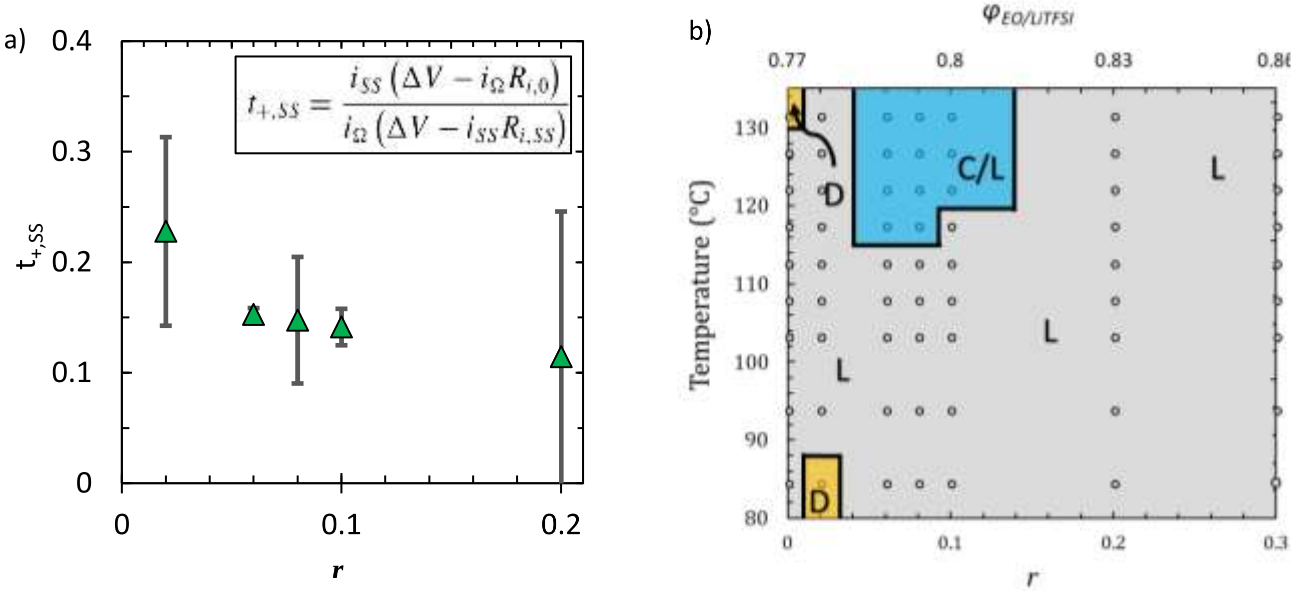

Figure 23. (a) Transference number measurements of poly(ethylene oxide) -*b*- poly(acryloisobutyl polyhedral oligomeric silsesquioxane) (PEO-POSS(5-6)). (b) phase diagram of PEO-POSS(5-1.9).

The team demonstrates that $t_{+,SS}$ values are within range of 0.1 to 0.25, which is comparable to that of PEO with molecular weight (5 kg mol^{-1})[1], the same molecular weight in the diblock copolymers. Thus, adding a non-conductive block to the polymer electrolyte does not appear to decrease the steady-state transference number. Future work includes determining the transference number and calculating diffusion coefficients of the hybrid organic-inorganic system of varying molecular weights synthesized in the first quarter. Further, the effect of phase behavior on electrochemical properties will be explored next quarter, along with lithium tomography experiments.

Patents/Publications/Presentations

Presentation

- American Physical Society (2018): "The Effect of Composition on the Morphology of Hybrid Inorganic-Organic Diblock Copolymer Electrolytes"; G. Sethi, I. Villaluenga, and N. Balsara.

Task 1.10 – Electrolyte/Binder for High Efficiency Lithium-Sulfur Battery: New Materials Design and Computation (Larry A. Curtiss, Zhengcheng Zhang, and Ahn Ngo, Argonne National Laboratory)

Project Objective. Lithium-sulfur batteries have received great attention because sulfur exhibits an order of magnitude higher theoretical capacity than that achievable with intercalation-type cathode materials in Li-ion batteries and is considered as a promising battery chemistry to power long-range, low-cost EVs. Sulfur is abundant in nature and non-toxic, which leads to low cost of the cell and environmental benefits. However, low active material utilization and poor cycle life hinder the practical application of Li-S batteries. The objective of this project is to develop new electrolyte materials to help overcome these challenges and enable high-efficiency Li-S batteries for vehicle application.

Project Impact. The development of novel functional electrolytes tailored for Li-S electrochemistry will enable improved materials utilization and longer cycle life as needed to take advantage of the high potential capacity of Li-S batteries to power long-range, low-cost EVs.

Approach. This project takes a new approach, combining organic synthesis and quantum chemistry computations to obtain an in-depth understanding of the interaction of the discharged lithium polysulfides with the electrolyte solvents and the lithium salt, aiming to develop new electrolyte materials for Li-S batteries. Based on the team's previous study, the fluorinated-ether-based electrolytes have shown very limited Li_2S_x solubility, and at the same time could effectively passivate the lithium anode surface affording a reversible electrochemistry with high CE. However, the low active material utilization compromises its advantages of high theoretical capacity and energy density. To overcome this, the team will investigate boron-containing fluorinated polyethers as a new class of electrolytes for Li-S batteries. To further improve the cycle life, the project also proposes to design and synthesize new polymer binders bearing a pentafluorophenyl group on the backbone. First principles density functional theory (DFT) and wave-function based quantum chemistry methods will be employed to provide accurate atomic/molecular level insight into the experimental studies. The team will also employ *ab initio* molecular dynamics (AIMD) simulations of the solvents for different finite temperatures and concentrations. The AIMD simulations will provide information on the structures of the electrolytes based on the fluorinated ethers synthesized in the experimental part of this project.

Out-Year Goals. The out-year goals are to find electrolytes that promote longer cycle life through electrolytes to reduce material loss.

Collaborations. This project engages in collaboration with Prof. Amin Salehi at University of Illinois at Chicago (UIC).

Milestones

1. Design, synthesis, and characterization of fluorinated solvents and studies of physical properties. (Q3, FY 2018; Completed)
2. Quantum chemical calculations of the binding energies of lithium polysulfides (Li_2S_x) with new solvents. (Q4, FY 2018; Initiated)

Progress Report

The Li-S battery still suffers from the rapid capacity fade during repeated cycling due to the gradual loss of active materials. To enhance the sulfur utilization, the team has designed new ether solvents containing a pentafluorophenyl group in the structures. Due to the strong electron-withdrawing effect of the five fluorines on the benzene ring, the pentafluorinated TFE-PFPE and TFE-PFBE compounds as shown in Figure 24 are expected to be excellent anion receptors that will strongly interact with polysulfides, especially the low order polysulfides, to form anion receptor complexes compared with the nonfluorinated ones, also shown.

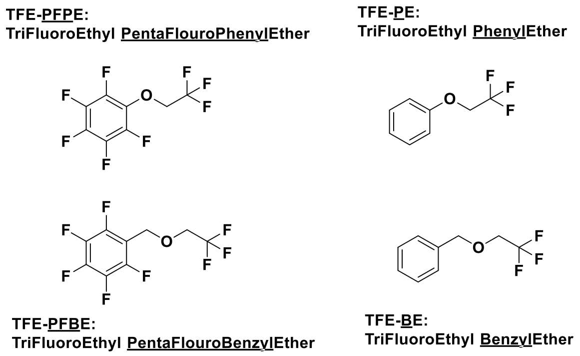

Figure 24. Structures of synthesized fluorinated ethers.

The TFE-PFBE compound was synthesized by reacting 2,2,2-trifluoroethanol and 1,2,3,4,5-pentafluorobenzyl bromide with DMF (50 mL) as a solvent by the reaction shown below. The crude was purified on a silica plug eluted with 0-5% EtOAc in hexane and then distilled under reduced pressure at 41ºC to provide the target compound as a clear colorless liquid in 55.3% yield (7.674 g, 27.394 mmol). The TFE-PFPE compound was also synthesized. The synthesized compounds were verified by NMR measurements.

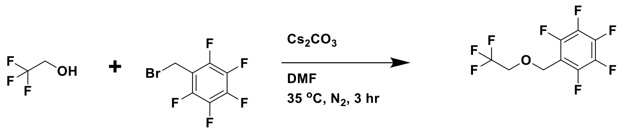

The voltage profiles are shown in Figure 25. Both fluorinated electrolyte cells showed a similar first charge discharge capacity of 800 mAh/g, which is lower than that of the DOL/DME baseline electrolyte due to its low conductivity. However, the charging curves are quite different. For the TFE-PFBE cell, a flat charging plateau is shown at ~ 2.6 V after the regular charging process. This plateau is a typical redox shuttling phenomenon of the dissolved polysulfides. This result confirms that TFE-PFBE is a stronger anion receptor than TFE-PFPE. The adjacent oxygen in the TFE-PFPE donates electrons to the benzene ring through the p-π conjugation, therefore decreasing the anion receptive strength of the solvents.

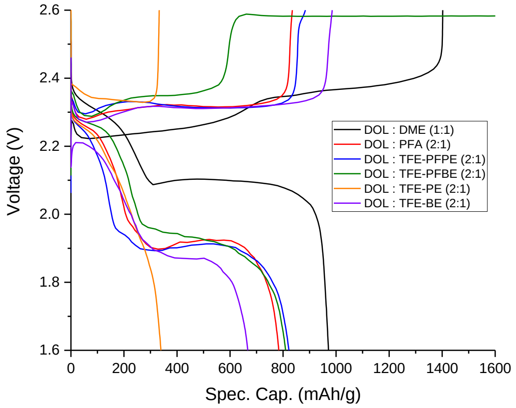

Figure 25. Voltage profiles of the Li-S cell with tetrafluorethylene – pentafluorinated perfluoro-polyether (TFE-PFPE) and TFE perfluorobutyl ethylene (TFE-PFBE) electrolytes. The sulfur electrode is made of commercial sulfur power, carbon black conducting agent, and polyvinylidene fluoride binder.

Patents/Publications/Presentations

The project has no patents, publications, or presentations to report this quarter.

TASK 2 – DIAGNOSTICS

Summary and Highlights

To meet the goals of the VTO Multi-Year Program Plan and develop lower-cost, abuse-tolerant batteries with higher energy density, higher power, better low-temperature operation, and longer lifetimes suitable for the next-generation of EVs, hybrid EVs (HEVs), and plug-in hybrid EVs (PHEVs), there is a strong need to identify and understand structure-property-electrochemical performance relationships in materials, life-limiting and performance-limiting processes, and various failure modes to guide battery development activities and scale-up efforts. In pursuit of batteries with high energy density, both high cell operating voltages and demanding cycling requirements lead to unprecedented chemical and mechanical instabilities in cell components. Successful implementation of newer materials such as silicon anode and high-voltage cathodes also requires better understanding of fundamental processes, especially those at the solid/electrolyte interface of both anode and cathode.

This Task takes on these challenges by combining model system, *ex situ*, *in situ*, and *operando* approaches with an array of the start-of-the-art analytical and computational tools. Three subtasks are tackling the chemical processes and reactions at the electrode/electrolyte interface. Researchers at LBNL use *in situ* and *ex situ* vibrational spectroscopy and far- and near-field scanning probe spectroscopy to understand the structure of active materials and the physio-chemical phenomena at electrode/electrolyte interfaces, particularly those of the high-voltage cathodes. GM is developing a number of *in situ* diagnostic techniques, including AFM, nanoindentor, dilatometer, and stress-sensor, to be combined with atomic/continuum modeling schemes to investigate and understand the coupled mechanical/chemical degradation of the SEI layer on Li-metal anode. ANL aims to first understand the pathways/mechanisms of the parasitic reactions the electrode/electrolyte interfaces and then stabilize them by developing functional surface coating and electrolyte additives. Subtasks at Brookhaven National Laboratory (BNL) and PNNL focus on the understanding of fading mechanisms in electrode materials, with the help of synchrotron-based X-ray techniques (diffraction and hard/soft X-ray absorption) at BNL and high-resolution transmission electron microscopy (HRTEM) and spectroscopy techniques at PNNL. UCSD is developing advanced diagnostic tools, including scanning transmission electron microscopy / electron energy loss spectroscopy (STEM/EELS), *operando* Bragg coherent diffraction imaging (BCDI) and *ab initio* computation, to probe anion redox and oxygen evolution in Li-excess NMC materials. At LBNL, model systems of electrode materials with well-defined physical attributes are being developed and used for advanced diagnostic and mechanistic studies at both bulk and single-crystal levels. These controlled studies remove the ambiguity in correlating material's physical properties and reaction mechanisms to its performance and stability, which is critical for further optimization. The final subtask at Stanford University / Stanford Linear Accelerator Center (SLAC) develops and utilizes a correlative X-ray microscopy platform to investigate the lithiation dynamics and understand factors that determine the rate capability and degradation mechanisms in cathode materials. The diagnostics team not only produces a wealth of knowledge that is key to the development of next-generation batteries, it also advances analytical techniques and instrumentation that have a far-reaching effect on material and device development in a variety of fields.

The highlights for this quarter are as follows:

- LBNL (Chen's group) used X-ray absorption spectroscopy (XAS) to reveal the chemical origin of cycling instability in a cation-disordered cathode.
- BNL (Yang and Bak) combined X-ray and neutron diffraction to track the changes in O-O bond distance and provided evidence for possible formation of O-O dimers in highly delithiated $LiCoO_2$.

- UCSD (Meng’s group) used electron diffraction (ED) analysis to show that bulk stacking faults generated during electrochemical cycling of layered oxide cathodes can be partially eliminated during heating, suggesting that heat treatment may be useful for structure and voltage recovery of cycled materials.
- PNNL (Wang’s Group) demonstrated that by infusing grain boundaries of secondary particles with a solid electrolyte, side reactions involving the liquid electrolyte can be minimized.

Task 2.1 – Model System Diagnostics for High-Energy Cathode Development (Guoying Chen, Lawrence Berkeley National Laboratory)

Project Objective. This project will use a rational, non-empirical approach to design and synthesize next-generation high-energy, high-voltage cathode materials. Combining a suite of advanced diagnostic techniques with model cathode materials and model electrode/electrolyte interfaces, the project will perform systematic studies to achieve the following goals: (1) obtain new insights into solid-state chemistry, particularly cationic and/or anionic redox activities during charge and discharge of high-capacity lithium TM oxides, (2) gain fundamental understanding on cathode/electrolyte interfacial chemistry and charge transfer process as a function of operating voltage, (3) reveal performance- and stability-limiting properties and processes in high-energy, high-voltage cathodes, and (4) develop strategies to mitigate the structural and interfacial instabilities.

Impact. The project will improve the commercial viability of next-generation high-energy cathode materials. The findings will enable more stable high-voltage cycling of existing Li-TM oxides as well as development of novel high-capacity cathode materials for advanced Li-ion batteries.

Approach. The project will prepare crystal samples of Li-stoichiometric and Li-excess TM oxides with well-defined physical attributes. It will perform advanced diagnostic and mechanistic studies at both bulk and single-crystal levels. Global properties and performance of the samples will be established from the bulk analyses, while the single-crystal-based studies will utilize time- and spatial-resolved analytical techniques to probe the material redox transformation process and failure mechanisms under battery operating conditions.

Out-Year Goals. In the out-years, the project will obtain fundamental knowledge on performance-limiting physical properties, phase transition mechanisms, parasitic reactions, and transport processes that prevent cathode materials from delivering higher capacities and achieving more stable cycling at high voltages. It will develop approaches to mitigate cathode structural and interfacial instabilities during high-voltage operation. Further, it will design and synthesize optimized Li-TM oxide cathodes as well as novel high-energy electrode materials.

Collaborations. This project collaborates with the following: G. Ceder, K. Persson, M. Doeff, B. McCloskey, and P. Ross (LBNL); V. Srinivasan (ANL); D. Nordlund and Y. Liu (Stanford Synchrotron Radiation Lightsource, SSRL); C. Wang (PNNL); C. Grey (Cambridge); and A. Huq and J. Nanda (Oak Ridge National Laboratory, ORNL).

`Milestones

1. Characterize oxygen activities during charge/discharge and extended cycling of Li-TM oxides and understand effect on cathode structural and electrochemical reversibility. (Q1, December 2017; Completed)
2. Investigate analytical techniques to determine the kinetics of anion redox process, and evaluate factors influencing rate capability of Li-TM oxide cathodes. (Q2, March 2018; Completed)
3. Apply advanced diagnostic techniques to investigate the reactivities of model oxide surfaces and understand their impact on oxide performance and safety. (Q3, June 2018; Completed)
4. *Go/No-Go Decision*: Reveal the impact of oxide chemistry and particle morphology on the extent of reversible oxygen redox versus lattice oxygen loss; understand how to fine tune oxygen activities at high voltages. *No-Go* if the processes of reversible oxygen redox and lattice oxygen loss cannot be decoupled with diagnostic studies. (Q4, September 2018; On schedule)

Progress Report

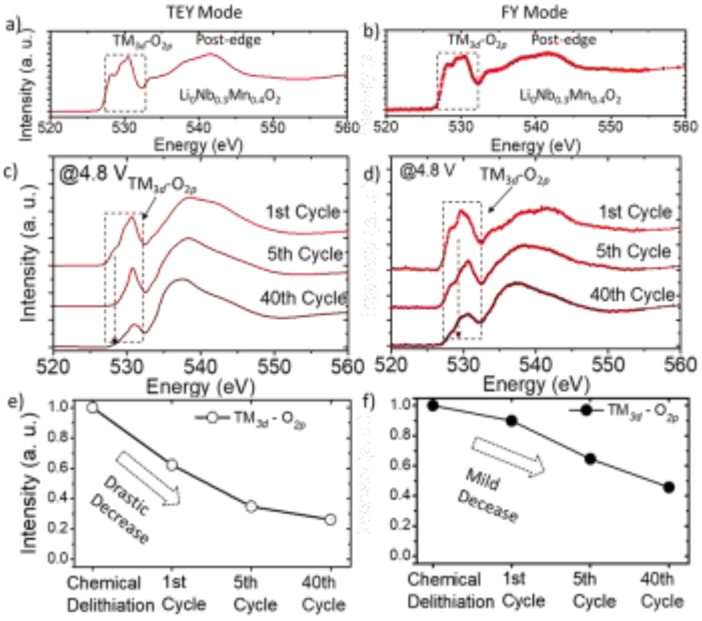

Figure 26. Oxygen *K*-edge X-ray absorption spectroscopy profiles of chemically delithiated $Li_0Nb_{0.3}Mn_{0.4}O_2$ (a-b) and $Li_{1.3}Nb_{0.3}Mn_{0.4}O_2$ cathodes charged to 4.8 V after various cycle numbers (c-d). (e-f) Intensity of the TM_{3d}-$O2_p$ absorption band as a function of the cycle number. (a), (c), and (e) were collected in the total electron yield mode; (b), (d), and (f) were collected in fluorescent yield mode.

The performance of rock-salt $Li_{1.3}Nb_{0.3}Mn_{0.4}O_2$ cathode was previously found to deteriorate quickly when cycled involving oxygen redox. This quarter, chemical origin of the cycling instability was investigated by surface sensitive soft XAS technique. Figure 26a-d shows the oxygen *K*-edge spectra collected in both total electron yield (TEY) and fluorescent yield (FY) modes, which probe the electronic structures of the specified element with a depth of ~ 5 and 50 nm, respectively. The pre-edge feature centered at ~530 eV is attributed to the transitions between O_{1s} to TM_{3d}-O_{2p} hybrid orbitals, which is strongly correlated to the changes in valence electrons of both oxygen and transition metal (TM), or the covalency between them. Monitoring the intensity changes in the TM_{3d}-O_{2p} peak, therefore, provides direct insights on oxygen redox activities. On both TEY and FY spectra, the chemically delithiated sample shows the highest TM_{3d}-O_{2p} pre-edge intensity (Figure 26a-b). The lower intensity observed on the cycled electrodes (Figure 26c-d) suggests less electron extraction or charge compensation from these hybrid orbitals. While the TEY intensity of TM_{3d}-O_{2p} pre-edge decreases drastically with cycling, with only ~ 60% and ~ 30% remaining after the 1st and 40th cycles, respectively, the reduction in FY intensity was much slower, with 90% remaining after the 1st cycle and 50% remaining after the 40th cycle (Figure 26e-f). This clearly indicates that the irreversibility in oxygen-related activities is more severe on the surface than that in the sub-surface region.

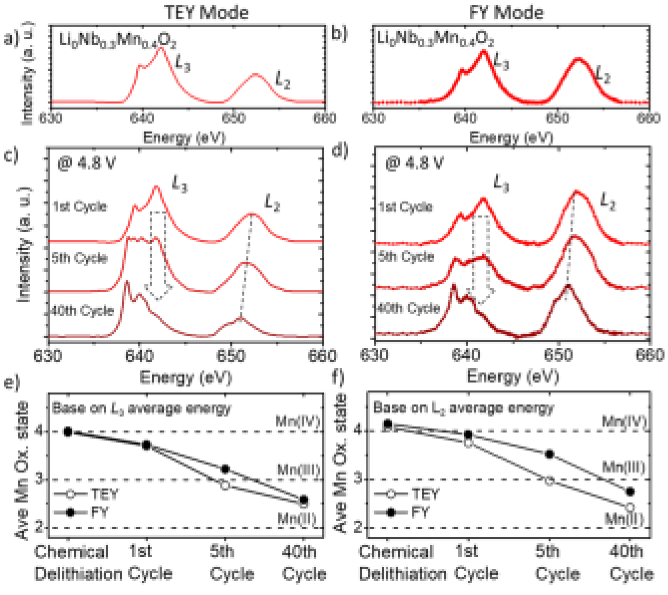

Figure 27. Manganese *L*-edge X-ray absorption spectroscopy profiles of chemically delithiated $Li_0Nb_{0.3}Mn_{0.4}O_2$ (a-b) and $Li_{1.3}Nb_{0.3}Mn_{0.4}O_2$ cathodes charged to 4.8 V after various cycle numbers (c-d). (e/f) Manganese oxidation state derived from average L_3 and L_2 band energies, respectively. (a) and (c) were collected in the totally electron yield mode; (b) and (d) were collected in in fluorescence yield mode.

Manganese *L*-edge soft XAS measurements were also performed to further compare the chemical changes on the surface and in the subsurface region. Figure 27 shows the spectra collected on fully chemically delithiated oxide (Figure 27a-b) and electrochemically charged $Li_{1.3}Nb_{0.3}Mn_{0.4}O_2$ after 1, 5, and 40 cycles (Figure 27c-d). Manganese oxidation state, derived from average L_2 (transition from Mn $2p_{1/2}$) and L_3 (transition from Mn $2p_{3/2}$) band energies, is plotted as a function of cycle number in Figure 27e-f. While manganese is fully oxidized to 4+ in both chemically delithiated $Li_0Nb_{0.3}Mn_{0.4}O_2$ and $Li_{1.3}Nb_{0.3}Mn_{0.4}O_2$ electrode after the first charge to 4.8 V, the L_2 and L_3 band features on TEY and FY indicate gradual reduction with cycling. After five cycles, the presence of Mn(III) multiplets along with Mn(IV) doublet was clearly observed. Manganese was further reduced to below 3+ after 40 cycles, as evidenced by the presence of a peak center at ~639 eV, signature of Mn(II) species. The broadly observed differences between the TEY and FY spectra suggest that manganese reduction is also more severe on the surface compared to that in the subsurface region.

Patents/Publications/Presentations

Publication

- Kan, W. H., B. Deng, Y. Xu, A. K. Shukla, T. Bo, S. Zhang, J. Liu, P. Pianetta, B.-T. Wang, Y. Liu, and G. Chen. “Visualizing the Effect of Local Short-Range Ordering on Lithium-Ion Diffusion in $Li_{1.3}Nb_{0.3}Mn_{0.4}O_2$ Single-Crystal Cathode.” *Chem* (2018). doi:10.1016/j.chempr.2018.05.008.

Presentation

- DOE AMR Meeting, Washington, D. C. (June 18–21, 2018): “Model System Diagnostics for High-Energy Cathode Development”; G. Chen.

Task 2.2 – Interfacial Processes – Diagnostics
(Robert Kostecki, Lawrence Berkeley National Laboratory)

Project Objective. This collaborative project will develop and apply advanced experimental methodologies to study and understand the mechanism of operation and degradation of high-capacity materials for rechargeable cells for PHEV and EV applications. The objective is to develop and apply *in situ* and *ex situ* far- and near-field optical multi-functional probes to obtain detailed insight into the active material structure and physio-chemical phenomena at electrode/electrolyte interfaces at a spatial resolution corresponding to the size of basic chemical or structural building blocks. The goal is to design new diagnostic techniques and experimental methodologies capable of unveiling the structure and reactivity at hidden or buried interfaces and interphases that determine material, composite electrode, and full-cell electrochemical performance and failure modes.

Project Impact. Instability and/or high resistance at the interface of battery electrodes limits electrochemical performance of high-energy-density batteries. A better understanding of the underlying principles that govern these phenomena is inextricably linked with successful implementation of high-energy-density materials in Li-ion and Li-based cells for PHEVs and EVs. The proposed work constitutes an integral part of the concerted effort within the BMR and supports development of new electrode materials for high-energy rechargeable cells.

Approach. The pristine and cycled composite electrode and model thin-film electrodes will be probed using various surface- and bulk-sensitive techniques, including FTIR, attenuated total reflectance (ATR)–FTIR, near-field infrared (IR) and Raman spectroscopy and microscopy, and scanning probe microscopy to identify and characterize changes in materials structure and composition. Novel *in situ/ex situ* far- and near-field optical multifunctional probes in combination with standard electrochemical and analytical techniques are developed to unveil the structure and reactivity at interfaces and interphases that determine materials electrochemical performance and failure modes.

Out-Year Goals. In the out-years, the project aims to: (1) determine the degradation mechanism(s) of high-voltage cathodes; and (2) propose and test effective remedies to intrinsic interfacial instability of these materials and composite electrodes.

Collaborations. Electrode materials and composite electrodes tested under different cycling regimes by M. Doeff (LBNL) and C. Ban (National Renewable Energy Laboratory, NREL) will be studied. The diagnostic studies will be carried out in sync with differential electrochemical mass spectrometry (DEMS) analysis by B. McCloskey (LBNL) and other diagnosticians in the BMR program. He will also work closely with V. Battaglia (LBNL) to obtain samples from full-cell cycling experiments.

Milestones

1. Controlled growth of model thin-film electrodes by pulsed laser deposition (PLD) as model system for fundamental electrochemical studies. *Go/No-Go Decision*: Stoichiometric thin films produced with sub-nanometer roughness. (December 2017; Completed)
2. Characterize bulk and surface structure of model PLD thin films and the relation to electrochemical properties. *Go/No-Go Decision*: Electrochemical performance of model system in line with that of bulk materials. (Q2, FY 2018; Completed March 2018)
3. Characterize chemistry of electrolyte decomposition at model PLD thin-film electrodes with near-field technique. (Q3, FY 2018; Completed)
4. Determine electrochemical impedance contribution from interface between organic electrolyte and electrode active material. *Go/No-Go Decision*: Development of model electrodes with high electrochemical stability and low impedance. (Q4, FY 2018; On schedule)

Progress Report

This quarter, the team characterized the morphology and chemical composition of the organic cathode electrolyte interfacial (CEI) layer on thin-film NMC-532 electrode after 3rd cycle by Neaspec scattering-type scanning near-field optical microscopy (NeaSNOM). Electrode potential was scanned by CV between 2-4.7 V, with lithium foil as CE in 1 M $LiPF_6$ in ethylene carbonate and diethyl carbonate (EC:DEC, 1:2 wt%) electrolyte in a Swagelok cell. After 3rd cycle (end at fully lithiated state), the electrode was washed in DEC for 5 s or 5 min to expose specifically the outer or inner organic CEI layer (experimental procedure was described last quarter). The AFM images show the pristine thin-film NMC-532 electrode (Figure 28a/d) consisting of closely packed 50- to 100-nm nanoparticles with surface roughness < 10 nm. Clearly, this PLD-made NMC-532 thin-film constitutes an excellent experimental platform for fundamental studies of interfacial processes.

The cycled NMC-532 electrode after soft (5 s) DEC washing (Figure 28b) shows clusters ca. 2~4-µm wide and 100-nm thick, unevenly distributed at the electrode surface. The corresponding IR absorbance image acquired by NeaSNOM of the same area is shown in Figure 28c. The bright areas indicate higher IR adsorption, whereas dark locations show no IR absorbance at the selected wavelength. Direct comparison of morphology (Figure 28b) and IR images (Figure 28c) reveals an overlap of the large clusters with the highly IR absorbing areas of the film at 1080 cm^{-1}, which corresponds to ν (C-O-C) from polyethylene glycol-type compounds.

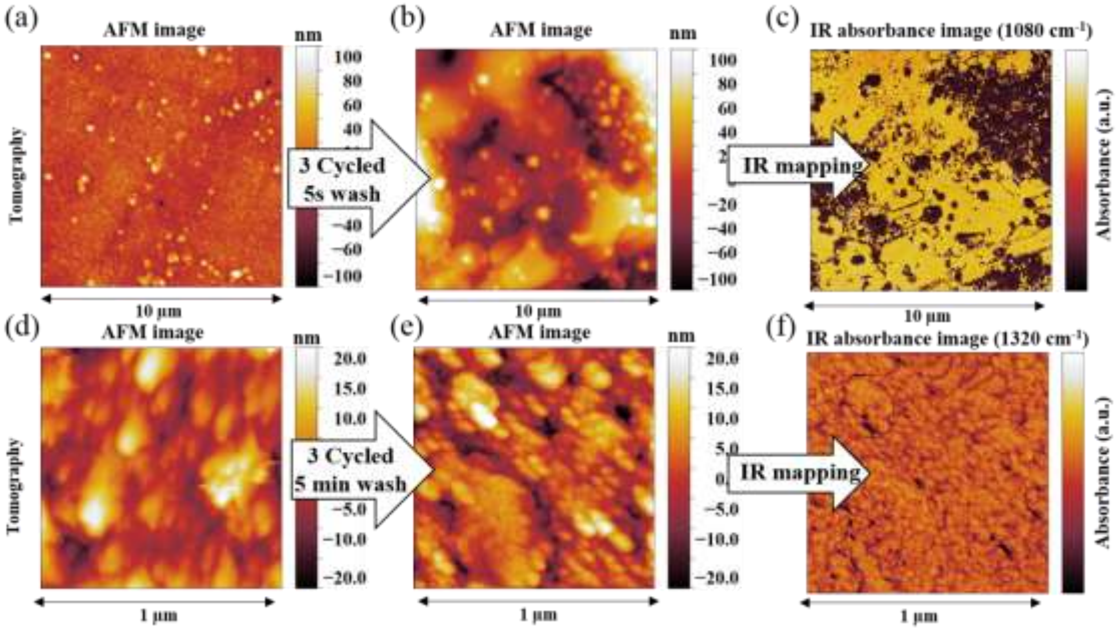

Figure 28. (a/d) Atomic force microscopy (AFM) morphology image of the pristine NMC thin-film electrode. (b) AFM morphology image and (c) near-field infrared (IR) adsorbance image of cycled NMC thin film after 5 s washing in diethyl carbonate (DEC). (e) AFM morphology image and (c) near-field IR absorbance image of cycled NMC thin film with 5 min washing in DEC.

To study the inner organic CEI layer, the non-uniform outer CEI film was removed by washing in DEC for 5 min. The AFM image (Figure 28e) gives no indication of thick deposits and displays similar surface morphology as the pristine electrode (Figure 28d). To unveil the surface chemical composition, NeaSNOM imaging was used again at 1320 cm^{-1}, which corresponds to ν(C-O) of the compounds observed in the inner organic layer (see last quarter's report). The IR absorbance image (Figure 28f) displays a uniform distribution of IR adsorption at the surface, indicating the organic species in the inner CEI layer are evenly spread out over the NMC-532 surface. In summary, the near-field IR analysis of the cycled thin-film NMC-532 surface revealed stratified CEI film that consists of thick glycol-type outer layer and thin inner layer. This completes the project's research efforts toward the third-quarter milestone.

Patents/Publications/Presentations

The project has no patents, publications, or presentations to report this quarter.

Task 2.3 – Advanced *In Situ* Diagnostic Techniques for Battery Materials (Xiao-Qing Yang and Seongmin Bak, Brookhaven National Laboratory)

Project Objective. The primary project objective is to develop new advanced *in situ* material characterization techniques and to apply these techniques to support development of new cathode and anode materials for the next generation of Li-ion batteries for PHEVs. To meet the challenges of powering the PHEV, Li-ion batteries with high energy and power density, low cost, good abuse tolerance, and long calendar and cycle life must be developed.

Project Impact. The VTO Multi-Year Program Plan describes the goals for battery: "Specifically, lower-cost, abuse-tolerant batteries with higher energy density, higher power, better low-temperature operation, and longer lifetimes are needed for development of the next-generation of HEVs, PHEVs, and EVs." The knowledge gained from diagnostic studies through this project will help U. S. industries develop new materials and processes for new generation Li-ion batteries in the effort to reach these VTO goals.

Approach. This project will use the combined synchrotron-based *in situ* X-ray techniques (X-ray diffraction, or XRD; hard and soft XAS) with other imaging and spectroscopic tools such as HRTEM and mass spectrometry (MS) to study the mechanisms governing performance of electrode materials.

Out-Year Goals. In the out years, the project will complete development of diagnostic techniques using X-ray pair distribution function (x-PDF), XRD, and XAS combined with neutron diffraction and neutron PDF (n-PDF), as well as STEM imaging and transmission X-ray microscopy (TXM) for cathode materials studies. It will then apply these techniques to study the structural changes of various new cathode materials.

Collaborations. The BNL team will work closely with material synthesis groups at ANL (Drs. Shin and Amine) for the high-energy composite and at PNNL for the Si-based anode materials. The project will also collaborate with industrial partners at GM and Johnson Controls, as well as with international collaborators.

Milestones

1. Complete the *in situ* TXM studies of $LiCoO_2$ cathode materials during charge-discharge cycling to evaluate the inhomogeneity of the charged (discharged) states among a large number of material particles and using a data mining technique to detect the under (over) reacted minority regions (particles). (Q1, December 2017; Completed)

2. Complete the neutron diffraction studies of $LiCoO_2$ as high-energy-density cathode material at high-voltage charge in comparison with the pristine state. (Q2, March 2018; Completed)

3. Complete the PDF studies of $LiCoO_2$ using both x-PDF and n-PDF probes to study the mechanism of anionic redox reaction in such widely used commercial cathode materials for Li-ion batteries and explore the potential of using this material for high-energy-density cell applications. (Q3, June 2018; Completed)

4. Complete the experimental design, data collection, and analysis of 3D STEM tomography studies of high-energy-density $Li_{1.2}Ni_{0.15}Co_{0.1}Mn_{0.55}O_2$ cathode materials at pristine state and after multiple cycling. (Q4, September 2018; In progress)

Progress Report

This quarter's milestone has been completed. BNL has been focused on the studies of structure change associated with the oxygen-related redox reaction (ORR). The $LiCoO_2$ cathode was charged to 4.6 V to reach a deeply delithiated state. Understanding the role of oxygen anions during electrochemical reaction requires a local probe. Both xPDF and nPDF were applied to the pristine sample and *ex situ* sample after charged to 4.6 V, with the data shown in Figure 29a/b, respectively. In Figure 29, xPDF data (a) and nPDF data (b) are plotted along with the contribution from O-O pairs. It can be clearly seen that in xPDF, O-O pairs make a minimum contribution to the whole pattern due to the small x-ray scattering cross section of oxygen. In contrast, the whole pattern of nPDF for the same sample is dominated by contribution from O-O pairs. Such difference can be understood by comparing the relative scattering power of lithium, cobalt, and oxygen for X-ray with those for neutron, as shown in Figure 29c. It can be seen from the lower panel of Figure 29b that there is an obvious peak (peak A) at around 2.63 Å, which is attributed to the shortest distanced O-O pairs. By checking with the structure determined from the NPD results, it is identified that the O-O pairs featuring such distance are those shared edges between neighboring CoO_6 octahedra, as shown in Figure 29d. Upon charging, peak A shifts to the left, becoming peak A' located at around 2.47 Å. Interestingly, this value is very close to the O-O bond distance (2.45 Å) observed previously by McCalla in Li-rich layered Li_2IrO_3, suggesting the possibility of formation of O-O dimers at the deeply delithiated state of conventional layered $LiCoO_2$ material.

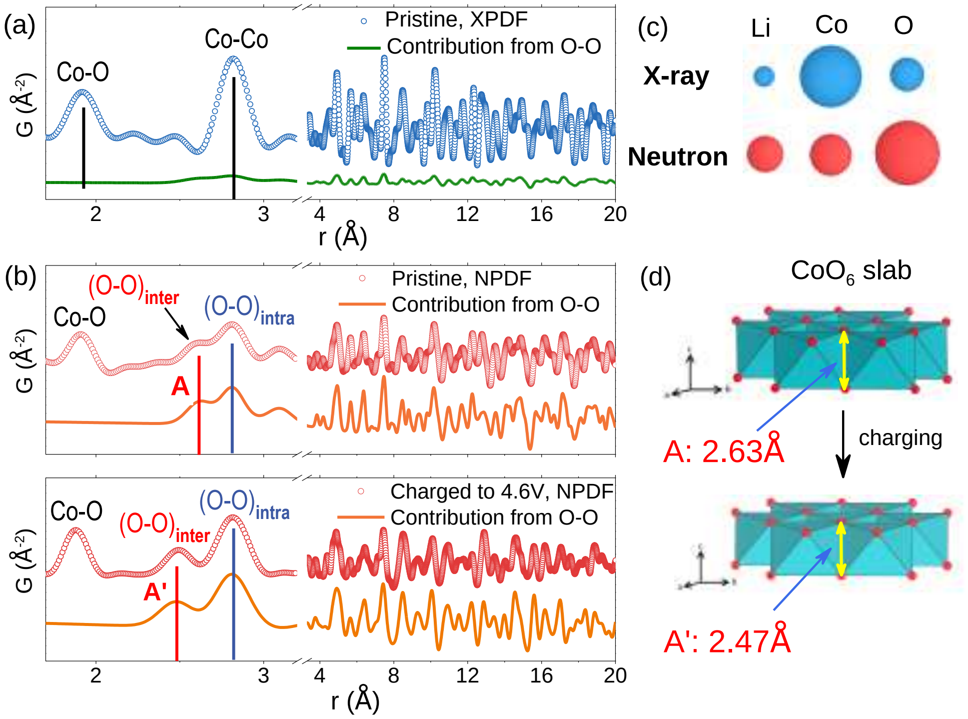

Figure 29. (a) X-ray pair distribution function data of pristine sample (symbol) and the O-O pair contribution (solid line). (b) Neutron pair distribution function data of both pristine and charged sample (symbol) and the O-O pair contribution (solid line). (c) The relative scattering power/length of lithium, cobalt, and oxygen for X-ray and for neutron scattering. (d) The change of the shortest O-O pair distance from pristine sample to charged sample.

Patents/Publications/Presentations

Publications

- Liu*, J., L. Yin, X-Q. Yang*, and P. G. Khalifah. "$Li_3VP_3O_9N$ as a Multielectron Redox Cathode for Li-Ion Battery." *Chemistry of Materials*. doi: 10.1021/acs.chemmater.8b01114 (web Publication Date: May 23, 2018).
- Liu*, J., L. Yu, E. Hu, B. S. Guiton, X-Q. Yang, and K. Page.* "Large-Scale Synthesis and Comprehensive Structure Study of δ-MnO_2." *Inorganic Chemistry* 57, no. 12 (2018): 6873–6882. doi: 10.1021/acs.inorgchem.8b00461 (Web Publication Date: May 30, 2018).
- Fan, X., E. Hu, X. Ji, Y. Zhu, F. Han, S. Hwang, J. Liu, S. Bak, Z. Ma, T. Gao, S-C. Liou, J. Bai, X-Q. Yang, Y. Mo, K. Xu, D. Su, and C. Wang. "High Energy-Density and Reversibility of Iron Fluoride Cathode Enabled via an Intercalation-Extrusion Reaction." *Nature Communications*. doi: 10.1038/s41467-018-04476-2 (Web Publication Date: June 13, 2018).

Presentation

- 13th China International Conference on the Frontier Technology of Advanced Batteries, CIBF2018, Shenzhen, China (May 22–24, 2018): "Using Synchrotron Based X-Ray Scattering and Absorption Spectroscopy as well as TXM and TEM Imaging Techniques to Study New Cathode Materials for Rechargeable Batteries"; E. Hu, X-Q. Yang, J. Liu, S-M. Bak, R. Lin, Z. Shadike, H-S. Lee, X. Wang, H. Xin, Y. Liu, X. Yu, X. Huang, and H. Li. Invited.

Task 2.4 – Advanced Microscopy and Spectroscopy for Probing and Optimizing Electrode-Electrolyte Interphases in High-Energy Lithium Batteries
(Shirley Meng, University of California at San Diego)

Project Objective. The proposed research aims to develop advanced microscopy and spectroscopy tools to probe, understand, and optimize the anion activities that govern the performance limitations such as capacity and voltage stabilities in high-energy Li-excess TM (such as nickel, cobalt, manganese) oxides cathode materials. The approach uniquely combines atomic resolution STEM, EELS, *operando* BCDI, and first-principles computation to probe anion redox and oxygen evolutions in Li-excess NMC materials. Furthermore, the project will track the lithium and oxygen dynamics under electrochemical testing via *operando* neutron diffraction, which will enhance understanding of the overall structural changes due to anion activities. Ultimately, this will hone in on the synthesis efforts to produce the modified materials with optimum bulk compositions and surface characteristics at large scale for consistently good performance. The above-mentioned characterization tools will be extended to diagnose various anode types, such as Li-metal anode.

Project Impact. If successful, this research will enable *operando* imaging at the single-particle level by advanced microscopy imaging and high-energy-resolution oxygen K-edge EELS. This work will provide an in-depth understanding of anion activities in high-voltage electrode materials, which can lead to significant improvement in stabilizing operation voltage and electrode-electrolyte interface for future generation high-energy-density electrodes.

Approach. This unique approach combines STEM/EELS, *operando* BCDI, and *ab initio* computation as diagnostic tools for probing anion redox and oxygen evolutions in Li-excess NMC materials. This allows for pinning down the atomistic/molecular mechanism of anion oxidation and determining the speciation compositions and surface characteristics for enabling high rate and long life in the proposed materials. Neutron enables the characterization of bulk material properties to enhance and further optimize high-energy electrode materials.

Out-Year Goals. The goal is to probe and control defects generation due to oxygen activity in the high-energy composite cathodes and to characterize electrode/electrolyte interface in lithium anodes so that their cycle life and efficiency can be significantly enhanced.

Collaborations. This work funds collaborations on EELS (Miaofang Chi, ORNL); neutron diffraction (Ken An, ORNL); and soft XAS (Marca Doeff, LBNL). It supports collaborative work with Zhaoping Liu and Yonggao Xia at Ningbo Institute of Materials Technology and Engineering in China. It also supports collaboration with the Battery500 Consortium.

Milestones

1. Benchmark electrode performance of bulk and surface modified Li-excess NMC. (Q2, March 2018; Completed)
2. Conduct BCDI and STEM/EELS characterization of modified Li-excess NMC single particle. (Q3, June 2018; Completed)
3. Propose strategies to optimize the anion activities in Li-excess NMC cathode materials. (Q4, September 2018; On track)

Progress Report

HRTEM/ED Characterization on Structural Recovery of Single Particle for Li-Rich Layered Oxide (LRLO) after Electrochemical Cycling. The previous report discussed demonstration that dislocations are generated and accumulated in the structure of LRLO material during electrochemical cycling. The nucleation of line defects dramatically modifies the local lithium environment by perturbing the ordering of oxygen stacking layers. To investigate stacking faults in detail, HRTEM combined with ED were applied for cycled LRLO material $Li[Li_{0.144}Ni_{0.136}Co_{0.136}Mn_{0.544}]O_2$. The diffraction streaks indicated by the red arrow in ED pattern represent superlattice ordering of single particle for LRLO. As shown in Figure 30a, the diffraction streaks in the ED pattern of cycled LRLO material are diffused, which indicates strong disorder in the layers stacking direction. After heat treatment at 300°C for one hour, the bulk structure still maintains the layer phase (Figure 30b). More importantly, the diffraction spots along the streaks in the ED pattern become more obvious compared with the cycled bulk structure. To show the changes clearly for different samples, the diffraction streaks intensity was quantified from line-scanning with position presented by red arrows. The peaks are more noticeable after the heat treatment compared with the sample after cycling. This observation can be well explained by the ED simulation result using SingleCrystal for LRLO material with different concentration of stacking faults (Figure 30c-d). Stacking faults are allowed only in between the −O−TM−O−Li− slabs and could never be generated inside the slabs. Three vectors defined as [0, 0, 1], [1/2, −1/6, 1], and [1/6, −1/6, 1] in the unit cell with conventional monoclinic cell definition represent all possible atomic configurations generated by the stacking faults. Different concentration of stacking faults was associated with the stacking probabilities of these stacking vectors. The ED analysis implies the stacking faults generated in the bulk structure during the electrochemical cycling can be partially eliminated by the heat treatment. The structure ordering along the layers stacking direction is partially restored. These findings well support the team's proposed heat treatment strategy for structure and voltage recovery of cycled LRLO material.

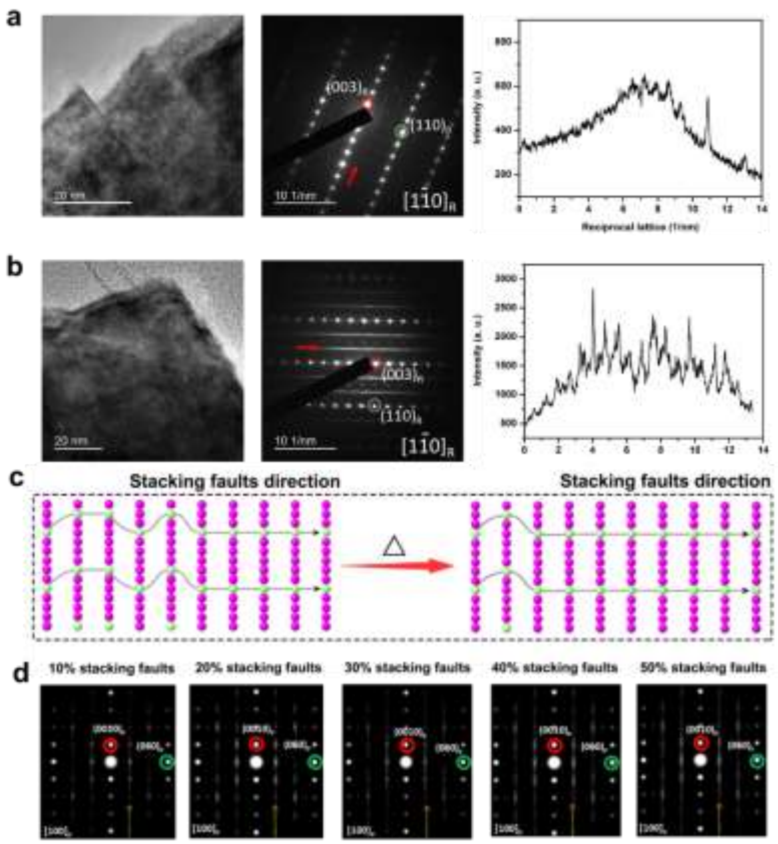

Figure 30. High-resolution transmission electron microscopy image, electron diffraction (ED), and intensity of reciprocal lattice from line-scanning on single particle for the Li-rich layered oxide (LRLO) sample after 50 cycles (a) and after heat treatment at 300°C (b). Models of cycled and heat treated LRLO for ED simulation (c). Simulated ED patterns for LRLO with different degree of stacking faults (d).

Influence of Metal-Ion Electrolyte Additive on Electrochemically Deposited Lithium Metal. To disclose the effect of Cs^+ and Zn^{2+} electrolyte additives, cryo-TEM was applied to explore the nanostructure of the deposited lithium metal. The cryo-TEM results (Figure 31a-c) exhibit that the lithium metal plated from Cs^+-containing electrolyte has a dense, uniform, and ultrathin SEI (< 1 nm) on the surface, which is similar to the SEI formed on graphite anode surface in the $CsPF_6$-containing electrolyte, demonstrating the positive effect of Cs^+ additive on the SEI formation. On the other hand, a conformal thick surface film was found along the surface of the lithium metal when the cell was cycled with Zn^{2+}-containing electrolyte. The surface is rough and about 10 nm in average thickness. The EDLi is consistently amorphous in the bulk with a partially-crystallized SEI—composed of LiF given characteristic bright spots (Figure 31f). Furthermore, the Li-Zn alloy is also amorphous without any characteristic bright rings and spots present in Figure 31e-f. Note that the Zn^{2+}-containing electrolyte has a higher CE and thicker surface layer than that of the pristine electrolyte. The Li-Zn alloy is believed to be distributed on the surface and to protect the lithium metal from electrolyte corrosion. Overall, both the EDLi from Cs^{+}- and Zn^{2+}-containing electrolytes are amorphous, suggesting there is little effect on lithium bulk structure; yet, they differ significantly in interfacial properties.

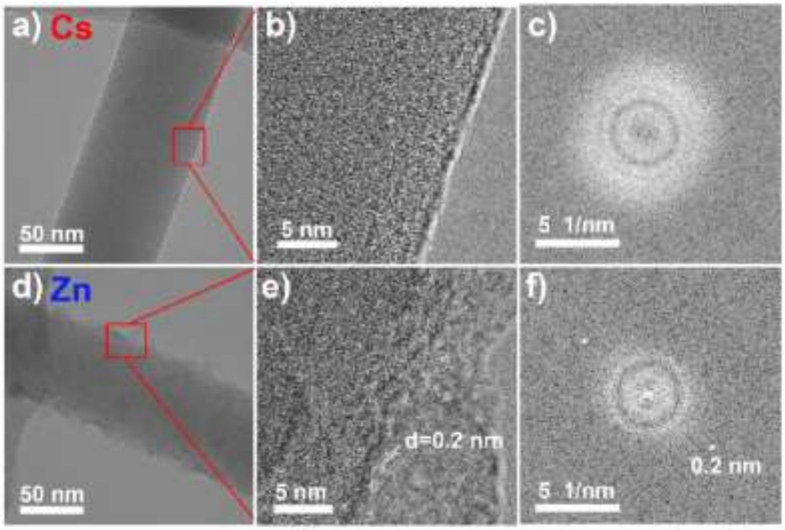

Figure 31. Cryo – transmission electron microscopy images (a, b, d, e) with their corresponding area fast Fourier transform analysis (c, f) of the deposited lithium metal using electrolytes containing Cs^{+} (a-c) and Zn^{2+} (d-f) additives at 400 kx magnification. The current density of the deposition is 0.5 mA/cm^{2}, and deposition time is 5 minutes.

Patents/Publications/Presentations

Publications

- Zhang, M., H. D. Liu, Y. S. Meng, et al. "Modified Co-Precipitation Synthesis of Meso-Structure Controlled Li-Rich Layered Oxides for Minimizing Voltage Degradation." ACS *Applied Energy Materials*. In print.
- Singer, A., M. Zhang, Y. S. Meng, et al. "Nucleation of Dislocations and Their Dynamics in Layered Oxides Cathode Materials during Battery Charging." *Nature Energy*. In print.

Presentations

- 233rd ECS Meeting, Seattle, Washington (May 13–17, 2018): "Structure and Voltage Recovery Driven by Defects Elimination in Li-Rich Layered Oxide Cathode Materials"; M. Zhang, H. D. Liu, and Y. S. Meng.
- 19th International Meeting on Lithium Batteries, Kyoto, Japan (June 17–22, 2018): "Role of Strain and Defects in Anion Redox Electrochemistry"; Y. S. Meng, M. Zhang, B. Qiu, and A. Singer. Keynote lecture.

Task 2.5 – *In Situ* Diagnostics of Coupled Electrochemical-Mechanical Properties of Solid Electrolyte Interphases on Lithium Metal Rechargeable Batteries

(Xingcheng Xiao, General Motors; Brian W. Sheldon, Brown University; Yue Qi, Michigan State University; and Y. T. Cheng, University of Kentucky)

Project Objective. The project objective is to develop a comprehensive set of *in situ* diagnostic techniques combined with atomic/continuum modeling schemes to investigate and understand the coupled mechanical/chemical degradation of the SEI layer/lithium system during lithium cycling. The goal of this understanding is to develop a new coating design strategy to achieve high cycle efficiency/dendrite free and extend the cycle life of high-energy-density batteries with lithium as the anode for EV application.

Project Impact. The fundamental understanding of the coupled mechanical/chemical degradation of the SEI layer during lithium cycling will enable the project to identify the desirable mechanical properties on SEI/lithium as a system and the specific transport properties that enable the homogenous lithium stripping/plating while avoiding the mossy structure. Furthermore, it will allow the project to develop a highly impactful strategy to protect lithium metal and achieve dendrite-free high cycle efficiency, which can dramatically increase the energy density of lithium batteries for EV applications.

Approach. Different *in situ* techniques, including AFM, nano-indentor, dilatometer, and stress-sensor, will be developed to investigate the mechanical compatibility between SEI and soft lithium and the relationship between surface morphology and current density distribution that results in an inhomogeneous lithium plating/stripping process. Multiple strategies will be developed to tailor the mechanical and transport properties of SEI and to properly engineer the protective coating/lithium interface.

Out-Year Goals. The out-year goals involve using *in situ* electrochemical tools to reveal failure mechanisms of SEI/lithium as whole electrode system, including correlating mechanical failure mechanisms of SEI/lithium, morphology evolution, cycle efficiency, and transport properties of SEI. Then, the project will develop continuum framework to establish the failure modes of SEI layer on lithium metal and provide the governing mechanical/material properties of SEI responsible for the critical failure mode based on the experimental results and atomic scale simulation.

Collaborations. Prof. Huajian Gao (Brown University) and Dr. Qinglin Zhang (GM) will be the key researchers involved in continuum simulation and postmortem analysis. Dr. Chongmin Wang (PNNL), Dr. Wangli Yang (LBNL), and Dr. Jie Xiao will be collaborators on advanced *in situ* analysis and electrolyte additives.

Milestones

1. A continuum model of SEI growth, which can predict potential SEI failure modes and incorporate them into the continuum model. (Q1, December 2017; Completed)
2. The impact of lithium deposition induced stress on lithium morphology and cycle efficiency. (Q2, March 2018; Completed)
3. The mechanical properties of SEIs measured by nanoindentation and the SEI composition measured by XPS. (Q3, June 2018; Completed)
4. Interface adhesion energy calculations; and predication of where interface delamination will occur. Lithium plating kinetics at a lithium/single-component SEI/electrolyte interface predicted by molecular dynamics (MD) simulation. (Q4, September 2018; On schedule)

Progress Report

A "Wrinkling-to-Ratcheting-to-Delamination" Failure Mechanism of Thin-Film Coatings as Artificial SEI Layer on Lithium Metal. In continuation of the team's previous studies on the wrinkling of a thin-film protective coating on a Li-metal electrode, a "wrinkling-to-ratcheting-to-delamination" failure mode was proposed, and an analytical model was developed to predict the design space for a mechanically stable coating that prevents interfacial delamination. In this model, the coating wrinkles during the first lithium deposition as the coating process induces a compressive stress in the coating. Thereafter, extensive plastic flow occurs in lithium during cyclic lithium deposition and stripping, leading to plastic ratcheting in the coating/Li system; this results in an accumulative increase of the amplitude of the wrinkled coating and thus increasing strain energy stored in the coating. After a sufficient number of cycles, the delamination of the coating from its underlying lithium metal becomes energetically favorable and occurs as the delamination energy release rate exceeds the interfacial toughness, which is detrimental to the battery performance due to the increased impedance through the loss of contact between the coating (as an artificial SEI layer) and lithium electrode.

The analytical model predicted a phase diagram of the failure mode with respect to the modulus and compressive stress of the coating normalized by the yield stress of lithium (Figure 32). The compositional strain in lithium, normalized interfacial toughness, and elastic limit of the coating were assumed to be 100%, 0.1%, and 0.3%, respectively. The orange line and red line in Figure 32 correspond to the predicted critical conditions for wrinkling and delamination, respectively. These two critical lines divide the phase diagram into three regions, representing three behaviors of the coating: no wrinkling, wrinkling, and wrinkling-induced interfacial delamination. The diagram affords a design space for a mechanically stable protective coating on lithium metal. To avoid delamination, the coating should have a moderate modulus, low compressive stress, high interfacial toughness, and low thickness.

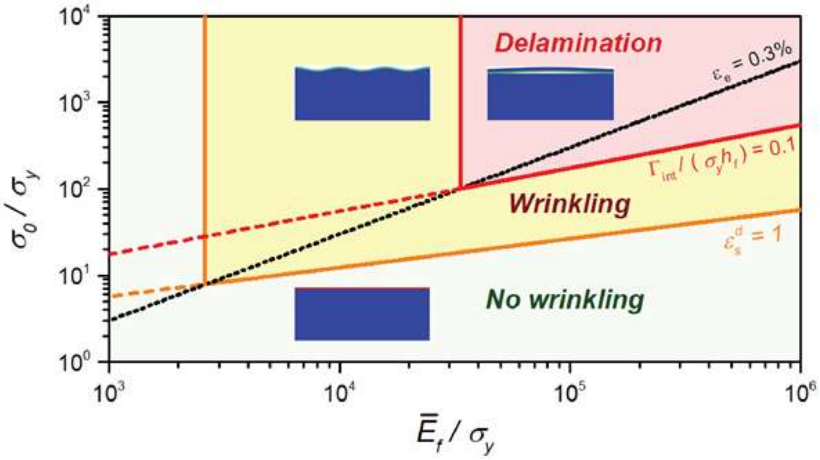

Figure 32. A phase diagram of wrinkling and delamination of a thin-film protective coating on a Li-metal electrode.

Surface Compositions of Lithium Electrodes Cycled in Four Different Electrolytes were Analyzed with XPS. To avoid air exposure, sample electrodes were stored in glove box and transferred to XPS and TOF-SIMS analysis chambers with respective special vessels. The same analyzing and sputtering parameters were applied to these samples. The XPS analyzing region has a diameter of 250 µm, and the sputtering region has a diameter of 1250 µm. In raw data, C-C peak at 285 eV may shift to a higher binding energy in some samples. Spectra curves shown later are calibrated based on the C-C peak at 285 eV. Figure 33 shows the XPS depth profiling spectra (Li 1s, C 1s, O 1s, F 1s, N 1s, S 2p) of lithium electrodes after the first plating (0.5 mA cm^{-2}, 4 mAh cm^{-2}) in four different electrolytes. For the SEI formed in the 4 M LiFSI DME electrolyte, Li_2CO_3, LiOH, LiF, Li_3N, and Li_2S are present on the surface. S 2p spectra indicate that the amount of Li_2S increases with the sputtering depth, reaching peak value after about 6 min. Li 1s and O 1s spectra show a small amount of Li_2O is on the surface and that its concentration increases and becomes stable after about 6 min of sputtering. On the contrary, F 1s spectra show LiF is distributing through the SEI and that its concentration deceases gradually. A similar phenomenon applies to Li_2CO_3, LiOH, Li_3N, and organic species such as RCOOLi and $ROCO_2Li$. For the SEI formed in the 0.4 M LiTFSI + 0.6 M $LiNO_3$ DOL-DME electrolyte, Li_2S only exists in the outer part of it and only a small amount of $Li_xS_yO_z$ species exists in the inner part. Other components have similar depth profiles compared with those formed in the 4 M LiFSI DME electrolyte. For the SEI formed in the 1 M LiTFSI DOL-DME electrolyte, learned from C 1s, F 1s, N 1s, and S 2p spectra, its surface layer contains some amount of LiTFSI salt because Li_3N, Li_2S, and $Li_xS_yO_z$ are decomposition products of LiTFSI. Residual LiTFSI disappeared after 30 s of sputtering. The sputtering interval is 30 s in this work. That means residual LiTFSI exists on the surface only. Other inorganic compounds on the surface include Li_2CO_3, LiOH, and LiF with decreasing concentrations, and Li_2O with increasing concentration. For the SEI formed in the 1 M $LiPF_6$ EC-DEC electrolyte, Li_2CO_3, LiOH, LiF, and Li_2O are present on the surface. The concentration of Li_2O increases with sputtering depth, while other components have decreasing concentrations.

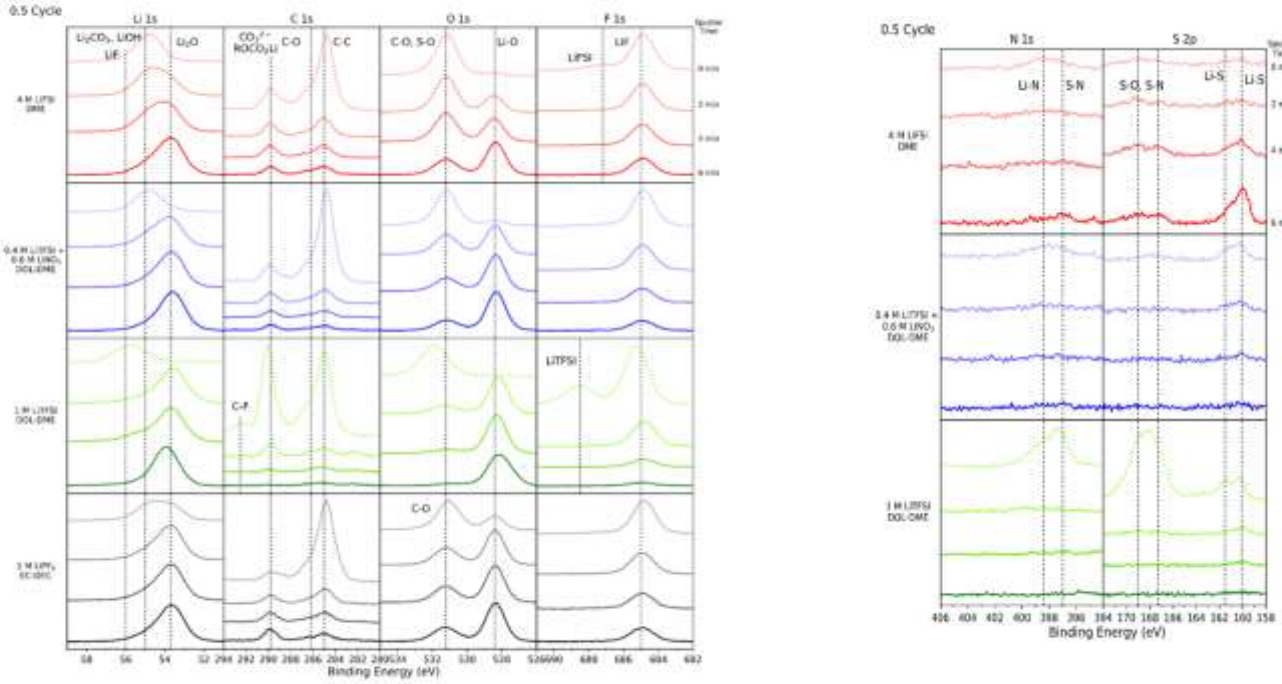

Figure 33. X-ray photoelectron spectroscopy depth profiling spectra (Li 1s, C 1s, O 1s, F 1s, N 1s, S 2p) of plated lithium surfaces after a half cycle (0.5 mA cm^{-2}, 4 mAh cm^{-2}) in four different electrolytes (4 M LiFSI DME, 0.4 LiTFSI + 0.6 M $LiNO^3$ DOL-DME, 1 M LiTFSI DOL-DME, and 1 M $LiPF^6$ EC-DEC).

Patents/Publications/Presentations

Publication

- Vinado, C., S. Wang, Y. Hec, X. Xiao, Y. Li, C. Wang, and J. Yang. "Electrochemical and Interfacial Behavior of All Solid State Batteries Using $Li_{10}SnP_2S_{12}$ Solid Electrolyte." *Journal of Power Sources* 396 (2018): 824–830.

Presentations

- 19th Annual Advanced Automotive Battery Conference, San Diego, California (June 4-5, 2018): "Surface and Interfacial Challenges and Opportunities in Rechargeable Lithium Batteries"; X. Xiao. Invited.
- 233rd ECS Meeting, Seattle, Washington (May 13–17, 2018): "*In Situ* Diagnostics of Coupled Electrochemical-Mechanical Failures of Solid Electrolyte Interphases on Lithium Metal for Rechargeable Batteries"; X. Xiao, J. Xu, B. Li, and Q. Zhang.
- 233rd ECS Meeting, Seattle, Washington (May 13–17, 2018): "Electrochemical Properties and Interfacial Behavior of All Solid-State Batteries Using $Li_{10}SnP_2S_{12}$ Solid Electrolyte"; C. Vinado, S. Wang, Y. Li, X. Xiao, and J. Yang.
- 233rd ECS Meeting, Seattle, Washington (May 13–17, 2018): "Mechanical Properties and Microstructure Evolution of Silicon Composite Electrodes"; Y. Wang, Q. Zhang, D. Li, J. Hu, J. Xu, D. Dang, X. Xiao, and Y. T. Cheng.
- DOE AMR, Washington, D. C. (June 18–21, 2018): "*In Situ* Diagnostics of Coupled Electrochemical-Mechanical Properties of Solid Electrolyte Interphases on Lithium Metal for Rechargeable Batteries"; X. Xiao.
- 18th U.S. National Congress for Theoretical and Applied Mechanics (USNCTAM), Chicago, Illinois (June 8, 2018): "Ratcheting-Induced Deformation and Failure in Li-ion Batteries"; K. Guo.

Task 2.6 – Microscopy Investigation on the Fading Mechanism of Electrode Materials (Chongmin Wang, Pacific Northwest National Laboratory)

Project Objective. The objective will be using a combination of *ex situ*, *in situ*, and *operando* HRTEM and spectroscopy to probe the fading mechanism of layer structured cathode under high-voltage operating condition. To complement the HRTEM study, *in situ* liquid cell SIMS and atom probe tomography (APT) will also be used to gain structural and chemical evolution of electrodes and correlate the structural and chemical evolution with battery performance.

Project Impact. The proposed characterization work focused on atomic level structural and chemical analysis and direct correlation with battery fading properties. The work can be directly used to guide the designing of electrode materials with tailored microstructure and chemistry for enhanced properties of increasing the energy density of Li-ion batteries and to accelerate market acceptance of EV, especially for PHEV required by the EV Everywhere Grand Challenge.

Approach. This project will use the unique *ex situ* and *in situ* TEM methods to probe the structure of Li-ion batteries, especially a biasing liquid electrochemical cell that uses a real electrolyte in a nano-battery configuration. It will also use various microscopic techniques, including *ex situ*, *in situ*, and especially the *operando* TEM system, to study the fading mechanism of electrode materials in batteries. This project will be closely integrated with other R&D efforts on high-capacity cathode and anode projects in the BMR Program to: (1) discover the origins of voltage and capacity fading in high-capacity layered cathodes, and (2) provide guidance for overcoming barriers to long cycle stability of electrode materials.

Out-Year-Goals. This project has the following out-year goals:

- Multi-scale (ranging from atomic-scale to mesoscale) *ex situ*/*in situ* and *operando* TEM investigation of failure mechanisms for energy-storage materials and devices. Atomic-level *in situ* TEM and STEM imaging to help develop fundamental understanding of electrochemical energy-storage processes and kinetics of electrodes.
- Extend the *in situ* TEM capability for energy storage technology beyond lithium ions, such as Li-S, Li-air, Li-metal, sodium ions, and multi-valence ions.

Collaborations. This project collaborates with Michael M. Thackeray and Jason Croy (ANL); Guoying Chen (LBNL); Jagjit Nanda (ORNL); Chunmei Ban (NREL); Khalil Amine (ANL); Donghai Wang (Pennsylvania State University); Arumugam Manthiram (University of Texas at Austin, UT Austin); Wei Tong (LBNL); Gao Liu (LBNL); Yi Cui (Stanford University); Jason Zhang (PNNL); Jun Liu (PNNL); Xingcheng Xiao (GM); Shirley Meng (UCSD); and Stan Whittingham (SUNY – Binghamton).

Milestones

1. Resolve the vacancy injection mechanism into the LM-NMC during the battery cycling and its correlation with battery fading mechanism. (Q2, March 31, 2018; Completed)
2. The functioning mechanism of electrolyte additive on the solid-liquid interphase in NMC cathode. (Q3, June 30, 2018; Completed)
3. Atomic level understanding of the mechanism of intergranular and intragranular cracking in NMC. (Q4, September 30, 2018; On schedule)

Progress Report

The key new information of this work is to report the functioning mechanism of enhanced cycling stability of cathode secondary particle in terms of capacity retention and voltage stability when the grain boundaries of the secondary particles are infused with a solid electrolyte.

It has been noticed that coating of NMC secondary particles with Li_3PO_4 and subsequent high-temperature annealing can lead to dramatic enhanced cycling stabilities of battery in terms of capacity retention, voltage decay, and thermal stability. Based on detailed STEM structural and chemical analysis, it is demonstrated that following the high-temperature annealing, the coated Li_3PO_4 is infused along the grain boundaries of the secondary particles. The infusion of grain boundary with solid electrolyte will eliminate penetration of liquid electrolyte into the grain boundaries of secondary particles, which subsequently eliminates the following detrimental factors: (1) intergranular cracking, (2) reaction of cathode with liquid, and (3) layer to disorder phase transition, as illustrated in Figure 34.

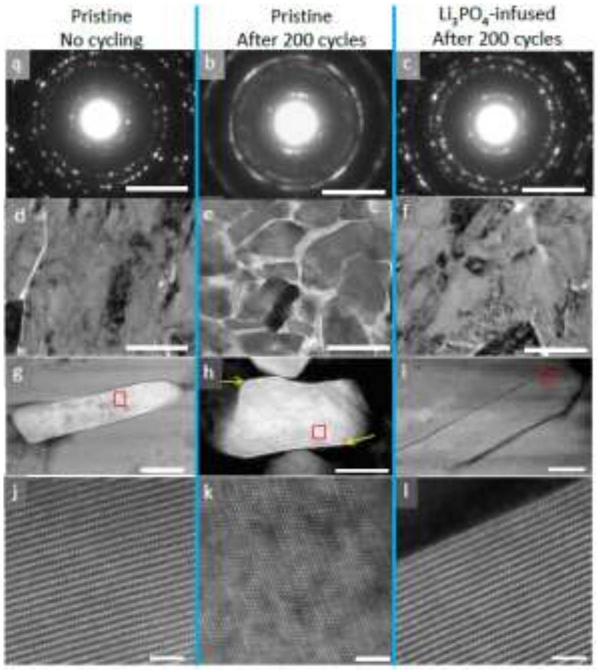

Figure 34. Infusion of Li_3PO_4 into secondary particles eliminates structural degradation. The structural degradations are evaluated by a combination of selected area electron diffraction (a-c), bright-field transmission electron microscopy imaging (d-f), scanning transmission electron microscopy – high-angle annular dark field (STEM HAADF) imaging (g-i), and atomic-level STEM-HAADF imaging (j-l, corresponding to the high magnification image of the redline marked regions). The left column corresponds to the pristine electrode without cycling, the middle column is the pristine electrode after 200 cycles, and the right column shows the Li_3PO_4-infused electrode after 200 cycles. These observations demonstrate that after 200 cycles, the pristine electrode shows significant structural degradation, featuring intergranular cracking and formation of amorphous phase within the grain boundaries (e), formation of surface reaction layer on each grain surface (indicated in h by the yellow arrows), and layered-to-spinel transformation (k), while these degradation features do not occur in the Li_3PO_4-infused electrode. The scale bars are 5 nm^{-1} in a-c, 500 nm in d-f, 100 nm in g-i, and 2 nm in j-l.

Further and most importantly, the present work indicates that cathode-liquid electrolyte interfacial reaction controls some of the critical steps that have been observed previously to contribute to the cycling stability of cathode. Therefore, the core step for addressing the barrier of cathode stability is to minimize the cathode-liquid electrolyte interaction.

The biggest challenge for the commercialization of layered structured nickel-rich lithium TM oxide cathode is the capacity and voltage fading. Resolving this problem over the years has followed an incremental progress. Tailoring of grain boundary structure and chemistry for optimization of materials behaviors and properties appears to be a classic protocol in material science. However, this strategy has hardly ever been used for the case of rechargeable battery. Herein, a new approach, based on tailoring grain boundary structure and chemistry in the secondary particles, has been developed to tackle these critical barriers in the system of Ni-rich layered cathode material, with $LiNi_{0.76}Mn_{0.14}Co_{0.10}O_2$ as a specific example.

The present work, for the first time, reveals unprecedented insight into how the cathode behaves in the case of not contacting with the liquid electrolyte, and ultimately points toward a general new route, via grain boundary engineering, for designing of better batteries of both solid-liquid and solid-state systems.

Patents/Publications/Presentations

Publication

- Yan, P., J. Zheng, J. Liu, B. Wang, X. Cheng, Y. Zhang, X. Sun, C. Wang, and J-G. Zhang. "Tailoring Grain Boundary Structures and Chemistry of Ni-Rich Layered Cathode for Enhanced Cycle Stability of Lithium-Ion Batteries." *Nature Energy* (Web Publication Date: June 2018).

Presentation

- Southern California Microscopy Society Meeting, University of Southern California (April 18, 2018): "Scanning/Transmission Electron Microscopy and Spectroscopy beyond Aberration Correction: *In Situ* Microscopy for Watching while It Happens"; C. M. Wang. Invited.

Task 2.7 – Understanding and Mitigating Interfacial Reactivity between Electrode and Electrolyte (Khalil Amine and Zhonghai Chen, Argonne National Laboratory)

Project Objective. To understand the pathway/mechanism of parasitic reaction between electrode materials and electrolyte for beyond Li-ion chemistries, and to stabilize the electrode/electrolyte interface for long life and safe battery chemistries.

Project Impact. The project is designed to have several areas of impact:

- To maximize the practical energy of battery chemistries beyond lithium ion,
- To improve the life and roundtrip energy efficiency of battery chemistries using S-based cathodes, and O_2-based cathodes, and
- To stabilize the lithium/electrolyte interface for high-energy-density lithium battery chemistries.

Approach. The project approach is multi-fold: (1) fundamental investigation of the pathway/mechanism of parasitic reactions between electrolytes and electrode materials, (2) rational mitigation of parasitic reactions based on the identified reaction pathway, (3) developing functional surface coating and electrolyte additives to suppress the chemical reactions between electrolytes and electrode materials, and (4) formulating new electrolyte to control the direct electrochemical reaction of electrolyte components.

Out-Year-Goals. When the electrode electrolyte interface is stabilized, the following results can be achieved:

- A cell with energy density of 600 Wh/kg, and
- A battery capable of operating for 500 cycles with low capacity fade.

Collaborations. The project collaborates with Dr. Gui-Liang Xu and Dr. Ang T. Ngo of ANL and with Prof. Chunsheng Wang of UMD.

Milestones

1. Synthesis of S/C composite cathode materials for Li/S batteries. (Q1, FY 2018; Completed)
2. Electrochemical characterization of S/C cathode. (Q2, FY 2018; Completed)
3. Investigation of the kinetics of parasitic reactions at the interface of S/C cathode. (Q3, FY 2018; Partially completed)
4. Investigation of the impact of sulfur load on both the electrochemical performance and kinetics of parasitic reactions. (Q4, FY 2018; In progress)

Progress Report

The dissolution of lithium polysulfide in the nonaqueous electrolytes during charge/discharge cycling of Li/S batteries has been widely considered the major contribution of low CE and poor life performance of Li/S batteries. Therefore, it is a widely adopted strategy to encapsulate the sulfur active material inside highly porous electric conductive medium, like nano-porous carbons, to reduce the direct exposure of lithium polysulfide toward the electrolyte. This quarter, the impact of the sulfur loading on the electrochemical performance of S/C was investigated.

Figure 35 shows the dependence of the electrochemical performance on the loading density of sulfur in the S/C composite. The electrolyte used for these cells is 1.0 LiTFSI in DOL/DME with 0.2 M $LiNO_3$ as the electrolyte additive. Without much surprise, the specific reversible capacity of the S/C electrode increases with the loading density of the sulfur, but the utilization of sulfur decreases with the loading density of sulfur. Meanwhile, the irreversible capacity loss decreases steadily the increase of the sulfur loading density (Figure 35b-c), although more unprotected sulfur is expected for high loading samples.

To gain more insight into the impact of sulfur loading on the dissolution of lithium polysulfide, a home-developed high precision leakage current measurement system was utilized to qualify the shuttling effect of lithium polysulfide inside the Li/S cell. Figure 36 shows the dependence of the static leakage current on both the working potential and the loading density of sulfur. When the potential is higher than 2.2 V, when sulfur is the dominant composition in the sulfur cathode, a small leakage current was observed, and the static leakage current showed no dependence on the loading density. The static leakage current peaks at about 2.1 V. At the low potential region (< 2.0 V), the static leakage current shows strong dependence on the loading density of sulfur; the higher the loading density, the smaller the leakage current is. Figure 36 suggests that more than one mechanism contribute to the shuttling effect of lithium polysulfide; the chemical details of these sides reactions will be further explored next quarter.

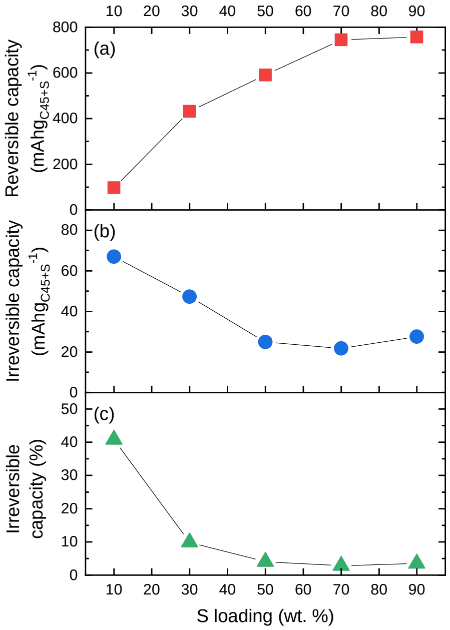

Figure 35. Dependence of (a) reversible capacity, (b) irreversible capacity loss, and (c) relative irreversible capacity loss of Li/C composite cathode on the loading density of sulfur in S/C composite.

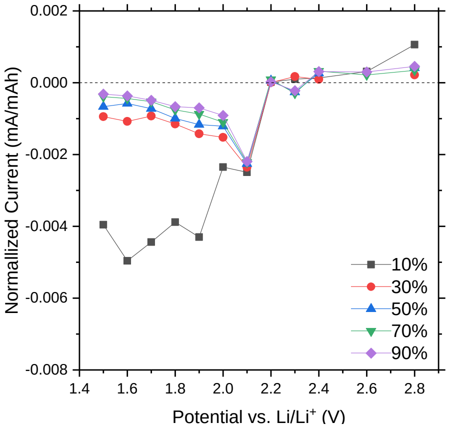

Figure 36. Dependence of the static leakage current on both the working potential and the loading density of sulfur in S/C composite.

Patents/Publications/Presentations

The project has no patents, publications, or presentations to report this quarter.

Task 2.8 – Correlative Microscopy Characterization of Electrochemical Hotspots in Oxide Electrodes (Yi Cui, William Chueh, and Michael Toney; Stanford/SLAC)

Project Objective. This project aims to develop and utilize a correlative microscopy platform to investigate the lithiation dynamics of LMR-NMC and NCA, with the specific goal of understanding factors that determine the rate capability and degradation mechanisms at the single primary particle length scale. By developing a nanoscale and single-particle understanding of lithiation, the project addresses specific engineering problems including electrochemical hotspot, electrode utilization, safety, and capacity/voltage fade.

Project Impact. Fundamental insights from this new diagnostic capability are expected to increase the power density and cycle life of oxide electrodes by improving electrode utilization, reducing electrochemical hotspots, decreasing capacity and voltage fade, and enhancing safety, which all improve the viability of Li-ion batteries for vehicle transportation. By understanding lithiation at the single-particle level, this project's success will contribute to improving on-vehicle battery management, such as charging/discharging protocol, and state-of-charge and state-of-health monitoring.

Approach. This project aims to develop a correlative microscopy platform to investigate the lithiation dynamics of LMR-NMC and NCA, with the specific goal of understanding factors that determine the rate capability and degradation mechanisms at the single primary particle length scale. On recharging time, the specific phenomena to be addressed include non-uniform current distribution and the correlation between surface property and the local lithiation rate. On degradation, phenomena to be addressed include correlating local chemistry and phases to capacity and voltage fading.

Out-Year Goals. Develop X-ray microscopy to investigate NMC and LMR-NMC cathodes at the single primary particle and single secondary particle level.

Collaborations. Commercial battery electrode particles are being supplied by Samsung.

Milestones

FY 2016

1. Development of correlative microscopy platform for imaging LMR-NMC cathodes. (Achieved)

FY 2017-2018

1. Synthesis and characterization of well-faceted NMC and NMC particles. Demonstrate *in situ* single particle imaging with spectro-ptychography of NMC. (Ongoing)
2. Use of correlative microscopy platform for imaging LMR-NMC and NMC cathode hotspots. (Ongoing)
3. Spectro-imaging of single NMC particles. (Ongoing)
4. *Ex situ* variable temperature (-20°C to +80°C) spectro-imaging of LMR-NMC particles. (Ongoing)

Progress Report

This quarter, the project investigated the apparent phase separation behavior in NMC cathodes. The team conducted *operando* XRD on single-layer pouch cells under mechanical compression using a specialized cell at Stanford Synchrotron Lightsource. Briefly, the cells are compressed by beryllium plates, which enables mechanical pressure while allowing X-rays to transmit. The team has obtained excellent agreement between state-of-charge determined electrochemically and via lattice constant refinements.

NMC-111 when delithiated to ~ 0.5Li is expected to exhibit a solid solution, though there has been reported phase separation under galvanostatic cycling experiments. Well-relaxed electrodes exhibit the expected Vegard relationship between lattice constant and the lithium content up to 0.5Li. However, upon galvanostatic charging, XRD reveals what appears to be phase separation, which intensifies with rate. Repeated cycling confirms that the phenomenon persists into later cycles, ruling out the effect of air reactivity, which has been observed in Ni-rich NMC. Electrode microstructure and thickness were controlled to avoid transport limitation within the porous electrode.

Preliminary modeling indicates that NMC-111, under sufficient current, is prone to "fictitious" phase separation, whereby a metastable mosaic distribution of fully lithiated and partially delithiated particles coexist within the same electrode. The modeling work was carried out in collaboration with Martin Bazant at Massachusetts Institute of Technology (MIT).

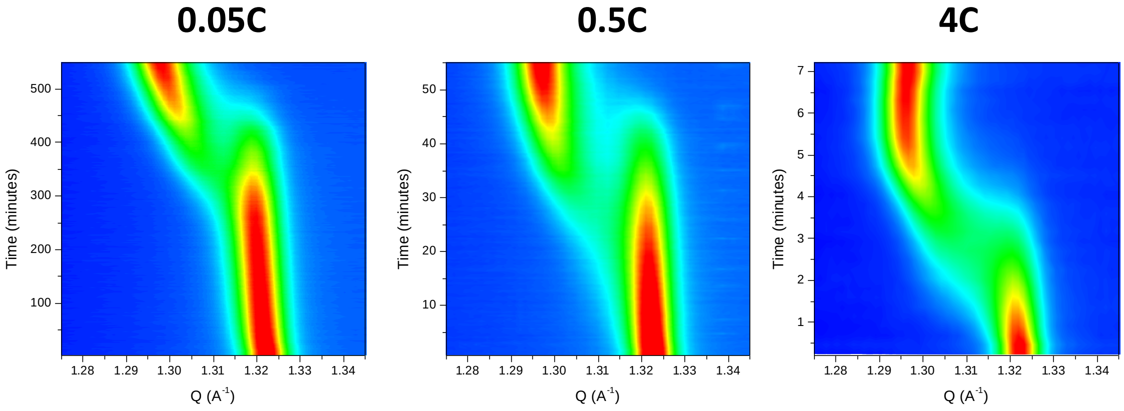

Figure 37. Rate-dependent *operando* X-ray diffraction of NMC-111 during first-cycle charging.

Patents/Publications/Presentations

Publication

- Hong, J., W. E. Gent, P. Xiao, K. Lim, D.-H. Seo, J. Wu, P. M. Csernica, C. J. Takacs, D. Nordlund, C.-J. Sun, K. H. Stone, W. Yang, D. Prendergast, G. Ceder, W. C. Chueh, and M. F. Toney. "Metal-Oxygen Decoordination Stabilizes Anion Redox in Li-Rich Oxides." Submitted (2018).

Presentations

- European Materials Research Society Meeting, Strasbourg, France (June 20, 2018); W. C. Chueh.
- Northwestern University, Department of Materials Science & Engineering, Evanston, Illinois (June 5, 2018); W. C. Chueh.
- MIT, Department of Materials Science & Engineering, Cambridge, Massachusetts (May 3, 2018); W. C. Chueh.
- Materials Research Society (MRS) Meeting, Phoenix, Arizona (April 3, 2018); W. C. Chueh.
- MRS Meeting, Phoenix, Arizona (April 2, 2018); W. C. Chueh.

TASK 3 – MODELING

Summary and Highlights

Achieving the performance, life, and cost targets outlined in the EV Everywhere Grand Challenge will require moving to next-generation chemistries, such as higher capacity Li-ion intercalation cathodes, silicon and other alloy-based anodes, Li-metal anode, and sulfur cathodes. However, numerous problems plague development of these systems, from material-level challenges in ensuring reversibility to electrode-level issues in accommodating volume changes, to cell-level challenges in preventing cross talk between the electrodes. In this task, a mathematical perspective is applied to these challenges to provide an understanding of the underlying phenomenon and to suggest solutions that can be implemented by the material synthesis and electrode architecture groups.

The effort spans multiple length sales from *ab initio* methods to continuum-scale techniques. Models are combined with experiments, and extensive collaborations are established with experimental groups to ensure that the predictions match reality. Efforts are also focused on obtaining the parameters needed for the models, either from lower-length scale methods or from experiments. Projects also emphasize pushing the boundaries of the modeling techniques used to ensure that the task stays at the cutting edge.

In the area of intercalation cathodes, the effort is focused on understanding the working principles of the high nickel layered materials with an aim of understanding structural changes and the associated changes in transport properties. Coatings, an effective strategy for high-voltage operation, are being explored with the aim of providing a rational design approach for new coating materials. In addition, focus is paid to the assembling of porous electrodes with particles to predict the conduction behavior and developing tools to measure electronic conduction.

In the area of silicon anodes, the effort is in trying to understand the interfacial instability and suggest ways to improve the cyclability of the system.

In the area of Li-metal anodes, the focus is on understanding how materials can be designed to prevent dendrite growth using continuum modeling approaches, combined with calculations on mobility in solid conductors. The results are used to guide materials development by providing the properties needed to prevent dendrites while also achieving the energy and power goals. Models are also starting to examine the role of the SEI on the morphology of the dendrite and to describe the mechanical-electrochemical coupled effects that are critical for dendrite formation.

Task 3.1 – Design of High-Energy, High-Voltage Lithium Batteries through First-Principles Modeling (Kristin Persson, Lawrence Berkeley National Laboratory)

Project Objective. This project supports VTO programmatic goals by developing next-generation, high-energy cathode materials and enabling stable cathode operation at high voltages through target particle morphology design, functional coatings, and rational design of electrolytes. The end-of-project goals include: (1) novel disordered, high-rate Li-excess cathodes, (2) new fundamental understanding of the cathode/electrolyte interface and the factors that control the interfacial chemistry and interfacial impedance, (3) critical surface and coating design and optimization strategies that will improve cycling of Li-ion battery cathodes, and finally (4) understanding of the factors that govern stability in nonaqueous electrolytes for Li-ion and Li-S systems.

Project Impact. To enhance the performance of Li-ion systems, improvements on the cathode and the electrolyte side are needed. This project is aimed to result in an improved understanding of the atomistic mechanisms underlying the surface behavior and performance of the Li-ion cathode materials, with the ultimate goal being to suggest strategies, such as coatings, surface protection, and particle morphology design. Furthermore, fundamental studies of electrolyte stability, as a function of solvent and salt concentrations, and components will be conducted.

Approach. First-principles calculations, both static and dynamic approaches, are used to model solid-state electrode material thermodynamics and kinetics. Liquid electrolytes are modeled through coupled classical MD and first-principles methods to accurately capture solvation structure as well as reactivity of liquid system.

Out-Year Goals. Stable interfaces will be determined by focusing initially on degradation mechanisms related to the release of surface oxygen at high charge. Tuning particle morphology and coating materials—both of crystalline as well as amorphous structure—will be explored using the Materials Project. For the electrolyte development, work will be aimed toward understanding the atomistic interactions underlying the performance of lithium electrolytes specifically elucidating the solvation structure (as a function of salt concentration) and its impact on the stability of different liquid constituent species.

Collaborations. This project is highly collaborative between BMR PIs G. Chen (LBNL), G. Ceder (LBNL), and V. Srinivasan (ANL). Cathode design and synthesis will be performed by Chen and Ceder, surface design by Persson, and electrolyte design and testing by Persson and Srinivasan.

Milestones

1. Finish modeling of $LiAsF_6$ in weakly dissociating solvent. Identification of concentration limit causing change in Li^+ solvation structure between contact-ion-pair and solvent separated species. (Q1, December 2017; Completed)
2. Finish modeling of $LiPF_6$ in weakly solvating solvent. Identification of concentration limit causing change in Li^+ solvation structure between contact-ion-pair and solvent separated species. (Q2, March 2018; Completed)
3. Modeling of dielectric constant of complex Li^+ electrolytes using MD. (Q3, June 2018; Completed)
4. *Go/No-Go Decision*: Test algorithm against experimental results to assess whether the project's model can quantitatively capture the change in dielectric behavior as a function of concentration and different solvation structures. If not, change approach. (Q3, June 2018; Completed)
5. Present simulated kinetic and thermodynamic evaluations of lithiation mechanisms of amorphous silicon and SiO_2. (Q4, September 2018; Completed)

Progress Report

The equilibrium potential profiles of the systems were found by the change in energy between each stable composition with respect to the change in lithium content. In the calculated voltage profile for Li_xSi, Figure 38a, the crystalline states follow a discrete pathway from 0.39 V to 0 V. In the amorphous lithium silicides, the lithiation voltage is initially found to be higher than the crystalline voltage, 0.54 V, until x_{Li}=0.5, where it drops below and follows the crystalline states.

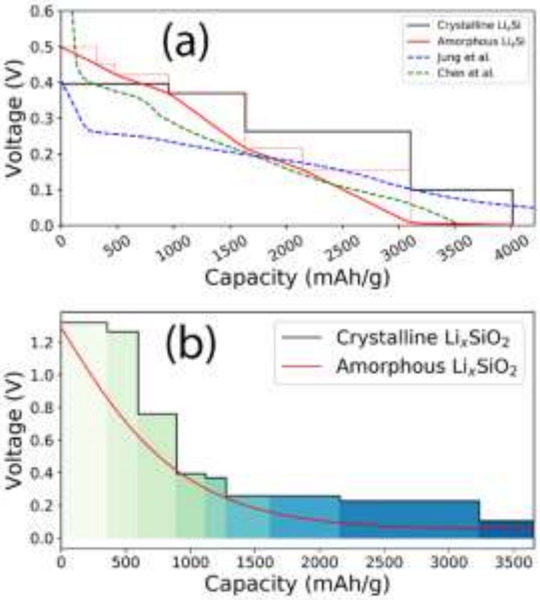

Figure 38. Predicted potential profiles for (a) silicon and (b) SiO_2, as referenced to the phase diagram.

Similar to the case of silicon lithiation, the potential profile for Li_xSiO_2 was derived from the chemical potential of lithium within the composition range between adjacent stable compositions. In the crystalline phases, the initial voltage of SiO_2 exceeds that of silicon by almost 1 V. As lithiation progresses and a Li-Si environment forms, the voltage drops to values closer to that of Li_xSi. The amorphous phases follow a similar trajectory, initially exhibiting a high potential of 1.29 V, and ending at 0.06 V. These findings agree qualitatively with previous studies on bulk SiO_2 that exhibit voltage profiles higher than that of silicon, between 1.0-1.5 V. The preferred equilibrium phase sequence upon lithiation shows the strength of, and preference toward, the formation of Li-Si and Li-O bonds at the expense of Si-O bonds. The formation of Li_xSi and Li_2O local environments will occur, even in the first charge, if the anode voltage drops below ~ 100 mV versus lithium metal. During discharge, the lithiated composite (surface phase and bulk) will delithiate in order of increasing potential such that the lithium silicides within the oxide layer and silicides in the bulk silicon will delithiate first, forming Li_xSi and Li_4SiO_4. Only after the Li_xSi phases have completely delithiated will Li_4SiO_4 be delithiated to form SiO_2.

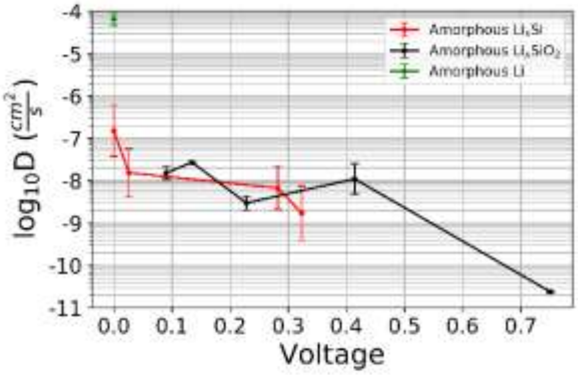

Figure 39. Lithium self-diffusivity diffusion coefficients in lithium silicides and lithium silicates as a function of voltage versus lithium.

Lithium self-diffusivities were calculated from AIMD simulations, with a fixed number of atoms, volume, and temperature (NVT), through the Stokes-Einstein relation over 200 ps trajectories at 500 K, 1000 K, and 1500 K. Room temperature lithium self-diffusivity is obtained from the Arrhenius relation. The team finds diffusivities on the order of 10^{-7} to 10^{-11} cm^2/s as shown in Figure 39, which is near the large range reported in literature, of 10^{-9} to 10^{-16} cm^2/s. The team observes an upward trend in diffusivity with decreasing voltage. Intuitively, as percolating Li-rich environments and pathways are formed within the amorphous matrix, the team expects the lithium diffusivity in Li-rich silicon to approach that of lithium metal.

Patents/Publications/Presentations

Presentation

- DOE AMR, Washington, D. C. (June 18–21, 2018): "Washington Predicting and Understanding Novel Electrode Materials From First-Principles"; Kristin A. Persson. Poster.

Task 3.2 – Addressing Heterogeneity in Electrode Fabrication Processes (Dean Wheeler and Brian Mazzeo, Brigham Young University)

Project Objective. The project goal is to better understand connections between fabrication conditions and undesired heterogeneity of thin-film electrodes by means of new nondestructive inspection techniques and computer models.

Project Impact. This work will result in new diagnostic and modeling tools for rapidly and conveniently interrogating how well homogeneity has been maintained in electrodes during fabrication and in subsequent cycling. Real-time measurement of heterogeneity will enable manufacturer quality control improvements. The measurement and modeling tools will further enable researchers to compare different electrodes, improve formulations and processes, and anticipate cell performance of new designs.

Approach. Two non-destructive inspection techniques will be developed or improved that will characterize electrochemical and mechanical uniformity of the electrodes. The first tool will be a flexible contact probe on a polymer substrate for rapidly measuring local electrical conductivity across electrodes of any geometry. The second tool will be a new acoustic probe that measures local elasticity and density of the composite film. These two prototyping efforts will be tied together by a particle-based microstructure model that allows prediction and correlation of electrode conductive and mechanical properties with fabrication conditions.

Out-Year Goals. This project was initiated October 2016 and concludes September 2019. Overall goals by fiscal year are as follows:

- **2017.** Fabricate first-generation flexible conductivity probe and proof-of-concept of acoustic probe. Improve microstructure model to match experiment.
- **2018.** Integrate flex probe with test fixtures suitable for assessment of large or continuous samples. Demonstrate measurement of localized ionic conductivity.
- **2019.** Assess affect of heterogeneity on cell charge and discharge performance. Further improve accuracy and reliability of probe and modeling technologies.

Collaborations. Ram Subbaraman and Jake Christensen (Bosch), Daniel Abraham (ANL), Steve Harris (LBNL), Bryant Polzin (ANL), and Chisu Kim (Hydro-Quebec, HQ) have provided battery materials for analysis. Other collaborations and the transfer of this technology to interested parties are being pursued.

Milestones

1. Integrate flex probe with off-the-shelf CNC positioning system to enable interrogation of large-format electrode films. (Q1, December 2017; Completed)
2. Integrate flex probe with prototype rolling apparatus to enable interrogation of continuous-roll electrode films. (Q2, March 2018; Completed)
3. *Go/No-Go Decision*: Demonstrate that localized conductivity probe has adequate reliability for continued development. Criteria: Localized ionic conductivity probe can match macroscopic results for a representative electrode sample. (Q3; Partially completed)
4. Quantify the durability of multiple flex probes to validate suitability for industrial use. (Q4; In progress)

Progress Report

Milestone 3 (Partially Complete). Methods exist for measuring ionic conductivity of battery films, but they generally measure bulk conductivity for large volumes. Taking measurements with a microprobe allows the possibility of determining local ionic conductivity and the degree of heterogeneity for this critical property. There is a great need to determine local ion transport, as this correlates with active material utilization and, in the case of anodes, the cause of localized lithium plating during fast charging. This quarterly milestone was to show proof of concept of measuring ionic conductivity with the conductivity microprobe previously designed at Brigham Young University (BYU).

Measurements were taken separately with electrolyte only, separator, anode, and cathode. Results indicate that the method clearly distinguishes between different conductivity values of these materials. However, a more detailed computer model must be completed to properly invert the experiments and make the method quantitative. For this reason, the milestone is considered partially complete. It is expected that the inversion model and therefore milestone will be fully completed next quarter.

Figure 40 shows the experimental set-up with an electrolyte-soaked electrode on the microprobe. In a given test, the probe is sampling conductivity for an electrode area of approximately 100 µm × 450 µm. When the conductivity is varied and other conditions are held constant, the EIS spectra show a clear trend with conductivity. Figure 41 shows typical Nyquist curves for different electrolytes, demonstrating that the method can distinguish even modest variations in conductivity.

This quarter a new research collaboration with Eagle Picher was developed. Collaborations with Robert Bosch NA and K2 were further developed.

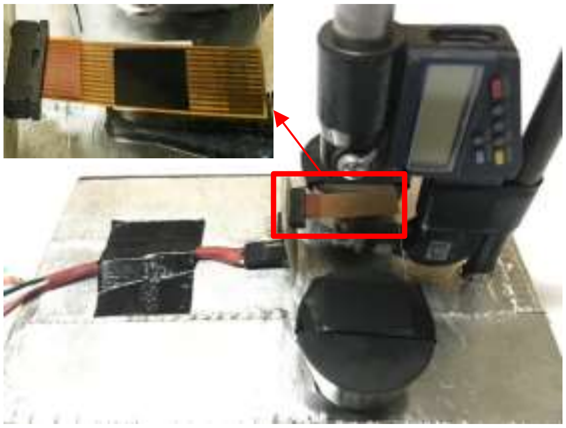

Figure 40. The experimental setup of micro-probe with a sample of delaminated cathode.

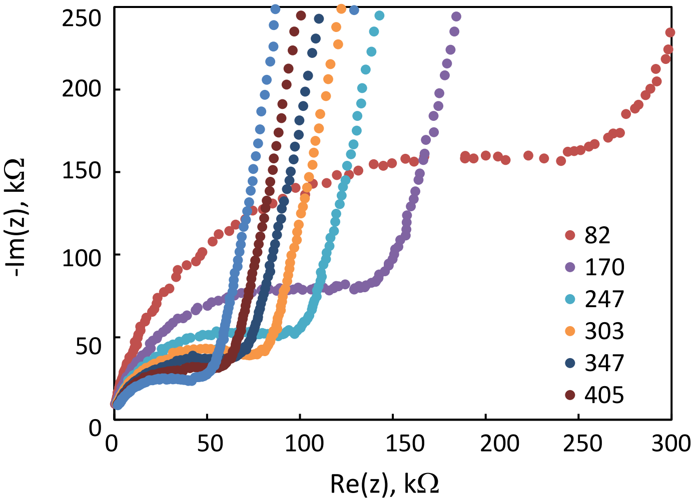

Figure 41. Electrochemical impedance spectroscopy Nyquist spectra of different electrolyte samples with conductivities varying from 82 to 443 µS/cm.

Patents/Publications/Presentations

Publications

- Forouzan, M. M., B. A. Mazzeo, and D. R. Wheeler. "Modeling the Effects of Electrode Microstructural Heterogeneities on Li-Ion Battery Performance and Lifetime." *Journal of the Electrochemical Society* 165, no. 10 (2018): A2127–A2144.
- Dallon, K. L., J. Yao, D. R. Wheeler, and B. A. Mazzeo "Characterization of Mechanical Properties of Battery Electrode Films from Acoustic Resonance Measurements." *Journal of Applied Physics* 123 (2018): 135102.

Presentations

- DOE AMR, Washington, D. C. (June 18–21, 2018): "Addressing Heterogeneity in Electrode Fabrication Processes"; B. A. Mazzeo and D. R. Wheeler.
- 233rd ECS Meeting, Seattle, Washington (May 13–17, 2018): "How to Deal with Electrode Heterogeneity in Cell-Level Battery Modeling"; D. R. Wheeler. Invited.
- 233rd ECS Meeting, Seattle, Washington (May 13–17, 2018): "Effects of Local Tortuosity and Porosity Heterogeneities on Charge and Discharge Performance of Li-Ion Batteries"; M. M. Forouzan, D. R. Wheeler, and B. A. Mazzeo.
- 233rd ECS Meeting, Seattle, Washington (May 13–17, 2018): "Local Variation in Microstructure Causes Heterogeneity in the Conductivity of Commercial Lithium-Ion Cathode Films"; J. E. Vogel, E. E. Hardy, S. Crawford, B. A. Mazzeo, and D. R. Wheeler.
- 233rd ECS Meeting, Seattle, Washington (May 13–17, 2018): "Slurry Model for Understanding Fabrication of Li-Ion Battery Electrodes"; M. Nikpour, J. Cordon, D. R. Wheeler, and B. A. Mazzeo.
- 233rd ECS Meeting, Seattle, Washington (May 13–17, 2018): "The Effect of Different Mixing Processes on the Ionic and Electronic Conductivities of Li-Ion Battery Electrodes"; F. Pouraghajan, A. I. Thompson, J. E. Vogel, B. A. Mazzeo, and D. R. Wheeler.

Task 3.3 – Understanding and Strategies for Controlled Interfacial Phenomena in Lithium-Ion Batteries and Beyond
(Perla Balbuena and Jorge Seminario, Texas A&M University; Partha Mukherjee, Purdue University)

Project Objective. The project objective is to evaluate and characterize interfacial phenomena in lithiated silicon and Li-metal anodes and to develop guidelines for potential solutions leading to controlled reactivity at electrode/electrolyte interfaces of rechargeable batteries using advanced modeling techniques based on first principles.

Project Impact. Understanding SEI growth on constantly evolving silicon surfaces and on highly reactive Li-metal surfaces is expected to define the electrolyte properties required in high-performance cells. Strategies to control the silicon anode instability and pulverization issues and the well-known safety and short effective lifetimes of Li-metal anodes will be developed by tuning the electrolyte composition, structure, dynamic, and stability, as well as that of the electrode morphology and interactions with the electrolyte, based on multiple characterizations of interfacial phenomena.

Approach. A comprehensive multiscale modeling approach including first-principles *ab initio* static and dynamics, classical MD, and coarse-grained mesoscopic models will focus on the roles of the electrolyte chemical, structural, and dynamical properties and of the electrode micro- and nano- structure on the formation and evolution of the SEI layer and associated electrochemical performance on silicon and on Li-metal anodes.

Out-Year Goals. Work will progress toward characterizing lithiation and SEI formation at silicon surfaces as well as the subsequent cracking and reforming events under the most realistic modeling conditions. Similarly, the project will investigate electrolyte effects on reactivity and dendrite formation in Li-metal surfaces. The project aims to capture how the chemistry of the various electrolyte components (mainly liquids, but also solid polymers and gels) affects the main issues that influence the electrode performance.

Collaborations. This project funds work at Texas A&M University (TAMU). Prof. G. Somorjai (UC Berkeley), Prof. Shahbazian Yassar (UIC), and Dr. Vijayakumar Murugesan have also contributed to the project.

Milestones

1. Complete analysis of effects of Li-substrate interactions on lithium deposition. (Q1, FY 2018; Completed)
2. Complete study of SEI reactions over lithium deposits. (Q2, FY 2018; Completed)
3. Complete analysis of operating conditions on dendrite growth. (Q3, FY 2018; Completed)
4. Complete evaluation of co-deposition effects. Establish comparisons with experimental trends. (Q4, FY 2018)

Progress Report

Chemistry of Lithium Plating. The team continued investigating the electronic structure of lithium during electro-deposition. Figure 42 illustrates how the *DFT-calculated* charge density difference (before and after electrodeposition) varies in the z-direction perpendicular to the surface for a pair $Li^+PF_6^-$ located in the proximity of the lithium surface. The ion is fixed to avoid the ion-pair formation. The surface has a defect of 4 lithium atoms defining a hollow site where the new lithium atom deposits. The charge density difference profile reveals how the charge accumulates in the vicinity of the deposited ion (yellow region), whereas it becomes depleted in the subsurface (light blue). A manuscript explaining these points is under review. This is only the first part of a series of investigations that is being carried out to evaluate with detail (for the first time) the electronic distribution during electrodeposition and the effects of the surrounding environment (SEI layer components).

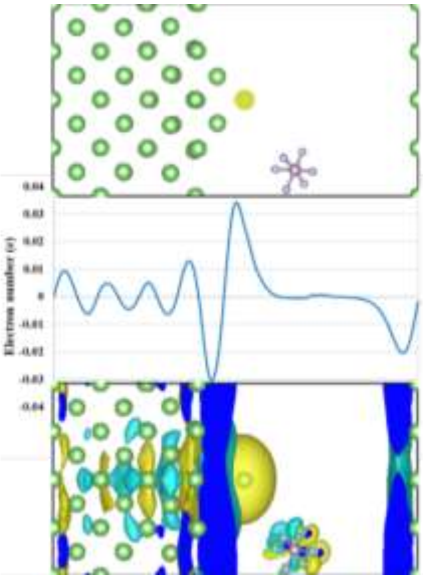

Figure 42. Charge density difference profile when a lithium ion is deposited on top of a defective lithium surface. Yellow: charge accumulation. Light blue: charge depletion.

Effects of Temperature and C-Rate on Dendrite Growth. *Classical MD* simulations of dendrite growth reported last quarter were further analyzed to study effects of higher temperatures and C-rates on dendrite growth. The study emulates charge of a battery with a Li-metal anode covered by a cracked LiF SEI film in contact with a liquid EC with 1 M $LiPF_6$ electrolyte. Preliminary observations indicate that: (a) the dendrite is porous; it is a low-density structure with void spaces; (b) high temperatures (400 K) favor smoother lithium deposition due to higher ionic diffusion, causing time to short-circuit to increase; and (c) high C-rate helps and low C-rate hinders the lithium dendrite formation. At high C-rate, the fast flow of ions deposits and reduces near the base of the dendrite creating an amorphous solid that exerts pressure from the dendrite base allowing its continuous growth. As they grow, dendrites become more porous with larger volume and height.

The same problem was studied with *mesoscale models*. A model for lithium electrodeposition was developed, taking into account three processes. In the vicinity of the SEI, lithium ions dissolve and adsorb on the SEI upper surface, and then diffuse through the SEI layer. At the Li-metal – SEI interface, lithium ions are reduced and directly deposited on the lithium anode surface, accompanied by electron transfer. A flat, homogeneous SEI layer is used to investigate lithium plating on the anode film. The battery operating temperature is set to 300 K. To quantify the roughening of Li-metal – SEI interface, the roughness parameter is defined as

$$R_a = \frac{1}{L}\int_0^L \left|x - x_c\right| \mathrm{d}y, \ (1),$$

where R_a is the arithmetical average deviation of the assessed profile, x is the vertical distance from the mean line, x_c is the height of the mean line, and y is the corresponding position in the horizontal direction. The interface roughness of the Li-metal – SEI was calculated as a function of local overpotential (synonymous with C-rate). The roughness exponentially increases with the local overpotential. Specifically, the roughness remarkably increases when the overpotential exceeds 0.22 V. Eventually, the drastic change in the roughness of undulating Li-metal – SEI interface initiates the formation of lithium dendrite. In this case (T = 300 K), lithium dendrite is initiated at the overpotential of 0.24 V. High overpotential yields high current density. lithium is prone to form dendrite under high current density. In addition, temperature could also affect lithium electrodeposition. For a given local overpotential, lithium is uniformly distributed over the anode surface at high temperature. However, as temperature decreases, the morphology could experience a transition from uniform lithium deposits to lithium dendrite. Li-ion diffusivity in SEI is significantly reduced as temperature goes down, and thus, the sluggish Li-ion transport is primarily responsible for lithium dendrite growth at relatively low temperature.

Patents/Publications/Presentations

Publications

- Qin, X., M. Shao, and P. B. Balbuena. “Elucidating Mechanisms of Lithium Plating on Lithium Anodes of Lithium-Based Batteries.” Under review.
- Tewari, D., Z. Liu, P. B. Balbuena, and P. P. Mukherjee. “Mesoscale Understanding of Lithium Electrodeposition for Intercalation Electrodes.” Under review.
- Bertolini, S., and P. B. Balbuena. “Buildup of Solid Electrolyte Interphase on Lithium-Metal Anode: Reactive Molecular Dynamics Study.” *Journal of Physical Chemistry C* 122 (2018): 10783–10791.
- Han, J. and P. B. Balbuena. “First-Principles Calculations of Oxidation Potentials of Electrolytes in Lithium-Sulfur Batteries and Their Variations with Changes in Environment.” *Physical Chemistry Chemical Physics.* In press.

Presentations

- ElecNano, Nancy, France (May 30, 2018): “Understanding the Origins of Dendrite Formation during Lithium Plating at the Nanoscale Level”; P. B. Balbuena, X. Qin, M. Shao, L. Camacho-Forero, S. Bertolini, E. Kamphaus, and M. S. Angarita-Gomez.
- DOE AMR Meeting, Washington, D. C. (June 20, 2018): “Understanding and Strategies for Controlled Interfacial Phenomena in Lithium-Ion Batteries and Beyond”; P. B. Balbuena. Poster b329.
- ElecNano, Nancy, France (May 31, 2018): “Molecular Dynamics Simulations of a Solid Electrolyte Interphase Cracking and Dendrite Formation in Silicon Anodes of a Li-ion Nanobattery”; J. M. Seminario, D. E. Galvez-Aranda, and L. A. Selis.
- NREL, Golden, Colorado (June 26, 2018): “Solid Electrolyte Interphase Cracking and Dendrite Formation in Silicon Anodes of a Li-Ion Nanobattery”; J. M. Seminario. Invited lecture.
- 233rd ECS Meeting, Seattle, Washington (May 15, 2018): “Cracks and Dendrites in Solid Electrolyte Interphases in Lithium-Ion Nanobatteries: Molecular Dynamics Simulations”; J. M. Seminario, D. E. Galvez-Aranda, and L. A. Selis.

Task 3.4 – Electrode Materials Design and Failure Prediction (Venkat Srinivasan, Argonne National Laboratory)

Project Objective. The project goal is to develop a continuum-based mathematical model to (i) investigate the impact of SEI layer on the growth of dendritic protrusions, and (ii) elucidate the deposition mechanism and deposit morphology observed on top of the carbon substrate in Li-S battery cathodes. Mechanical stiffness and transport mechanism of lithium through the SEI layer can significantly affect the nucleation of dendritic protrusions on top of Li-metal anodes. Effectiveness of protective layers in preventing the growth of lithium dendrites can also be studied by using this methodology. Next-generation, high-energy-density Li-S batteries experience limited capacity due to cathode surface passivation because of the precipitation of Li-sulfides during the discharge process. Understanding the morphology of precipitates can significantly help to develop strategies that can minimize the surface passivation and improve the practical specific capacity of Li-S batteries. The main focus will be to develop microscale models capable of successfully capturing the multiscale multiphysics phenomena that occur during Li-metal and Li-sulfide deposition processes.

Project Impact. Based on the work conducted as part of this project, better understanding of the different mechanisms responsible for degradation in Li-metal anodes and Li-S batteries can be developed. Based on these understandings, different strategies can be devised to minimize the impact of degradation mechanisms and enhance the performance and lifetime of next-generation Li-ion batteries.

Project Approach. The approach used here is to develop mesoscale models, based on continuum modeling, to describe the critical processes in the materials and combining them with electrochemical, microscopic, and spectroscopic data to ensure parameter estimation and model validation. The model is then used to provide insights to impact of material properties on performance and life, and guidance for design of new materials.

Out-Year Goals. At the end of this project, mathematical models will be developed that can capture the impact of diffusivity, conductivity, transference number, solubility, and mechanical stiffness of various species on the morphology of lithium and Li-sulfide deposits on top of Li-metal and carbon substrates, respectively.

Collaborations. This project has no collaborations this period.

Milestones

Incorporate SEI Layer in Li-Metal Dendrite Model

1. Incorporate SEI layer in lithium dendrite growth model and analyze its influence on growth of dendritic protrusions. (Q1, December 31, 2017; Completed)

2. Evaluate the impact of mechanical properties and thickness of SEI layer on propensity for dendrite growth. (Q2, March 31, 2018; Completed)

Mathematical Model for Sulfur Redistribution

3. Develop a model to examine the precipitation process of lithium sulfide during battery discharge. (Q3, June 30, 2018; Completed)

4. Develop a mathematical model to describe surface morphology evolution in sulfur cathode. (Q4, September 30, 2018; In progress)

Progress Report

Develop Mathematical Models to Evaluate the Precipitation Process of Lithium-Sulfide during Battery Discharge Process. Much published research has indicated that active surface passivation caused by Li_2S precipitation can significantly reduce sulfur utilization and greatly limit battery charge-storage capacity and cycle life. This quarter, research work targeted evaluating this precipitation process of Li_2S on the active sulfur electrode surface by mathematical modeling. Based on electrochemical kinetics and thermodynamics, a phase field modeling approach was developed to describe "deposition" of Li_2S during battery discharge process and "removal" of Li_2S during charge process on the active cathode surface. As shown in Figure 43, a one-dimensional geometry is applied, in which two reactions are assumed to describe Li_2S film generation (discharge) and removal (charge), respectively. Meanwhile, for simplicity, a few assumptions are applied: reactions are only considered on the active carbon surface, and nucleation of Li_2S in the electrolyte is neglected. Because Li_2S has very low electron conductivity ($\sim 10^{-13}$ S/m), the surface passivation process is simulated through surface coverage increase of Li_2S on the active carbon surface along with the discharge process.

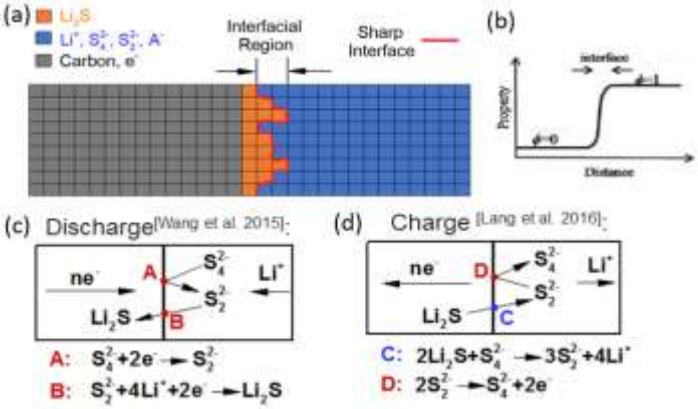

Figure 43. (a) One-dimensional model geometry for the electrode-electrolyte interfacial region. (b) Phase field model converts the sharp interface into a continuous interfacial region by a phase parameter. (c) Electrochemical reactions assumed for the Li_2S precipitation process in the battery discharge process. (d) Electrochemical/chemical reactions assumed for Li_2S removal during battery charge process.

Modeling results are shown in Figure 44. On the carbon surface, as shown in Figure 44a, Li_2S film growth (precipitation process) and removal in discharge-charge process follow different trends. This originates from the different electrochemical/chemical reactions taking place during discharge and charge. Under different discharge/charge current conditions, model indicates that current increase can greatly reduce the time needed for Li_2S growth until its surface coverage reaches 100% (Figure 44b), while its influence on the time needed for Li_2S removal in the charge process is not comparable (Figure 44c). This implies high C-rates can potentially lead to Li_2S accumulation on the active electrode surface in the discharge-charge cycles, since the time needed for Li_2S film growth could be longer than that needed for Li_2S film removal.

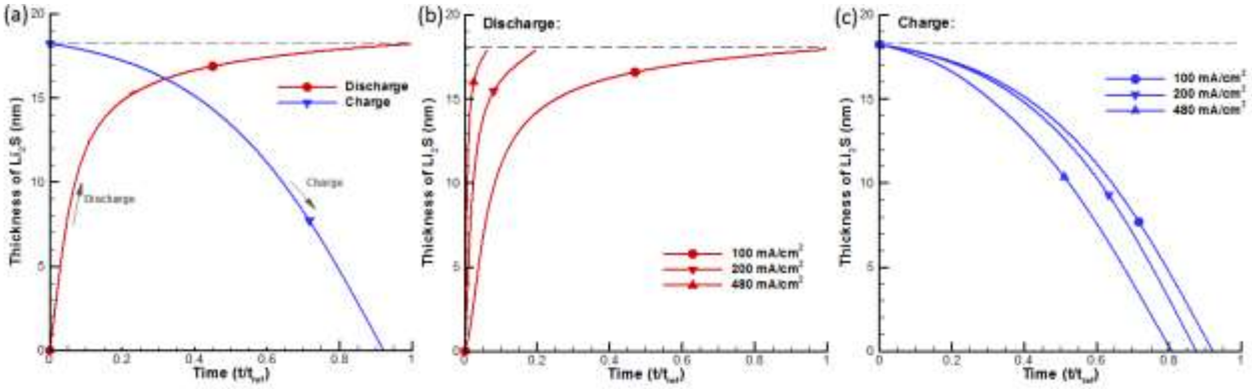

Figure 44. (a) Modeled Li_2S film growth on the active carbon surface in the discharge, and Li_2S film removal in the charge. (b) Li_2S film thickness growth under different discharge current conditions: 100 mA/cm², 200 mA/cm², and 480 mA/cm². (c) Simulated Li_2S film thickness variation under different charge current conditions.

Patents/Publications/Presentations

Presentation

- 233rd ECS Meeting, Seattle, Washington (May 13–17, 2018): “Mathematical Modeling of the Li_2S Precipitation Process in Li-S Battery”; Y. Xie and V. Srinivasan.

Task 3.5 – First-Principles Calculations of Existing and Novel Electrode Materials (Gerbrand Ceder, Lawrence Berkeley National Laboratory)

Project Objective. The main project objectives are as follows: (1) develop very high-capacity, layered cathodes with high structural stability (> 250 mAh/g) and high surface stability; (2) clarify the role that Li-excess and cation disorder play in capacity and structural stability; (3) develop predictive modeling of oxygen charge transfer and oxygen loss, and find ways to make oxygen redox beneficial in terms of increase capacity; and (4) develop materials with engineered surface passivation that does not lead to impedance increase.

Project Impact. The project will lead to insight in how Li-excess materials work and ultimately to higher capacity cathode materials for Li-ion batteries. The project will help in the design of high-capacity cathode materials that are tolerant to TM migration.

Out-Year Goals. Future goals include the following: (1) develop higher capacity Li-ion cathode materials, and novel chemistries for higher energy density storage devices, and (2) guide the field in the search for higher energy density Li-ion materials.

Collaborations. This project collaborates with K. Persson (LBNL), C. Grey (Cambridge), G. Chen (LBNL), and B. McCloskey (UC Berkeley).

Milestones

1. Assess, through modeling, the viability of fluorination of disordered-rocksalt cathodes to reduce the oxygen activity. (Q1, FY 2018; Completed)
2. Synthesize one partially fluorinated cathode material and demonstrate fluorination through NMR, TEM, XRD, or other characterization tool. (Q2, FY 2018; Completed)
3. Demonstrate viability of reducing TM valence in Li-excess materials to create higher capacity (for example, use Mn^{2+} or V^{3+} or more Ni^{2+}). (Q3, FY 2018; Completed)
4. Demonstrate capacity > 200mAh/g in a novel fluorinated disordered rocksalt. (Q4, FY 2018)

Progress Report

Recently, the team designed a class of high-capacity disordered rocksalt cathodes relying on only reversible TM redox and assessed their synthetic accessibility by constructing the phase diagram. By combining the active $Mn^{2+/4+}$ and $V^{4+/5+}$ couples, as well as fluorination, the team has removed all redox-inactive metal species, maximizing the specific energy density granted by TM redox. Furthermore, the team computed the voltage curve and analyzed the delithiation mechanism from DFT calculations [Kitchaev, D. A., Z. Lun, et al., *Energy & Environmental Science* (2018)].

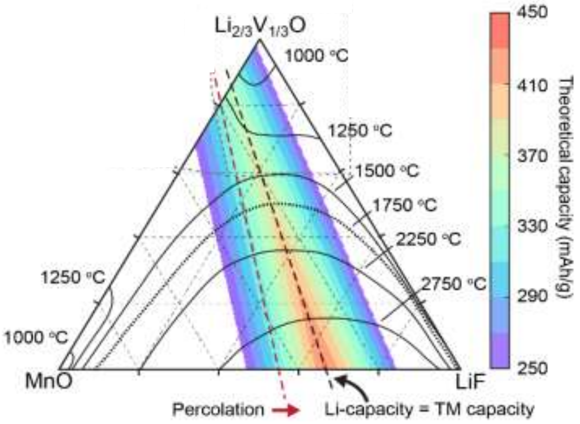

Figure 45. Computed phase diagram of the $MnO/Li_2VO_3/LiF$ alloy space.

Figure 45 shows the computed phase diagram of the $MnO/Li_2VO_3/LiF$ alloy space. According to the phase diagram, accessible compositions by both high-temperature solid-state synthesis (solid lines) and high-energy ball-milling (dotted line) can be identified. The team also plotted the theoretical capacity of possible compositions in this chemical space, given as a color-coded overlay in Figure 45. According to the theoretical capacity, the $Mn^{2+/4+}$ and $V^{4+/5+}$ redox couples are fully accessible, unless limited by the lithium content in the structure. Because of the high content of light, redox-active TMs, theoretical TM capacities are very high, reaching above 300 mAh/g for synthetically accessible oxides and oxyfluorides. The team picked a representative, $Li_{1.166}Mn_{0.333}V_{0.500}O_{1.833}F_{0.166}$ (ST-LMVF), from the phase diagram to study the delithiation behavior of this class of materials.

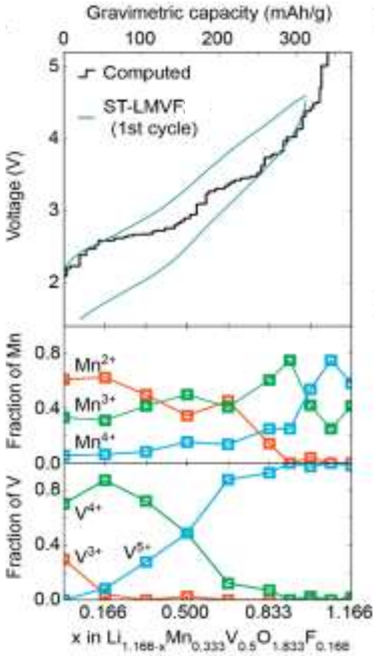

Figure 46. Computed voltage profile and evolution of manganese and vanadium oxidation states (from density functional theory).

Figure 46 shows the calculated voltage profile and delithiation mechanism during electrochemical cycling for ST-LMVF. Calculations suggest an initial mixed population of Mn^{2+}, Mn^{3+}, V^{3+}, and V^{4+} due to partial charge transfer from Mn^{2+} to V^{4+}. As lithium is extracted from the structure, for $0 < x < 0.166$, the population of V^{3+} decreases rapidly while that of V^{4+} increases. For $0.166 < x < 0.666$, the population of V^{5+} increases at the expense of V^{4+}. Between x = 0.666 and x = 0.916, the population of Mn^{3+} increases at the expense of Mn^{2+}, while for $0.916 < x < 1.08$, Mn^{3+} begins to oxidize to Mn^{4+}. For $1.08 < x < 1.166$, oxygen begins to be oxidized preferentially to Mn^{3+}, illustrating oxygen redox. Based on the team's calculation, ST-LMVF shows a redox mechanism consisting of low-voltage V^{4+} / V^{5+} redox combined with high-voltage Mn^{2+} / Mn^{4+} redox, partially overlapping with oxygen oxidation at high voltage; it should deliver a large capacity (~ 300 mAh/g) within a reasonable voltage window (1.5-4.6 V) largely relying on TM capacity.

Patents/Publications/Presentations

The project has no patents, publications, or presentations to report this quarter.

Task 3.6 – Dendrite Growth Morphology Modeling in Liquid and Solid Electrolytes (Yue Qi, Michigan State University)

Project Objective. The project goal is to develop a validated model to predict lithium dendrite morphology evolution in both liquid and solid electrolytes during electrodeposition and stripping to accelerate the adoption of Li-metal electrodes in current and emerging battery technologies. To achieve this goal, the project has four objectives: (1) formulate a general framework that captures the electrochemical-mechanical driving forces for lithium morphology evolution; (2) consider the role of the nm-thin SEI in liquid electrolytes as well as the microstructures of mm-thick solid electrolytes for lithium morphology evolution; (3) connect micron-scale phase-field models and atomic-scale DFT-based simulations via parameter- and relationship-passing to predict lithium dendrite nucleation and growth kinetics and morphology; and (4) validate the key input parameters and main conclusions of the multi-scale model as new capabilities are being developed step-by-step.

Project Impact. This atomically informed, fully coupled, electrochemical-mechanical dendrite morphology evolution model will allow the project to design the desired properties of artificial SEI coatings, the microstructure of solid electrolyte materials, and the corresponding battery operating conditions, so as to avoid dendrite growth during cycling. It will accelerate design of durable and safe lithium anodes for Li-S, Li-air, and all-solid Li-ion batteries. Thus, it directly impacts emerging technologies, such as Li-S, Li-air, and all-solid Li-ion batteries, which aim to meet the DOE target of the high-energy-density battery cells (> 350 Wh/kg) for EV applications and to push the cost below \$100/kWh$_{\text{use}}$.

Approach. A multiscale model approach is taken to connect micron-scale phase-field models and atomic-scale DFT-based simulations via parameter- and relationship-passing.

Out-Year Goals. The second-year goal is to establish the model to simulate metallic lithium precipitation in solid electrolytes while further developing the understanding of lithium dendrite growth in liquid electrolytes. To reach this goal, mechanical and electrochemical driving forces for lithium dendrite growth in solid electrolytes will be coupled in phase field model, while DFT is used to address the lithium plating tendency in various solid electrolyte and coating materials. Validation of the model will come from experiments to correlate the distinctive transport properties of artificial SEI layers with their impact on lithium dendrite morphology.

Collaborations. This project collaborates with UMD, Sandia National Laboratories (SNL), PNNL, University of Arkansas, and University of Houston.

Milestones

1. Compare lithium morphology obtained from experiments and modeling. *Go/No-Go Decision*: Determine if effect of SEI on dendrite growth should be modeled implicitly or explicitly. (Q1, December 30, 2017; *Go*)
2. Identify electronic pathway of lithium dendrite growth inside $Li_7La_3Zr_2O_{12}$ (LLZO). (Q2, March 31, 2018; Completed)
3. Identify Li-ion pathway of lithium dendrite growth inside LLZO. (Q3, June 30, 2018; Completed)
4. Develop multiphase multigrain phase-field model that incorporates mechanical and electrochemical driving forces for lithium dendrite growth in polycrystalline solid electrolyte. (Q4, October 31, 2018; In progress)

Progress Report

Solid Electrolyte. The project's previous studies on the lithium nucleation tendency in the cubic $Li_7La_3Zr_2O_{12}$ (c-LLZO) and the atomic layer deposited-Li_2PON_2 (ALD-LiPON) have shown that the surface electronic states in LLZO can be the pathway for electron transport and the traps for excess electrons to nucleate lithium. To assess the lithium nucleation tendency in other solid electrolyte materials, γ and β Li_3PS_4 phases were investigated with DFT calculations. The band gap on the surface, the location of the excess electrons, and the fracture energies are compared in Table 3. Although there is no additional surface state, the excess electrons are mainly localized on top of surface sulfur atoms and around phosphorus atoms for both γ-Li_3PS_4 and β-Li_3PS_4. Thus, the predicted order of lithium nucleation tendency will be LLZO (cubic and tetragonal) > β-Li_3PS_4 > γ-Li_3PS_4 > Li_2PO_2N. Li_3PS_4 also has much lower fracture energy than the oxide solid electrolytes (LLZO and Li_2PO_2N); this will also contribute to the different lithium dendrite morphology observed in sulfide and oxide-based electrolytes.

Table 3. Comparison of several solid electrolytes.

	Fracture Energy (J/m^2)	Bulk Band Gap (eV)	Surface Band Gap (eV)	Location of Excess electrons
c-LLZO	1.72	4.3	2.3	Surface
t-LLZO	2.08	4.3	2.8	Surface
Li_2PO_2N	0.92	6.2	4.2	Bulk
β-Li_3PS_4	0.38	2.8	2.6	Surface
γ-Li_3PS_4	0.20	2.9	2.6	Surface

The contribution of the surface states to lithium dendrite growth needs to be captured in the mesoscale as a new implementation, by incorporating a thermodynamics consistent description of electrons to the phase-field model. More specifically, the chemical potential of electrons becomes a function of the distance to the surface/grain boundaries. Thus, the DFT calculated open circuit fermi level values at the surface and bulk of different solid electrolyte materials (for example, LLZO, LiPON, etc.) are inputs to the phase-field model. The calculated equilibrium Li-ion and electron concentration distribution at a straight LLZO grain boundary under the applied overpotential were plotted together with the electric field in Figure 47. Due to the large difference in their diffusion coefficients, electrons transport orders of magnitude slower than lithium ion, and the equilibrium electron concentration profiles barely change with varying applied voltage (Figure 47a-d). Further, the electron concentration at the grain boundary region is prominently higher than the bulk, which is in agreement with the DFT calculation. Based on this test result, it is computationally efficient to formulate the electron concentration as a function of the local structure (phase order parameter), voltage, and the solid electrolyte materials surface states.

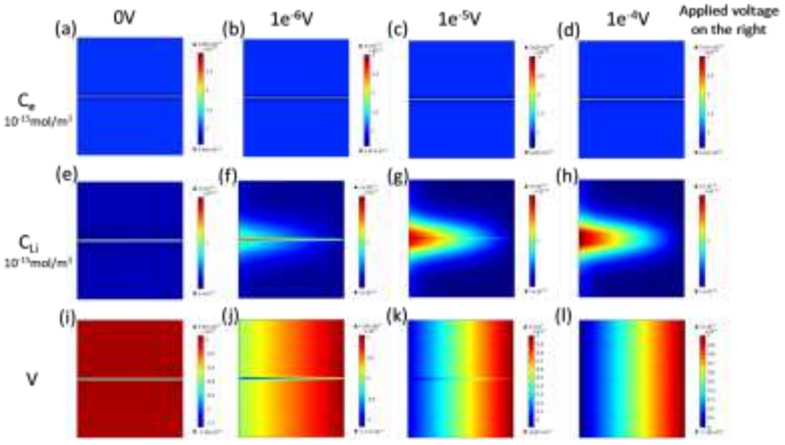

Figure 47. The equilibrium electron, Li-ion concentration, and the electric field distribution profile under different applied voltages.

The coupling of electron concentration formulation with phase morphological evolution is ongoing.

Patents/Publications/Presentations

Publications

- Li, Y. S., and Y. Qi. “Transferable SCC-DFTB Parameters for Li-Metal and Li-Ions in Inorganic Compounds and Organic Solvents.” *Journal of Physical Chemistry C* 122 (2018): 10755.
- Tian, H. K., B. Xu, and Y. Qi. “Computational Study of Li Nucleation Tendency in LLZO and Rational Design of Interlayer Materials to Prevent Li Dendrites.” *Journal of Power Source* 382 (2018): 79–86.
- Cheng, Q., L. Wei, Z. Liu, N. Ni, Z. Sang, B. Zhu, W. Xu, L-Q. Chen, W. Min, and Y. Yang. “*In-Operando*, Three Dimensional, and Simultaneous Visualization of Ion Depletion and Lithium Growth by Stimulated Raman Scattering Microscopy.” *Nature Communications* (2018). Accepted.
- Li, G., Z. Liu, Q. Huang, Y. Gao, M. Regula, D. Wang, L-Q. Chen, and D. Wang. “Stable Metal Anodes Enabled by Electrokinetic Phenomena.” *Nature Energy*. Under review.
- Liu, Z., P. Lu, Q. Zhang, X. Xiao, Y. Qi, and L.-Q. Chen. “A Bottom-up Formation Mechanism of Solid Electrolyte Interphase (SEI) Revealed by Isotope-Assisted Time-of-Flight Secondary Ion Mass Spectrometry (TOF SIMS).” Pending submission.
- Li, Y. S., and Y. Qi. “Energy Landscape of the Charge Transfer Reaction at the Complex Li/SEI/Electrolyte Interface.” Pending submission.

Presentations

- MRS Meeting, Phoenix, Arizona (April 5, 2018): “Phase-Field Method of Li Dendrite Formation During Electrodeposition”; Z. Liu, L. Chen, Y. Qi, X. Xiao, Q. Zhang, and L-Q. Chen. Invited.
- MRS Meeting, Phoenix, Arizona (April 5, 2018): “Computational Study of Li Nucleation Tendency in LLZO and Rational Design of Interlayer Materials to Prevent Li Dendrites”; H. K. Tian, B. Xu, and Y. Qi.
- 233rd ECS Meeting, Seattle, Washington (May 14, 2018): “Simulation of Lithium Ion Transport Through the Complex Electrode/SEI/Electrolyte Interface”; Y. Qi. Invited.
- 233rd ECS Meeting, Seattle, Washington (May 14, 2018): “Comparison of the Interfacial Reaction Kinetics and Plating Morphology of Lithium and Magnesium Anodes”; Y. Li, Z. Liu, Y. X. Lin, Y. Yao, L. Q. Chen, and Y. Qi. Invited.

Task 3.7 – First-Principles Modeling and Design of Solid-State Interfaces for the Protection and Use of Lithium-Metal Anodes
(Gerbrand Ceder, UC Berkeley)

Project Objective. The project objective is to determine the design principles that control the solid electrolyte/lithium electrode interfaces by determining the reaction products stemming from pairing solid electrolytes and lithium metal. The project will conduct rigorous analysis based on computing electrolyte phase-diagrams closed and open to lithium. Li-ion transport properties in bulk electrolytes and interfacial products will be assessed through AIMD and nudged elastic band (NEB) calculations. Simultaneously, a robust framework will be developed to identify factors controlling Li-dendrite propagation within solid electrolytes and interfacial products by accounting for irregularities, defects, and grain boundaries, through a model that includes elements of fracture mechanics, thermodynamics, and electrochemistry.

Project Impact. The project will lead to understanding of the complex evolution of lithium metal/SEI during electrochemical cycling. The understanding of this process is necessary to determine design principles to develop reliable all solid-state batteries.

Approach. By incorporating NEB and AIMD methods, high-throughput computation is used to screen candidate solid electrolyte with high electro-chemical stability and high ionic conductivity. DFT is used to calculate bulk elastic constants of materials, surface energies, and interface de-cohesion energies of grain boundaries; continuum theory (elastic-plastic-fracture mechanics) is used to assess the resilience of solid electrolytes and grain/particle boundaries toward lithium dendrite growth and propagation. The finite element method is used to couple several physical processes, including electro-chemical deposition, ionic diffusion, thermal expansion, and mechanical contacting.

Out-Year Goals. The out-year goals include the following: (1) obtain design criteria for solid electrolytes that can resist unstable lithium propagation by computing elastic properties, surface energies, and decohesion energies, and (2) adapt fracture mechanics models describing crack propagation to lithium dendrite propagation in different scenarios.

Collaborations. There are no collaborative activities this quarter.

Milestones

1. Development of metal-electrolyte electrochemical-mechanical interface model. (Q1, FY 2018; Completed)
2. Stability screening of candidate material for good SSE. (Q2, FY 2018; Completed)
3. Determine critical stress conditions that yield fracture in ceramic electrolytes during lithium deposition. (Q3, FY 2018; Completed)
4. Lithium conductivity screening using AIMD and NEB method to screen for materials with high lithium mobility. (Q4, FY 2018; In progress)

Progress Report

Lithium Conductivity Screening Using AIMD and NEB Method. After stability screening of candidate material for good SSE against lithium metal, the team started lithium conductivity screening using AIMD and NEB calculations. The single-vacancy migration mechanism was first studied using NEB method in a lithium nitride material, as shown in Figure 48. Lithium vacancy diffuses in a 2D plane with an activation energy of 284 meV, which is comparable to several state-of-the-art Li-ion conductors. This result indicates that good ionic conductivity could be potentially achieved in these lithium nitrides. More systematical work will be conducted in the next period.

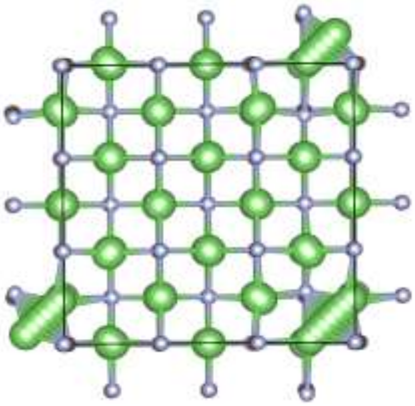

Figure 48. Single lithium vacancy migration path in a nitride lattice.

Study of Critical Stress Conditions that Yield Fracture in Solid Electrolyte. Experimental work has shown that solid lithium deposited at the interface is able to crack the surface of the solid electrolyte and penetrate into the bulk. For a fracture to propagate in the relatively hard ceramic material, there must be a large enough stress concentration at the crack tip. Therefore, it is important to study the local values of critical stress that yield fracture. To quantify the relation between external pressure, surface roughness, and critical stress, and to understand how the increase in tip stress will lead to fracture propagation, the team constructed a simplified model, as shown in Figure 49. The team found that due to the surface roughness and imperfections, a stress concentration will be developed at protrusions of the rough surface. This stress can be several orders of magnitude greater than the yield stress of lithium, and it can approach the fracture stress of solid electrolyte. Such a high stress concentration could further crack the solid electrolyte.

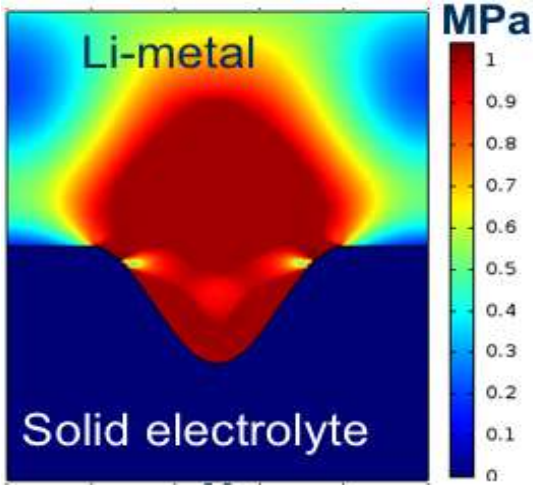

Figure 49. Mechanical model to study stress concentration at rough surface.

Patents/Publications/Presentations

The project has no patents, publications, or presentations to report this quarter.

Task 3.8 – Large-Scale *Ab Initio* Molecular Dynamics Simulations of Liquid and Solid Electrolytes (Lin-Wang Wang, Lawrence Berkeley National Laboratory)

Project Objective. The project goal is to use large-scale AIMD simulations and other computational approaches to study the discharging mechanism in Li-S battery, especially for polysulfur interaction with liquid electrolyte solvent molecules, and cathode materials, as well as lithium diffusion mechanisms in various systems. The long-term goal is to use such theoretical understanding to provide guidance to develop better electrolyte and cathode systems to overcome the bottlenecks that prevent commercialization of the Li-S battery. One major issue is solvation of Li_2S_n molecules in the electrolyte. The team is working to find the solution to this problem by both understanding the Li_2S_n-electrolyte interaction and discovering better cathode materials for optimal Li_2S_n-cathode binding. Specifically, the team seeks to: (1) develop reliable methods that combine classical force field (CFF) simulations with *ab initio* calculations to study thermal dynamic properties of Li_2S_n in different electrolytes, as well as interactions with different species within the electrolytes; and (2) study Li_2S_n interaction with different cathode materials, especially for 2D cathode materials consisted of light elements in the right-upper corner of the periodic table. The goal is to have sufficient binding energy between the Li_2S_n molecules and the cathode material, so, thermodynamically, the Li_2S_n will not be dissolved in the electrolyte. To study the Li_2S_n-electrolyte interaction, the team needs to accurately calculate the molecule entropy inside the solvent, which is a challenging task. The team plans to combine CFF with *ab initio* calculations for that study. To study Li_2S_n and cathode interaction, the team will calculate the phase diagrams of the systems with different number *n* and will hence obtain the binding energies and voltages at every step of the discharging process.

Project Impact. Making the Li-S battery a commercial reality will have a major impact on society and also help to realize the VTO goal of 500 km per charge for EV. However, the nature of chemical reaction makes it different from the traditional intercalation-based Li-ion battery. The molecular nature of Li_2S_n also allows solvation in the electrolyte. To address these problems, it is essential to have fundamental studies and understandings of the underlying mechanisms. The theoretical simulation can also play an important role in discovering and designing new cathode materials.

Out-Year Goals. In the outgoing years, the team will further develop computational methods for more accurate entropy and interaction energy calculations for the electrolyte. This is a critical capability to study the battery system. The team will also explore different cathode materials and morphologies. In particular, there is a vast space to explore using 2D materials as Li-S battery cathodes and using curved amorphous structures to increase capacity. The key is to investigate all the effects and competitions of different reactions.

Collaborations. The project will collaborate with G. Liu's group for cathode design. It has also collaborated with Prof. F. Pan of Beijing University for lithium battery research in general.

Milestones

1. Set up the Li_2Sn calculation with charge polarization model (CPM) solvent model without explicit solvent molecule. (Completed)
2. Carry out Li_2S_n/cathode structure calculations using CPM solvent model, with different cathode structures. (Completed)
3. Continue the $Li2S_n$ calculation with explicit solvent molecules; carry out direct CFF and AIMD simulations. (In progress)
4. Continue calculation of $Li2S_n$/cathode binding energies and phase diagrams, discovering new adequate cathode materials and morphologies. (In progress)

Progress Report

The project has finished its study of 2D hexaaminobenzene as Li-S battery cathode material. The 2D hexaaminobenzene is consisted of a carbon-nitride sheet with carbon in a benzene ring and nitrogen atom binding with a TM. The team found high energy density (1300 Wh/kg) and relatively good stability against Li_2S_n dissolvation. The results have been summarized in a paper that has just been accepted by *Advanced Energy Materials*. The team is continuing this study of 2D hexaaminobenzene. One issue of such 2D material as cathode is how to increase volumetric energy capacities. To do that, the team has designed a sandwich structure with alternating 2D hexaaminobenzene and Li-S layers, as shown in Figure 50. Surprisingly, such structure only has a few percent volume expansion upon full lithiation. The weight energy capacity of the system remains high, above 1000 Wh/kg. One issue is the lithium diffusion inside such a system. As can be seen from the top view, there is a big hole in the structure, which allows the lithium atoms to diffuse down, and the lithium atoms only need to diffuse a short distance sideways between the layers. Nevertheless, it will be extremely useful if the team can calculate the lithium diffusion constant quantitatively within such a system. Unfortunately, for such amorphous systems, conventional diffusion constant calculations based on barrier heights are impossible due to the large number of possible configurations. On the other hand, the direct MD simulations cannot be run long enough to reveal the diffusion path. To overcome this problem, the team is developing a new method, where an atomic force applied to one lithium atom will force it to move, and the trajectory of this lithium atom is analyzed to reveal the information of the barrier height. This is an ongoing development; if successful, it can be used in many battery studies.

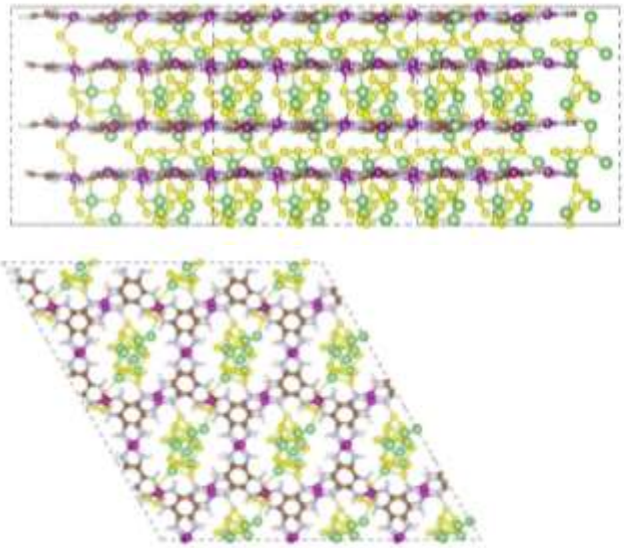

Figure 50. The sandwich structure of hexaaminobenzene and Li-S. (Left, side view; Right, top view)

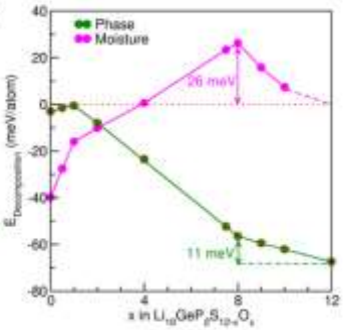

Figure 51. The decomposition energy as phase separation (into ternaries) and moisture reaction. Negative value means unstable.

The team has also studied the design and improvement of solid electrolyte: $Li_{10}GeP_2S_{12}$ (LGPS). This germanium thiophosphate has one of the highest lithium conductivities (20 mS/cm) among all the known solid electrolytes. Unfortunately, it is moisture unstable. Through *ab initio* calculation, the team found that the instability comes from the PS_4 tetrahedron. It is possible to replace the PS_4 with PO_4; hence, the team arrived at a new compound: $Li_{10}(GeS_4)(PO_4)_2$. The team found that not only is this compound moisture stable, it has even higher lithium mobility than the original LGPS. This is unlike the $Li_{10}GeP_2O_{12}$ counterpart, where the lithium mobility is low due to the small size of GeO_4 tetrahedron. The team found that the existence of GeS_4 retains the lithium diffusion channels. Furthermore, using linear programing, they found that the $Li_{10}(GeS_4)(PO_4)_2$ is stable against decomposition into binary compounds, although it might not be thermal dynamically stable against decomposing into ternary compounds of Li_4GeS_4 and Li_3PO_4. But this is the same situation as for $Li_{10}GeP_2O_{12}$, which is also thermal dynamically unstable against the decomposition into Li_4GeO_4 and Li_3PO_4. The team argues that a kinetic barrier exists against the decomposition into ternary compounds. Finally, they found that the $Li_{10}(SnS_4)(PO_4)_2$ is an even better solid electrolyte with even higher lithium mobility. This overcomes the scarcity of germanium. This work provides a new way to design lithium solid electrolyte. A manuscript is under review.

Patents/Publications/Presentations

Publications

- Yang, L., J. Zheng, M. Xu, Z. Zhuo, W. Yang, L. W. Wang, L. Dai, J. Lu, K. Amine, and F. Pan. “Short Hydrogen Bonds on Reconstructed Nanocrystal Surface Enhance Oxygen Evolution Activity.” ACS *Catalysis* 8 (2018): 466.
- Duan, Y., B. Zhang, J. Zheng, J. Hu, J. Wen, D. J. Miller, P. Yan, T. Liu, H. Guo, W. Li, X. Song, Z. Zhuo, C. Liu, H. Tang, R. Tan, Z. Chen, Y. Ren, Y. Lin, W. Yang, C. M. Wang, L. W. Wang, J. Lu, K. Amine, and F. Pan. “Excess Li-Ion Storage on Nanocrystal Reconstructed Surface to Boost Battery Performance.” *Nano Letters* 17 (2017): 6018.
- Wu, J., and L. W. Wang. “2D Frameworks C2N as a Potential Cathode for Lithium Sulfur Batteries: An *Ab Initio* Density Functional Study.” *Journal of Materials Chemistry A* 6 (2018): 2984.
- Li, Y., F. Ma, and L. W. Wang. “Phosphorene Oxides as Promising Cathode Material for Sealed Non-Aqueous Li-Oxygen Battery.” *Journal of Materials Chemistry A* 6 (2018): 7815.
- Gao, G., F. Zheng, F. Pan, and L. W. Wang. “Theoretical Investigation of 2D Conductive Microporous Coordination Polymers as Li-S Battery Cathode with Ultrahigh Energy Density.” *Advanced Energy Materials*. Accepted.

Task 3.9 – *In Operando* Thermal Diagnostics of Electrochemical Cells (Ravi Prasher, Lawrence Berkeley National Laboratory)

Project Objective. Effective heat dissipation in batteries is important for multiple reasons including performance, reliability, and safety. Currently, the thermal management of battery cells is provided at the system level by either forced air or liquid cooling, leading to reduced system-level energy densities and more failure-prone complex system designs. Furthermore, even given theoretically infinite system level cooling applied to the external battery surface, peak temperature rise within a cell would still easily exceed acceptable threshold values due to the poor thermal transport properties within the cell itself. It has not yet been possible to thermally profile a real cell during operation to provide a spatially resolved map of heat transfer properties throughout the cell. The objective of this research is to create a metrology capable of spatially resolved *in operando* thermal property profiling, and then use this tool to reveal the largest thermal bottlenecks within a functioning Li-ion cell and create a complete materials-level cell thermal model.

Project Impact. The intrinsic thermal resistance of Li-ion cells is currently far higher than the theoretical value predicted by simply combining the known thermal properties of each macro component into an appropriate thermal model. The spatially resolved thermal transport property measurements from this project will reveal what key piece of information is missing. Preliminary data suggest that more than 75% of the total battery thermal resistance may be due to a single interface between the cathode and separator, previously unknown. An accurate understanding of the cell internal thermal transport is necessary to successfully optimize cell thermal performance to meet the challenges of extreme fast charging, mitigating thermal runaway, and improving battery performance, reliability, and safety.

Approach. To accomplish the project goals, the team will utilize two state-of-the-art thermal metrology techniques. They will build an in-house adapted 3ω technique to measure thermal transport properties throughout the bulk of a Li-ion cell while it is in operation, without affecting the operation of the cell. The 3ω system will work by using mm-scale sensors on the electrode current collectors to send variable-frequency thermal waves into the operational battery to quantitatively measure heat transport through different layers and interfaces. The team will also use the ultrafast optical time domain thermoreflectance (TDTR) technique to measure nanoscale thermal transport properties of constituent components of the cathode composite. They will then combine these results to create an "all-scale" accurate thermal model of the cell that—unlike existing models—agrees with the empirical measurements of cell thermal performance.

Out-Year Goals. In outgoing years, the project will design, build, and implement the adapted 3ω metrology. This will involve developing and testing the metrology itself along with accompanying theory, designing compatible battery samples, and finally applying the technique to live cells. The team will use the already built TDTR system at LBNL to measure epitaxially grown cathode materials provided by collaborators. Combined, this will provide enough data to construct and validate a realistic all-scale thermal model of the battery.

Collaborations. This project collaborates with two LBNL groups, Vincent Battaglia's for cell assembly for 3-Omega studies and Robert Kostecki's for pristine battery active material growths for TDTR studies.

Milestones

1. TDTR measurements of ideal battery samples. (Q1, FY 2018; Completed)
2. 3-Omega sensing and heating lines fabricated, and metrology developed. (Q2, FY 2018; Completed)
3. Electrochemical cells with 3-Omega sensors integrated on the electrodes. (Q3, FY 2018; Completed)
4. *Go/No-Go Decision*: Baseline *in operando* thermal diagnostics and measurement with 3-Omega technique performed. (Q4, FY 2018; On schedule)

Progress Report

Quarter 3 milestone met. The team has successfully integrated 3-omega sensors onto electrodes in the electrochemical cells. They tried six different approaches to successfully electrically insulate the sensors from the electrodes. Most passivation layer combinations were either too thick and thermally resistive and blocked too much heat, destroying the sensors' sensitivity, or were too fragile and cracked or otherwise failed during sample handling. A final process of 0.4-µm parylene with 40 nm of ALD Al_2O_3 yielded consistent and robust results. The sensors were then deposited on top of this insulation, wired with silver epoxy, and covered by a hollowed-out protective Teflon shield. This stack was then integrated into a vacuum-sealed pouch cell with electrolyte to form a live electrochemical cell with integrated sensors (Figure 52). The team was then able to successfully measure a 3ω signal from within the battery (Figure 53), demonstrating the efficacy of the sample design. Full data analysis will require future development of a complete mathematical thermal model of the multi-layer geometry for the 3ω signal.

3ω sensors deposited on top of cathode current collector

Sensors sealed under protected Teflon shield with internal cavity

Electrode with sensors put in sealed pouch cell with electrolyte. Live cell.

Figure 52. Process flow showing integration of 3-omega sensors onto electrodes within electrochemical cells.

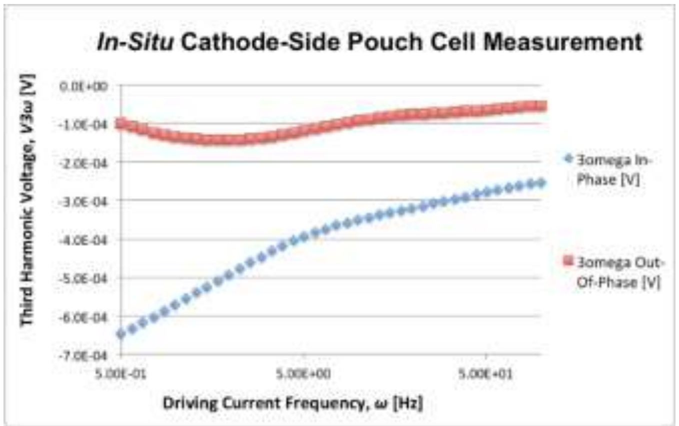

Figure 53. Raw data from *in situ* measurement of full electrochemical cell using internally integrated 3ω sensors.

Patents/Publications/Presentations

The project has no patents, publications, or presentations to report this quarter.

Task 3.10 – Multi-Scale Modeling of Solid-State Electrolytes for Next-Generation Lithium Batteries (Anh Ngo, Larry A. Curtiss, and Venkat Srinivasan, Argonne National Laboratory)

Project Objective. This project is part of a multi-scale modeling effort to obtain an in-depth understanding of the interaction of the electrode and the solid electrolyte aimed at developing highly efficient SSE batteries for vehicle applications. Input parameters needed for mesoscale (continuum) level calculations are being obtained from atomistic calculations including DFT and classical MD simulations. This atomistic input will enable a multi-scale computational procedure for SSEs that is capable of successfully capturing the physicochemical aspects during charge and discharge process including lithium transport mechanisms, interfacial phenomena during the insertion and extraction of lithium ions, and mechanical deformation of SSE.

Project Impact. A major safety concern experienced with commercially available Li-ion batteries under some scenarios is leakage of the liquid electrolyte, which can potentially catch fire. Replacement of the liquid electrolyte is necessary to decrease the fire hazard and improve safety associated with present-day Li-ion batteries. In addition, use of solid electrolytes provides a path to prevent dendrites in Li-metal anodes, thereby leading to batteries with significantly higher energy density. The impact of this project will be to help in development of good SSEs as a replacement for the commercially used organic liquid electrolytes to improve safety and energy density in Li-ion batteries.

Approach. Parameters needed for mesoscale modeling of grain-interior, grain-boundary, and electrode-electrolyte interface will be calculated by DFT-based calculations along with Monte Carlo (MC) and MD simulations. The calculations will be used to determine properties of the electrode with the solid electrolyte as well as in grain-boundary regions of the solid electrolyte. This will include calculations of structure, stability, ionic conductivity, Young's modulus, fracture toughness, exchange current density, and other properties.

Out-Year Goals. The out-year goals of this work are to calculate other properties such as fracture toughness and include other SSEs and coatings in the multi-scale modeling.

Collaborations. This project collaborates with Venkat Srinivasan at ANL.

Milestones

1. AIMD of the interface structure of the LLZO solid electrolyte lithium anode and MC simulations of LLZO grain boundaries. (Q2, FY 2018; Completed)
2. Calculations of Young's modulus at grain-interior and grain-boundary region for LLZO solid electrolytes. (Q3, FY 2018; Completed)
3. Calculations of exchange current density at the electrode-electrolyte interface. (Q4, FY 2018; Initiated)

Progress Report

The use of lithium metal in Li-ion batteries requires protection of the lithium surface such as by a ceramic solid electrolyte to prevent propagation of lithium dendrites, which can cause safety problems and capacity fade. Multi-scale modeling of SSEs can provide insight into the mechanism for dendrite growth and other instabilities for guidance on how to improve performance. At the mesoscale (continuum) level of modeling atomistic level, input is required from theory or experiment to accurately capture physicochemical aspects during charge and discharge processes of a Li-ion battery with SSE. One of these inputs is the Young's Modulus, which is a fundamental property of every material and is very important in batteries material research. This constant can provide information as to when a structure will deform.

In this work, the Young's modulus was calculated for bulk regions of LLZO and its grain boundaries. The atomic structure/stoichiometry of LLZO grain boundaries (GB) was previously established by MC simulations using about 35,000 atoms. The MC calculations provided the structures of four low-angle GB [$\Sigma_3(112)$, $\Sigma_5(210)$, $\Sigma_5(310)$, $\Sigma_9(221)$]. During this quarter, the team used these results to carry out MD simulations with the Large-Scale Atomic/Molecular Massively Parallel Simulator (LAMMPS) code and soft Butler-Volmer (BV) potentials. About 1,720,000 atoms were used for LLZO to calculate the Young's modulus. The Young's modulus, *E*, can be calculated from tensile stress-strain graphs in the linear regime. The slope of the graph is used to calculate *E* when the material obeys Hooke's law. The team divided it into contributions from the bulk region of the simulation cell (fractional coordinates $0.2 < x < 0.3$ and $0.7 < x < 0.8$) and GB region (fractional coordinates $0.95 < x < 0.05$ and $0.45 < x < 0.55$). The team has strained LLZO in each direction, and a summary of results is given in Figure 54 for bulk and the $\Sigma_3(112)$ GB. A linear fit gave an average value of Young's Modulus *E*=138 GPa for bulk LLZO and E=117 GPa for the $\Sigma_3(112)$ GB.

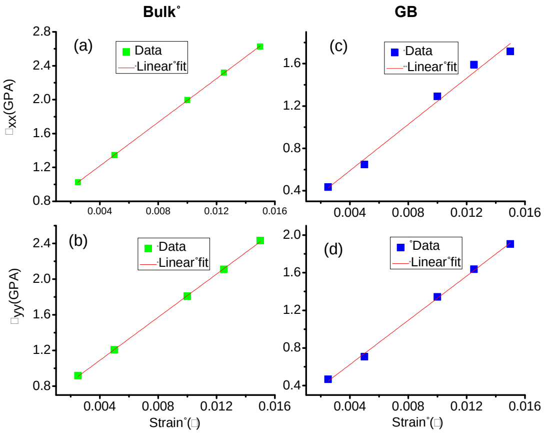

Figure 54. The x, y components of the Young's Modulus obtained from the project's model. (a) and (b) are for the bulk region, while (c) and (d) are for grain boundary regions of the $\Sigma_3(112)$ grain boundary.

Young's modulus provides an estimation of the deformability of any solid material. This parameter helps to estimate the evolution of stress within solids subjected to a certain amount of deformation. Because ceramic-based SSEs are very stiff, the magnitude of their Young's modulus is also very high (approximately 10 to 15 times larger than that of lithium). Due to lithium deposition, a small amount of deformation at the electrode-electrolyte interface can lead to development of compressive stress, which can significantly impact the state of the electrochemical potential observed at the lithium/ceramic-electrolyte interface. As evolution of mechanical stress, and effectively Young's modulus, directly affects the overpotential observed during the lithium deposition process, it is very important to estimate the exact magnitude of Young's modulus for the ceramic SSEs for use in multi-scale modeling. Differences in Young's moduli between the bulk and GB of electrolyte can also impact the reaction current observed in each of the phases.

Patents/Publications/Presentations

The project has no patents, publications, or presentations to report this quarter.

TASK 4 – METALLIC LITHIUM

Summary and Highlights

The use of a metallic lithium anode is required for advanced battery chemistries like Li-ion, Li-air, and Li-S to realize dramatic improvements in energy density, vehicle range, cost requirements, and safety. However, the use of metallic lithium with liquid and polymer electrolytes has so far been limited due to parasitic SEI reactions and dendrite formation. Adding excess lithium to compensate for such losses effectively negates the high energy density for lithium in the first place. For a long lifetime and safe anode, it is essential that no lithium capacity is lost either (1) to physical isolation from roughening, dendrites, or delamination processes, or (2) to chemical isolation from side reactions. The key risk and current limitation for this technology is the gradual loss of lithium over the cycle life of the battery.

The BMR, Battery500, and other DOE programs are addressing this challenge with many innovative and diverse approaches. Key to all is the need for a much deeper analysis of the degradation processes and new strategies to maintain a dense, fully connected lithium and a dendrite-free electrolyte so that materials can be engineered to fulfill target performance metrics for EV application, namely 1000 cycles and a 15-year lifetime, with adequate pulse power. Projecting the performance required in terms of just the lithium anode, this requires a high rate of lithium deposition and stripping reactions, specifically about 30 μm of lithium per cycle, with pulse rates up to 10 and 20 nm/s (15mA/cm^2) charge and discharge, respectively, with little or no excess lithium inventory. This is daunting in the total mass and rate of material transport that must be achieved without failures.

The efficient and safe use of metallic lithium for rechargeable batteries is then a great challenge, and one that has eluded R&D efforts for years. This Task takes a broad look at this challenge for both solid-state batteries and batteries continuing to use liquid electrolytes. For the liquid electrolyte batteries, steady improvement has been realized by PNNL researchers through use of dual lithium salts and organic additives to the typical organic solvent electrolytes to impede lithium corrosion and roughening. Now, MIT is investigating halide and other additives to form self-healing SEI coatings. Engineered coating and 3D-anode structures continue to offer promising results. These include application of various 2D coating materials under investigation at Stanford University and use of 3D-copper-foam structures at University of Pittsburgh. An increasing number of programs are turning to various composites of polymer and ceramic electrolytes to address mechanical and ion transport challenges. ORNL is continuing investigation of spray-coated composite polymer electrolytes, while UT Austin and PNNL are also initiating work in this direction. A breakthrough is needed to promote facile Li-ion transport between the ceramic and organic polymer or liquid electrolytes. Two highly successful programs using ceramic solid electrolytes, specifically the LLZO garnets, were completed. Both demonstrated a great decrease in the area specific resistance (ASR) of the garnet-Li interface, reaching values of just a few ohms. This was accomplished variously using coating to promote wetting, treatments to ensure the surface is free of flaws and contamination, or higher interface areas to decrease the current density. As the ASR decreased, the interface adhesion and the critical current density achievable without forming Li-metal shorts increased. Fundamental aspects of this work on inorganic solid electrolytes are being continued by ANL researchers and others. The last project is focused on the properties of lithium metal itself. Past work using nanoindentation showed that lithium plating under high currents can exert large stresses at the lithium SEI. Following this, ORNL with Michigan Technological University and University of Michigan will initiate work to create lithium stability maps to understand conditions where the lithium morphology becomes difficult to control. Each of these projects involves a collaborative team of experts with the skills needed to address the challenging materials studies of this dynamic electrochemical system.

Highlights. Progress for this quarter is summarized below. The approaches to stabilizing the Li-metal anode are varied and encompass the following: new formulations of the electrolyte solutions to promote more stable and efficient lithium plating; addition of robust barrier coatings at the lithium surface to block dendrites; and use of ceramic and polymer solid electrolytes to confine the lithium. Each path offers some improvement.

With liquid electrolytes:

- Lithium difluorophosphate (LiDFP) was shown to be effective as a dendrite-suppressing additive for standard $LiPF_6$/carbonate electrolyte by forming a compact and stable SEI on the lithium anode. With an optimal LiDFP content, Li||Li symmetric cells cycled stably for more than 500 and 200 h at 0.5 and 1.0 mA cm^{-2}, respectively; this is much longer than the control electrolyte without LiDFP additive.
- Lithium metal exposed to a fluoroethylene carbonate (FEC)-containing liquid electrolyte formed an SEI with a much higher fluorine concentration and the signature XPS peaks consistent with LiF formation. The LiF, with a high electronic resistivity, forms a superior SEI. The FEC additive is part of a self-healing electrolyte for which a patent application was submitted.
- Cycling was improved by surface engineered (SE) interesting ridge features into the metallic lithium anode. When the SE and pristine (P) lithium metal are compared, both the Sand's time for onset of dendrite formation and the capacity retention for coin cells of Li/$LiMn_2O_4$ were extended for SE compared to P Li-metal anodes.
- To increase the effective electrochemical area of the anode current collector, a thin graphene film was deposited onto the clean copper current collector by chemical vapor deposition (CVD). The graphene film is effective to reduce electrochemical polarization and enhance charge/discharge reversibility. The morphology suggests there is better bonding of metallic lithium to the carbon, than to copper.

Forming barrier materials at the lithium surface:

- Novel 3D electrodes were prepared using ALD-coated HCS. The thin ALD coating seals the micropores of HCS to keep the electrolyte from contacting lithium occupying the center; the liquid electrolyte only contacts the outer surface of ALD Al_2O_3/HCS. 500 cycles, over 3 months, were achieved without the initiation of fluctuations in the measured CE.

Performance with solid electrolytes:

- Using composite electrolytes containing 50 vol% Ohara ceramic powders, Li/$LiFePO_4$ batteries achieved good capacity only when a thin LiPON or polymer electrolyte layer separated the Ohara from the lithium metal and prevented reaction.
- A new type of composite gel electrolyte was prepared using a one-pot synthesis; the room-temperature ionic conductivity of the composite gel membrane was 1×10^{-4} S/cm.
- Many Li/LLZO/Li samples were evaluated for the critical current densities at room temperature to 70°C. The apparent Arrhenius behavior exhibiting an activation energy of 0.25eV is being analyzed to fit the activation energy to a physical model, with an emphasis on balancing the lithium flux at the Li-LLZO interface.

Task 4.1 – Lithium Dendrite Prevention for Lithium Batteries
(Wu Xu and Ji-Guang Zhang, Pacific Northwest National Laboratory)

Project Objective. The project objective is to enable lithium metal to be used as an effective anode in rechargeable Li-metal batteries for long cycle life at a reasonably high current density. The investigation in FY 2018 will focus on effects of various lithium salt mixtures, inorganic fillers and polymer types on ionic conductivity, lithium CE, Li-anode morphology, and battery performances in terms of long-term cycling stability at room temperature and elevated temperatures and at various current density conditions, rate capability, and low-temperature discharge behavior. The compatibility of such electrolytes with 4-V NMC cathode will be investigated.

Project Impact. Lithium metal is an ideal anode material for rechargeable batteries. Unfortunately, uncontrollable dendritic lithium growth and limited CE during repeated lithium stripping/deposition processes have prevented their practical applications. This work will explore the new hybrid composite electrolytes that can lead to dendrite-free lithium deposition with high CE. The success of this work will increase energy density of Li-metal and Li-ion batteries and accelerate market acceptance of EVs, especially for PHEVs as required by the EV Everywhere Grand Challenge.

Out-Year Goals. The long-term goal of the proposed work is to enable lithium and Li-ion batteries with > 120 Wh/kg (for PHEVs), 1000 deep-discharge cycles, 10-year calendar life, improved abuse tolerance, and less than 20% capacity fade over a 10-year period.

Collaborations. This project collaborates with Chongmin Wang, PNNL, on characterization by TEM/SEM; Bryant Polzin, ANL, on electrodes sampling; and Hongfa Xiang, Hefei University of Technology, on LiDFP additive study.

Milestones

1. Develop a lithium salt mixture that has an ambient melting temperature and an ionic conductivity over 1 mS/cm. (Q1, December 31, 2017; Completed)
2. Investigate effects of inorganic fillers and polymers on hybrid composite electrolytes. (Q2, March 31, 2018; Completed)
3. Develop an inorganic/polymeric hybrid composite electrolyte with ionic conductivity over 1 mS/cm and lithium CE over 99%. (Q3, June 30, 2018; Completed)
4. Achieve over 300 cycles for 4-V Li||NMC batteries with ~ 2 mAh/cm^2 cathode loading. (Q4, September 30, 2018; Ongoing)

Progress Report

This quarter, the electrochemical performances of "polymer-in-salt" electrolytes were investigated. As shown in Figure 55, this polymer-in-salt electrolyte has an ionic conductivity of 4.2×10^{-5} S/cm at 25°C and 1.1×10^{-3} S/cm at 70°C (Figure 55a), and an oxidation stability voltage of 4.5 V on SS substrate (Figure 55b). When this polymer-in-salt electrolyte was assembled into the Li||LFP coin cell and tested at 60°C in the voltage range of 2.5-4.2 V, the cycling efficiency was 83% for the first cycle and then reached 91% and 92% for the second and the third cycles (Figure 55c), respectively. When tested in Li||NMC-622 coin cells at the same conditions, this polymer-in-salt electrolyte gave 79% and 87% cycling efficiency for the first two cycles, respectively. These cells are still being tested. Further development and evaluation of the polymer-in-salt electrolytes with and without inorganic fillers are in progress.

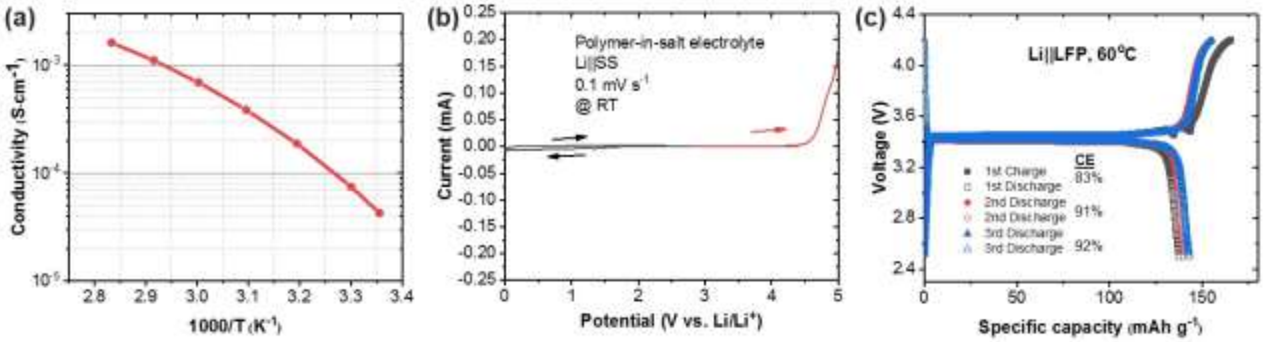

Figure 55. (a) Temperature dependence of ionic conductivity of a polymer-in-salt electrolyte. (b) Electrochemical stability of the polymer-in-salt electrolyte in Li||SS cells at a scan rate of 0.1 mV/s and room temperature. (c) Charge/discharge voltage profiles for the first three cycles of a Li||LFP cell with the polymer-in-salt electrolyte at 60°C.

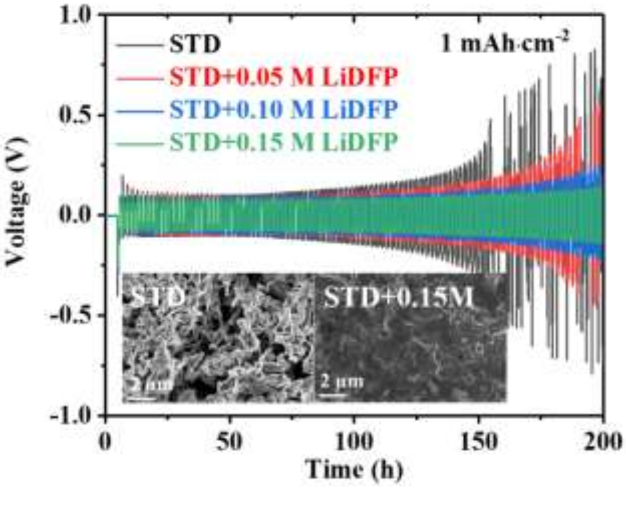

Figure 56. Comparison of cycling stability of Li||Li symmetric cells using electrolytes with different amounts of lithium difluorophosphate additive and scanning electron microscopy images of lithium morphologies from cycled cells.

In addition, the stability of Li-metal anode and Li-metal batteries was also investigated by using LiDFP as an additive in a conventional $LiPF_6$/carbonate electrolyte. It is found that the lithium CE can be largely improved from 84.6% in the conventional $LiPF_6$-based electrolyte to 95.2% by the addition of an optimal concentration of LiDFP at 0.15 M. The optimal LiDFP-containing electrolyte can allow the Li||Li symmetric cells to cycle stably for more than 500 and 200 h at 0.5 and 1.0 mA cm^{-2}, respectively; this is much longer than the control electrolyte without LiDFP additive (Figure 56). Meanwhile, this LiDFP-containing electrolyte also plays an important role in enhancing the cycling stability of the Li||NMC-333 cells with a moderately high mass loading of 9.7 mg cm^{-2}. Detailed characterizations by using EIS, SEM, XPS, and FTIR indicate that LiDFP can be preferentially reduced on Li-metal anode to form a compact and stable SEI film enriched with LiF and phosphates, leading to enhanced protection to the metallic lithium anode, inhibition of lithium dendrite growth, and improved stability of Li-metal anode and the related batteries.

Patents/Publications/Presentations

Publication

- Shi, P., L. Zhang, H. Xiang, X. Liang, Y. Sun, and W. Xu. “Lithium Difluorophosphate as a Dendrite-Suppressing Additive for Lithium Metal Batteries.” ACS *Applied Materials & Interfaces* 10 (2018): 22201–22209**.**

Presentations

- Energy Storage System Safety and Reliability Forum 2018, Seattle, Washington (March 28-29, 2018): “Nonflammable Electrolytes for Lithium-Ion Batteries”; W. Xu, S. Chen, X. Cao, and J.-G. Zhang. Invited.
- 233rd ECS Meeting, Seattle, Washington (May 13–17, 2018): “Guided Growth and Smooth Deposition of Lithium Metal Film through Electrolyte Strategy”; W. Xu, F. Ding, Y. Zhang, J. Qian, X. Ren, X. Li, and J.-G. Zhang. Invited.
- 2018 China International Conference on the Frontier Technology of Advanced Batteries, Shenzhen, Guangdong, China (May 22–24, 2018): “Imide-Orthoborate Salts/Carbonate Electrolytes for Fast Charging and Stable Cycling of Rechargeable Lithium Metal Batteries”; W. Xu, X. Li, J. Zheng, S. Jiao, H. Xiang, X. Chen, and J.-G. Zhang. Invited.
- DOE AMR Meeting, Washington, D. C. (June 18–21, 2018): “Lithium Dendrite Prevention for Lithium Batteries”; W. Xu, and J.-G. Zhang. Poster.

Task 4.2 – Self-Assembling and Self-Healing Rechargeable Lithium Batteries (Yet-Ming Chiang, Massachusetts Institute of Technology; Venkat Viswanathan, Carnegie Mellon University)

Project Objective. The project objectives are as follows: (1) investigate formation of lithium halide containing SEI, (2) characterize the structure and composition of the SEI surface film and morphology of the electrochemically deposited lithium, and (3) develop combinations of electrolytes (solvents + salts) and electrolyte additives that produce a highly Li-ion conducting, mechanically robust, and self-healing SEI to suppress lithium dendrite formation and improve CE.

Project Impact. Efforts to achieve practical use of the Li-metal anode in rechargeable lithium batteries have long been plagued by lithium dendrite formation and low CE. Lithium dendrites cause battery short-circuits, leading to serious safety hazards. The low CE of Li-metal anodes demands use of excess lithium to offset the lithium loss during cycling, which lowers the overall energy density of the battery. If successful, this project will enable self-forming and self-healing SEI containing alkali and/or alkaline earth halides that can suppress dendrite formation and improve CE. This will eventually enable high-energy-density (> 400 Wh/kg) and long-cycle-life (> 500 cycles, 80% capacity retention) Li-metal batteries.

Approach. The project approach involves the following: (1) identifying suitable combinations of solvents, Li-electrolyte salts, and halide and other additives that can produce highly Li-ion conducting, mechanically robust, and self-healing SEI, (2) using integrated theory and experiment, and (3) assembling and testing symmetric and asymmetric cells and Li-metal batteries comprising a high areal-capacity cathode (> 3 mAh/cm^2) and a capacity-limited Li-metal anode (< 130% lithium excess).

Out-Year Goals. The project will down-select electrolyte compositions, develop designs for prototype full cells of > 10 mAh capacity, and fabricate and deliver cells to DOE-specified laboratories for testing and evaluation.

Collaborations. This project collaborates with 24M Technologies Inc. on 18 cm^2/80 cm^2 pouch cell fabrication and tests.

Milestones

1. Demonstrate Li-Li asymmetric cell using halide additives that outperforms additive-free cell according to criteria in Q3 and Q4. (Q1, December 2017; Completed)
2. Deliver structural and chemical characterization results for baseline halide films on lithium metal. (Q2, March 31, 2018; Completed)
3. Deliver structural and chemical characterization results for self-healed halide films on lithium metal. (Q3, June 30, 2018; Completed)
4. Establish quantitative theoretical criteria for effectiveness and reproducibility in dendrite-suppression experiments. (Q4, September 30, 2018; Ongoing)
5. *Go/No-Go Decision*: Demonstrate Li-Li symmetric cells that meet established criteria cycling at ≥ 3 mAh/cm^2 at C/5 rate over 30 cycles. (Q1, FY 2019; Ongoing)

Progress Report

This quarter, structural and chemical characterization results for self-healing halide films on lithium metal are reported. Specifically, the milestone to "deliver structural and chemical characterization results for baseline halide films on lithium metal" is addressed.

XPS measurements were carried out on lithium metal deposited in electrolyte with seal-healing functionality. XPS is a surface-sensitive technique that can probe the composition of the SEI on the surface of the deposited lithium. 3.0 mAh/cm^2 lithium was first deposited onto a copper substrate at a current density of 0.6 mA/cm^2. The sample was rinsed using dimethyl carbonate (DMC) several times and dried under vacuum before the XPS measurements. The sample was transferred into the chamber of the XPS instrument using a specialized sample-transfer holder filled with argon gas. Here, the team focuses on results from a model electrolyte formulation that used FEC as the LiF forming additive, which produces the baseline halide films.

A much higher fluorine concentration of 12.1% was observed in the SEI formed in FEC-containing electrolyte (Figure 57a), compared to 2.7% fluorine when using a control electrolyte without FEC (as reported last quarter). The F 1s spectra can be further resolved into peaks corresponding to LiF at 684.8 eV and C-F bonds at 686.6 eV (Figure 57b). Based on peak area, the SEI film formed from FEC-containing electrolyte has a higher LiF fraction, 92.3%, than the SEI formed in FEC-free electrolyte, 71.7% (see last report). In this example, it is clear that more LiF forms in the presence of FEC than without it.

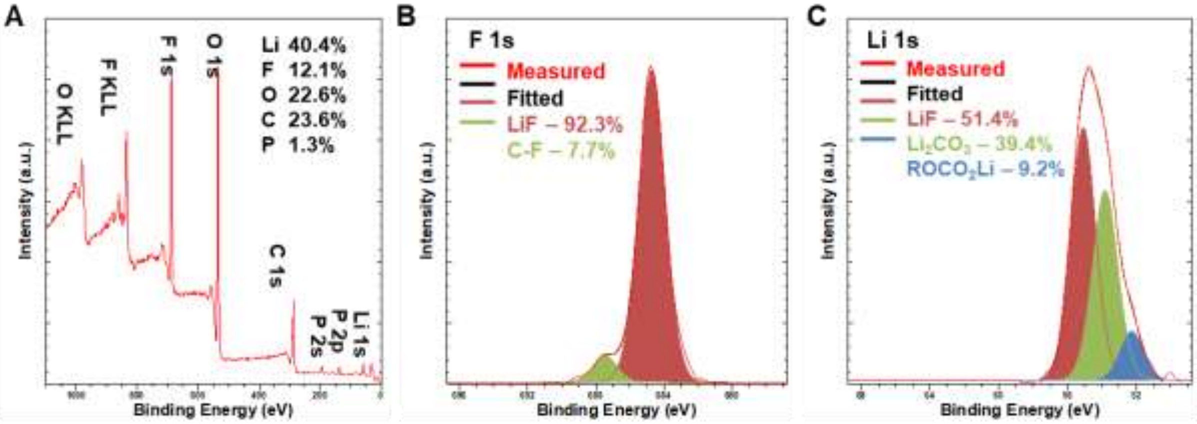

Figure 57. X-ray photoelectron spectroscopy studies of the SEI formed in LiPF$_6$/carbonate-based electrolyte with fluoroethylene carbonate additive.

The LiF-rich SEI is the product of spontaneous reactions between fresh lithium and FEC. LiF is critical in promoting the formation of stable and uniform SEI. LiF is highly electronically insulating (≈ 10^{-31} S/cm) and can prevent electrons from crossing the SEI film and causing side reactions. On the other hand, LiF is reported to have a low lithium diffusion activation energy and a high surface energy, which enhances surface diffusion of Li$^+$ during electrodeposition and promotes a uniform and dendrite-free morphology. In the Li 1s spectra, Figure 57c, the peak of LiF (55.7 eV) is also enhanced in the FEC-induced SEI film. Therefore, by introducing FEC into the electrolyte, an LiF-rich SEI film is achieved, which has been shown effective in suppressing lithium dendrite formation and improving Li-metal cycling CE (reported in the first quarterly report this fiscal year). With these results, this milestone is completed.

Patents/Publications/Presentations

Patent

- Chiang, Y-M., et al. Electrolytes for Alkali Metal Electrodes and Rechargeable Batteries Using Same. U. S. patent; filed May 15, 2018.

Task 4.3 – Engineering Approaches to Dendrite-Free Lithium Anodes (Prashant Kumta, University of Pittsburgh)

Project Objective. This project will yield Li-metal anodes with specific capacity ≥ 2000 mAh/g (≥ 10 mAh/cm^2), ~ 1000 cycles, CE loss ≤ 0.01%, and CE ≥ 99.99% with superior rate capability. The goal is to (1) systematically characterize different approaches for generation of dendrite-free Li-metal anodes while also providing understanding of the scientific underpinnings, and (2) evaluate the microstructure and electrochemical performance of dendrite-free Li-metal anodes. Generation of high-performance, dendrite-free Li-metal anodes will successfully demonstrate generation of novel sulfur cathodes, affording fabrication of Li-S batteries meeting the targeted gravimetric energy densities ≥ 350 Wh/kg and ≥ 750Wh/l with a cost target $125/kWh and cycle life of at least 1000 cycles for meeting the EV Everywhere Grand Challenge blueprint.

Project Impact. Dendrite formation in electrochemical systems occurs due to inhomogeneous current densities coupled with local diffusion gradients, surface roughness, and kinetic roughening. Lithium dendrite formation and growth are, however, not well understood; adding to the complexity is SEI formation. Control and elimination of Li-metal dendrite formation is a veritable challenge. If overcome, it would render universal adoption of Li-anode batteries for stationary and mobile applications. This project is a scientific study of novel approaches to address dendrite formation in Li-anode batteries, electrolyte decomposition, and associated cell failure. Development of dendrite-free, high-performance lithium anodes will enable the use of Li-free cathodes, opening myriad possibilities to push the envelope in terms of cathode capacity and battery energy density.

Approach. This project will explore several approaches focused on engineering new structurally isomorphous metallic alloys combined with engineering the surface of metallic lithium as well as the current collectors, including development of novel high Li-conducting conjugated polymers and composite structures. The unifying theme is to initiate a uniform nucleation with homogenous growth, eliminating preferential reversible plating and de-plating and thus resulting in dendrite-free, high-energy-density Li-metal anodes.

Out-Year Goals. This project comprises three major phases to be successfully completed in three years:

- Year 1 – Synthesis, characterization, and scale up of suitable porous foams (PF) for use as current collectors for lithium anodes and Li-ion conductor (LIC) materials to prepare multilayer porous foams (MPF).
- Year 2 – Development of Li-rich structurally isomorphous alloy (SIA) anodes. Generation of composite multilayer anodes (CMAs).
- Year 3 – Advanced high-energy-density, high-rate, extremely cyclable cell development.

Collaborations. The project works with Dr. M. K. Datta and Dr. O. I. Velikokhatnyi (University of Pittsburgh) as co-PIs. It also collaborates Dr. A. Manivannan (Global Pragmatic Materials), XPS analysis; Dr. D. Krishnan Achary (University of Pittsburgh), solid-state magic angle spinning NMR (MAS-NMR) characterization; and Dr. J. R. Gaines (Kurt Lesker), thin-film system fabrication/ characterization.

Milestones

1. Synthesis and testing of SIA electrodes. (Q3, April 2018; Completed)
2. Optimization of MPFs to improve capacity and stability for scaling. (Q4, July 2018; Ongoing)
3. Synthesis of MPFs exhibiting: specific capacity ≥ 1000 mAh/g (≥ 4 mAh/cm2), > 400 cycles without cell failure), and initial CE of ≥ 95% with ≤ 0.05% loss per cycle. (October 2018; Ongoing)
4. First-principles investigations into identifying electronically and ionically conductive materials capable of acting as SIA compositions over a range of lithium compositions. (October 2018; Ongoing)
5. Fabrication/characterization of thick electrodes for 10-mAh cell configurations. (October 2018; Ongoing)

Progress Report

Last quarter, the concept of surface engineering of lithium metal to control the nucleation and growth of dendritic structure was introduced. It has been shown that the suitable surface engineering of lithium metal helps to control the nucleation overpotential.

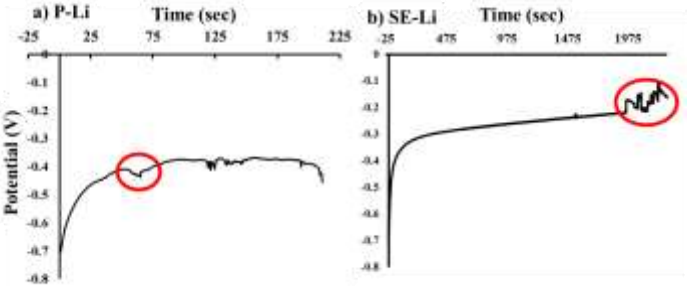

Figure 58. Sand's time experiment showing potential versus time for symmetric Li/Li cells for pristine lithium and surface-engineered lithium.

This quarter, considerable attention was directed toward understanding the "planar/non-planar" growth behavior of the surface engineered lithium metal (SE-Li) during long-term cycling. To this end, Sand's time analysis, post cycling SEM analysis, and full cell testing with high-voltage $LiMn_2O_4$ cathode were conducted to study the planar/non-planar growth behavior of SE-Li in 1 M $LiPF_6$ in EC:DEC:FEC=45:45:10 (vol%) electrolyte. Sand's time experiment (Figure 58) was conducted in a symmetric Li/Li in a three electrode Swagelok cell with SE-Li as the working electrode. The cell was charged (lithium plating) at an areal current density (I_{AD}) of 10 mA/cm^2. The onsets of voltage fluctuations indicate the onset of unstable lithium plating (non-planar lithium growth). As shown in Figure 58, pristine lithium (P-Li) and SE-Li show fluctuations at ~ 60 s and ~ 1940 s, corresponding to areal charge density (Q_{AD}) of ~ 0.17 mAh/cm^2 and ~ 5.39 mAh/cm^2, respectively, which indicates the delayed mossy lithium plating on SE-Li. The post plated SEM study (Figure 59b) of SE-Li showed preferential plating (I_{AD}=0.5mA/cm^2, t=1h) in the high energy regions due to surface engineering. P-Li under the same conditions, however, shows random plating of lithium. Post cycling SEM image (Figure 59c) of SE-Li after 10 cycles, (I_{AD}=0.5mA/cm^2, t=1h) shows gradual buildup of SEI layer in the high energy regions, still retaining the engineered surface features.

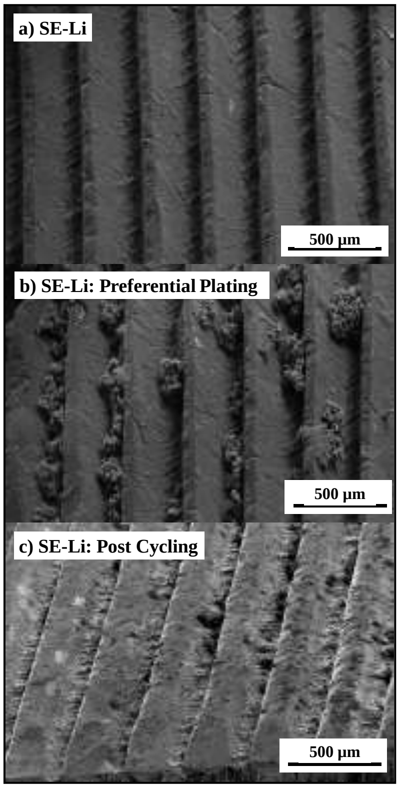

Figure 59. Scanning electron microscopy images of (a) surface-engineered lithium (SE-Li), (b) lithium plating on SE-Li, and (c) cycled SE-Li.

Full cell cycling Figure 60) of SE-Li and P-Li with $LiMn_2O_4$ cathode (~ loading: 11-15 mg/cm^2) was further conducted in a coin cell cycled between 3-4.3 V at a current of 100 mA/g (I_{AD}~1.5mA/cm^2) with analysis of the cycling performance. P-Li/$LiMn_2O_4$ shows rapid fade in specific capacity after 160 cycles, while SE-Li/$LiMn_2O_4$ shows stable cycling till 400 cycles (Figure 60). Premature capacity fade seen in P-Li electrode can be attributed to the unstable mossy plating on P-Li leading to rapid SEI layer buildup contrasted to SE-Li.

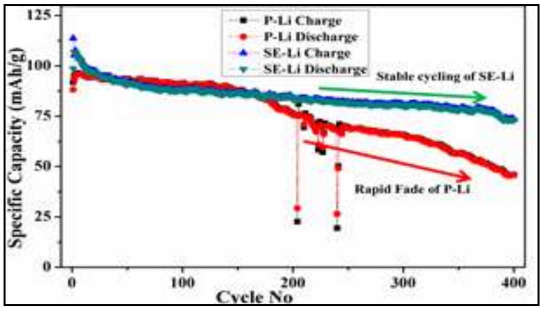

Figure 60. Cycling behavior of $LiMn_2O_4$ cathode tested against pristine lithium and surface-engineered lithium.

Patents/Publications/Presentations

Presentations

- 223rd ECS Meeting, Seattle, Washington (May 13–17, 2018): "Suppression of Dendrites in Lithium Sulfur Batteries Using a Composite Polymer Electrolyte (CPE)"; B. Gattu, P. Murugavel Shanthi, P. Thanapisitikul, B. A. Day, M. K. Datta, O. I. Velikokhatnyi, and P. N. Kumta.
- 223rd ECS Meeting, Seattle, Washington (May 13–17, 2018): "Surface Patterning of Lithium Metal: Novel Approach to Stable Li Metal Anodes"; P. Thanapisitikul, B. Gattu, P. M. Shanthi, B. A. Day, M. K. Datta, and P. N. Kumta.
- 223rd ECS Meeting, Seattle, Washington (May 13–17, 2018): "Surface Modification of Porous Foam Electrodes: Stabilization of Solid Electrolyte Interphase Formation in Li-Metal Batteries"; B. A. Day, B. Gattu, P. M. Shanthi, M. K. Datta, and P. N. Kumta.

Task 4.4 – Nanoscale Interfacial Engineering for Stable Lithium-Metal Anodes
(Yi Cui, Stanford University)

Project Objective. This study aims to render Li-metal anode with high capacity and reliability by developing chemically and mechanically stable interfacial layers between lithium metal and electrolytes, which is essential to couple with sulfur cathode for high-energy, Li-S batteries. With the nanoscale interfacial engineering approach, various kinds of advanced thin films will be introduced to overcome issues related to dendritic growth, reactive surface, and virtually "infinite" volume expansion of Li-metal anode.

Project Impact. Cycling life and stability of Li-metal anode will be dramatically increased. The success of this project, together with breakthroughs of sulfur cathode, will significantly increase the specific capacity of lithium batteries and also decrease cost, thereby stimulating the popularity of EVs.

Out-Year Goals. Along with suppressing dendrite growth, the cycle life, CE, and current density of Li-metal anode will be greatly improved (that is, no dendrite growth for current density up to 3.0 mA/cm^2, with CE greater than 99.5%) by choosing the appropriate interfacial nanomaterial along with rational electrode material design.

Milestones

1. Further improve the efficacy of Li-metal protection layers. (Q1, December 2017; Completed)
2. Improve the CE > 99.2%. (Q2, FY 2018; Completed)
3. Demonstrate > 800 cycles of Li-metal anode with stable host and interphase. (In progress)

Progress Report

Of the various approaches to maximizing Li-metal anode performance, design of lithium hosts (3D lithium) to accommodate the large volume change of lithium during cycling along with development of stable interfaces to minimize parasitic reactions are the most promising. One major type of 3D lithium consists of hollow electrodes that can accommodate electrochemically plated lithium. However, the preparation of hollow hosts via template-assisted methods requires subsequent removal of templates, which inevitably leaves micropores on the shell. Therefore, it is essential to prepare a stable interface on the surface of lithium hosts to completely seal pathways for the electrolyte to react with lithium. Here the team reports on design and development of a novel 3D electrode using ALD-coated HCS. The microporous carbon shell acts as a mechanically sturdy frame to confine electrochemical lithium plating. Importantly, the thin ALD coating seals the micropores of HCS to keep the electrolyte from contacting lithium and deactivates defective HCS surfaces (Figure 61). Through this design, the liquid electrolyte only contacts the outer surface of ALD Al_2O_3/HCS and cannot penetrate the hollow sphere. Therefore, SEI forms only on the outside of the ALD-coated HCS upon cycling.

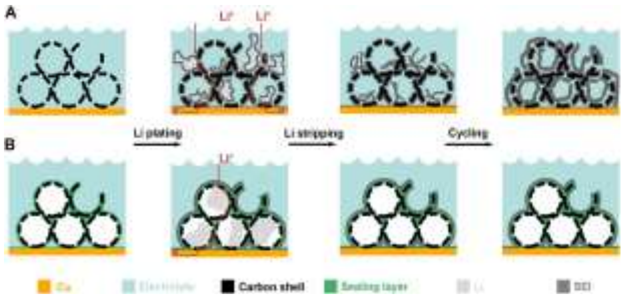

Figure 61. Schematic of lithium plating/stripping in lithium hosts (a) without and (b) with the sealing layer.

To further validate and visualize electrolyte infiltration, the team performed SEM/FIB characterization of HCS electrodes and ALD AL_2O_3/HCS electrodes dried in saturated aqueous solution of NaCl. The electrodes were immersed in the solution overnight, then taken out of the solution, gently wiped to remove excess solution on the surface, and dried. Salt precipitations can be observed inside the cavity of HCS, while no precipitates were identified within ALD Al_2O_3/HCS cavities (Figure 62). This confirms the feasibility of ALD coatings as a sealant for nanoporous carbon.

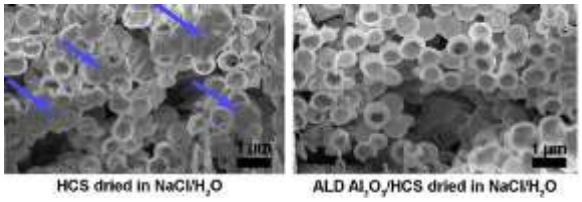

Figure 62. Scanning electron microscopy of hollow carbon spheres (HCS) and atomic layer deposition Al_2O_3 Al_2O_3/HCS electrodes soaked and dried in saturated NaCl solution. $LiPF_6$/EC/DEC electrolyte or saturated NACL/H_2O solution.

The cycle performance of ALD Al_2O_3/HCS electrodes was evaluated in ether-based electrolyte (Figure 63). For pristine HCS electrodes, the CE approached 98% during the first 200 cycles and then began to fluctuate in later cycles. More specifically, the CE sometimes reached a low value and then followed with an abnormally high value (> 100%) in later cycles. These observations could be related to the formation of dead lithium in the HCS electrode. For comparison, the CE versus cycle number curve of the two ALD Al_2O_3/HCS electrodes was always stable and smooth for the entire 500 cycles. The average CE of both electrodes tested was about 99% for 3 months of testing and, to the best of the team's knowledge, represents one of the most stable Li-metal anodes cycled in ether electrolyte. The ultralong cycle life, along with high CE, demonstrates the importance of avoiding parasitic reactions through segregation of liquid electrolyte and electrodeposited lithium.

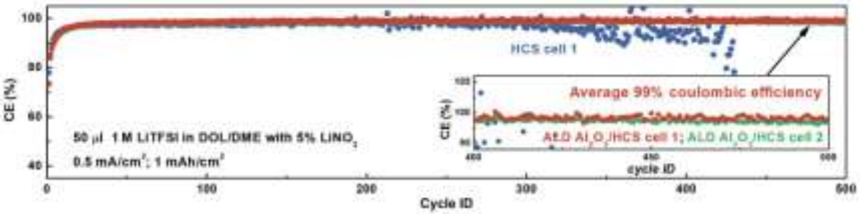

Figure 63. Cycling performance.

Patents/Publications/Presentations

Publication

- Xie, J., Y. Cui, et al. "Engineering Stable Interfaces for Three-Dimensional Lithium Metal Anodes." *Science Advances*. In press.

Task 4.5 – Composite Electrolytes to Stabilize Metallic Lithium Anodes
(Nancy Dudney and X. Chelsea Chen, Oak Ridge National Laboratory)

Project Objective. The project has several objectives: (1) prepare composites of representative polymer and ceramic electrolyte materials to achieve thin membranes that have the unique combination of electrochemical and mechanical properties required to stabilize the metallic lithium anode while providing for good power performance and long cycle life, (2) understand the Li-ion transport at the interface between polymer and ceramic solid electrolytes, which is critical to effective conductivity of the composite membrane, (3) identify key features of composite composition, architecture, and fabrication that optimize performance, and (4) using practical and scalable processing, fabricate thin electrolyte membranes to use with a thin metallic lithium anode to provide good power performance and long cycle life.

Project Impact. A stable lithium anode is critical to achieve high energy density with excellent safety, lifetime, and cycling efficiency. This study will identify key design strategies that should be used to prepare composite electrolytes to meet the challenging combination of physical, chemical, and manufacturing requirements to protect and stabilize the Li-metal anode for advanced batteries. By utilizing well characterized and controlled component phases, design rules developed for composite structures will be generally applicable toward substitution of alternative and improved solid electrolyte component phases as they become available. Success will enable DOE technical targets: 500-700 Wh/kg, 3000-5000 deep discharge cycles, and robust operation.

Approach. This project seeks to develop practical solid electrolytes to provide stable, long-lived protection for the Li-metal anode. Current electrolytes have serious challenges when used alone; oxide ceramics are brittle, sulfide ceramics are air sensitive, polymers are too resistive and soft, and many electrolytes react with lithium. Composites provide a clear route to address these issues. This project does not seek discovery of new electrolytes; rather, the goal is to study combinations of well-known electrolytes. The project emphasizes investigation of polymer-ceramic interfaces formed as bilayers and as simple composite mixtures where effects of interface properties can be readily isolated. In general, the ceramic phase is several orders of magnitude more conductive than the polymer electrolyte, and interfaces can contribute an additional source of resistance. Using finite element simulations as a guide, composites with promising compositions and architectures are fabricated and evaluated for Li-transport properties using AC impedance and DC cycling with lithium in symmetric or half cells. General design rules will be determined for wide application to other solid electrolyte combinations.

Out-Year Goal. The goal is to use advanced manufacturing processes where the architecture of the composite membrane can be developed and tailored to maximize performance and cost-effective manufacturing.

Collaborations. Work is conducted by Dr. Y. Zhang and Dr. X. Chen. Dr. J. Chen (ORNL) assisted with electron microscopic characterization and Dr. R. Ruther (ORNL) with Raman spectroscopy. Electrolyte powders are obtained from Ohara Corporation and Prof. Sakamoto (University of Michigan).

Milestones

1. Fabricate a full battery using aqueous spray coating for both the composite electrolyte and cathode incorporating a protected Li-metal anode. (Q4 FY 2017 stretch goal; Completed)
2. Accurately determine the polymer/ceramic electrolyte interface resistance for PEO and Ohara. Revisit effect of DMC on interface ASR. (Q1, FY 2018; Completed)
3. Minimize interface ASR by chemical and mechanical treatment with a goal of < 100 ohm. (Q2, FY 2018; ongoing, as ASR is > 100 ohm)
4. Move beyond model materials like Ohara and PEO, to include polymer gels. Identify promising polymer ceramic systems with interfacial ASR less than 10 ohm. (Q3, FY 2018; Ongoing – new polymer gel)
5. Assess the feasibility of slurry spray coating to form the thin membrane of new materials. (Q4, FY 2018)

Progress Report

The project performed extensive cycling tests on the two cells built last quarter, as shown in Figure 64. The two cells consisted of $LiFePO_4$ cathode, polymer catholyte, CPE|PE bilayer electrolyte or PE single-layer electrolyte, and lithium anode. At 50°C, the Li|PE|CPE|LFP cell had higher discharge capacity than the PE single layer at all tested rates. The PE cell could not endure C/5 rate as could CPE|PE bilayer electrolyte. The impedance spectroscopy results showed a decreased impedance of all interfaces after 20 cycles. The interfacial resistance of PE|cathode interface is much higher than that of CPE|cathode interface. The team is still trying to understand this observation.

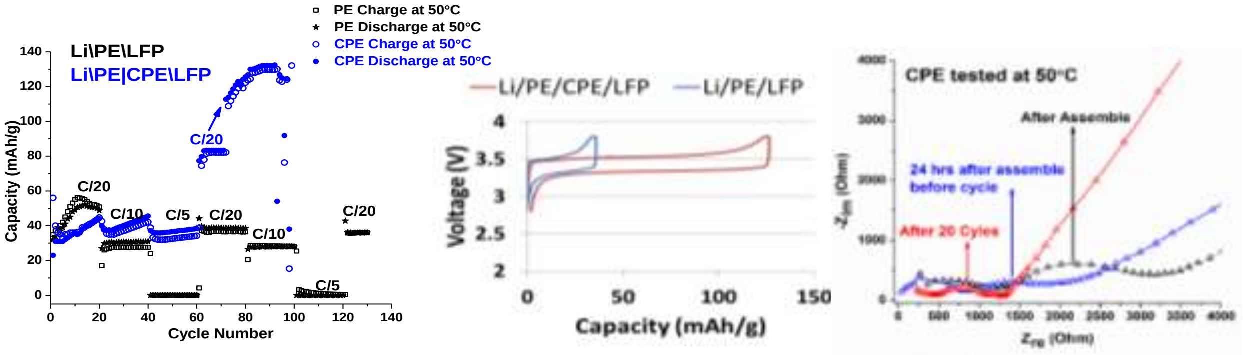

Figure 64. (left) Discharge and charge capacity as a function of cycle number for two all-solid-state cells at 50°C. (middle) Discharge and charge voltage profile at cycle 80. (right) Impedance spectra of Li|PE|CPE|LFP cells at different stages.

In addition, the team built two other cells with the following design: Li|CPE|LFP and Li|LiPON|CPE|LFP. They found that the cell containing CPE as the single layer of electrolyte did not cycle well with low discharge capacity (Figure 65). After 20 cycles, the voltage profile was abnormal, indicating reactions between lithium anode and Ohara ceramic. This may have led to dendrite growth in the cell. With 1-µm thick LiPON coating, the lithium interface was well protected and the LiPON|CPE cell was able to deliver higher capacity.

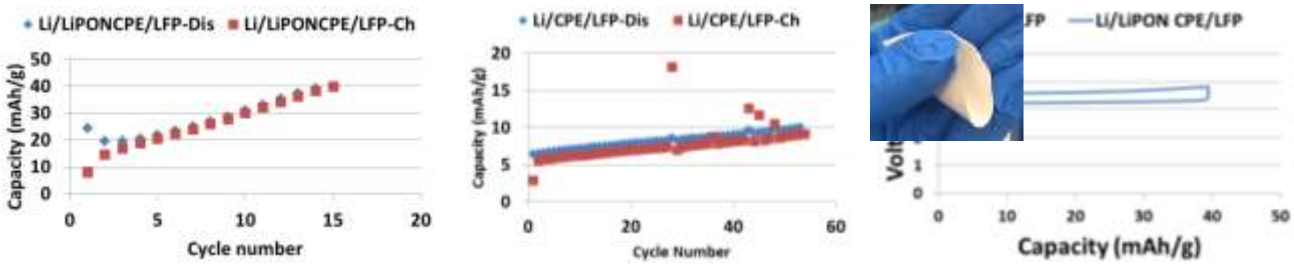

Figure 65. Discharge and charge capacity as a function of cycle number for Li|LiPON|CPE|LFP cell (left) and Li|CPE|LFP cell (middle), at 50°C. Discharge and charge voltage profile at cycle 15 for Li|Lipon|CPE|LFP cell and cycle 40 for Li|CPE|LFP cell (right).

This quarter, the team developed a new type of composite electrolyte: composite gel electrolyte. A one-pot synthesis containing oligomers, lithium salt, and ceramic powder was performed. The resulting membrane was a very homogenous and mechanically flexible membrane, as shown in Figure 66. The room-temperature ionic conductivity of the composite gel membrane was 1×10^{-4} S/cm. This is the same as the sintered ceramic plate and more than 1 order of magnitude higher than the project's previous composite electrolyte membranes with the same ceramic loading (Figure 66). Next quarter, the team will further assess properties of the composite gel electrolytes, particularly, the ion conduction path.

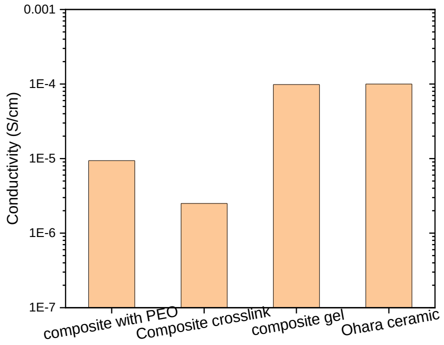

Figure 66. Ionic conductivity of previous composite electrolytes and composite gel electrolyte at 30°C.

Patents/Publications/Presentations

Publication

- Pandian, A. S., X. C. Chen*, J. Chen, B. S. Lokitz, R. E. Ruther, G. Yang, K. Lou, J. Nanda, F. M. Delnick, and N. J. Dudney*. "Facile and Scalable Fabrication of Polymer-Ceramic Composite Electrolyte with High Ceramic Loadings." *Journal of Power Sources* 390 (2018): 153–164.

Presentation

- DOE AMR Meeting, Washington, D. C. (June 18–21, 2018): "Composite Electrolyte to Stabilize Metallic Lithium Anodes"; N. J. Dudney, X. C. Chen, A. S. Pandian, Y. Zhang, and F. M. Delnick. Poster.

Task 4.6 – Lithium Batteries with Higher Capacity and Voltage (John B. Goodenough, University of Texas at Austin)

Project Objective. The project objective is to develop an electrochemically stable alkali-metal anode that can avoid the SEI layer formation and the alkali-metal dendrites during charge/discharge. To achieve the goal, a thin and elastic solid electrolyte membrane with a Fermi energy above that of metallic lithium and an ionic conductivity $\sigma > 10^{-4}$ S cm^{-1} will be tested in contact with alkali-metal surface. The interface between the alkali-metal and the electrolyte membrane should be free from liquid electrolyte, have a low impedance for alkali-metal transport and plating, and keep a good mechanical contact during electrochemical reactions.

Project Impact. A safe alkali-metal anode that can be plated/stripped reversibly at low resistance and high rates over many thousands of charge/discharge cycles would maximize the volumetric energy density for a given cathode of a rechargeable battery for powering an all-electric road vehicle. Such a battery could also be used for stationary back-up storage of electric power from energy sources other than fossil fuels.

Approach. The project will design, make, and test cells. The approach is to introduce a solid-electrolyte interfacing the anode and a coating on the anode current collector that is wet by a lithium anode. The solid electrolyte should also be wet by the anode to create a bond that is strong enough to constrain the anode volume changes to be perpendicular to the anode/electrolyte interface.

Out-Year Goals. The out-year goal is to develop coin cells that are safe and low-cost with a long cycle life at a voltage $V > 3.0$ V that can compete with the internal combustion engine for powering a road vehicle.

Collaborations. This project collaborates with A. Manthiram at UT Austin and K. Zaghib at HQ.

Milestones

1. Test the cyclability of plating of metallic lithium through a conventional polymer/ceramic or ceramic Li^+ electrolyte. (Q1, FY 2018; Completed)
2. Test relative energies of Cu^+/Cu^0 redox couple and energy of plating/stripping of lithium on/from copper. (Q2, FY 2018; Completed)
3. Test plating/stripping of metallic lithium on a carbon-coated copper current collector with different electrolytes. (Q3, FY 2018; Ongoing)
4. Demonstrate a low-cost, 3-V cell with a copper current collector as cathode. (Q4, FY 2018)

Progress Report

The project has tested plating/stripping of metallic lithium on a carbon-coated copper current collector with different electrolytes. Lithium metal is a promising anode material owing to its high Fermi level and specific capacity of 3861 mAh g^{-1}. Despite advantages in voltage and capacity, dendritic growth of lithium during battery operation has banned its commercial application. One potential solution to mitigate the dendrite issue is to reduce the effective current density during lithium growth. After a literature survey, the team found that the nucleation density of the lithium deposit is not high compared to total available surface of the current collector. Complete use of the current collector should be a starting point to solve the dendrite issue.

To increase the effective electrochemical area, the team coated a thin graphene film on a clean copper current collector with CVD. Defect density was monitored to get a high-quality graphene film. Half-cells with lithium as anode and copper as cathode were assembled. The team tested several liquid electrolytes such 1 M $LiPF_6$ in EC/DEC (1/1) and 1 M $LiPF_6$ in EC/DMC (1/1) because a solid electrolyte makes it difficult to probe the morphology of lithium deposit after an electrochemical reaction. All the cells were tested at room temperature.

Galvanostatic lithium deposition showed notable contrasts between the bare and graphene-coated copper current collectors, but not between the different liquid electrolytes. Figure 67 shows charge/discharge voltage curves at 0.5 mA cm^{-2} (discharge for 2 h, charge up to 2 V; 5th cycle). CE and average lithium deposition voltage of the bare and graphene-coated copper current collectors are 94.6% versus 96.2% and -27.7 mV versus -22.3 mV, respectively. It is apparent that the graphene film is effective to reduce electrochemical polarization and enhance charge/discharge reversibility. The team is testing long-term stability of the graphene film.

To explain the contrasts in the electrochemistry, the team has observed surface morphologies of the lithium deposits on the two different current collectors. In this experiment, shown in Figure 68, lithium metal was deposited at 1 mA cm^{-2} for 6 h. First, it was observed that the graphene layer was not effective to prohibit the dendritic lithium growth. However, the utilization of the current collector was remarkably different with the presence of graphene. Scattered island-type lithium growth was observed on the bare copper, but the lithium deposition on the graphene-coated copper is much more uniform. Moreover, mechanical adhesion of lithium deposit on the graphene-coated copper is far stronger. Lithium on the bare copper was easily peeled off. The morphological characterization suggests that the better lithium deposition kinetics and higher CE on the graphene-coated copper are mainly the result of better bonding of metallic lithium to the carbon than to copper.

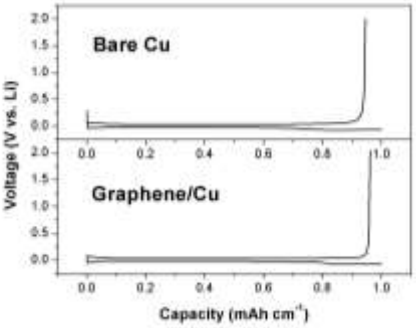

Figure 67. Charge/discharge voltage curves of bare and graphene-coated copper current collectors at 0.5 mA cm^{-2} (discharge for 2 h, charge up to 2 V; 5th cycle).

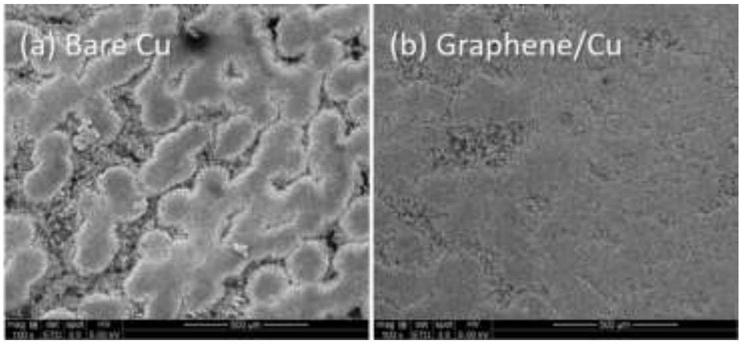

Figure 68. Scanning electron microscopy images of lithium deposit on the bare and graphene-coated copper current collectors. Lithium deposition was performed at 1 mA cm^{-2} for 6 h at room temperature.

Patents/Publications/Presentations

The project has no patents, publications, or presentations to report this quarter.

Task 4.7 – Advancing Solid-State Interfaces in Lithium-Ion Batteries
(Nenad M. Markovic and Larry A. Curtiss, Argonne National Laboratory)

Project Objective. The project objectives are multifaceted, including development of a new mechanically and chemically stable and Li-ion conductive ($\geq 2 \times 10^{-4}$ S/cm at 298 K) solid electrolyte for a solid-state battery encompassing a Li-metal anode, Li-oxide-based cathode, and nonflammable crystalline and amorphous solid electrolytes that can operate at cathode potentials > 5 V (denoted as a S_{Li}-S_{EL}-S_{C} system).

Project Impact. Protective organic and inorganic compounds can enhance stability of the interface, improve Li-ion interfacial transport, minimize dendrite formation, and increase safety in Li-ion batteries.

Approach. The project proposes to develop and use interdisciplinary, atomic-/molecular-level insight obtained from integrating both experimental- and computational-based methodologies to define the landscape of parameters that control interfacial properties for a new generation of the Li-ion solid-solid battery systems. The strategy will involve transferring knowledge gained from well-characterized thin-film materials to real-world materials. This strategy forms a closed loop wherein the knowledge gained from model systems is used to design more complex, real-world materials, and vice versa. The work will focus on utilizing existing in-house synthesis and characterization methods to enable rapid transition from fundamental science to realistic cells.

Out-Year Goals. The out-year goals are to use and develop the physical and chemical synthesis methods for design of solid-solid interfaces with unique chemical/mechanical/conductivity properties. The proposed work will develop and exploit a variety of *ex situ* and *in situ* experimental optical and surface sensitive techniques and electrochemical methods to explore and explain bulk and interfacial properties of the selected materials. The results will serve to unravel many puzzling bulk and interfacial properties of S_{Li}-S_{EL}-S_{C} systems, including various types of ceramic and glass materials.

Collaborations. This project funds work at ANL. It will establish collaboration with Jeff Sakamoto at University of Michigan.

Milestones

1. Development of new synthesis and characterization methods for controlled deposition of lithium on crystalline LLZMO (M = Nb, Ta, Al) materials on the appropriate substrate. (Q1, FY 2018; Completed)

2. Use electrochemical methods to investigate the efficiency as well as charge-discharge cyclability for selected LLZMO materials; Characterize the interface stability of lithium in contact with LLTO solid electrolyte with different orientation. (Q2, FY 2018; Completed)

3. Development of chemical- and physical-based synthesis method to make amorphous Li_2S-P_2S_5 (~ 10^{-3} S/cm at room temperature) and LLZMO solid electrolytes with fast ionic transport of lithium and to elucidate the chemical interaction of lithium with such a glass material. (Q3, FY 2018)

4. Introduce new experimental and computational tools for characterizing *ex situ* and *in situ* interaction of lithium and $LiCoO_2$ with amorphous solid electrolytes. (Q4, FY 2018)

Progress Report

Transition from Well-Ordered Systems to Disordered Systems: Sulfide Solid Electrolytes – LPS (75Li_2S-25P_2S_5). LPS glass was synthesized through bulk processing from Li_2S + P_2S_5 (3:1). It is an amorphous material with an ionic conductivity of 10^{-4} – 10^{-3} S cm^{-1} at room temperature and has been reported to have a low charge-transfer resistance against metallic lithium despite the high reactivity expected when in contact with lithium. Samples were loaded as-received into the glove box, and likely contain a reaction layer due to exposure to residual H_2O and O_2 during shipment. Lithium metal was sputtered directly onto as-received, unpolished LPS samples, and XPS spectra were measured before (red) and after (black) lithium sputtering. The lithium target contains 2-3% copper as an impurity from the target fabrication, leading to the observed copper peaks in the survey and core level spectra; however, as lithium is significantly more reactive than copper, the team does not anticipate any significant modification to the chemistry of the reaction. The XPS measurements clearly show that even unpolished LPS reacts with lithium metal, with the evolution of new features in the core level spectra (Figure 69). Surprisingly, the samples appear to be oxidized in contact with lithium, with the appearance of peaks to higher binding energy relative to those present on the as-received samples; however, at this time the team cannot rule out the presence of differential charging that would also lead to the presence of such peaks at higher binding energy. A recent report suggests that LPS decomposes to form Li_2S and Li_3P phases in contact with lithium [*Nature Communications* 9 (2018): 2490]; however, the project results suggest the reactions that take place on air/moisture-exposed surfaces may be more complicated than simple decomposition.

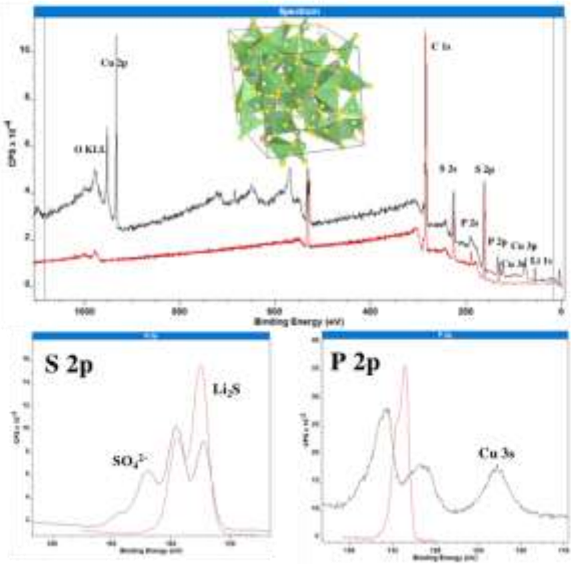

Figure 69. Survey (top) and S 2p and P 2p (bottom) core level X-ray photoelectron spectra before (red) and after (black) lithium sputtering show clear reaction of LPS with lithium metal.

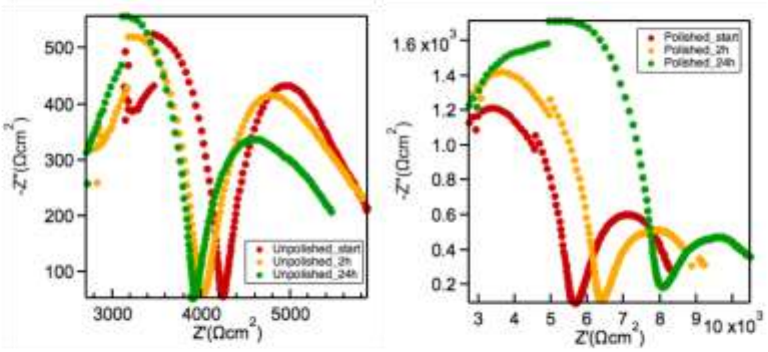

Figure 70. The impedance spectrum of unpolished (left) and polished (right) Li-LPS-Li symmetric cells at room temperature.

LPS Interface Stability Correlation with Impedance. One of the biggest challenges in pairing LLZO with lithium was the formation of a Li_2CO_3 oxidation layer that decreased the lithium wettability and led to an increase in the impedance of the LLZO/Li interface. In the case of LPS, the biggest challenge is its extreme sensitivity to moisture that quickly degrades the sample surface. The team prepared all of the Li-LPS-Li symmetric coin cells in a glove box: they were assembled with vacuum-deposited lithium present on both LPS surfaces and cleaned lithium foil pressed on both sides of unpolished and sandpaper-polished LPS samples. After cell assembly, the team followed the evolution of the cell impedance (Figure 70) to shed light on how the Li-LPS interface changes with time. For the sample with an unpolished surface (Figure 70, left), the team observed a slight decrease in impedance over the first 24 hours, which could be due to improved lithium contact with LPS due to interaction with the surface reaction layer. With polished LPS, both bulk and interfacial impedance is higher than for the unpolished sample (Figure 70, right), and a consistent increase in impedance is observed over the first 24 hours that suggests significantly higher chemical instability and reactivity with lithium relative to the unpolished sample. For both samples, however, it was not possible to measure impedance after 48 hours, suggesting that despite the higher initial stability of the unpolished sample, both samples eventually exhibit extensive reactivity with lithium. The project is currently analyzing these samples further and performing additional XPS measurements on polished and unpolished surfaces to gain deeper insight into the interfacial chemistry that guides the observed electrochemical response.

Patents/Publications/Presentations

Publications

- Connell, J. G., Y. Zhu, P. Zapol, S. Tepavcevic, J. Sakamoto, L. A. Curtiss, D. D. Fong, J. W. Freeland, and N. M. Markovic. "Crystal Orientation-Dependent Reactivity of Oxide Surfaces in Contact with Lithium Metal." ACS *Applied Materials & Interfaces* 10 (2018): 17471–17479.
- Zhu, Y., J. G. Connell, P. Zapol, S. Tepavcevic, J. Sakamoto, L. A. Curtiss, D. D. Fong, J. W. Freeland, and N. M. Markovic. "Surface Chemistry and Intrinsic Stability of Doped Lithium Lanthanum Zirconium Oxides." In preparation.

Presentation

- MRS Meeting, Phoenix, Arizona (April 2–6, 2018): "Interface Stability of Al, Ta, Nb-Doped $Li_7La_3Zr_2O_{12}$ in Contact with Lithium Metal"; Y. Zhu, J. G. Connell, P. Zapol, S. Tepavcevic, J. Sakamoto, L. A. Curtiss, D. D. Fong, J. W. Freeland, and N. M. Markovic.

Task 4.8 – Mechanical and Defect Properties at the Protected Lithium Interface (Nancy Dudney, Oak Ridge National Laboratory; Erik Herbert, Michigan Technological University; Jeff Sakamoto, University of Michigan)

Project Objective. A new project objective will be to understand the evolution of lithium metal upon cycling in contact with a generic solid electrolyte under various intrinsic and extrinsic conditions. The team plans to construct a set of stability maps that will describe the predominate mass transport process and defect structure evolution in lithium metal. Simple maps may address current density, areal capacity, and layer thickness. Then, maps extending to many other cell designs, interfacial factors, and duty cycle parameters are envisioned. A key activity in FY 2018 will be to develop experimental tools with which to probe lithium morphology in real time. While initial work will focus on experimental characterization, modeling will be introduced to interpret kinetic processes and extrapolate for alternative properties and designs and extended cycling.

Project Impact. Stability maps can guide realistic design choices for solid electrolytes and cell design. Ideally, lithium is deposited and removed uniformly to maintain a fully dense anode in good contact with the solid electrolyte. However, in practice, this may not be realized depending on cycling conditions, nature of the electrolyte, nature of the lithium, and cell architecture. Mapping the lithium defect evolution will offer insight for when, how, and why the lithium structure is altered, along with a much deeper analysis of the degradation. With this insight, the team can realistically project the performance of optimized Li-metal anodes. Materials and cells can be engineered to fulfill the target level of performance for EV batteries, namely 1000 cycles, 15-year lifetime, with adequate pulse power.

Approach. For the initial one-year effort, the project will work to develop experimental tools to probe the lithium structure and its interfaces with mechanical, imaging, and electrochemical methods during mass transport and relaxation. Different constructions for the stability maps will be explored to identify the most useful graphical representation of what is expected to be a rich and detailed analysis of the formation and annealing of lattice and extended defects in the lithium metal.

Out-Year Goals. In the out-years, modeling efforts will be integrated to interpret and extrapolate the results to wide cycling conditions and detailed analysis of the solid electrolytes being used to stabilize the lithium metal.

Collaborations. This project funds work at ORNL, Michigan Technological University, and University of Michigan.

Milestones

1. Characterize *in situ* changes in lithium anode from a single stripping/plating half cycle. (FY 2017; Ongoing)
2. Identify two experimental tools to probe the defect structure of lithium created under cycling. (Q2, FY 2018; Completed)
3. Cycle lithium under conditions expected to create different defect structures and morphologies to begin creation of stability maps. (Q3, FY 2018; Ongoing)
4. Design and construct stability diagrams to map the evolution of the defects structure and morphology for lithium metal under a variety of cycling conditions and with different model solid electrolytes. (Q4, FY 2018)

Progress Report

Equipment is assembled at Michigan Technological University for tests of lithium properties using nanoindentation during or immediately after cycling. Initial results will be reported next quarter.

Evidence for excellent cycling of lithium with garnet LLZO solid electrolyte disks continues to be collected. Current samples have an ASR interface resistance of only 2 ohms cm^2. These samples are used to investigate changes in the lithium metal with extended cycling using a wide range of current densities and temperatures.

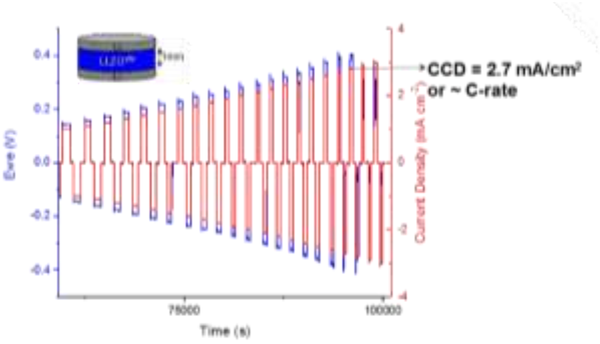

Figure 71. Li-LLZO-Li room-temperature cycling data. A critical current density of 2.7 mA/cm^2 (avg; stdev ~ 0.5 mA/cm^2; n=12) was achieved.

Figure 71 shows determination a critical current density (CCD) of 2.7 mA/cm^2 for symmetric Li-LLZO-Li cells measured at room temperature. Here, the LLZO interface was carefully prepared and was free of any interface coating, such as gold, often used to improve the wetting.

Statistics for many measurements of the CCD at room and elevated temperatures are collected in the table included in Figure 72. The CCD appears to follow Arrhenius behavior (Figure 72), exhibiting an activation energy of 0.25eV. The team is analyzing the data to fit the activation energy to a physical model, with an emphasis on balancing the lithium flux at the Li-LLZO interface.

Table 4. Averages and standard deviations for critical current density as a function of temperature.

Temperature	25°C	40°C	60°C	80°C	100°C
Average CCD (mA·cm^{-2})	0.93	1.48	2.67	4.07	6.70
Standard Dev. (mA·cm^{-2})	0.24	0.24	0.70	0.31	1.21

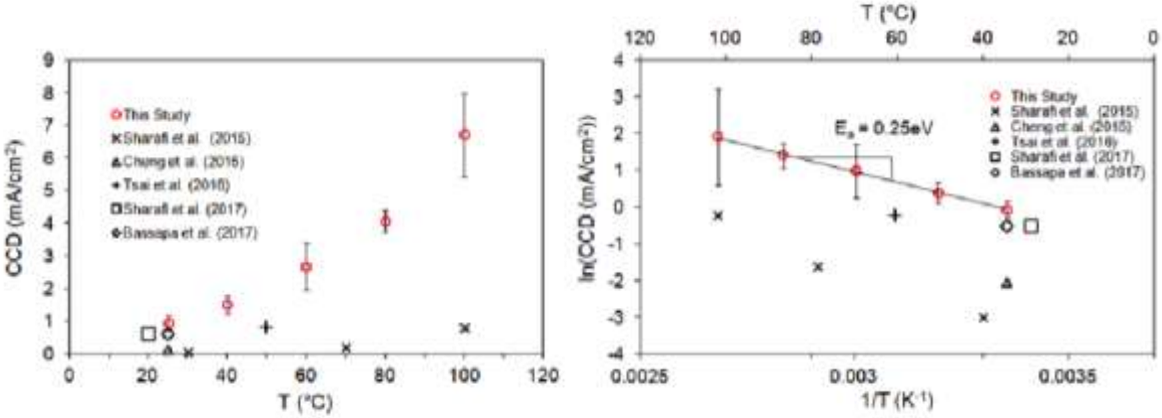

Figure 72. Critical current density (CCD) as a function of temperature in Li-LLZO-Li cells (top left) and the logarithm of CCD as a function of the inverse of temperature (top right). Both plots include reported CCDs from the literature for comparison.

Patents/Publications/Presentations

Publications

- Taylor, N. J., S. Stangeland-Molo, C. G. Haslam, A. Sharafi, T. Thompson, M. Wang, R. Garcia-Mendez, and J. Sakamoto. "Demonstration of High Current Densities and Extended Cycling in the Garnet $Li_7La_3Zr_2O_{12}$ Solid Electrolyte." *Journal of Power Sources* 396 (2018): 314–318.
- Herbert, E. G., P. S. Phani, N. J. Dudney, and S. A. Hackney. "Nanoindentation of High Purity Vapor Deposited Lithium Films: The Elastic Modulus." *Journal of Materials Research* 33, no. 10 (2018): 1335.
- Herbert, E. G., S. A. Hackney, N. J. Dudney, V. Thole, and P. S. Phani. "Nanoindentation of High Purity Vapor Deposited Lithium Films: A Mechanistic Rationalization of Diffusion-Mediated Flow." *Journal of Materials Research* 33, no. 10 (2018): 1347.
- Herbert, E. G., S. A. Hackney, N. J. Dudney, V. Thole, and P. S. Phani. "Nanoindentation of High Purity Vapor Deposited Lithium Films: A Mechanistic Rationalization of the Transition to Dislocation-Mediated Flow." *Journal of Materials Research* 33, no. 10 (2018): 1361.

Presentations

- Department of Energy, U. S.–China Battery Workshop, San Diego, California (May 2018): "Garnet Based Li-Metal Batteries"; J. Sakamoto. Invited.
- MRS Meeting, Phoenix, Arizona (April 2018): "What Governs the Stability of the Li-LLZO Interface at High Current Density?"; J. Sakamoto. Invited.
- 233rd ECS Meeting, Seattle, Washington (May 2018): "What Governs the Stability of the Li-LLZO Interface at High Current Density?"; J. Sakamoto. Invited.

TASK 5 – SULFUR ELECTRODES

Summary and Highlights

Advances in Li-ion technology have been stymied by challenges involved in developing high reversible capacity cathodes and stable anodes. Hence, there is a critical need for development of alternate battery technologies with superior energy densities and cycling capabilities. In this regard, Li-S batteries have been identified as the next flagship technology, holding much promise due to the attractive theoretical specific energy densities of 2,567 Wh/kg. In addition, realization of the high theoretical specific capacity of 1,675 mAh/g corresponding to formation of Li_2S using earth-abundant sulfur renders the system highly promising compared to other available cathode systems. Thus, the research focus has shifted to developing Li-S batteries. This system, however, suffers from major drawbacks, as elucidated below:

- Limited inherent electronic conductivity of sulfur-based and sulfur-compound-based cathodes;
- Volumetric expansion and contraction of both the sulfur cathode and lithium anode;
- Soluble polysulfide formation/dissolution and sluggish kinetics of subsequent conversion of polysulfides to Li_2S, resulting in poor cycling life;
- Particle fracture and delamination resulting from the repeated volumetric expansion and contraction;
- Irreversible loss of lithium at the sulfur cathode, resulting in poor CE; and
- High diffusivity of polysulfides in the electrolyte, resulting in plating at the anode and consequent loss of driving force for lithium diffusion (that is, drop in cell voltage).

These major issues cause sulfur loss from the cathode, leading to mechanical disintegration. Additionally, surface passivation of anode and cathode systems results in a decrease in the overall specific capacity and CE upon cycling. Consequently, the battery becomes inactive within the first few charge-discharge cycles. Achievement of stable, high capacity Li-S batteries requires execution of fundamental studies to understand the degradation mechanisms in conjunction with devising engineered solutions.

This Task addresses both aspects with execution of esoteric, fundamental *in situ* XAS and *in situ* electron paramagnetic resonance (EPR) studies juxtaposed with conducting innovative applied research comprising use of suitable additives, coatings, and exploration of composite morphologies as well as appropriate engineered strategies. Both ANL and LBNL use X-ray based techniques to study phase evolution and loss of CE in S-based and S-Se-based electrodes, primarily by the former during lithiation/delithiation while understanding polysulfide formation in sulfur and oligomeric PEO solvent by the latter, respectively. Work from PNNL, University of Pittsburgh, and Stanford demonstrates high areal capacity electrodes exceeding 4 mAh/cm^2. Following loading studies, PNNL performed *in situ* EPR to study reaction pathways mediated by sulfur radical formation. Coating/encapsulation approaches adopted by University of Pittsburgh and Stanford comprise flexible sulfur wire electrodes coated with LIC by University of Pittsburgh, and TiS_2 encapsulation of Li_2S in the latter, both ensuring polysulfide retention at sulfur cathodes. BNL work, on the other hand, has focused on benchmarking of pouch-cell testing by optimization of the voltage window and study of additives such as LiI and $LiNO_3$. *Ab initio* studies at Stanford and University of Pittsburgh involve calculation of binding energies, diffusion coefficients, ionic conductivities, and reaction pathways determination, augmenting the experimental results. Similarly, AIMD simulations performed at TAMU reveal multiple details regarding electrolyte decomposition reactions and the role of soluble polysulfides on such reactions. Using kinetic MC simulations, electrode morphology evolution and mesostructured transport interaction studies were also executed. Studies at PNNL suggest that proper control of electrode porosity/thickness is essential for obtaining high-energy Li-S batteries.

Porosity shows strong dependence on calendering pressure because of low tap densities of electrode components such as sulfur and carbon. Increasing the calendering-pressure from 0.2 to 1.5 ton (T) leads to rapid decrease of electrode porosity, resulting in improvement of electrode volumetric energy density.

Measured electrode volumetric energy density increased from 650 Wh L^{-1} for as-cast electrode (120-μm thick) to 1300 Wh L^{-1} for electrode compressed to 60 μm. Additionally, Pennsylvania State University has shown use of dimethyl disulfide as a functional co-solvent, demonstrating its ability to show an alternate electrochemical reaction pathway for sulfur cathodes by formation of dimethyl polysulfides and lithium organosulfides as intermediates and reduction products. Further, University of Wisconsin at Milwaukee (UWM) has conducted high-performance liquid chromatography (HPLC)-MS studies and has determined the distribution of polysulfides at various discharge and recharge reactions. UT Austin, at the same time, has shown that by integrating polysulfide-filter-coated separators fabricated with cellulose nanofiber, the cells retain 50% of the initial capacity after storing for one year and exhibit a low self-discharge rate of only 0.14% per day.

Each of these projects has a collaborative team of experts with the required skill set needed to address the EV Everywhere Grand Challenge of 350 Wh/kg and 750 Wh/l and cycle life of at least 1000 cycles.

Highlights. This Task reports the following project highlights for this quarter:

- Work in Dr. P. Mukherjee's group (Purdue University) and with Perla Balbuena (TAMU) has focused on using mesoscale modeling for understanding of the transport of active species in the electrolyte in response to (i) a concentration gradient – diffusion as well as (ii) a potential gradient resulting in migration in the carbon-sulfur cathode architecture. This work has demonstrated that the formation of S-C chemical bonds at the synthesis stage favors the discharge reaction during lithiation of S-C cathodes. Advantages include the suppression of the formation of long-chain polysulfide species, and the contribution of carbon to enhance the overall cathode capacity.
- Dr. H. Gan (BNL) has identified TiS_2 to be an effective multifunctional cathode additive for Li-S batteries due to its high electronic conductivity, electrochemical activity, and polysulfide (PS) adsorption ability. High surface area, 2D TiS_2 nano-sheets additive when cycled at C/5 discharge rate, shows much better capacity retention and higher sulfur utilization over 200 cycles. This observed better electrochemical performance is attributed to the improved PS adsorption and the uniform distribution of 2D TiS2 nano-sheets within the sulfur cathode.
- D. Qu (UWM) and X-Q. Yang (BNL) copolymerized sulfur with p-phenylene vinylene derivative (denoted as Xant-) to form a new conductive cross-linked polysulfur-random-PPV (denoted as S/Xant-) copolymer cathode material S/Xant- (70 wt% S) in one pot. The S/Xant- exhibits a high initial capacity of 720 mAh g-1(based on S/Xant- or 1029 mAh g^{-1} based on sulfur) at 100 mA g^{-1} discharge rate exhibiting good electrochemical stability showing promise of further improvement.

Task 5.1 – Novel Chemistry: Lithium Selenium and Selenium Sulfur Couple (Khalil Amine, Argonne National Laboratory)

Project Objective. The project objective is to develop a novel S_xSe_y cathode material for rechargeable lithium batteries with high energy density and long life, as well as low cost and high safety.

Project Impact. Development of a new battery chemistry is promising to support the goal of PHEV and EV applications.

Approach. The dissolution of lithium polysulfides in nonaqueous electrolytes has been the major contribution to the low energy efficiency and short life of Li-S batteries. In addition, the insulating characteristics of both end members during charge/discharge (sulfur and Li_2S) limit their rate capacity. To overcome this problem, sulfur or Li_2S is generally impregnated in a carbon-conducting matrix for better electronic conductivity. However, this makes it difficult to increase the loading density of practical electrodes. It is proposed to solve these barriers using the following approaches: (1) partially replace sulfur with selenium, (2) nano-confine the S_xSe_y in a nanoporous conductive matrix, and (3) explore advanced electrolytes with suppressed shuttle effect.

Out-Year Goals. This new cathode will be optimized with the following goals:

- A cell with nominal voltage of 2 V and energy density of 600 Wh/kg.
- A battery capable of operating for 500 cycles with low capacity fade.

Collaborations. This project engages in collaboration with the following: Professor C. Wang of UMD, Dr. Y. Ren and Dr. C. Sun of Advanced Photon Source at ANL, and Dr. L. A. Curtiss at ANL.

Milestones

1. Exploration of novel siloxane-based electrolytes for Li-Se and Se-S systems. (Q1, FY 2018; Completed)
2. Development of high-performance Li/Se-S batteries using optimized siloxane-based electrolytes. (Q2, FY 2018; Completed)
3. Computational modeling on the working mechanism of high-concentration siloxane-based electrolytes. (Q3, FY 2018; Ongoing)
4. *In situ/ex situ* diagnostic on the function mechanism of high-concentration siloxane-based electrolytes. (Q4, FY 2018)

Progress Report

Li-salt concentration was proposed recently as an important control parameter of reduced polysulfide dissolution in Li/S batteries. This quarter, the team further conducted first principles DFT AIMD to simulate the solvation behavior of high-concentration siloxane electrolytes. During this process, the chemical processes and properties such as stability of intermediates, solvation of polysulfides, and reactivity toward the nonaqueous electrolytes could reveal the underlying function mechanism of high-concentration siloxane-based electrolytes for Li/Se-S batteries. The premilinary results are discussed below.

Figure 73 shows the initial and optimized structure of high-concentration LiTFSI in DOL+ANL-2, as computed by DFT. The team finds that with increasing concentration of LiTFSI salt, the Li-O bonds start to break, which means that the solvation of Li^+ and $TFSI^-$ toward the free solvents (mixtures of DOL and ANL-2) start to increase. Therefore, with increasing LiTFSI concentration, the free DOL and ANL-2 solvents were both significantly decreased, which would lower the amount of the solvated polysulfides and thus decrease the polysulfides dissolution. Results showed that 5 M is an optimized concentration for LiTFSI as the solvation of Li^+ and $TFSI^-$ became less preferred due to less free solvents.

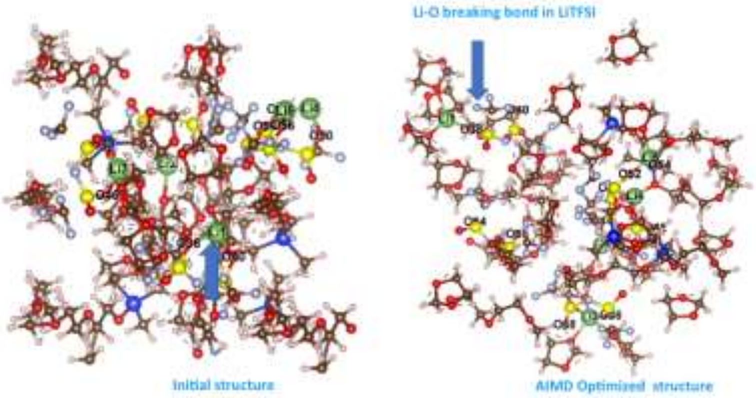

Figure 73. Initial (left) and optimized (right) structure of high-concentration siloxane-based electrolytes using *ab initio* molecular dynamic simulation.

In the next step, the team further evaluated solvation of polysulfides (for example, Li_2S_6) in the high-concentration siloxane electrolytes. As shown in Figure 74, the result showed that there is no chemical bond breaking of Li_2S_6. This means there is no interaction between Li_2S_6 and the surronding environment, that is, high-concentration siloxane-based electrolytes. This is because the solvation of Li^+ and $TFSI^-$ toward the solvents (mixture of DOL and ANL-2) are both stronger than the solvation between Li_2S_6 and the solvents. Hence, AIMD simulation results showed that the concentration of Li-salt, the solvation capability of salt with the solvents, and the solvation capability of polysulfides toward the solvents play a crucial role in suppressing polysulfides/poyselenides dissolution. Next quarter, the team will further use experimental techniques such as *in situ* X-ray absorption near-edge structure (XANES) and *in situ* Raman spectroscopy to directly confirm suppression of polysulfides/ polyselenides formation, and also other techniques such as XPS to look into the interface.

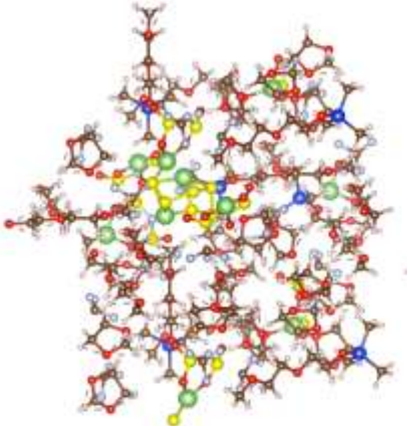

Figure 74. Computed structure of Li_2S_6 in high-concentration siloxane-based electrolytes.

Patents/Publications/Presentations

Presentation

- 2018 Advanced Automobile Battery Conference, San Diego, California (June 4–7, 2018): “Novel Chemistry for Automotive Application: Lithium-Selenium and Selenium-Sulfur Couple”; G.-L. Xu, Z. Chen, and K. Amine. Invited.

Task 5.2 – Development of High-Energy Lithium-Sulfur Batteries

(Jun Liu and Dongping Lu, Pacific Northwest National Laboratory)

Project Objective. The project objective is to develop high-energy, low-cost Li-S batteries with long lifespan. All proposed work will employ thick sulfur cathode (≥ 2 mAh/cm^2 of sulfur) at a relevant scale for practical applications. The diffusion process of soluble polysulfide out of thick cathode will be revisited to investigate cell failure mechanism at different cycling. The fundamental reaction mechanism of polysulfide under the electrical field will be explored by applying advanced characterization techniques to accelerate development of Li-S battery technology.

Project Impact. The theoretical specific energy of Li-S batteries is ~ 2300 Wh/kg, which is almost three times higher than that of state-of-the-art Li-ion batteries. The proposed work will design novel approaches to enable Li-S battery technology and accelerate market acceptance of long-range EVs required by the EV Everywhere Grand Challenge.

Approach. The project proposes to (1) identify and address key issues of applying high-energy sulfur cathodes including materials, binders, electrode architectures and functional electrode additives, (2) advance mechanism study of sulfur cathode and electrolyte by using *in situ*/*ex situ* techniques and custom-designed hybrid cell setup, and (3) verify effectiveness of the new approaches with coin/pouch cells by using high-loading electrodes (> 4 mg/cm^2), limited lithium (< 200% lithium excess), and lean electrolyte (E/S < 4 μL/mg).

Out-Year Goals. This project has the following out-year goals:

- Fabricate Li-S pouch cells with thick electrodes to understand sulfur chemistry/electrochemistry in environments similar to real application.
- Leverage the Li-metal protection project funded by the DOE and PNNL advanced characterization facilities to accelerate development of Li-S battery technology.
- Develop Li-S batteries with a specific energy of 400 Wh/kg at cell level, 1000 deep-discharge cycles, improved abuse tolerance, and less than 20% capacity fade over a 10-year period to accelerate commercialization of EVs.

Collaborations. This project engages in collaboration with the following: Dr. X-Q. Yang (BNL), Dr. D. Qu (UWM), Dr. X. Xiao (GM), and Dr. J. De Yoreo (PNNL).

Milestones

1. Study of electrolyte compatibility with different carbon host materials and binders and their effects on reversible sulfur utilization. (Q1, December 31, 2017; Completed)

2. Design and demonstration of an electrochemical cell by using ceramics Li$^+$ conductive separator for focused cathode or anode mechanism study for Li-S. (Q2, March 31, 2018; Completed)

3. Study failure mechanism of Li-S cell under lean amount of liquid electrolyte by decoupling the interference of lithium anode using liquid/solid electrolyte hybrid cell. (Q3, June 30, 2018; Completed)

4. Develop functionalized separators to suppress polysulfide shuttle and improve interfacial stability of lithium anode. (Q4, September 30, 2018; In progress)

Progress Report

Last quarter, a novel solid/liquid electrolyte hybrid-cell without the interferences of the lithium anode was designed for a focused study of sulfur cathodes. Functionality and sealing of the device were verified. This quarter, performance of sulfur cathodes was investigated under different conditions, including electrode wetting process and sulfur utilization in sulfur cathodes of high sulfur loading with different electrolyte/sulfur ratios. With the help of the hybrid cell and meticulously designed sealing parts, accurate electrolyte control within the cathode and cell dead-volume can be realized. For example, minimal dead-volume can be reached by properly matching the cell dimension and electrode size. This makes it possible to quantify the minimum electrolyte amount required for a specific electrode architecture and composition design. Before the study, the compatibility of the liquid and solid electrolyte was first evaluated. The Indium (In) and stainless steel (SS) blocking electrodes were used in such In-SE-LE-SS cell configuration, wherein the solid electrolyte (SE) contacts with liquid electrolyte (LE) directly. In contrast to the reported results, the DME solvent is found to be incompatible with the garnet solid electrolyte. After 10 hours of contact with the DME electrolyte, an additional semicircle appeared in the EIS and increased with time (Figure 75a). Formation of a new interfacial layer on the garnet pellet is possible. On the other hand, when DOL-based electrolyte is used, the EIS plot indicates stable response throughout the whole test. Thus, 1 M LiTFSI/DOL was used as the electrolyte in the subsequent studies of electrode wetting and evaluation of cell performance. As one of the main study foci, electrolyte infiltration in sulfur electrodes of high loading was investigated under lean electrolyte conditions, which mimics electrode wetting in high-energy Li-S pouch cells. The In electrode was lithiated by electrochemical method and used for the InLi/SE/LE/SS cell. EIS of the cell was monitored for 22 hours after injecting the 1M LiTFSI/DOL electrolyte. Almost identical EIS spectra during this period further confirmed the stability of SE with the electrolyte and the excellent sealing of the system (Figure 75c). Then, a sulfur electrode (sulfur mass loading ~ 4 mg/cm^2) was added into the cathode chamber. A lean amount of electrolyte was applied. In addition, the minimized dead-volume design will eliminate any excess electrolyte out of the InLi/SE/LE/Sulfur cell. The EIS monitoring started immediately after the cell assembly. At the very beginning, the overall charge transfer resistance (R_{ct}) is low and comparable to that of a blank test without a sulfur electrode (Figure 75c). However, the R_{ct} increases significantly, even after one hour of rest. The trend of resistance increase accelerates in the first 12 hours, then slows down and achieves stability after 18 hours (Figure 75d/inset). Compared to the stable R_{ct} observed in the blank test (Figure 75c), significant change observed in the EIS spectra may be explained by the slow electrode wetting in the high loaded sulfur electrodes. During the resting period, the limited electrolyte in between the sulfur electrode and SE will infiltrate into the electrode architecture, penetrating into the individual S/C secondary particles. This results in the shortage of electrolyte at the electrode interface, and thus leads to the increase in R_{ct}. After about 18 hours of rest, the cell resistance stabilizes, indicating complete electrolyte infiltration or the electrolyte is uniformly distributed. This stabilization time has been applied in the preparation and test of high energy Li-S pouch cells with similar electrode loadings.

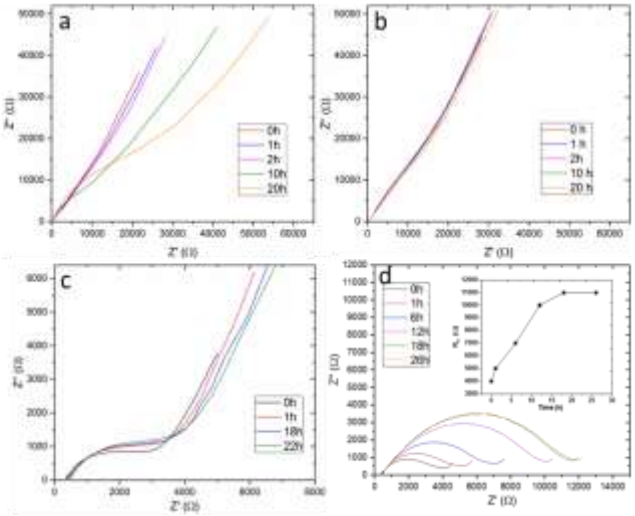

Figure 75. Electrochemical impedance spectra (EIS) evolution in the first 20 hours of In-SE-LE-SS cell with electrolytes (a) 1 M LiTFSI/ DME and (b) 1 M LiTFSI/DOL. (c) EIS evolution of InLi/SE/LE/SS and (d) InLi/SE/LE/S with 1 M LiTFSI/DOL. EIS test (5 mv, 105-10-1 Hz).

Patents/Publications/Presentations

Publications

- Liu, J., D. Lu, J. Zheng, P. Yan, B. Wang, X. Sun, Y. Shao, C. Wang, J. Zhang, and J. Liu. “Minimizing Polysulfide Shuttle Effect in Lithium Sulfur Batteries by Anode Surface Passivation.” ACS *Applied Material & Interfaces* 10, no. 26 (2018): 21965–21972.
- Lu, D., Q. Li, J. Liu, J. Zheng, Y. Wang, S. Ferrara, J. Xiao, J. Zhang, and J. Liu. “Enabling High Energy Density Cathode for Lithium-Sulfur Batteries.” ACS *Applied Material & Interfaces* 10, no. 27 (2018): 23094–23102.

Task 5.3 – Nanostructured Design of Sulfur Cathodes for High-Energy Lithium-Sulfur Batteries (Yi Cui, Stanford University)

Project Objective. The charge capacity limitations of conventional TM oxide cathodes are overcome by designing optimized nano-architectured sulfur cathodes. This study aims to enable sulfur cathodes with high capacity and long cycle life by developing sulfur cathodes from the perspective of nanostructured materials design, which will be used to combine with Li-metal anodes to generate high-energy Li-S batteries. Novel sulfur nanostructures as well as multi-functional coatings will be designed and fabricated to overcome issues related to volume expansion, polysulfide dissolution, and the insulating nature of sulfur.

Project Impact. The capacity and the cycling stability of sulfur cathode will be dramatically increased. This project's success will make Li-S batteries to power EVs and decrease the high cost of batteries.

Out-Year Goals. The cycle life, capacity retention, and capacity loading of sulfur cathodes will be greatly improved (200 cycles with 80% capacity retention, > 0.3 mAh/cm^2 capacity loading) by optimizing material design, synthesis, and electrode assembly.

Collaborations. This project engages in collaboration with the following:

- BMR PIs,
- SLAC National Accelerator Laboratory: *In situ* X-ray, Dr. M. Toney, and
- Stanford: Professor Nix, mechanics; and Professor Bao, materials.

Milestones

1. Elucidate different adsorption mechanisms and probe possible adsorption species. (Q2, FY 2018, January 2018; Completed)
2. Develop multi-functional sulfur cathode binder capable of controlling the polysulfide shuttling and facilitating Li-ion transport. (Q3, FY 2018, April 2018; Completed)
3. Demonstrate the flame-retardant property of binder to improve safety and propose flame-retardant mechanism. (Q4, FY 2018, July 2018; Completed)
4. Build *in situ* characterization platform to monitor nucleation/dissolution of sulfur/Li_2S_n. (Q1, FY 2019, October 2018; Ongoing)

Progress Report

Last quarter, the team developed an aqueous inorganic polymer, ammonium polyphosphate (APP), as a novel multifunctional binder to address the issues existing in Li-S batteries. The strong binding affinity of the main chain of APP with lithium polysulfides blocks diffusion of polysulfide anions and inhibits their shuttling effect. The coupling of APP with Li-ion facilitates ion transfer and promotes the kinetics of the cathode reaction. In this report, the team demonstrates that APP bestows the sulfur cathode with significantly improved flame-retardant property, thus improving the safety of Li-S batteries.

The safety issues of Li-S batteries originating from the flammability of lithium, sulfur electrodes, and the organic liquid electrolytes can be alleviated by engineering battery structure, employing SSE, and optimizing electrode design. APP binder employed here not only improves the polysulfide adsorption capability but also endows sulfur electrode flame-retardant properties to effectively improve the safety of Li-S batteries. To demonstrate the flame-retardant property of APP, sulfur cathodes with APP and PVDF binders were exposed to a direct flame until they ignited, after which the direct flame was removed. Sulfur cathode with traditional PVDF binder was tested using this method, as shown in Figure 76a. Upon exposure to direct flame for ~ 1 s, the sulfur cathode was ignited, and the flame burned vigorously and spread quickly. The specific burning time, that is, the burning time divided by the mass of sulfur, was calculated to be ~ 519 s g^{-1}, reflecting the high flammability of sulfur cathode (Figure 76c). The sulfur cathode with APP binder was tested using the same method. In contrast, APP binder is efficient in reducing the burning time of the sulfur cathode. After being ignited, the flame is suppressed and finally self-extinguished (Figure 76b-c). The specific burning time was significantly decreased to ~ 289 s g^{-1}, indicating the flame-retardant properties of the APP binder based sulfur cathode. The flame-retardant mechanism of the APP binder can be proposed as follows: during the combustion process, APP decomposes and releases ammonia/water gas, and crosslinks to form an insulating polymer layer (Figure 76d). This insulating polymer layer acts as a physical barrier to heat, fuel, and oxygen transfer, thus building up an isolation layer between the condensed and gas phases and effectively protecting the underlying sulfur from catching fire (Figure 76d).

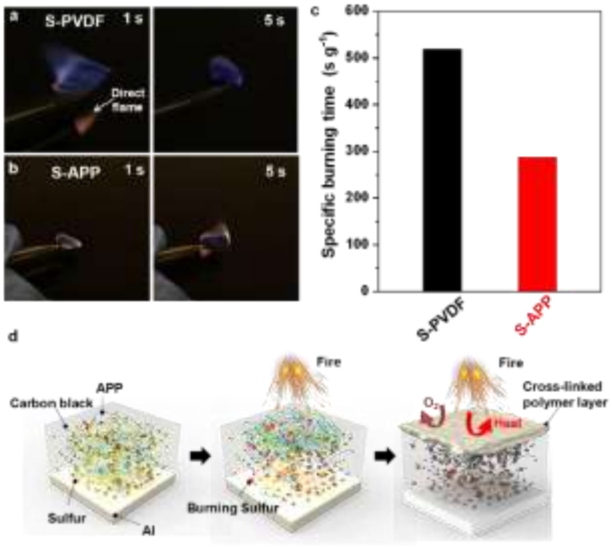

Figure 76. The specific burning time test of sulfur electrodes with (a) sulfur – polyvinylidene fluoride (S-PVDF) electrode and (b) sulfur – ammonium polyphosphate (S-APP) electrode. The time indicated in the pictures is counted as soon as the electrodes are exposed to the direct flame from a lighter, indicated by the white arrow in (a). (c) The specific burning time of the sulfur cathodes with APP and PVDF binders. (d) Schematic showing the flame-retardant mechanism of the APP binder based sulfur electrode.

To confirm the proposed flame-retardant mechanism, the team did a burning test on S-APP and S-PVDF electrodes; after the fire was self-extinguished, XPS and SEM were used to understand the mechanism. XPS analysis clearly shows the presence of nitrogen, sulfur, and phosphorous elements in the S-APP electrode from the survey spectrum (Figure 77b). After burning, the intensity of the N 1s signal significantly decreases, while the intensity of the phosphorous signal is almost the same, indicating decomposition and release of NH_3, as well as generating a cross-linked polymer, as proposed in Figure 77a. It should be noted that the sulfur signal only slightly decreases, suggesting that the APP binder protects the underlying sulfur from burning and halts the further spread of the fire. This is quite different for the S-PVDF electrode based on the S 2p XPS spectrum analysis, in which the intensity of the sulfur signal obviously decreases, suggesting most of the sulfur materials are burned away. Further evidence can be obtained from the SEM postmortem analysis of the electrodes after burning. The overall morphology and structure were well preserved for S-APP electrode (Figure 77d), demonstrating that the protective layer produced by APP decomposition helps prevent further combustion of sulfur. However, due to the weak protection offered by PVDF binder, a large quantity of sulfur is evaporated from the sulfur cathode, leaving many holes in the electrode after burning (Figure 77h) which is in agreement with the previous analysis. The corresponding sulfur and phosphorus elemental maps of the S-APP electrode after burning indicate sulfur is protected and phosphorous is retained in the electrode (Figure 77e-f), which is consistent with the energy dispersive spectroscopy (EDS) results that the intensity of the sulfur signal is much higher compared with the carbon signal from the electrode (Figure 77g). In contrast, holes are found on the sulfur cathode with PVDF binder (Figure 77h), and the sulfur signal is missing in these areas (Figure 77i), indicating poor protection of sulfur combustion by PVDF. In addition, the sulfur signal is much lower than the carbon signal after burning (Figure 77k), confirming the evaporation of sulfur from sulfur cathode during the burning process.

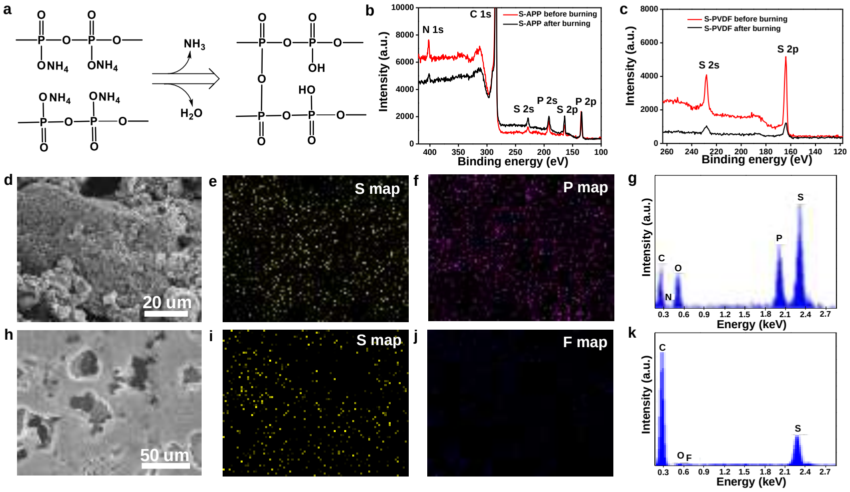

Figure 77. (a) Chemical reaction for flame-retardant mechanism. (b) X-ray photoelectron spectroscopy (XPS) spectra of the surface chemical composition of the sulfur – ammonium polyphosphate (S-APP), before and after burning. (c) S 2p XPS spectra of the S-PVDF electrode before and after burning. (d) Scanning electron microscopy (SEM) image and the corresponding (e) sulfur and (f) phosphorus elemental maps of the S-APP electrode after burning. (g) Energy dispersive spectroscopy (EDS) of the S-APP electrode after burning. (h) SEM image and the corresponding (i) sulfur and (j) fluorine elemental maps of the S-PVDF electrode after burning. (k) EDS of the S-PVDF electrode after burning.

Patents/Publications/Presentations

The project has no patents, publications, or presentations to report this quarter.

Task 5.4 – Addressing Internal “Shuttle” Effect: Electrolyte Design and Cathode Morphology Evolution in Lithium-Sulfur Batteries
(Perla Balbuena, Texas A&M University; Partha Mukherjee, Purdue University)

Project Objective. The project objective is to overcome the Li-metal anode deterioration issues through advanced Li-anode protection/stabilization strategies including (1) *in situ* chemical formation of a protective passivation layer and (2) alleviation of the “aggressiveness” of the environment at the anode by minimizing the polysulfide shuttle with advanced cathode structure design.

Project Impact. Through formulation of alternative electrolyte chemistries as well as design, fabrication, and test of improved cathode architectures, it is expected that this project will deliver Li/S cells operating for 500 cycles at efficiency greater than 80%.

Approach. A mesoscale model including different realizations of electrode mesoporous structures generated based on a stochastic reconstruction method will allow virtual screening of the cathode microstructural features and the corresponding effects on electronic/ionic conductivity and morphological evolution. Interfacial reactions at the anode due to the presence of polysulfide species will be characterized with *ab initio* methods. For the cathode interfacial reactions, data and detailed structural and energetic information obtained from atomistic-level studies will be used in a mesoscopic-level analysis. A novel sonochemical fabrication method is expected to generate controlled cathode mesoporous structures that will be tested along with new electrolyte formulations based on the knowledge gained from the mesoscale and atomistic modeling efforts.

Out-Year Goals. By determining reasons for successes or failures of specific electrolyte chemistries, and assessing relative effects of composite cathode microstructure and internal shuttle chemistry versus that of electrolyte chemistry on cell performance, expected results are as follows: (1) develop an improved understanding of the Li-S chemistry and ways to control it, (2) develop electrolyte formulations able to stabilize the lithium anode, (3) develop new composite cathode microstructures with enhanced cathode performance, and (4) develop a Li-S cell operating for 500 cycles at an efficiency greater than 80%.

Collaborations. This is a collaborative work combining first-principles modeling (Perla Balbuena, TAMU), mesoscopic-level modeling (P. Mukherjee, Purdue University), and synthesis, fabrication, and test of Li/S materials and cells (V. Pol, Purdue University). Balbuena also collaborates with M. Vijayakumar from PNNL.

Milestones

1. Elucidate effects of PS migration and reduction at the anode on overall performance. (September 30, 2018; Ongoing)
2. Investigate charge reactions of nucleating Li_2S structures. (September 30, 2018; Ongoing)

Progress Report

Electrochemical Complexations due to Chemical Reactions at Anode. Work in Mukherjee's group has focused on using mesoscale modeling for understanding these issues. Transport of active species in the electrolyte is driven in response to (i) a concentration gradient–diffusion as well as (ii) a potential gradient–migration. During operation of a Li-S cell, polysulfides and dissolved sulfur consequently transport to anode surface where due to extreme reactivity of lithium metal, they can undergo chemical reduction. Such chemical reduction complicates the speciation and in turn alters the electrochemical evolution of the cell (as shown in the previous report). As a result of these combined transport + reaction interactions, the identity of active sulfur species changes, which in turn reflects as changes in both the potential profile as well as achievable capacity. Both discharge plateaus shorten since the electroactive sulfur simultaneously undergoes chemical reduction at the anode and in turn represents a capacity defect.

As the cells are operated at higher and higher rates, the timescale for electrochemical reactions decreases (chemical reaction timescale does not change with current), and in turn, capacity defect decreases at higher rates. Moreover, at higher rates, the higher order polysulfides react to a greater extent at cathode before they can be transported to the anode. The polysulfide flux coming at anode successively consists of smaller chain polysulfides as operating currents are increased. Equivalently, the chemical reduction at anode largely results in Li_2S formation at the anode. The Li_2S at the anode cannot be decomposed and amounts to an irreversible capacity loss.

Cathode specifications such as porosity and sulfur-to-electrolyte ratio determine the ionic concentrations in the electrolyte phase and consequently the electrolyte transport evolution. For lower sulfur contents, polysulfide species can easily transport to the anode and partake in chemical reactions. On the other hand, at high sulfur contents, electrolyte transport is severely hindered and limits electrochemical operation. The intermediate sulfur loadings represent a balance between reduced anode centric chemical interactions as well as not so rate limiting cathode processes, such as reduced electrolyte conductivity, and identifies the set of cathode specifications that result in well performing cells.

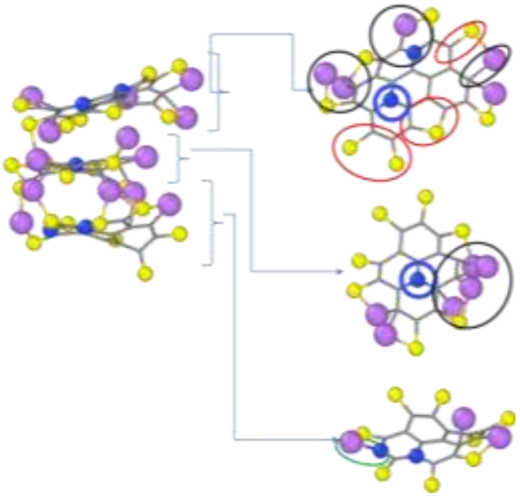

Figure 78. Multilayer graphene structure showing the incorporation of nitrogen into the C rings in pyridinic (not shown), graphitic (blue circle), and pyrrolic (green circle) positions and their interactions with lithium. Note that: (1) graphitic nitrogen does not interact with lithium, (2) pyrrolic nitrogen bonds to lithium, and (3) as discussed last quarter, carbon backbone also participates in the electrochemical reduction of sulfur.

Carbon-Sulfur Cathode Architecture and Chemistry. In the team's previous work, they demonstrated that the formation of S-C chemical bonds at the synthesis stage favors the discharge reaction during lithiation of S-C cathodes. Advantages include suppression of the formation of long-chain polysulfide species, and the contribution of carbon to enhance the overall cathode capacity. This behavior is similar to that found experimentally using sulfurized poly-acrylonitrile (S-PAN) as cathode material. However, the previous model was only composed of carbon and sulfur. Therefore, new AIMD simulations are being carried out to elucidate the role of nitrogen (Figure 78). The team has completed the lithiation process and obtained the voltage profile that qualitatively agrees with the experimental reports. They are now characterizing the delithiation (charge) process. Results will be reported.

Patents/Publications/Presentations

Publications

- Perez-Beltran, S., and P. B. Balbuena. "Formation of Multi-Layer Graphene Domains with Strong Sulfur-Carbon Interaction and Enhanced Sulfur Reduction Zones for Lithium-Sulfur Battery Cathodes." *ChemSusChem* 11 (2018): 1970–1980.
- Liu, Z., H. Deng, W. Hu, F. Gao, S. Zhang, P. B. Balbuena, and P. P. Mukherjee. "Revealing Reaction Mechanisms of Nanoconfined Li_2S: Implications for Lithium-Sulfur Batteries." *Physical Chemistry Chemical Physics* 20 (2018): 11713–11721.
- Mistry, A., and P. P. Mukherjee. "Electrolyte Transport Evolution Dynamics in Li-Sulfur Batteries." Under review.
- Perez-Beltran, S., and P. B. Balbuena. "First-Principles Explorations of the Electrochemical Lithiation Dynamics of a Multilayer Graphene Nanosheet-Based Sulfur-Carbon Composite." Under review.
- Mistry, A., and P. P. Mukherjee. "'Shuttle' in Polysulfide Shuttle: Friend or Foe?" Under review.

Presentations

- Li-SM^3 Conference, Chicago, Illinois (April 23, 2018): "Influence of Cathode Architecture on the Discharge and Charge Reactions of Li/S Batteries"; P. B. Balbuena. Invited.
- 233rd ECS Meeting, Battery Division, Seattle, Washington (May 13, 2018): "Microscopic Structure and Electrolyte Nature Effects on Discharge Products of C-S Cathodes in Li-S Batteries"; P. B. Balbuena, S. Perez Beltran, E. P. Kamphaus, A. E. Torres, and F. A. Soto.
- 233rd ECS Meeting, Seattle, Washington (May 16, 2018): "Multiscale Analysis of Polysulfide Shuttle Effects at the Li Metal Anode and Cathode Morphology Evolution in Li-S Batteries"; P. B. Balbuena, J. M. Seminario, P. P. Mukherjee, and V. Pol. Invited.
- NREL (June 26, 2018): "Addressing Main Issues of Lithium-Sulfur Batteries"; P. B. Balbuena. Invited.
- 233rd ECS Meeting, Seattle, Washington (May 2018): "Transport and Electrochemical Dynamics in the Li-S Battery Electrolyte"; A. Mistry and P. P. Mukherjee.
- Li-SM^3 Conference, (Lithium-Sulfur Batteries: Mechanisms, Modeling, and Materials), Chicago, Illinois (April 2018): "Probing the Evolutionary Dynamics in Li-S Battery Electrodes"; P. P. Mukherjee and A. Mistry. Invited.

Task 5.5 –Investigation of Sulfur Reaction Mechanisms
(Deyang Qu, University of Wisconsin at Milwaukee; Xiao-Qing Yang, Brookhaven National Laboratory)

Project Objective. The primary objectives are (1) to conduct focused fundamental research on the mechanism of "shuttle effect" inhibition for the rechargeable Li-S batteries, and (2) to develop electrode and electrolyte systems that can mitigate "shuttle effect" so low self-discharge and long cycle life can be achieved. Special attention will be paid to the following: investigating chemical interactions between additives and dissolved polysulfides, management for solubility of polysulfide ions, formation of SEI layer and dead lithium on surface of lithium anode, and exploration of electrode and cell designs. Through such investigations, the Li-S chemistry will be studied systematically, and scientific understanding of the inhibition mechanism for "shuttle effect" can be well utilized to guide system engineering design. The goal is to develop a practical rechargeable Li-S battery to meet the challenges of powering next-generation EVs beyond Li-ion technologies.

Project Impact. With the unique *in situ* electrochemical-HPLC/MS technique developed in this program, the mechanisms of all reactions in a Li-S cell can be revealed. The interactions between additives and the soluble polysulfides can be investigated in real-time toward mitigation of "shuttle effect." The results will guide development of sulfur cathode and Li-S designs for EVs.

Approach. This project will use *in situ* electrochemical-MS, electrochemical-HPLC/MS, XPS, SEM, and XRD to study electrochemical reactions associated with sulfur electrodes. Electrochemical techniques such as AC impedance, rotation ring disk electrode, and galvanostat will be used to study the electrode process kinetics. The project will use an *in situ* electrochemical optical method to investigate the surface of lithium anode during cycling of a Li-S cell.

One-Year Goals. The one-year goals include the following: (1) complete preliminary investigations of the inhibition mechanism for the "shuttle effect" and evaluation of "shuttle effect" inhibitors, and (2) complete preliminary design and tests of sulfur-containing electrodes and electrolytes.

Collaborations. The PI, D. Qu, is the Johnson Controls Endowed Chair Professor; thus, the UWM and BNL team has close collaboration with Johnson Controls' scientists and engineers. This collaboration enables the team to validate the outcomes of fundamental research in pilot-scale cells. This team has been closely working with top scientists on new material synthesis at ANL, LBNL, and PNNL, with U. S. industrial collaborators at GM, Duracell, and Johnson Controls as well as international collaborators in China, Japan, and South Korea. These collaborations will be strengthened and expanded to give this project a vision on both today's state-of-the-art technology and tomorrow's technology in development, with feedback from the material designer and synthesizers upstream and from industrial end users downstream.

Milestones

1. Complete the investigation and determination of the possible chemical reactions between dissolved polysulfide ions with the materials in a Li-S cell, both active and non-active during the storage, and thus the stability of battery components. (Q1, December 31, 2017; Completed)
2. Complete tabulating the list of materials to be tested as inhibitive additives to mitigate "shuttle effect"; start the tests and develop understanding of the mechanism of such effects. (Q2, March 31, 2018; Completed)
3. Complete testing the inhibitive additives; start to explore and design sulfur-containing electrode materials. (Q3, FY 2018; Completed on June 30, 2018)
4. Complete the preliminary engineering design and test for the new sulfur-containing electrode materials. (Q4, FY 2018; Ongoing)

Progress Report

This quarter, the team continued to synthesize new polymer materials for sulfur cathode. The main purpose is to localize the dissolved polysulfide ions in the cathode matrix. The team is exploring to bond the polysulfide species on the backbone materials, either modified carbon or polymers through chemical bonds.

The team started to copolymerize sulfur with *p*-Phenylene vinylene derivative (denoted as Xant-) to form a new conductive cross-linked Polysulfur-*random*-PPV (denoted as S/Xant-) copolymer cathode material in one pot. Taking advantage of the diradical character of *p*-Phenylene vinylene intermediate, the diradical polymeric sulfur can be intercepted and stabilized by the formation of strong covalent bonds between sulfur and carbon. The cross-linked polymer framework will help to self-protect and confine polysulfide and sulfur dissolution, and thus avoid the detrimental shuttling effects. Poly(*p*-Phenylene vinylene) (PPV) and its derivatives are conjugated conductive materials and with their inclusion in the cross-linked copolymer framework, fast electron conducting channels would be provided, which will improve conductivity of the sulfur-containing polymer. Figure 79 shows photographs of S/Xant-copolymer with different sulfur contents.

Figure 79. Photographs of S/Xant- copolymer with 90% (a), 70% (b), and 50% sulfur (c).

Figure 80 shows the rate performance of as-synthesized S/Xant- (70 wt% sulfur). The preliminary result indicates that the S/Xant- has a high initial capacity of 720 mAh g^{-1} (based on S/Xant- or 1029 mAh g^{-1} based on sulfur) at 100 mA g^{-1} discharge rate. The capacity decreases as the discharge rate increases; for example, at high rate (> 1 mA g^{-1}), the capacity is relatively low, probably resulting from the aggregation of S/Xant- copolymer in the electrode, which could limit the ionic diffusion. On one hand, the aggregation of S/Xant- copolymer could confine the polysulfide ions within the cathode; on the other hand, it might also hinder the mass transfer of Li$^+$ in and out of the cathode matrix. The limitation of the Li-ion diffusion would induce the low capacity at high rates. As shown in Figure 80, when the current density was reduced back to 100 mA g^{-1} after 30 cycles, the reversible capacity went back to ~ 610 mAh g^{-1} (S/Xant-), suggesting good stability of the electrode. The performance of S/Xant- electrode could be further improved by optimizing the electrode structure.

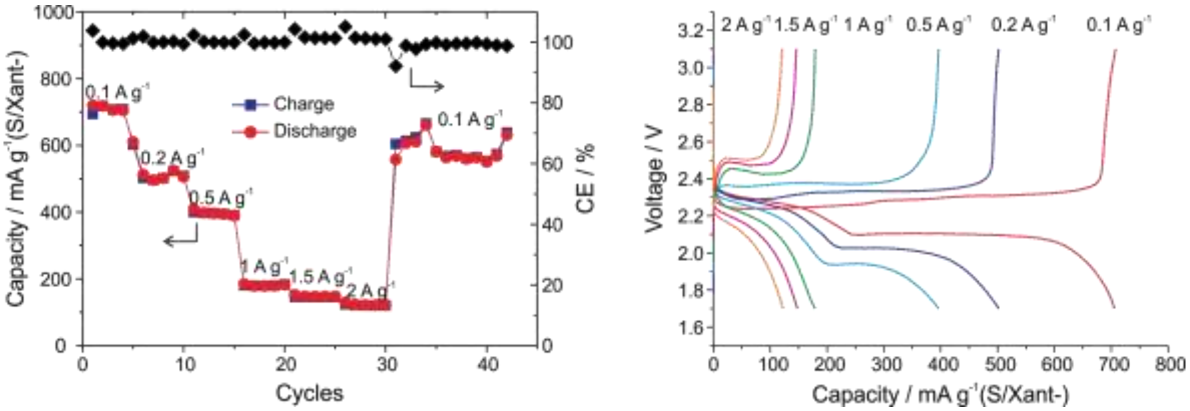

Figure 80. Rate performance of S/Xant- (70% sulfur). The testing was done in a coin cell.

Patents/Publications/Presentations

Publication

- Zheng, D., G. Wang, D. Liu, J. B. Harris, T. Ding, J. Si, D. Qu, X. Yang, and D. Qu. "Systematic and Rapid Screening for the Redox Shuttle Inhibitors in Lithium-Sulfur Batteries." *Electrochimica Acta* 282 (2018): 687–693.

Task 5.6 – Statically and Dynamically Stable Lithium-Sulfur Batteries
(Arumugam Manthiram, University of Texas at Austin)

Project Objective. The project objective is to develop statically and dynamically stable Li-S batteries by integrating polysulfide-filter-coated separators with a protected Li-metal anode through additives or a modified Li_2S cathode with little or no charge barrier during first charge. The project includes demonstration of electrochemically stable cells with sulfur capacities of > 1000 mAh g^{-1} and cycle life in excess of 500 cycles (dynamic stability) along with positive storage properties (static stability) at > 70 wt% sulfur content and ~ 5 mg cm^{-2} loading.

Project Impact. The combination of polysulfide-filter (PS-filter)-coated separator, Li-metal-protection additives, and Li_2S cathode modifications offers a viable approach to overcome the persistent problems of Li-S batteries. This project is systematically integrating the basic science understanding gained in its laboratory of these three aspects to develop the Li-S technology as the next-generation power source for EVs. The project targets demonstrating cells with sulfur capacities of over 1000 mA h g^{-1} and cycle life in excess of 500 cycles along with good storage properties at high sulfur content and loading that will make the Li-S technology superior to the present-day Li-ion technology in terms of cost and cell performance.

Approach. Electrochemical stability of the Li-S cells is improved by three complementary approaches. The first approach focuses on establishment of an electrochemically stable cathode environment by employing PS-filter-coated separators. The PS-filter coatings aim to suppress the severe polysulfide diffusion and improve the redox capability of Li-S cells with high-sulfur loadings. The study includes an understanding of materials characteristics, fabrication parameters, electrochemical properties, and battery performance of the PS-filter-coated separators. The second approach focuses on electrode engineering from two aspects. First, investigation of a Li-metal anode with coating- and additive-supporting approaches is aimed at improving the safety of Li-S cells. Second, research on activated-Li_2S cathode with little or no charge-barrier will promote performance and safety of the C-Li_2S cells. Integration of the first two approaches would create statically and dynamically stable Li-S batteries for EVs.

Out-Year Goals. The overall goal is to develop statically and dynamically stable Li-S batteries with custom cathode and stabilized anode active materials. In addition to developing a high-performance battery system, a fundamental understanding of the structure-configuration-performance relationships will be established. Specifically, the optimization of the electrochemical and engineering parameters of PS-filter-coated separators aims at comprehensively investigating different coating materials and their corresponding coating techniques for realizing various high-performance custom separators. The developed PS-filter-coated separators can be coupled with pure sulfur cathodes with high-sulfur loading and content. Multi-functional PS-filter-coated separators, high-loading sulfur cathodes, stabilized-Li-metal anodes, activated-Li_2S cathodes, and novel cell design are anticipated to provide an in-depth understanding of the Li-S battery chemistry and to realize statically and dynamically stable Li-S batteries.

Collaborations. There are no collaborative activities this quarter.

Milestones

1. Develop Li-metal anodes with high electrochemical stability. (Q1, December 2017; Completed)
2. Develop Li_2S cathodes with low activation barrier and polarization. (Q2, March 2018; Completed)
3. Demonstrate high-loading coin cells and pouch cell prototypes. (Q3, June 2018; Completed)
4. *Go/No Go Decision*: Study cost and environmental impact assessment of the technology. (Q4, September 2018; Ongoing)

Progress Report

Currently, it is recognized that the necessary parameters to develop high-energy-density Li-S batteries include a sulfur loading of at least 7–10 mg cm^{-2}, a sulfur content of over 65 wt%, and a low electrolyte/sulfur (E/S) ratio of less than 11 µL mg^{-1}. This quarter, the team demonstrated a high-loading, lean electrolyte sulfur cathode by assembling two carbon-paper sheets as a cathode substrate, into which Li_2S_6 polysulfide catholyte was added. Two cathodes were fabricated with this design: one with 13 mg cm^{-2} and 75 wt% sulfur with an E/S ratio of 4.0 µL mg^{-1}, and the other with 17 mg cm^{-2} and 80 wt% sulfur with an E/S ratio of 3.9 µL mg^{-1}, based on the total mass of the cathode including the carbon paper. Operating under such strict cell-design conditions, the cells with 13 and 17 mg cm^{-2} showed high charge-storage capacities of, respectively, 717 and 593 mAh g^{-1} at a C/10 rate with high capacity-retention rates of 71% and 85% after 200 cycles (Figure 81).

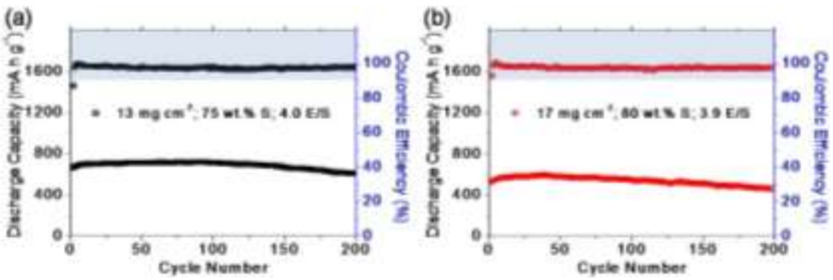

Figure 81. Long-term cyclability of the cells fabricated with the three-dimensional carbon-paper cathodes with a sulfur loading, sulfur content, and electrolyte/sulfur ratio of, respectively, (a) 13 mg cm^{-2}, 75 wt%, and 4.0 µL mg^{-1} , and (b) 17 mg cm^{-2}, 80 wt%, and 3.9 µL mg^{-1}.

Based on the understanding obtained with the project's cathode design, the team developed a Li-sulfur pouch cell with a high sulfur loading (7 mg cm^{-2}) cathode covered with a carbon-paper interlayer. Specifically, an 80 wt% sulfur slurry was coated onto an aluminum-foil current collector, and a carbon-paper sheet was directly placed on the coated slurry as an interlayer. With this design, sulfur has intimate contact with the conductive materials, and electrons can easily transfer from the current collector and the conductive carbon sheet to sulfur particles. Furthermore, the carbon-paper layer acts as a protective layer to prevent the active material from delamination. More importantly, the carbon paper is able to limit the migration of polysulfides to the anode during cycling. The prepared sulfur cathode was cut into a rectangular size of 47.8 mm × 81.5 mm (length × width). A lithium foil was cut into a size of 48.3 mm × 81.5 mm (length × width). A sheet of coated separator was then placed between the two electrodes to prevent short-circuit. The assembled cell was sealed in a plastic film pouch with an E/S ratio of 5 µL mg^{-1}. The assembled cells were rested for 3 h and then cycled in the range of 1.6-3.0 V. During the formation step, a C/15 rate was employed. During the regular cycling step, a C/5 rate was employed. Figure 82 shows the performance of the developed pouch cells. The cell displayed a discharge capacity of 900 mAh g^{-1} at C/15 rate and ~ 600 mAh g^{-1} at C/5 rate. The performance demonstrates the excellent electrochemical reversibility of the developed Li-S pouch cells, giving the team confidence to build on further pouch cells to improve the cycle life.

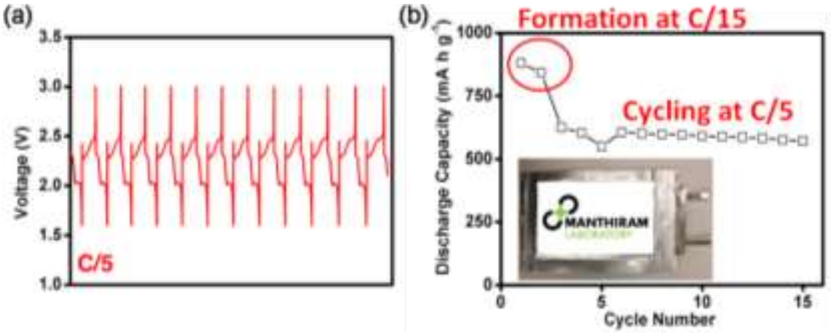

Figure 82. Cycling performance of a lithium-sulfur pouch cell with a sulfur loading of 7 mg cm^{-2}, sulfur content of 70 wt% based on the total mass of the cathode, and an electrolyte/sulfur ratio of 5 µL mg^{-1}: (a) charge/discharge curves and (b) cyclability at a C/5 rate.

Patents/Publications/Presentations

Publications

- Luo, L., S.-H. Chung, and A. Manthiram. "Rational Design of a Dual-Function Hybrid Cathode Substrate for Lithium-Sulfur Batteries." *Advanced Energy Materials* (2018). doi: 10.1002/aenm.201801014.
- Chung, S.-H., C.-H. Chang, and A. Manthiram. "Progress on the Critical Parameters for Lithium-Sulfur Batteries to be Practically Viable." *Advanced Functional Materials* (2018). doi: 10.1002/adfm.201801188.
- Nanda, S., A. Gupta, and A. Manthiram. "A Lithium-Sulfur Cell Based on Reversible Lithium Deposition from a Li_2S Cathode Host onto a Hostless-Anode Substrate." *Advanced Energy Materials* (2018). doi: 10.1002/aenm.201801556.

Presentations

- International Symposium on Functional Materials (ISFM-2018), Chandigarh, India (April 13–15, 2018): "Materials Challenges and Prospects of Electrical Energy Storage"; A. Manthiram. Invited plenary talk.
- Central Electrochemical Research Institute, Chennai, India (April 20, 2018): "Next Generation Battery Chemistries: Materials Challenges and Prospects"; A. Manthiram. Invited talk.
- 2nd International Materials Science and Engineering for Green Energy Conference, Rabat, Morocco (April 25, 2017): "Next-Generation Battery Technologies: Materials Challenges and Prospects"; A. Manthiram. Invited plenary talk.

Task 5.7 – Electrochemically Responsive, Self-Formed, Lithium-Ion Conductors for High-Performance Lithium-Metal Anodes

(Donghai Wang, Pennsylvania State University)

Project Objective. The project objective is to develop and deliver an electrochemically responsive self-formed hybrid LIC as a protective layer for Li-metal anodes, enabling Li-metal anodes to cycle with a high efficiency of ~ 99.7% at high electrode capacity (> 6 mAh/cm^2) and high current density (> 2 mA/cm^2) for over 500 cycles. The project will also demonstrate prototype ~ 300 mAh Li-S battery cells with energy densities of ~ 200 Wh/kg and ~ 80% capacity retention for ~ 300 cycles at ~ 80% depth of discharge using Li-metal anodes with this protective layer.

Project Impact. This project aims to develop a new hybrid LIC that enables safe and high-performance Li-metal anodes. The use of these high-performance Li-metal anodes in turn enables Li-S batteries with high energy density and long cycling life. Such anodes can also lead to a 50% increase in the energy density of conventional Li-ion batteries with Li-metal oxide cathodes. Meeting the technical targets will potentially develop a new high-energy-density lithium battery, promote increased adoption of EVs and PHEVs, and reduce petroleum consumption in the transportation sector by helping battery-powered vehicles become accepted by consumers as a reliable source of transportation.

Approach. The novel multiphase organo-Li_xS_y or organo-$Li_xP_yS_z$ hybrid ion conductors with tunable multi-functional organic components and controlled Li_xS_y and $Li_xP_yS_z$ inorganic components will be designed and prepared, and thus enable safe use of lithium metal with high CE. In the second year, the team will develop the 2nd generation of organo-Li_xS_y lithium protection layers with tuned functionality: (1) finding appropriate composition, (2) developing appropriate synthesis and fabrication methods, and (3) optimizing organic components in a protection layer to further improve CE and Li-S battery performance.

Out-Year Goals. Work will progress toward development of the 2nd generation of organo-Li_xS_y lithium protection layers with tuned functionality. Characterization, performance, and compatibility tests on materials and systems will be conducted. Uniform and dendrite-free lithium deposition under the protection of the 2nd generation of organo-Li_xS_y lithium protective layers will be demonstrated, and CE will be further improved.

Collaborations. There are no active collaborations.

Milestones

1. Development of the 2nd generation of organo-Li_xS_y lithium protection layers with tuned functionality. Conduct characterization and performance tests on the materials. (Q1, FY 2018; Completed)
2. Demonstrate uniform and dendrite-free lithium deposition under protection of the 2nd generation of organo-Li_xS_y lithium protective layers. (Q2, FY 2018; Completed)
3. Optimize the 2nd generation of organo-Li_xS_y lithium protective layer and demonstrate lithium anodes cycling with ~ 98.8% CE for ~ 200 cycles. (Q3, FY 2018; Completed)
4. Demonstrate lithium anodes with optimized 2nd generation of organo-Li_xS_y lithium protective layer and ~ 99.2% CE for ~ 300 cycles. (Q4, FY 2018)

Progress Report

SEI layers formed from electrolyte containing PSD-90 were characterized. First, the composition of the SEI layers was investigated using XPS. The SEI layers were obtained from C-Ely (1 M LiTFSI+4%$LiNO_3$/DOL+DME) and PSD-90-Ely (1 M LiTFSI+8%PSD-90+4%$LiNO_3$/DOL+DME) after 100 cycles of lithium deposition/dissolution and named C-SEI and PSD-90-SEI, respectively. In S 2p XPS spectra (Figure 83a), two strong peaks at 160.5 and 161.7 eV for the PSD-90-SEI indicate the presence of Li_2S and Li_2S_2; the peak located at 162.2 eV that corresponds to the S 2p3/2 for lithium organosulfides (RS_4Li_4) confirms that lithium organosulfides exist in the PSD-90-SEI layer. The peak at 163.3 eV is assigned to lithium polysulfides (Li_2S_x) and organopolysulfides (RS_xLi_4), which overlap and make the peak stronger. The 2p XPS spectra of PSD-90-SEI reflect the existence of lithium organosulfides/organopolysulfides along with the Li_2S/Li_2S_2 in the SEI layer. The C 1s XPS spectra of C-SEI (Figure 83b) contain a peak at ~292.1 eV assigning to the functional group –CF3 from the decomposition of LiTFSI. This peak almost disappears when PSD-90 is added in the electrolytes (PSD-90-Ely), indicating the decomposition of LiTFSI is dramatically suppressed in the presence of PSD-90. Moreover, the F 1s XPS spectra (Figure 83c) display a relatively lower intensity of peak assigned to –CF3 in the PSD-90-SEI, reconfirming the suppression of LiTFSI decomposition in the presence of PSD-90.

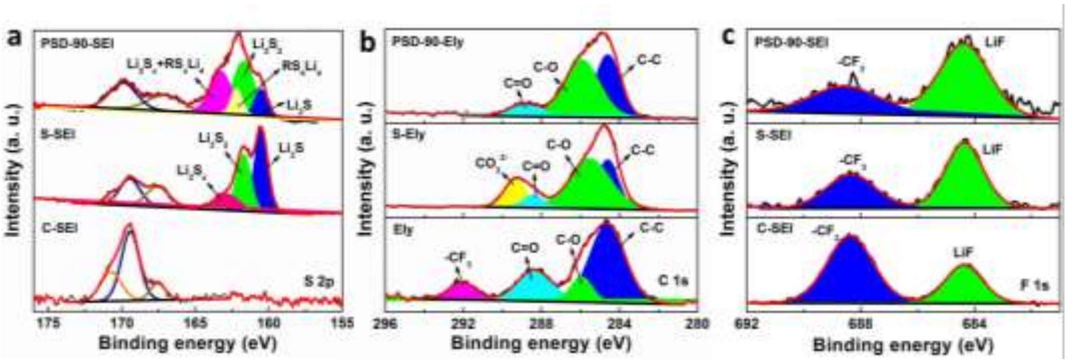

Figure 83. The X-ray photoelectron spectroscopy (XPS) spectra of SEI layers formed from the electrolytes containing different additives. S 2p XPS spectra (a), C 1s XPS spectra (b), and F 1s XPS spectra (c) of the SEI layers formed from different electrolytes.

Figure 84 shows that FTIR spectra of C-SEI and PSD-90-SEI are quite different. The FTIR spectra of PSD-90-SEI show prominent peaks at 1600, 1575, and 1558 cm^{-1}, which correspond to the vibration of carbon-carbon double bond of the phenyl group. The peak at ~ 790 cm^{-1} is the vibration characteristic of C-H bond of the 1, 3-substituted phenyl groups, which can prove the presence of 1, 3-substituted phenyl groups. All of the peaks can also be found in the pure PSD-90, demonstrating that the organosulfides originate from the PSD-90.

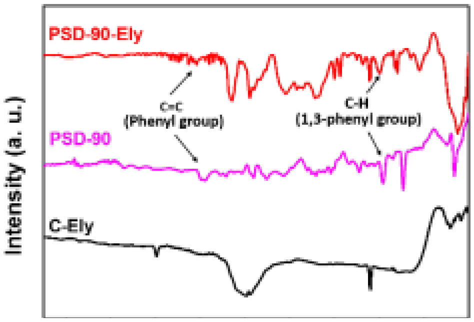

Figure 84. Fourier transform infrared of SEI layers obtained from the C-Ely (C-SEI) and the PSD-90-Ely (PSD-90-SEI).

Surface morphologies of the C-SEI and PSD-90-SEI layers studied by AFM (Figure 85a-b) and SEM (Figure 85e-f) consistently show a porous, fractured, and loose structure observed in C-SEI (Figure 85a/e); in comparison, a mostly planar, smooth, and uniform structure is shown in the PSD-90-SEI layer (Figure 85b/f). Indentation curve of C-SEI (Figure 85c) shows the loading and unloading curves almost overlap and the slopes are very high, implying that the C-SEI layer is rigid and its viscoelasticity is negligible. The reduced modulus of the C-SEI is calculated to be 903 MPa from the Johnson-Kendall-Roberts (JKR) model fit (Table 5). By contrast, a more substantial deformation and hysteresis between the loading and unloading curves of PSD-90-SEI layer (Figure 85d) reflects flexible characteristic under the mechanical deformation. The PSD-90-SEI layer exhibits a lower modulus of 340 MPa (Table 5), indicating this SEI layer becomes soft and viscoelastic.

Table 5. The reduced modulus of SEI layers formed from the C-Ely and PSD-90-Ely.

Electrolyte	SEI layer	Reduce modulus (JKR model)/MPa
C-Ely	Inorganic layer (C-SEI)	903
PSD-90-Ely	Inorganic/organic layer (PSD-90-SEI)	340

The stable SEI layer fabricated from PSD-90-Ely dramatically improves the lithium deposition/dissolution CE. The cycling performance of lithium deposition/dissolution using PSD-90-Ely is shown in Figure 86. At a capacity of 1 mAh cm^{-2} and a deposition capacity of 2 mA cm^{-2}, a high average CE of 99.1% can be maintained for 420 cycles.

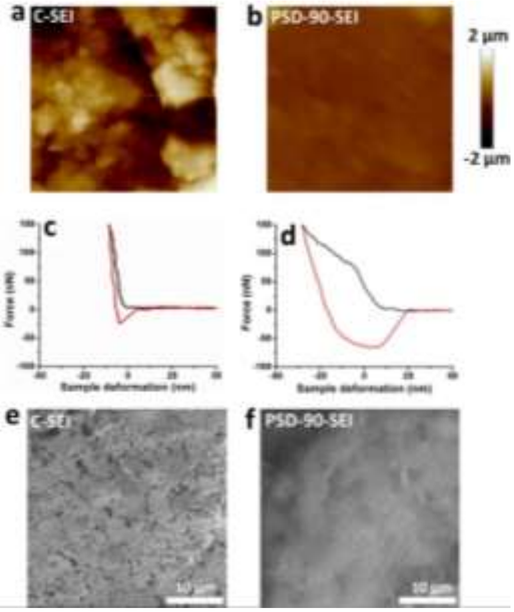

Figure 85. Atomic force microscopy (AFM) images and indentation study of SEI layers obtained from C-Ely (a/c) and PSD-90-Ely (b/d). Scanning electron microscopy images of SEI layers obtained from C-Ely (e) and PSD-90-Ely (f). The scan size for AFM images is 10×10 μm^2.

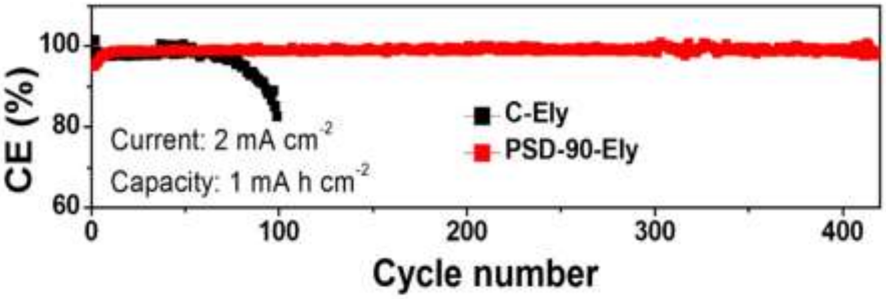

Figure 86. Cycling performance of cells using PSD-90-Ely electrolyte.

Patents/Publications/Presentations

Publication

- Li, G. X., Q. Q. Huang, X. He, Y. Gao, D. W. Wang, S. H. Kim, and D. H. Wang. "Self-Formed Hybrid Interphase Layer on Lithium Metal for High Performance Lithium-Sulfur Batteries." ACS *Nano* 12, no. 2 (2018): 1500–1507.

Presentations

- 233rd ECS Spring Meeting, Seattle, Washington (May 15, 2018): "Manipulation of Structure and Morphology of Solid-Electrolyte Interphase Layer for High-Performance Li Metal Batteries"; D. Wang. Invited.
- MRS Meeting, Phoenix, Arizona (April 4, 2018): "Design and Engineering of Interfaces/Interphases for Stable Li Anodes" D. Wang. Invited.

Task 5.8 – Materials and Cell Design Optimization for Lithium-Sulfur Battery Technology (Hong Gan, Brookhaven National Laboratory)

Project Objective. Develop a low-cost battery technology for PEV application utilizing the Li-S electrochemical system by incorporating new materials (cathode, electrolyte, additives), consistent with DOE's long-term goals.

Project Impact. The Li-S battery system has gained significant interest due to its low material cost potential (35% cathode cost reduction over Li-ion) and its attractive 2.8x (volumetric) to 6.4x (gravimetric) higher theoretical energy density compared to conventional Li-ion benchmark systems. Commercialization of this technology requires overcoming several technical challenges. This effort will focus on improving the cathode energy density, power capability, and cycling stability by introducing optimized multifunctional cathode additives (MFCA) and multifunctional electrolyte (MFE) and conductive carbon host. The primary deliverable of this project is to boost the sulfur utilization and further improve the energy efficiency and the energy density at the cell level for Li-S battery technology.

Approach. In the past three years, the team successfully completed the project "*Multi-Functional Cathode Additives (MFCA) for Li-S Battery Technology*." The layer structured TiS_2 has been identified as the true MFCA for Li-S cells, which is conductive electronically, active electrochemically, and with ability to adsorb polysulfide. By incorporating all the improvements—including the TiS_2 additive, the formulation optimization, the new binder and new carbon host for high sulfur loading, the electrode processing optimization, the electrode density control, and the electrolyte fill weight control—2032 coin cells with > 4 mAh delivered capacity with excellent cycle life have been demonstrated. This year, the team will build on previous work by incorporating MFE studies, in addition to the cathode material studies to further optimize Li-S cell performance.

Out-Year Goals. To address the system level interactions, one area of research will be the electrolyte and electrolyte additives, since electrolyte is a critical component in the Li-S battery for polysulfide dissolution, lithium anode SEI protection, and cathode interface reaction control. The project will continue to look into electrolytes with reduced polysulfide solubility, and the electrolytes/additives with ability to improve sulfur utilization to achieve long cycle life and high energy-efficiency. Improvement of sulfur utilization and the delivered energy density at the electrode level will also be achieved by introducing the 2D-nano-sheet TiS_2 with reduced particle size and increased Brunauer–Emmett–Teller (BET) surface area for maximized polysulfide–TiS_2 interaction, and by introducing the new carbon host of high pore volume and high BET surface area with controlled particle size distribution for high sulfur loading.

Collaborations. This project collaborates with D. Su (BNL), X. Tong (BNL), Q. Wu and Y-C. K. Chen-Wiegart (SBU, BNL), A. Marschilok (SBU), K. Takeuchi (SBU), and E. Takeuchi (SBU, BNL).

Milestones

1. Electrolyte with low polysulfide solubility. (Q1, December 2017; Completed)
2. Electrolyte additive investigation for improved sulfur utilization. (Q2, March 2018; Completed)
3. Proof-of-concept testing of 2D TiS_2 as MFCA in sulfur electrode. (Q3, March 2018; Completed June 2018)
4. Alternative high pore volume and high BET surface area carbon host investigation. (Q4; Initiated June 2018)

Progress Report

TiS_2 has been identified as an effective MFCA for Li-S batteries due to its high electronic conductivity, electrochemical activity, and polysulfide (PS) adsorption ability. To maximize its PS adsorbing capability, high surface area TiS_2 is desirable. Synthesis of 2D TiS_2 nano-sheets and the studies of its impact on Li-S cell electrochemical performance were carried out this quarter.

2D TiS_2 Nano-Sheets Synthesis. Synthesis of 2D TiS_2 nano-sheets was successfully achieved by using a two-step sonication method after TiS_2 lithiation. TiS_2 particle size was reduced to ~ 1 µm in a-axis along the basal plane and nano-scale in the c-axis (Figure 87) direction. The crystallite size reduction is also evidenced by XPD, as shown in Figure 88, with significant peak broadening for the 2D material. Based on the Debye-Scherrer equation, the average-thickness of TiS_2 sheets for the synthesized and raw TiS_2 (commercial pristine) samples is estimated to be ~ 9 nm and ~ 73 nm, respectively.

Polysulfide Adsorption Color Test. The 2D TiS_2 nano-sheets material with much smaller particle size in all dimensions (Figure 87) is expected to have more exposed surface area than the raw TiS_2. Its interaction with PS should be stronger than that of the control sample. Consistent with previous reporting, the lightened color of PS solution was observed in the presence of TiS_2 (Figure 89) against the control PS solution. In addition, significant color difference is also observed between the two samples containing raw TiS_2 and 2D TiS_2 nano-sheets, with the latter resulting in lighter color, indicating more efficient PS adsorption by the 2D TiS_2 nano-sheets material.

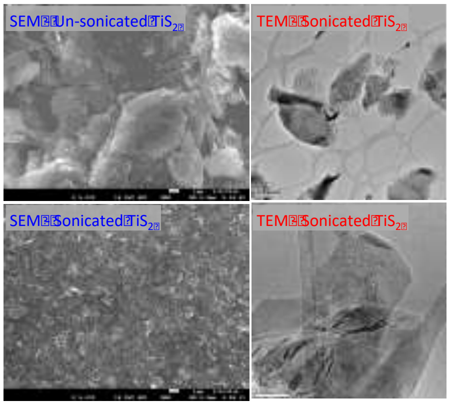

Figure 87. Two-dimensional TiS_2 sheet synthesis.

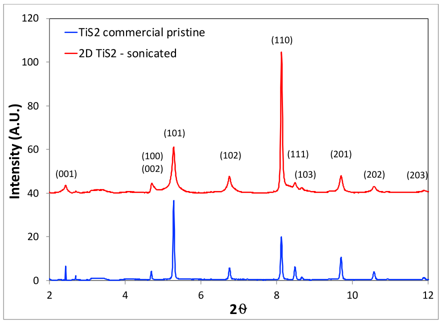

Figure 88. XPD of two-dimensional sheet TiS_2.

Electrochemical Performance. TiS_2 is used as cathode additive in sulfur electrode to replace part of the carbon black. 2032-coin cells were prepared. The rate test (C/20 to 2C) was performed, followed by cycling test. The Li-S cells with 2D TiS_2 nano-sheets additive exhibit better sulfur utilization than that of Li-S cells with raw TiS_2 additive at all discharge rates (Figure 90). In addition, the cells with 2D TiS_2 nano-sheets also delivered more capacity than the control cells at C/20, C/10, and C/5 discharge rates. The advantage of 2D TiS_2 nano-sheets additive is more pronounced during the cell cycling study at C/5 discharge rate, which shows much better capacity retention and higher sulfur utilization over 200 cycles. The better electrochemical performance is attributed to improved PS adsorption and uniform distribution of 2D TiS_2 nano-sheets within the sulfur cathode. These results clearly demonstrate the beneficial effect of 2D TiS_2 nano-sheets on the Li-S cell electrochemical performance.

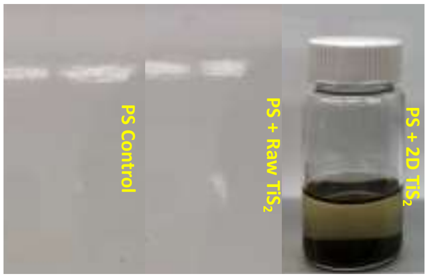

Figure 89. Polysulfide adsorbing color test.

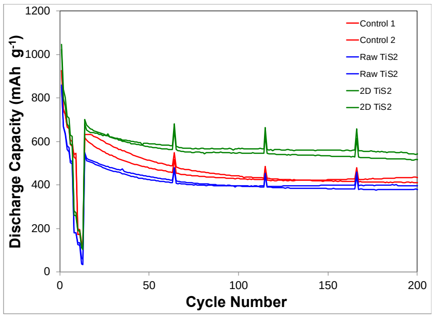

Figure 90. Electrochemical testing.

Patents/Publications/Presentations

Publication

- Sun, K., Q. Wu, X. Tong, and H. Gan. "Electrolyte with Low Polysulfide Solubility for Li-S Batteries." ACS *Applied Energy Materials* 1 (2018): 2608–2618. doi: 10.1021/acsaem.8b00317.

Presentations

- American Institute of Chemical Engineers (AIChE) Southern Regional Conference (SRC), Louisiana State University, Baton Rouge, Louisiana (April 6–7, 2018): "Lithium Batteries: Loading and Density Effect of Sulfur Cathode"; A. K. Matarasso, K. Sun, and H. Gan. Poster.
- National Synchrotron Light Source II (NSLS-ll) and Center for Functional Nanomaterials (CFN) Users' Meeting, Brookhaven National Laboratory, Long Island, New York (May 21–23, 2018): "*Operando* Chemical and Structural Evolution of TiS_2 in Li-Ion and Na-Ion Batteries"; C-H. Lin, K. Sun, E. Stavitski, K. Attenkofer, P. Northrup, G. J. Williams, J. Thieme, H. Gan, and Y-C. K. Chen-Wiegart. Poster.
- 19th International Meeting on Lithium Batteries, Kyoto, Japan (June 16–22, 2018): "Effect of Cell Design on Li-S Battery Power Capability"; K. Sun, A. K. Matarasso, R. Epler, and H. Gan. Poster.

TASK 6 – AIR ELECTRODES / ELECTROLYTES

Summary and Highlights

High-density energy storage systems are critical for EVs required by the EV Everywhere Grand Challenge. Conventional Li-ion batteries still cannot fully satisfy the ever-increasing needs because of their limited energy density, high cost, and safety concerns. As an alternative, the rechargeable lithium-oxygen (Li-O_2) battery has the potential to be used for long-range EVs. The practical energy density of a Li-O_2 battery is expected to be ~ 800 Wh kg^{-1}. The advantages of Li-O_2 batteries come from their open structure; that is, they can absorb the active cathode material (oxygen) from the surrounding environment instead of carrying it within the batteries. However, the open structure of Li-O_2 batteries also leads to several disadvantages. The energy density of Li-O_2 batteries will be much lower if oxygen must be provided by an onboard container. Although significant progress has been made in recent years on fundamental properties of Li-O_2 batteries, research in this field is still in an early stage, with many barriers to be overcome before practical applications. These barriers include:

- Instability of electrolytes—The superoxide species generated during discharge or O_2 reduction process is highly reactive with electrolyte and other components in the battery. Electrolyte decomposition during charge or O_2 evolution process is also significant due to high over-potentials.
- Instability of air electrode (dominated by carbonaceous materials) and other battery components (such as separators and binders) during charge/discharge processes in an O-rich environment.
- Limited cyclability of the battery associated with instability of the electrolyte and other battery components.
- Low energy efficiency associated with large over-potential and poor cyclability of Li-O_2 batteries.
- Low power rate capability due to electrode blocking by the reaction products.
- Absence of a low-cost, high-efficiency oxygen supply system (such as oxygen selective membrane).

The main goal of this Task is to provide a better understanding on the fundamental reaction mechanisms of Li-O_2 batteries and identify the required components (especially electrolytes and electrodes) for stable operation of Li-O_2 batteries. PNNL researchers will investigate new approaches to improve stability of Li-metal anode in Li-O_2 batteries and develop thick carbon/catalyst composite air electrodes for practical Li-O_2 batteries. Li-metal anodes will be protected using two approaches: (1) *in situ* formation of a stable SEI layer before Li-O_2 cell operation through various electrolyte formulations and treatment protocols, and (2) *ex situ* formation of stable inorganic/polymeric hybrid electrolyte layers through dip-coating or tape casting method to coat the inorganic/polymeric hybrid electrolyte layer on Li-metal surface. Thick carbon/catalyst composite air electrodes based on carbon nanotubes (CNTs) and transient metal oxides such as RuO_2 and with ≥ 4 mg/cm^2 areal loading will be developed. At ANL, new cathode materials and electrolytes for Li-air batteries will be developed for Li-O_2 batteries with long cycle life, high capacity, and high efficiency. The state-of-the-art characterization techniques and computational methodologies will be used to understand the charge and discharge chemistries. Success of this project will establish a solid foundation for further development of Li-O_2 batteries toward practical applications for long-range EVs. The fundamental understanding and breakthrough in Li-O_2 batteries may also provide insight on improving the performance of Li-S batteries and other energy storage systems based on chemical conversion processes.

Highlight. This quarter, the ANL group discovered that the Ir_3Li core-shell nanoparticles reduce charge overpotentials in Li-O_2 batteries.

Task 6.1 – Rechargeable Lithium-Air Batteries (Ji-Guang Zhang and Wu Xu, Pacific Northwest National Laboratory)

Project Objective. The project objective is to develop rechargeable Li-O_2 batteries with long-term cycling stability. The team has found that the corrosion of Li-metal anode is a critical degradation mechanism of Li-O_2 batteries. Realization of very high energy density of Li-O_2 batteries strongly depends on the stability of Li-metal anodes. In FY 2018, the focus will be on protection of Li-metal anodes for Li-O_2 batteries. Several approaches, including *in situ* and *ex situ* methods, will be used to study the corrosion of Li-metal anode in Li-O_2 cells under different treatment/protection conditions.

Project Impact. Li-air batteries have a theoretical specific energy more than five times that of state-of-the-art Li-ion batteries and are potential candidates for use in next-generation, long-range EVs. Unfortunately, the poor cycling stability and low CE of Li-air batteries have prevented their practical application. This work will explore well-protected Li-metal anodes, new electrolytes, and high-loading air-electrodes that could lead to long cyclability and high CE in high-energy Li-air batteries that can be used in the next-generation EVs required by the EV Everywhere Grand Challenge.

Approach. Li-metal anodes will be protected using *in situ* formation of a stable SEI layer before Li-O_2 cell operation through various electrolyte formulations and treatment protocols and *ex situ* formation of stable inorganic/polymeric hybrid electrolyte layers through dip-coating or tape casting method to coat the inorganic/polymeric hybrid electrolyte layer on Li-metal surface. Thick carbon/catalyst composite air electrodes based on CNTs and transient metal oxides such as RuO_2 and with ≥ 4 mg/cm^2 areal loading will be developed. The lithium anodes and Li-O_2 cells at different stages of cycling (including as-prepared, after discharge, after recharge, and after cycling) will be analyzed by microscopy and spectroscopy techniques such as SEM, EDX, XRD, and XPS.

Out-Year-Goals. The long-term goal is to enable rechargeable Li-air batteries with a specific energy of 800 Wh/kg at cell level, 1000 deep-discharge cycles, improved abuse tolerance, and less than 20% capacity fade over a 10-year period to accelerate commercialization of long-range EVs.

Collaborations. This project collaborates with Chongmin Wang of PNNL on characterization of cycled air electrodes by TEM/SEM.

Milestones

1. Investigate electrolyte additives to form stable SEI layer on Li-metal anode of Li-O_2 batteries. (Q1, December 31, 2017; Completed)
2. Develop inorganic/polymeric composite hybrid electrolyte membranes to protect Li-metal anode in Li-O_2 batteries. (Q2, March 31, 2018; Completed)
3. Develop thick air electrodes of at least 4 mg/cm^2 areal loading for Li-O_2 batteries. (Q3, June 30, 2018; Ongoing)
4. Evaluate cycling performance of Li-O_2 batteries with protected Li-metal anode and thick air electrode. (Q4, September 30, 2018; Ongoing)

Progress Report

Although significant progress has been made in catalyst materials development, few studies have been devoted to preparation of high areal-loading air electrode for practically meaningful high-energy Li-O_2 batteries. Although carbon-based air cathode materials have demonstrated ultrahigh gravimetric capacities (mAh/g), most of the reported results were obtained with very small areal loadings that rarely surpassed 1 mg cm^{-2}. This quarter, high areal-loading air-electrodes have been developed to boost the practical energy density of Li-air batteries. First, RuO_2/CNT composites were successfully synthesized by using hydrothermal method. Then, RuO_2/CNTs/PVDF slurry was coated on the carbon paper. Finally, thick air-electrodes (loading: 2 mg cm^{-2}, 3 mg cm^{-2}, and 4 mg cm^{-2}) composed of RuO_2/CNT and PVDF (4:1 by weight) were obtained after drying under vacuum. The optical image of uniform high areal-loading air-electrode with 4 mg cm^{-2} loading is shown in Figure 91a. Feasibility of using these thick air-electrodes was evaluated in CR2032-type Li-O_2 coin cells. Figure 91b shows the electrochemical performance of Li-O_2 cells with thick air-electrodes cycled at a current density of 0.1 mA cm^{-2} with a cutoff voltage window of 2.2 V to 4.2 V in 1 M Lithium trifluoromethanesulfonate (LiTf)/ Tetraethylene glycol dimethyl ether (TEGDME) electrolyte at room temperature. Areal capacities of Li-O_2 cells with RuO_2/CNT air-electrodes with different loading of 2 mg cm^{-2}, 3 mg cm^{-2}, and 4 mg cm^{-2} are as high as 6.8 mAh cm^{-2}, 5.2 mAh cm^{-2}, and 4.3 mAh cm^{-2}, respectively (Figure 91b); this is superior over average areal capacity (~3 mAh cm^{-2}) of electrodes in existing Li-ion batteries. Importantly, although the thickness of above high-loading air-electrodes increases significantly when compared to that of previously reported thin air-electrodes (less than 1 mg cm^{-2}), the as-fabricated RuO_2/CNT catalyst decorated on gas-diffusion layer made of carbon paper still exhibits excellent efficiency and favor decomposition of various discharge products during charge process and improvement for CE during discharge/charge processes. Therefore, these high loading air-electrodes can greatly enhance practical energy density of Li-O_2 batteries.

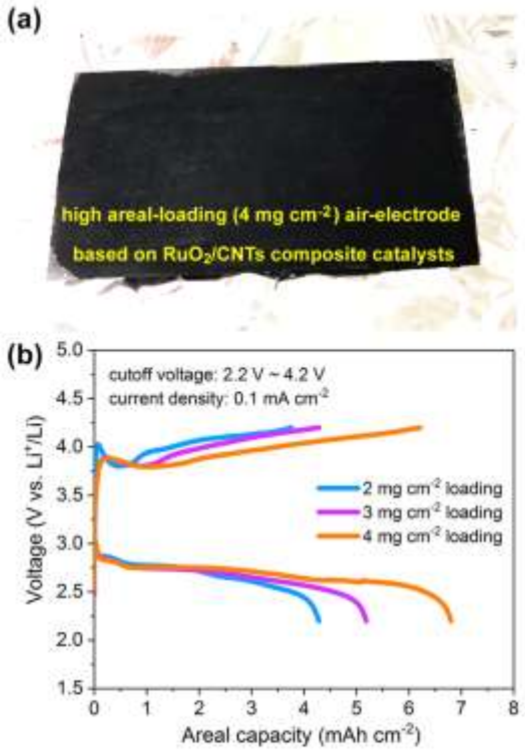

Figure 91. (a) Optical image of as-prepared high-loading (4 mg cm^{-2}) air-electrode based on RuO_2/CNT composite catalysts. (b) Deep discharge/charge curves of Li-O_2 cells cycled between 2.2 V and 4.2 V at a current density of 0.1 mA cm^{-2} in 1 M LiTf-TEGDME electrolyte at room temperature.

Patents/Publications/Presentations

The project has no patents, publications, or presentations to report this quarter.

Task 6.2 – Lithium-Air Batteries
(Khalil Amine and Larry A. Curtiss, Argonne National Laboratory)

Project Objective. This project will develop new cathode materials and electrolytes for Li-air batteries for long cycle life, high capacity, and high efficiency. The goal is to obtain critical insight that will provide information on the charge and discharge processes in Li-air batteries to enable new advances to be made in their performance. This will be done using state-of-the-art characterization techniques combined with state-of-the-art computational methodologies to understand and design new materials and electrolytes for Li-air batteries.

Project Impact. The instability of current nonaqueous electrolytes and degradation of cathode materials limits the performance of Li-air batteries. The project impact will be to develop new electrolytes and cathode materials that are stable and can increase cycle life and improve efficiency of Li-air batteries.

Approach. The project is using a joint theoretical/experimental approach for design and discovery of new cathode and electrolyte materials that act synergistically to reduce charge overpotentials and increase cycle life. Synthesis methods, in combination with design principles developed from computations, are used to make new cathode architectures. Computational studies are used to help understand decomposition mechanisms of electrolytes and how to design electrolytes with improved stability. The new cathodes and electrolytes are tested in Li-O_2 cells. Characterization along with theory is used to understand the performance of the materials used in the cell and make improved materials.

Out-Year Goals. The out-year goals are to find catalysts that promote discharge product morphologies that reduce charge potentials and find electrolytes for long cycle life through testing and design.

Collaborations. This project engages in collaboration with Prof. K. C. Lau (UC at Norridge), Prof. Y. Wu (Ohio State University), Dr. D. Zhai (China), and R. Shahbazian-Yassar (UIC).

Milestones

1. Investigation of highly uniform Pt_3Co nanoparticles in biphasic nitrogen-doping cobalt@graphene heterostructures as cathode materials. (Q1, FY 2018; Completed)
2. Computational studies of dependence of stability and composition of discharge products in Li-O_2 batteries on ether-based electrolytes. (Q2, FY 2018; Completed)
3. Use of highly uniform small iridium clusters supported on reduced graphene oxide to study formation of Ir_3Li alloys for lithium-superoxide-based batteries. (Q3, FY 2018; Completed)
4. Investigation of dependence of discharge composition on type of ether used in electrolytes from experimental studies. (Q4, FY 2018; Initiated)

Progress Report

One of the major challenges for Li-oxygen batteries is the high charge overpotential, which results in a low energy efficiency. It was recently shown that lithium superoxide, which is a good electronic conductor and has a low charge overpotential, can be formed in a Li-O_2 battery using iridium as a catalyst, but little is known about the role of iridium in the lithium superoxide formation. It was speculated that an Ir_3Li alloy forms that acts as effective template for growth of the LiO_2. In this work, size-selected subnanometer iridium clusters were used to generate uniformly sized iridium nanoparticles on reduced graphene oxide based cathodes to gain new insight into the mechanism by which the iridium particles evolve and function during discharge when the LiO_2 forms. It is found that during discharge the iridium nanoparticles surprisingly evolve to larger ones while incorporating lithium from LiO_2 to form core-shell structures with Ir_3Li shells.

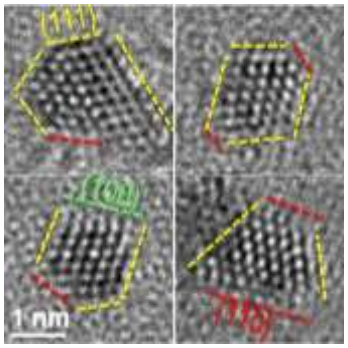

Figure 92. High-resolution transmission electron microscopy image of annealed Ir_8 clusters on an rGO cathode showing crystalline facets of the iridium nanoparticles.

The cathode material for the Li-O_2 cell used in this study was prepared by depositing ligand-free subnanometer Ir_n clusters of a specific size on reduced graphene oxide (rGO). The rGO surface is covered by a fraction of a monolayer with size-selected Ir_n clusters of sizes 2, 4, and 8 atoms. The size and crystallinity of the deposited nanoclusters were further tuned by annealing of the samples under vacuum. For the iridium clusters, the team has chosen one size (n=8), which has been annealed to larger particles (~ 1.5 nm). From HRTEM studies, the iridium nanoparticles have crystalline facets, as shown in Figure 92. During discharge it is found that LiO_2 forms in the Li-O_2 cell with a TEGDME electrolyte. The evidence for LiO_2 formation was from Raman spectra and titration of the discharge product, as well as DEMS measurement during discharge that showed one electron used per O_2.

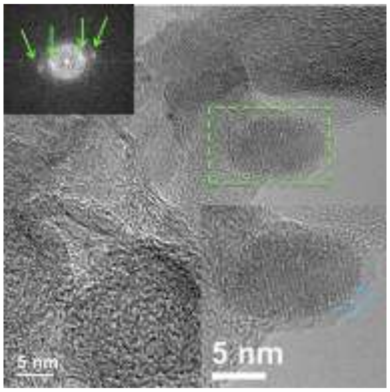

Figure 93. Green rectangle shows a typical ~ 5 x 10 nm particle formed on the Ir-rGO cathode with white lines corresponding to Ir_3Li spacing ; the upper left inset shows a fast Fourier transform (FFT) on the nanoparticle surface with the diffraction peaks consistent with Ir_3Li; lower right inset shows a close up of the nanoparticle with a thin layer of ~ 1-2 nm marked by dashed cyan line on the surface of the nanoparticle, due to the discharge product.

HRTEM was used to characterize the evolution of the iridium nanoparticles. The HRTEM images showed that the iridium nanoparticles, which started out as ~ 1.5 nm, had unexpectedly evolved during the discharge process and formed larger particles, most being ~ 5 to 10 nm in size. Figure 93 shows one of the ~ 5 x 10 nm nanoparticles where the iridium lattice spacing has increased as indicated by white lines in the image in what appears to be an outer shell. From HRTEM imaging, the shell has a lattice spacing of ~ 0.41 nm, which matches with that of an Ir_3Li lattice. Electron diffraction patterns also confirm that the shell is Ir_3Li, as it shows an additional diffraction ring with dots corresponding to the double lattice spacing of Ir_3Li. Thus, these results show that the 1.5 nm Ir particles grow during discharge to form larger core-shell Ir/Ir_3Li nanoparticles. The Ir_3Li shell can act as a template for the growth and stabilization of crystalline LiO_2. The crystallinity can suppress disproportionation to the thermodynamically more stable products of Li_2O_2 and O_2. The Ir_3Li core-shell nanoparticles discovered here provide a new direction in nanomaterials research for reducing charge overpotentials and finding a closed system in Li-O_2 batteries.

Patents/Publications/Presentations

Publication

- 27th Austin Symposium on Molecular Structure and Dynamic, Dallas, Texas (March 3–5, 2018): “Subnanometer Metal Clusters as Catalysts for Energy Conversion and Storage”; L. A. Curtiss.

TASK 7 –SODIUM-ION BATTERIES

Summary

During FY 2019, the BMR will add five new projects, including several in the area of sodium-ion batteries. The sodium-ion battery will require investigations to identify optimal electrode materials, electrolytes, separators, and binders to reach its full potential. The BMR program will therefore have a limited effort directed toward identifying sodium-ion battery materials that have potential value for vehicle applications. These projects will be included in this new section as they get underway. More detailed information on this BMR Task will be provided in upcoming reports.

Task 7.1 – Exploratory Studies of Novel Sodium-Ion Battery Systems (Xiao-Qing Yang and Seongmin Bak, Brookhaven National Laboratory)

Project Objective. The primary objective of this proposed project is to develop new advanced *in situ* material characterization techniques and to apply these techniques to explore the potentials, challenges, and feasibility of new rechargeable battery systems beyond the lithium-ion batteries (LIBs), namely the Na-ion battery systems for PHEV. To meet the challenges of powering the PHEV, new rechargeable battery systems with high energy and power density, low cost, good abuse tolerance, and long calendar and cycle life need to be developed. This project will use the synchrotron-based *in situ* X-ray diagnostic tools developed at BNL to evaluate the new materials and redox couples, to explore in fundamental understanding of the mechanisms governing the performance of these materials.

Project Impact. In the VTO MYPP, the goals for battery are described as: "Specifically, lower-cost, abuse-tolerant batteries with higher energy density, higher power, better low-temperature operation, and longer lifetimes are needed for the development of the next-generation of HEVs, PHEVs, and EVs." The knowledge learned from diagnostic studies and collaborations with U. S. industries through this project will help U. S. industries to develop new materials and processes for new generation of rechargeable battery systems, namely Na-ion battery system in their efforts to reach the VTO goals.

Approach. This project will use the synchrotron-based *in situ* X-ray diagnostic tools developed at BNL to evaluate the new materials and redox couples to enable a fundamental understanding of the mechanisms governing the performance of these materials and provide guidance for new material and new technology development regarding Na-ion battery systems.

Out-Year Goals. Complete the synchrotron-based *in situ* XRD and *ex situ* XAS studies of $Na_{0.66}Mn_{0.6}Ni_{0.2}Mg_{0.2}O_2$ as new cathode material for Na-ion batteries during charge-discharge cycling.

Collaborations. BNL team has been closely working with top scientists on new material synthesis at ANL, LBNL, and PNNL, with U. S. industrial collaborators at General Motors and Johnson Controls; as well as international collaborators.

Milestones

1. Complete i*n situ* XRD and *ex situ* XAS studies and the evaluation of lattice parameter changes of new $NaCrS_2$ layer structured cathode materials during the charge-discharge cycling. (Q1, December 2017; Completed)
2. Complete the synchrotron-based XRD studies with Rietveld refinement of $Na_3VP_3O_9N$, as well as XANES and extended X-ray absorption fine structure (EXAFS) investigation of this new cathode material for Na-ion batteries at pristine and fully charged states. (Q2, March 2018; Completed)
3. Complete the synchrotron based *in situ* XRD studies of $Na_{0.66}Mn_{0.6}Ni_{0.2}Mg_{0.2}O_2$ as new cathode material for Na-ion batteries during charge-discharge cycling. (Q3, June 2018; Completed)
4. Complete the synchrotron-based XANES studies of $Na_{0.66}Mn_{0.6}Ni_{0.2}Mg_{0.2}O_2$ as new cathode material for Na-ion batteries during charge-discharge cycling. (Q4, September 2018; In progress)

Progress Report

The third quarter milestone for FY 2018 was completed, and progress began on the fourth quarter milestone. BNL has been focused on the *in situ* XRD studies of $Na_{0.66}Mn_{0.6}Ni_{0.2}Mg_{0.2}O_2$ as new cathode materials for Na-ion batteries. To monitor the structural changes of $Na_{0.66}Mn_{0.6}Ni_{0.2}Mg_{0.2}O_2$ during sodium extraction and insertion, *in situ* XRD was conducted at various charge/discharge states in a voltage range of 1.5-3.8 V versus Na^+/Na. The results are presented in Figure 94. During the charge process, most diffraction peaks shift continuously to higher angles, indicating the shrinking of the unit cells of $Na_{0.66}Mn_{0.6}Ni_{0.2}Mg_{0.2}O_2$ upon sodium deintercalation in a solid-solution behavior. At the end of the charge, a new peak can be observed, indicating a new phase is formed.

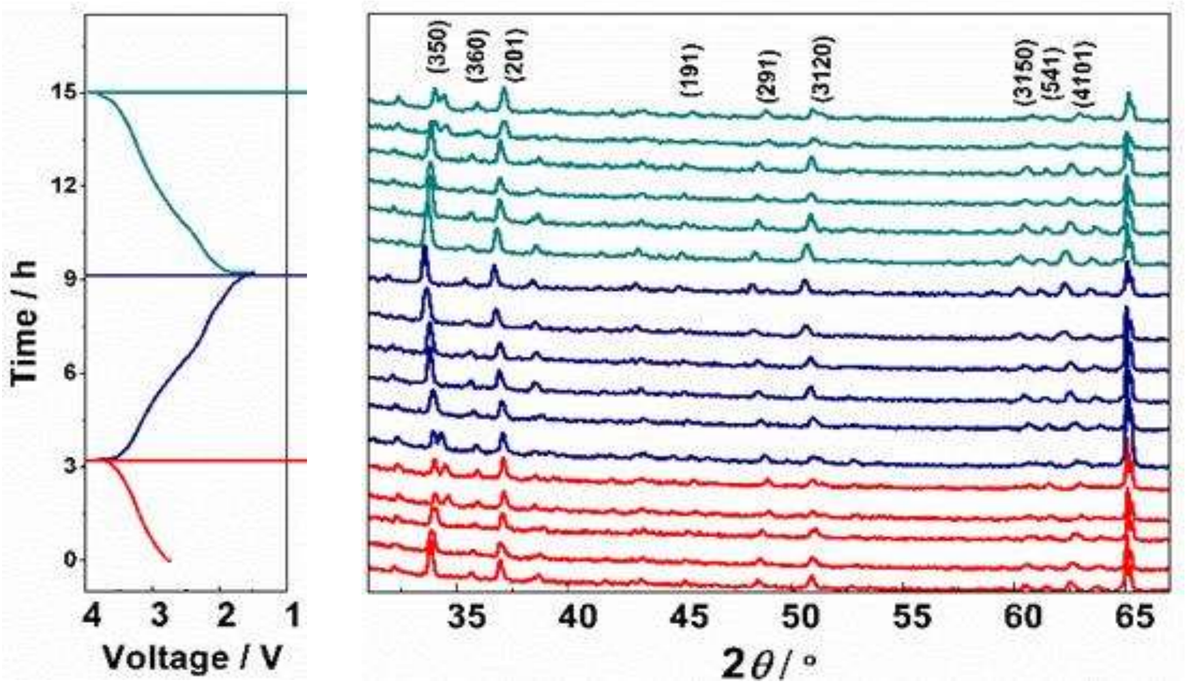

Figure 94. ***In situ*** **X-ray diffraction patterns collected during the first charge/discharge and the second charge of** $Na/Na_{0.66}Mn_{0.6}Ni_{0.2}Mg_{0.2}O_2$ **cells at a current rate of 0.2 C in the potential range between 1.5 and 4.3 V.**

Patents/Publications/Presentations

Publication

- Liu, J., L. Yu, E. Hu, B. S. Guiton, X-Q. Yang, and K. Page, "Large-Scale Synthesis and Comprehensive Structure Study of δ-MnO_2." *Inorganic Chemistry* 57, no. 12 (2018): 6873–6882. doi: 10.1021/acs.inorgchem.8b00461 (Web Publication Date: May 30, 2018).

Presentation

- CIBF2018, Shenzhen, China (May 22–24, 2018): "Using Synchrotron Based X-ray Scattering and Absorption Spectroscopy as well as TXM and TEM Imaging Techniques to Study New Cathode Materials for Rechargeable Batteries"; E. Hu, X-Q. Yang, J. Liu, S-M. Bak, R. Lin, Z. Shadike, H-S. Lee, X. Wang, H. Xin, Y. Liu, X. Yu, X. Huang, and H. Li. Invited.

Innovation Center for Battery500
(Jun Liu, PNNL; Yi Cui, Stanford University)

Project Objective. The project aims to develop commercially viable lithium battery technologies with a cell-level specific energy of 500 Wh/kg through innovative electrode and cell designs that enable the extraction of the maximum capacity from advanced electrode materials. In addition to achieving high specific energy, the project aims to be able to achieve 1,000 cycles for the developed technologies.

Project Impact. The Battery500 Consortium will develop the next-generation lithium battery technologies that will significantly increase energy density, improve cycle life, and reduce cost. This will greatly accelerate the deployment of EVs and reduce carbon emission associated with fossil fuel consumption. The consortium will utilize first class expertise and capabilities in battery research in the United States and develop an integrated and multidisciplinary approach to accelerate development and deployment of advanced electrode materials in commercially viable high-energy batteries. The advances made in this consortium will also benefit the improvement of current Li-ion battery technologies.

Approach. This project will utilize an assortment of national resources located at the national laboratory level and university level. The lithium anode combined with a compatible electrolyte system and two cathodes—one high-Ni $LiNi_xMn_yCo_zO_2$ and another sulfur—will be studied and developed to reach high-energy density. The project focus is to design novel electrode and cell architectures to meet the 500 Wh/kg goal. The consortium will work closely with R&D companies, battery/materials manufacturers, and end users/OEMs to ensure that the developed technologies are aligned with industry needs and can be transitioned to production.

Out-Year Goals. This project aims for the following out-year goals. (1) Integrate materials and components developed in FY 2018 into 1 Ah pouch cell and demonstrate 350 Wh/kg cell with more than 50 charge discharge cycles, and provide analytical results for materials selection, cell design and fabrication, and further refinement for FY 2019. (2) Evaluate the seedling projects for key findings that can be incorporated into the consortium.

Collaborations. The collaboration among consortium team members will be well coordinated by the leadership team, which includes the keystone project leads and co-leads along with PIs at all member institutions. Collaboration with the community outside of this consortium and with industry will be facilitated by the executive committee, the advisory board, and the industry committee.

Milestones

1. Scale up the synthesis capacity of high-Ni-content NMC to 500 g; Incorporate cathode surface modification in coin cells with greater than 2 mAh/cm^2 loading. (Q1, December 2017; Completed)
2. Establish the high-nickel NMC coin cell properties using the materials synthesized by the team and supplied by other sources; Develop stage 1 pouch cell testing protocols and provide updated component parameters toward 350 Wh/kg; Establish baseline properties of Li-S coin cells using parameters required to reach 350 Wh/kg. (Q2, March 2018; Completed)
3. Provide feedback on characterization of new materials and concepts by the characterization team; Develop procedures to identify lithium anode failure in coin cells and pouch cells. (Q3, June 2018; In progress)
4. Establish coin cell performance with 30% weight reduction in the anode current collector; Develop and implement methods to improve and understand cycle and calendar life limitations of pouch cells. (Q4, September 2018; In progress)

Progress Report

The third milestone for FY 2018 has been completed. Feedback on characterization of the new materials and concepts was provided by the characterization team. The procedures to identify lithium anode failure in coin cells and pouch cells were developed.

This quarter, the FY 2018 second quarter review was held May 10–11 in Seattle, Washington. The PIs, postdocs, and students of Battery500 Consortium team gave 19 oral and 20 poster presentations. Two posters were rewarded as best posters of the review meeting. The active involvement of the young scientists in the review meeting resulted in many interesting discussions during and after the review meeting as well as many post-meeting collaborative research activities.

Also this quarter, more than 15 invited talks were delivered by PIs of Battery500 Consortium and 8 papers were published or accepted for publication in peer-reviewed journals. Further, about 11 technical teleconferences were held for scientific information exchange, and three working group teleconferences were held for managing the consortium project.

The technical portion of this report is organized under three Keystone projects, as presented below.

Keystone Project 1: Materials and Interfaces

High-Nickel NMC. *Determine attributes of NMC-811 versus NCA:* The thermal stability of NCA versus NMC-811 charged to either 4.4 V or 4.7 V was determined. It was reported that the presence of aluminum in the layered oxide structure can improve the thermal stability of layer structured cathode materials. The team's results in Figure 95a-b show that in the presence of electrolyte, both delithiated NMC-811 and NCA have similar thermal stabilities. Both decompose at temperatures below 250ºC; the similarity indicates that in operating battery, NCA does not have significant thermal stability advantage over NMC-811. The different cut-off voltage results further showed that samples charged to 4.4 V and 4.7 V have similar thermal stabilities in NMC-811 and NCA. However, the team physically observed much more gassing from 811 than from NCA; that is, the differential scanning calorimetry (DSC) holders popped open for 811, but not for NCA. These observations are consistent with earlier discussions that in Li-metal batteries, the lithium anode is the major concern rather than the cathode. Therefore, the team initiated a study of the thermal stability of the anode/electrolyte combinations.

The cell capacity retention for Li/NMC-811 cell using lean electrolyte is much worse than for flooded electrolyte cells, and has been associated with reaction of the lithium metal with the electrolyte. The team confirmed that graphite anodes do not have the same capacity fade issue for lean electrolyte, as shown in Figure 95c.

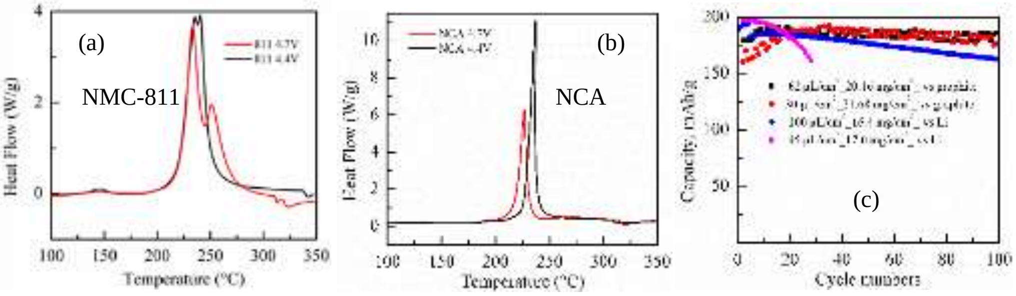

Figure 95. Differential scanning calorimetry profiles of (a) NMC-811 and (b) NCA charged to different cut-off voltages. (c) Capacity retention of a graphite/NMC-811 cell, compared with a Li/NMC-811 cell.

Lithium Anode. Recently, the team developed a fire-retardant localized high-concentration electrolyte consisting of 1.2 M LiFSI in a mixture of flame-retardant triethylphosphate/bis(2,2,2-trifluoroethyl) (TEP/BTFE) ether (1:3 by molar ratio) that is stable to both lithium metal and NMC. This electrolyte greatly enhances the cycling performance of Li-metal batteries. A Li||$LiNi_{0.6}Mn_{0.2}Co_{0.2}O_2$ battery using this electrolyte can retain > 97% capacity after 600 cycles at 1C rate (ca. 1.6 mA cm^{-2}), corresponding to a negligible capacity decay of < 0.005% per cycle when tested in coin cells. More importantly, this new electrolyte is also stable when used in cells with combination of lean electrolyte and thin Li-foil anode, resulting in stable operation of high-capacity (Li||NMC-811, 1 to 2.5Ah), high-energy-density (> 300 Wh/kg) pouch cells for more than 200 cycles. Characterization of this fire-retardant electrolyte is shown in Figure 96. More work will follow to improve the operating temperature window and reduce cost of these electrolytes.

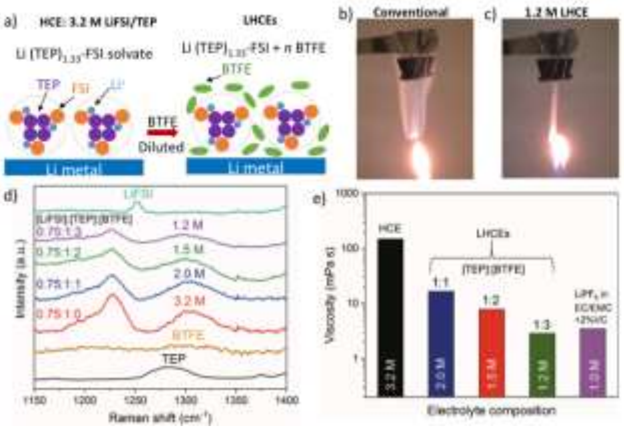

Figure 96. Characterization of fire-retardant localized high-concentration electrolyte (LHCE). (a) Schematic illustration for dilution by BTFE of an HCE consisting of 3.2 M LiFSI/TEP to form LHCEs. (b-c) Photographs of ignition tests of glass fibers saturated with the conventional electrolyte (b) and the 1.2 M LHCE (c). (d) Raman spectra of pure TEP, pure BTFE, LiFSI, the HCE, and LHCEs with different LiFSI salt concentrations and TEP/BTFE molar ratios. (e) Viscosity of different electrolytes.

Keystone Project 2: Electrode Architecture

The goal of the Keystone 2 is to design, model, fabricate, and characterize the effect of electrode architecture on electrode and cell performance in support of reaching the project goal of 500 Wh/kg cell specific energy. Included in this Keystone are architecture design of thick cathodes (UCSD), Li-metal electrode architectures (PNNL and Stanford), inorganic (UT-Austin) and polymer (Stanford) electrolytes, and electrode performance modeling (UW). Highlighted here are recent advancement at Stanford on development of new polymer electrolytes and continued characterization of thick cathodes at UCSD.

The research group of Z. Bao at Stanford University has been developing suitable polymers as coating protection layer for lithium metal or as SSE with a focus on understanding the molecular design of polymers that impact transference number. The vast majority of solid polymer electrolyte (SPE) research in the past 40 years has focused on PEO-based polymers, which have low conductivities (~ 10^{-5} S cm^{-1}) and transference numbers with t_{Li+} of only 0.2. The team hypothesizes that a polymer with more sterically hindered oxygen (for example, poly(tetrahydrofuran), or PTHF; Figure 97a), may create loose coordination to Li^+. To overcome the poor mechanical and thermal properties of the PTHF polymer, the group employed a chemical cross-linking procedure to create mechanically-robust, free-standing membranes. These crosslinked electrolytes show a cation transference number of 0.53, which is among the highest of any reported SPE based on a single polymer component with no additives. Furthermore, the Li-ion conductivity of the xPTHF electrolytes is higher than that of the xPEO electrolytes across a wide range of molecular weights, as shown in Figure 97b. MD and DFT simulations confirmed that the improved transference number of PTHF SPEs is due to the loose coordination of the polymer backbone to Li^+ compared to PE (Figure 97c). The average number of oxygens solvating lithium in the PEO system is ~ 6 compared to only ~ 4 oxygens solvating Li^+ in PTHF. These results suggest that PTHF coordinates less strongly to lithium than PEO does. The ^7Li NMR spectra in Figure 97d show that the ^7Li peak is shifted downfield in the PTHF-based electrolyte compared to PEO. This downfield shift is indicative of reduced electron density around the lithium atom, signifying looser coordination with the highly donating oxygen electrons in the polymer backbone. This loose coordination is expected to enable the high Li-ion conductivity and high transference number, as discussed above. The new polymer is thermally stable up to 230°C, electrochemically stable up to 4 V versus Li/Li^+ and can operate in a Li|SPE|$LiFePO_4$ battery at elevated temperature for over 100 cycles with an average CE of 99.58%. Overall, the concept of tuning the interaction between the polymer backbone and Li^+ is an exciting approach to develop improved SPEs for Li-ion batteries and potentially polymer coatings for lithium metal.

In the cathode work, UCSD has continued its evaluation of thick electrodes. By using a dry electrode manufacturing method, Maxwell Technology is capable of making Ni-rich NMC thick electrodes with various active mass loadings, porosities, and thicknesses. These electrode properties have an influence on the electrochemical performance of the batteries. Table 6 correlates the initial capacity and CE with different electrode loading, porosity, and thickness. The electrochemical evaluation was performed in CR2032 coin cells, with 50 µL electrolyte and 1-mm-thick lithium disc. In the first two cycles, the electrodes were activated at C/10; in the following cycles the cells were charged at C/10 and discharged at C/3, between 2.8 to 4.4 V versus Li/Li^+. Although the active material loading of the Maxwell NMC-811 (40 mg/cm^2) is 10 mg/cm^2 more than that of the Maxwell NMC-622-3 (30 mg/cm^2), its capacity is still ~12 mAh/g higher. Considering that these two electrodes have similar porosity, the improved capacity can be ascribed to the increased nickel content in the NMC-811 material. A comparison between Maxwell NMC-622-2 and Maxwell NMC-622-3 indicates that reducing the porosity in the electrode helps to improve the electrochemical performances. Though it might appear surprising, this may be due to the more compact electronic conductive network in the electrode with the lower porosity. The low porosity still allows electrolyte to fill the pores and maintains good ionic conductivity. A comparison between the Maxwell NMC-622-1 and Maxwell NMC-622-2 electrodes, as well as Maxwell NMC-622-3 and Maxwell NMC-622-4, suggests that less active material loading gives better electrochemical performance, which, however, reduces the energy density of the battery. In summary, the NMC-811 material with 20 porosity and 30-40 mg/cm^2 active mass loading offers a good candidate to achieve high-energy batteries. More work will follow to optimize the electronic transport properties of the thick electrodes.

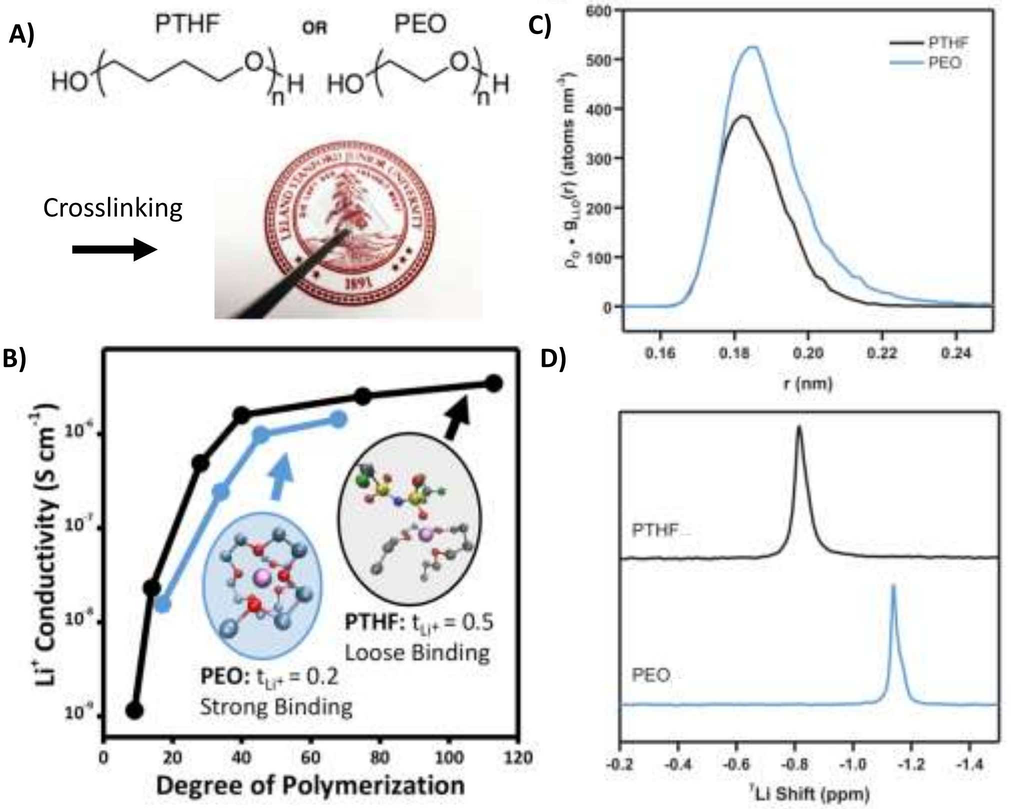

Figure 97. (a) Chemical structures of PEO and PTHF precursors that are used in the crosslinking reaction to create robust, free-standing solid polymer electrolyte (SPE) films. (b) Graph showing the ionic conductivity versus the degree of polymerization of the polymers in the crosslinked network for xPEO and xPTHF SPEs. The inset shows molecular dynamics simulations of LiTFSI dissolved in the polymer backbones. (c) Density-weighted lithium-oxygen radial distribution functions (atoms per nm^3) in PTHF and PEO. (d) Experimental ^7Li NMR spectra for LiTFSI in PEO and PTHF.

Table 6. The relationship between the physical properties and electrochemical performance of the Ni-rich NMC thick electrodes provided by Maxwell Technology.

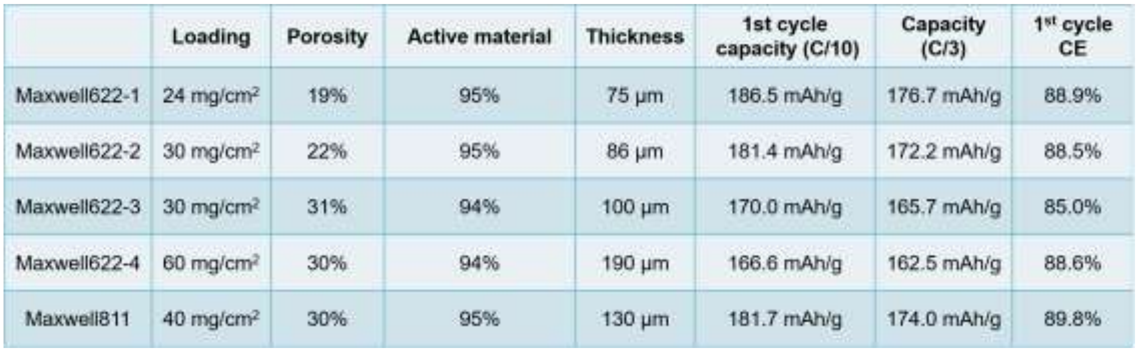

	Loading	Porosity	Active material	Thickness	1st cycle capacity (C/10)	Capacity (C/3)	1st cycle CE
Maxwell622-1	24 mg/cm^2	19%	95%	75 µm	186.5 mAh/g	176.7 mAh/g	88.9%
Maxwell622-2	30 mg/cm^2	22%	95%	86 µm	181.4 mAh/g	172.2 mAh/g	88.5%
Maxwell622-3	30 mg/cm^2	31%	94%	100 µm	170.0 mAh/g	165.7 mAh/g	85.0%
Maxwell622-4	60 mg/cm^2	30%	94%	190 µm	166.6 mAh/g	162.5 mAh/g	88.6%
Maxwell811	40 mg/cm^2	30%	95%	130 µm	181.7 mAh/g	174.0 mAh/g	89.8%

In summary, the consortium continues to make advancements in both cathode and lithium anode architectures. Recent work shows NMC with loadings of 30-40 mg/cm^2 and 20% porosity is a potential candidate for realizing the next-generation consortium demonstration cells. Progress in polymer electrolyte shows the possibility for Li-metal protection coatings with high ion conductivity and mechanical robustness.

Keystone Project 3: Cell Fabrication, Testing, and Diagnosis

Efforts to better understand electrode structure and cell failure highlighted activities during this quarter. On the electrode structure side, two distinct computational efforts were undertaken. In the first, novel structures with arrays of electrode material and fixed-width, low-tortuosity gaps were investigated. Finite-element simulations (FEM) of these architectures using macro-homogeneous models of Newman and co-workers were undertaken to help determine the optimal distribution of electrode mass for a fixed thickness and overall capacity, and to understand material utilization at high rates of galvanostatic discharge.

Figure 98 depicts discharge curve simulations for an NMC cathode. The discharge simulation is terminated either when the cell voltage falls below the cutoff value, or when the electrolyte concentration in the cathode toward the current collector drops below a certain minimum value. When used to identify enhanced utilization of cathode material, it was identified that increased utilization is obtained over the homogeneous for $W_d/L_p = 1$ and lower. At a configuration of $W_d/L_p \sim 0.5$, nearly 95% utilization is achieved where W_d is the domain width and L_p is the domain thickness. The pseudo-3D model permits parametric variations that allow simulation of low electronic-conductivity regimes, and as such is a generalized framework that can be used to simulate any combinations of anode/cathode chemistries, and different property combinations of electrodes, separator, and electrolytes.

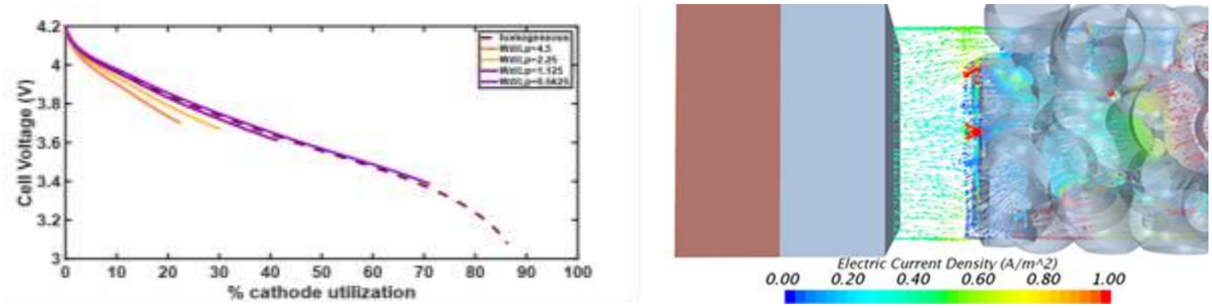

Figure 98. Discharge curves at ~ 6 mA/cm^2 to understand cathode utilization (right). Current density variation computations (left) of cathode chemistries.

In a complementary computational work, the current density distribution in a cathode and the subsequent localized current density at the opposing Li-metal negative electrode were investigated using a 3D model. These computations found that not only does the localized current density at the lithium metal correlate with the structure of the cathode, but also that the size of particles used in the cathode impacts localized current density. Indeed, when moving from 3- µm to 9-µm cathode particles, more than a 2x increase in variability is seen.

Experimentally, analysis of full pouch cells and coin cells using limited electrolyte and lithium metal indicated that it is possible to characterize aging processes and to relate variations in aging that occur for calendar and cycle life cells. For calendar life cells, it has been observed that cells see little loss in performance over the course of more than six months. The most distinct areas of performance loss for calendar life cells are a general increase in cell impedance and a gradual shift in the ability to fully charge the cell within the prescribed charging regime. Both modes can be linked with evolving interfaces within the cell. Similar modes of failure are seen for the cycle life cells, but with an additional loss of cathode active material over the course of 275 cycles. The magnitude of performance loss due to interfacial processes is similar for both calendar and cycle life cells, suggesting that the repeated plating and stripping has limited impact on cell failure at a C/20 rate.

Patents/Publications/Presentations

Patents

- Fang, C., X. Wang, and Y. S. Meng. TGC Method and System for Metal Quantification. UD00000763.
- Wang, S., et al. Battery Separator with Lithium Ion Conductor Coating. Provisional Patent Application, June 19, 2018.

Publications

- Li, J., W. Li, S. Wang, K. Jarvis, J. Yang, and A. Manthiram. "Facilitating the Operation of Lithium-Ion Cells with High-Nickel Layered Oxide Cathodes with a Small Dose of Aluminum." *Chemistry of Materials* 30, no. 9 (2018): 3101–3109.
- Li, Y., X. Chen, A. Dolocan, Z. Cui, S. Xin, L. Xue, H. Xu, K. Park, and J. B. Goodenough. "Garnet Electrolyte with an Ultralow Interfacial Resistance for Li-Metal Batteries." *Journal of the American Chemical Society* 140, no. 20 (2018): 6448–6455.
- Li, Y., H. Xu, P. Chien, N. Wu, S. Xin, L. Xue, K. Park, Y. Hu, and J. B. Goodenough. "A Stable Perovskite Electrolyte in Moist Air for Li-Ion Batteries." *Angewandte Chemie International Edition* (May 2018).
- Liu*, J., L. Yin, X-Q. Yang*, and P. G. Khalifah. "$Li_3VP_3O_9N$ as a Multielectron Redox Cathode for Li-Ion Battery." *Chemistry of Materials*. doi: 10.1021/acs.chemmater.8b01114 (Web Publication Date: May 23, 2018).
- Jue Liu*, L. Yu, E. Hu, B. S. Guiton, X-Q. Yang, and K. Page*. "Large-Scale Synthesis and Comprehensive Structure Study of δ-MnO_2." *Inorganic Chemistry* 57, no. 12 (2018): 6873–6882. doi: 10.1021/acs.inorgchem.8b00461 (Web Publication Date: May 30, 2018).
- Fan, X., E. Hu, X. Ji, Y. Zhu, F. Han, S. Hwang, J. Liu, S. Bak, Z. Ma, T. Gao, S-C. Liou, J. Bai, X-Q. Yang, Y. Mo, K. Xu, D. Su, and C. Wang. "High Energy-Density and Reversibility of Iron Fluoride Cathode Enabled via an Intercalation-Extrusion Reaction." *Nature Communications*. doi: 10.1038/s41467-018-04476-2 (Web Publication Date: June 13, 2018).

- Chen, S., J. Zheng, L. Yu, X. Ren, C. Niu, H. Lee, X. Wu, J. Xiao, J. Liu, and J. Zhang. "High Efficiency Lithium Metal Batteries with Fire-Retardant Electrolytes." *Joule*. doi: https://doi.org/10.1016/j.joule.2018.05.002 (Web Publication Date: May 29, 2018).
- Jiao, S., X. Ren, R. Cao, M. H. Engelhard, Y. Liu, D. Hu, D. Mei, J. Zheng, W. Zhao, Q. Li, N. Liu, B. D. Adams, C. Ma, J. Liu, J-G. Zhang, and W. Xu. "Stable Cycling of High-Voltage Lithium Metal Batteries in Ether Electrolytes." *Nature Energy* (2018). doi: https://doi.org/10.1038/s41560-018-0199-8.

Presentations

- Advanced Automotive Battery Conference (AABC), San Diego, California (June 5, 2018): "Assessing Critical Pathways to Next Generation High Energy Safe Lithium Batteries"; Y. S. Meng. Invited.
- Advanced Battery Power – Kraftwerk Batterie, Münster, Germany (April 11, 2018): "Li-Ion: Where from and Where to?"; M. S. Whittingham. Invited.
- Münster Electrochemical Energy Technology (MEET), University of Münster, Munster, Germany (April 13, 2018): "Li-Ion Batteries: Present Status and Materials Limitations"; M. S. Whittingham. Invited.
- 48th Power Sources Conference, Denver, Colorado (June 12, 2018): "The Past, the Present and Future Trends for Li Batteries"; M. S. Whittingham. Invited.
- MRS Meeting, Phoenix, Arizona (April 3-6, 2018): "Highly Stable Lithium Metal Batteries Enabled by Localized High Concentration Electrolytes"; J.-G. Zhang, S. Chen, and J. Zheng. Invited.
- CIBF2018, Shenzhen, China (May 22–24，2018): "High Efficiency Lithium Metal Batteries Enabled by Localized High Concentration Electrolytes"; J.-G. Zhang. Invited.
- 233rd ECS Meeting, Seattle, Washington (May 13–17, 2018): "One Step Synthesis of Li-Alkyl Carbonates and Their Application as Coatings on Li Anode"; P. Liu, et al. Invited.
- MRS Meeting, Phoenix, Arizona (April 4, 2018): "Solution Based Synthesis of Solid Electrolytes"; P. Liu, et al. Invited.
- ISFM-2018, Chandigarh, India (April 13–15, 2018): "Materials Challenges and Prospects of Electrical Energy Storage"; A. Manthiram. Invited plenary talk.
- Samsung SDI, Seoul, South Korea (April 17, 2018): "Investigation and Reduction of Residual Lithium in Nickel-Rich Cathode Materials"; A. Manthiram. Invited.
- Central Electrochemical Research Institute, Chennai, India (April 20, 2018): "Next Generation Battery Chemistries: Materials Challenges and Prospects"; A. Manthiram. Invited.
- 2nd International Materials Science and Engineering for Green Energy Conference, Rabat, Morocco (April 25, 2017): "Next-Generation Battery Technologies: Materials Challenges and Prospects"; A. Manthiram. Invited plenary talk.
- 233rd ECS Meeting, Seattle, Washington (May 13–17, 2018): "Bulk and Surface Chemistry of High-Nickel Layered Oxide Cathodes"; A. Manthiram. Invited.
- 8th Forum on New Materials: Materials Demands Towards New Generation Electrochemical Energy Storage Systems, International Conference on Materials and Technologies (CIMTEC 2018), Perugia, Italy (June 10–14, 2018): "High-Nickel Layered Oxide Cathodes for Next Generation Lithium-Ion Batteries"; A. Manthiram. Invited.